Aston University

Some pages of this thesis may have been removed for copyright restrictions.

If you have discovered material in Aston Research Explorer which is unlawful e.g. breaches copyright, (either yours or that of a third party) or any other law, including but not limited to those relating to patent, trademark, confidentiality, data protection, obscenity, defamation, libel, then please read our Takedown policy and contact the service immediately (openaccess@aston.ac.uk)

THE RELATIONSHIP OF MINERALIZATION TO PETROLOGY AT PARYS MOUNTAIN, ANGLESEY

A THESIS

SUBMITTED IN PARTIAL FULFILMENT OF THE REQUIREMENTS FOR

THE DEGREE OF

DOCTOR OF PHILOSOPHY

IN ACCORDANCE WITH THE SPECIAL REGULATIONS

OF

THE UNIVERSITY OF ASTON IN BIRMINGHAM

17966 12 DEC 1974

BY

T. THANASUTHIPITAK

NOVEMBER, 1974

THESIS 552 104 29 THA

SUMMARY

The Lower Palaeozoic succession at Parys Mountain overlies a Precambrian basement (the Mona Series). This succession consists of Ordovician slates, overlain by, and in part interbedded with, Ordovician dacitic and rhyolitic volcanics, which in turn are unconformably overlain by Silurian slates. Both basement and Palaeozoic rocks have been deformed during Caledonian and Variscan orogenies. The resultant structure of Parys Mountain is interpreted as an east-north-easterly trending, single syncline overturned to the north.

Many primary extrusive characters are retained by the volcanic rocks, despite the high degree of deformation. The lithologies and textures allow subdivision and interpretation of these rocks as dacite, lithic tuff, siliceous sinter, rhyolitic tuff, rhyolitic ignimbrite, rhyolitic tuff-lava, and rhyolitic lava.

The results of 61 bulk chemical analyses are interpreted to show that the volcanism was of the orogenic calc-alkaline type from a continental margin/island arc environment. The magmas probably result from either partial melting of the crustal part of the oceanic lithosphere on a Benioff zone, or partial melting of the mantle, above a Benioff zone, under high load pressures and high water pressures.

The mineral deposits are largely confined within the volcanic succession though some occur in the Ordovician and Silurian slates near to their contacts with the volcanics. The majority of the deposits form conformable lenses and tabular bodies, with subordinate

deposits as veins and stockworks. The ore mineral assemblages are of chalcopyrite, galena, sphalerite, and pyrite. The general paragenetic sequence (73 sections) is pyrite--chalcopyrite--galena--sphalerite. The main mineralization episode is interpreted to be syngenetic, genetically related to the volcanism. The veins and stockworks probably result from Caledonian and Variscan remobilization of the primary mineralization.

Trace element analyses (Cu, Zn, Pb, Ni, Co, Cd, Cr, Hg, Ba, Sr), on 350 specimens, detected anomalous concentrations of these elements around the mineralized zones, though some occur where no mineralization was found. The analyses also indicate a close relationship between the mineralization and the volcanic horizons, especially the siliceous sinter.

ACKNOWLEDGEMENTS

I am especially in debted to Dr. J. W. Gaskarth for his advice, criticism, and encouragement during his supervision of this study.

I wish to thank Canadian Industrial Gas and Oil Limited, and intermine Limited of Toronto, who were in charge of the exploration programme at Parys Mountain during this study, for permission to use the data and core specimens. The kindness and co-operation of Mr. E. Cockshutt, the caretaker of the companies, is gratefully acknowledged.

I also wish to thank the British Council for the scholarship awards for this study.

Dr. R. A. Ixer must be thanked for his advice, suggestions, and useful discussion on the polished section studies. Mr. F. B. Frost is thanked for his discussion and permission to use the computer programme.

I wish to express my gratitude to all members of the staff and technicians of the Department of Geological Sciences, University of Aston in Birmingham, for their consideration and much useful advice received during my studying here. Special thanks are due to Mr. J.H. Williams for his help in preparation of the plates used in this work, Mr. P. Brueton and Mrs. M.V. James for their care and skill in preparation of the many polished and thin sections, and Miss H.J. Couper for her kindness in proof reading of the thesis.

Mrs. E. J. Montgomery is highly thanked for her care and skill in preparation of the many diagrams and tables, and also her kind and useful advice during preparation of this thesis.

TABLE OF CONTENTS

page

SUMMARY i

ACKNOWLEDGEMENTS iii

TABLE OF CONTENTS iv

LIST OF FIGURES viii

LIST OF PLATES x

LIST OF TABLES xii

CHAPTER 1 INTRODUCTION 1

1.1 General Geology of Parys Mountain 1

1.2 Interpretations of the Geological History of Parys Mountain 6

1.3 Mineralization at Parys Mountain 9

1.4 Mining and Exploration History 10

1.5 Aims of the Present Investigation 13

1.6 Terminology 15

CHAPTER 2 STRATIGRAPHY 19

2.1 Precambrian 19

2.2 Ordovician 23

2.3 Silurian 26

CHAPTER 3 IGNEOUS ROCKS 28

3.1 Volcanic Rocks 28

3.1.1 Introduction and general succession . 28

3.1.2 Dacitic rocks 32

3.1.3 Lithic tuffs 38

3.1.4 Siliceous sinter 39

3.1.5 Rhyolitic rocks 41

3.2 Intrusive Rocks 50

		page
CHAPTER 4	STRUCTURAL GEOLOGY	54
	4.1 Introduction	54
	4.2 Caledonian Structures	55
	4.3 Post-Caledonian Structures	57
CHAPTER 5	MINERALIZATION	59
	5.1 General Characteristics of the Ore Bodies	59
	5.2 General Description of Ore Minerals	63
	5.2.1 Rutile	65
	5.2.2 Pyrite	66
	5.2.3 Marcasite	88
	5.2.4 Pyrrhotite	91
	5.2.5 Arsenopyrite	93
	5.2.6 Chalcopyrite	94
	5.2.7 Sphalerite	97
	5.2.8 Galena	108
	5.2.9 Tennantite	110
	5.2.10 Tetrahedrite	110
	5.2.11 Native Bismuth	112
	5.2.12 Bismuthinite	112
	5.2.13 Bismuth sulphosalts	114
	5.2.14 Bournonite	116
	5.2.15 Haematite	118
	5.2.16 Covellite	118
	5.2.17 Bornite	118
	5.2.18 Siderite	118
	5.2.19 Gangue Minerals	120
	5.3 Ore Mineral Paragenesis	121
	5.3.1 Rutile	123
	5.3.2 Pyrite 1	124
	5.3.3 Marcasite	125
	5.3.4 Pyrrhotite	126
	5.3.5 Pyrite 2	126
	5.3.6 Arsenopyrite	126

page

5.3.7 Chalcopyrite 127
5.3.8 Galena 127
5.3.9 Sphalerite 128
5.3.10 Tetrahedrite group, native bismuth, bismuthinite, and bismuth sulphosalts . . . 128
5.3.11 Pyrite 3 128
5.3.12 Secondary minerals 129
5.3.13 Gangue minerals 129

CHAPTER 6 GEOCHEMISTRY 132
6.1 Introduction 132
6.2 Bulk Chemistry 135
6.3 Discussion of Bulk Chemical Results 143
6.4 Trace Element chemistry 151
6.5 The Study of Wall Rock Alteration 170

CHAPTER 7 PETROGENESIS 171
7.1 General Statement 171
7.2 The Ordovician Slates 172
7.2.1 The Ordovician Depositional Basin in Anglesey 172
7.2.2 Source of the Ordovician Sediments . . . 174
7.3 The Volcanic Rocks 176
7.3.1 Previous Interpretations 176
7.3.2 Evidence used in the petrogenetic interpretation 177
7.3.3 Origin of Magma and Regional Tectonics . 181

CHAPTER 8 ORE GENESIS 187
8.1 Introduction 187
8.2 Previous interpretations 191
8.3 Depositional Environment and Method of Emplacement of stratiform Massive Sulphide Deposits. 192
8.4 Genesis of sulphide deposits at Parys Mountain and their relationship with volcanism 195

page

CHAPTER 9 SUMMARY OF CONCLUSIONS 200

9.1 Introduction 200

9.2 Origin of the 'felsite', the Carreg-y-doll, and the White Rock Formation 200

9.3 Relationship between the Volcanic Rocks and the Enclosing Sedimentary Strata 201

9.4 Origin of the Mineral Deposits 202

REFERENCES CITED 205

Appendix A Specimen Collection 216

Appendix B Sketch Geologic Sections for the Various Diamond Drill Holes and Correlations between them 221

Appendix C Geochemical Techniques 245

Appendix D Bulk Chemical Analysis 256

Appendix E Statistical Techniques 264

LIST OF FIGURES

page

Figure 1 Sketch map of Anglesey to show the study area . . 2

Figure 2 Simplified geological and tectonic map of Anglesey 3

Figure 3 Geological map of Parys Mountain (in pocket)

Figure 4 Sections through Parys Mountain to show different structural interpretations 5

Figure 5 Early Caradocian Palaeogeography of the British Caledonides 7

Figure 6A Sketch map to show the positions of boreholes drilled during 1961-1962 12

Figure 6B Sketch map to show the positions (and bearings) of the diamond drill holes 14

Figure 7 Sections of boreholes to show contact relationship between volcanic and sedimentary rocks 29

Figure 8 Generalized stratigraphic column 31

Figure 9 Block diagram to show geological interpretation from borehole data . . . . . (in pocket)

Figure 10 Sketch geological plan with cross sections to show locations of ore lodes 60

Figure 11 Sketch of polished specimens to show some macroscopic features of the ore 131

Figure 12 Niggli alk-si diagram 136

Figure 13 Differentiation Index vs SiO_2 diagram 138

Figure 14 Normative colour index vs normative plagioclase composition diagram 140

page

Figure 15 Normative An-Ab-Or diagram 141

Figure 16 MgO vs Fe_2O_3 diagram 142

Figure 17 AFM diagram 144

Figure 18 Harker Diagrams 146-8

Figure 19 Plot of principal component co-ordinate along boreholes C4, M10, and H17A. 158-160

Figure 20 Plot of factor scores along borehole C4 164

Figure 21 Plot of factor scores along borehole M10 165

Figure 22 Plot of factor scores along borehole IM9 166

Figure 23 Plot of factor scores along borehole H17A 167

Figure 24 Sketch to show the position of Anglesey with respect to the plate tectonic interpretation of the regional structure 185

Figure 25 Sketch diagrams to show the development of the Ordovician volcanism and sedimentation . .(facing p. 202

Figure 26 Synoptic diagram to illustrate the general geologic history of Parys Mountain area . . . . . .(facing p. 204

Figure 27 Sketch map to show the exposure ares of rocks at Parys Mountain 217

Figure 28 Sketch map to show surface samples' location 218

Figure 29 Sketch map to show position (with bearing) of diamond drill holes 219

Figure 30 Diagramatic sections of boreholes 241- 243

Figure 31 Generalized borehole logs and tentative correlation 244

Figure 32 Diagram to show the construction of the decomposition vessel used for dissolution of samples for A.A.S. 249

Figure 33 Sketch diagram to show instrumental set up for the determination of mercury by cold vapour method 253

LIST OF PLATES

		page
Plate 1	General appearance of porphyritic dacites in hand specimen, and their photomicrographs	34
Plate 2	General appearance of aphanitic dacites in hand specimen and in thin section	36
Plate 3	Aphanitic dacite with welded and flow-like textures	37
Plate 4	General appearance of lithic tuff in hand specimen and their photomicrographs	40
Plate 5	Photomicrographs of siliceous sinter (A,B,C, and D), and interlayering of rhyolitic tuff and Ordovician slate in hand specimen (E and F)	43
Plate 6	Photomicrographs of rhyolitic tuff (A,B,C, and D), general appearance of rhyolitic ignimbrite in hand specimen (E) and in thin section (F)	44
Plate 7	Photomicrographs of rhyolitic ignimbrite	46
Plate 8	Photomicrographs of rhyolitic ignimbrite	47
Plate 9	Photomicrographs of rhyolitic ignimbrite (A and B), general appearance of rhyolitiv tuff-lava in hand specimen (C), and photomicrographs of rhyolitic tuff-lava	49
Plate 10	Photomicrographs of rhyolitic tuff-lava (A,B and C) and rhyolitic lava (D,E, and F)	51
Plate 11	Photomicrographs of dolerite	53
Plate 12	Photomicrographs of rutile and pyritohedral pyrite	67
Plate 13	Photomicrographs of anhedral and framboidal pyrite	70

Plate	Photomicrographs of	page
14 and 15	Framboidal pyrite	71 and 73
16, 17, and 18	Colloform pyrite	74, 77 and 78
19 and 20	Secondary overgrowths in pyrite	80 and 82
21	Secondary overgrowths and corrosion in pyrite	83
22	Corrosion and zoning in pyrite	85
23	Zoning in pyrite	86
24	Poikilitic and cataclastic textures in pyrite	89
25	Special fabrics in pyrite	90
26	Marcasite and pyrrhotite	92
27	Arsenopyrite and chalcopyrite	95
28 and 29	Chalcopyrite	96 and 98
30, 31, 32, 33, 34, 35 and 36	Sphalerite	99, 101, 102, 103, 105, 106, and 107
37	Galena	109
38	Galena and tennantite	111
39	Tennantite and tetrahedrite	113
40 and 41	Native bismuth, bismuthinite, bismuth-sulphosalts, covellite, and bornite	115 and 119

LIST OF TABLES

Table		page
1	General stratigraphic sequence at Parys Mountain	20
2	Comparison of interpretations of the Mona Complex	21
3	The economic minerals and their associated host rocks in the four ore types of Parys Mountain	64
4	Paragenetic sequence of the ore minerals	122
5	Correlation matrices	152, 153 and 154
6	Inferred depositional events in Anglesey from Precambrian to early Silurian, with probable depositional environments related to the status of the Irish Sea Landmass.	175
7	Sulphide mineral assemblages and their associated host rocks.	190
8	Number of specimens collected and method of study	220
9	Information on locations and treatment of specimens, and analytical results (A.A.S)	222
10	Materials and solvents used in preparation of stock solutions for A.A.S	250
11	Bulk chemical analytical results	257
12	Norm calculated result of bulk chemical analyses	259
13 (A,B)	Statistical data	266 and 267
14	Total variance for Principal Component Analysis of 289 samples	268
15	Matrix of Principal Component Analysis for 289 samples	269
16	Matrix of factor loadings for 289 samples	270

Table		page
17	Total variance for Principal Component Analysis of 61 samples	271
18	Matrix of Principal Component Analysis for 61 samples	272
19	Matrix of factor loadings for 61 samples	273
20	Matrix of principal component co-ordinates for borehole C4	274
21	Matrix of factor scores for borehole C4	275
22	Matrix of factor scores for borehole M10	276
23	Matrix of factor scores for borehole IM9	277
24	Matrix of factor scores for borehole H17A	278
25	Matrix of principal component co-ordinates for boreholes M10, IM9, H17A, IM6	279
26	Matrix of factor scores for borehole IM6,H14, and H16	283

CHAPTER 1

INTRODUCTION

1.1 General Geology of Parys Mountain

Parys Mountain is situated about 6.5km south of the town of Amlwch in the north-east corner of the island of Anglesey, North Wales (Fig.1). It forms a topographical feature trending ENE-WSW which is some 150m high over an area of 2400 by 800m.

Two thirds of the area of Anglesey is occupied by Precambrian rocks (Fig.2), and the rest is approximately equally occupied by Ordovician and Carboniferous rocks, with subsidiary quantities of Cambrian, Silurian, and Devonian rocks (the disposition of these rocks is described by Wheatley (1971a), and Greenly (1919).

A simplified tectonic map of Anglesey (Fig.2) shows Parys Mountain to be situated on the north-eastern side of the north-westerly trending syncline, which crosses the north-western part of the island.

Parys Mountain is underlain by the Precambrian Mona Series and a succession of Lower Palaeozoic sedimentary and volcanic rocks most of which, except the Silurian sediments, are intruded by a group of doleritic sills. The Precambrian rocks consist of chlorite schists, micaceous and granitoid gneisses, and quartzitic gneisses. The Lower Palaeozoic succession consists of Ordovician slates, Ordovician dacitic and rhyolitic volcanic rocks, and Silurian slates. The doleritic intrusions are probably contemporaneous with the volcanic rocks (late Ordovician).

The rocks of the Precambrian Mona Series, exposed in the northern and southern parts of the Parys Mountain area, are thrust over

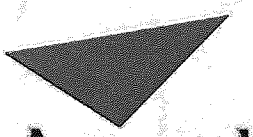

Aston University

Content has been removed for copyright reasons

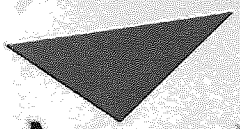

Aston University

Content has been removed for copyright reasons

the younger rocks along several low angle thrust faults (the Carmel Head, Corwas, and Nebo Thrusts - Fig.3, in pocket). The northern outcrops consist of chlorite schists, and those in the south are of micaceous, granitoid, and quartzitic gneisses. Ordovician slates are exposed around the core of the mountain in the northern, western, and southern parts of the area (Fig.3). These slates are overlain by, and have gradational contacts with, volcanic rocks of late Ordovician age. Silurian slates form the core of the mountain and are enclosed by the volcanic rocks (Fig.3). The doleritic rocks form small sill-like intrusions (10 to 20m thick), and have a generally easterly or north-easterly strike. They intrude the Precambrian and Ordovician rocks but not the Silurian slates.

The most comprehensive geological account of Parys Mountain, including a detailed (6inches to 1mile) geological map, is in the Geological Survey Memoir on Anglesey by Greenly (1919). This work identified and defined the major rock types, and gave a detailed description of the overall geology. The rocks of the area were described as consisting of the Precambrian Mona Complex, Ordovician slaty shales, Silurian graptolitic shales, and intrusive sills of "felsite". The structure of the area was interpreted as being two overturned synclines, with an intervening, complementary, anticline, in the Ordovician and Silurian rocks, and the "felsite" (Fig.4-1,and 2). These folds were thought to be truncated in depth by the Rhwch Thrust. Later Manning (1959) interpreted the structure as that of a single syncline overturned to the north (Fig.4-3), and he considered the "felsite" to be a two-pronged dyke and not a sill. However, Hawkins (1966), Bates (1964,1966), and Wheatley (1971a,b) all favour

FIGURE 4

CROSS SECTIONS ILLUSTRATING THE STRUCTURAL INTERPRETATIONS OF PARYS MOUNTAIN

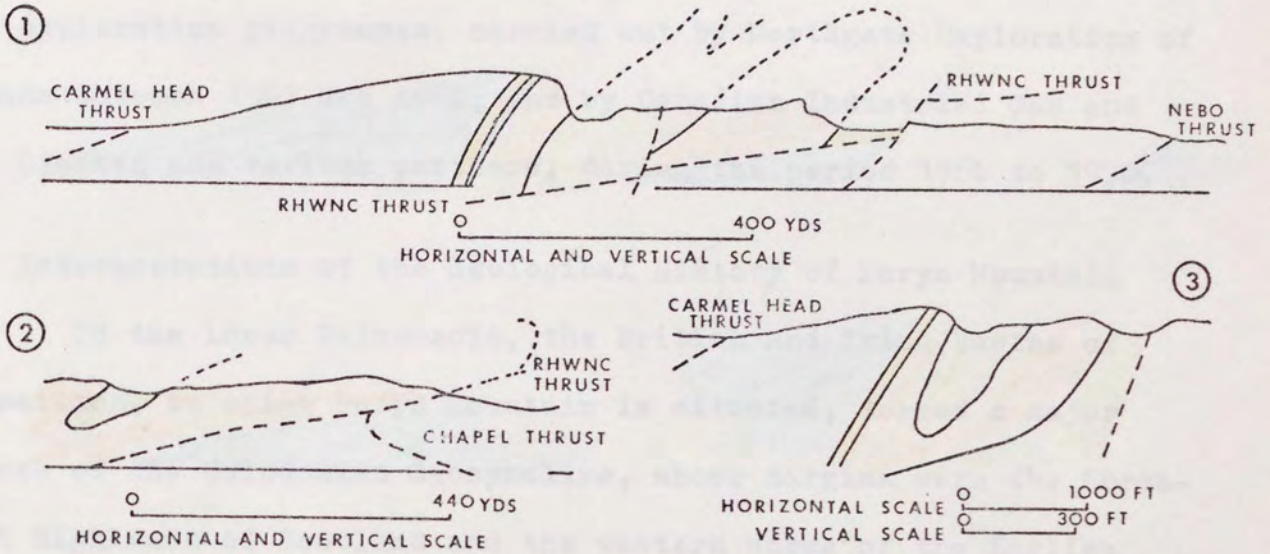

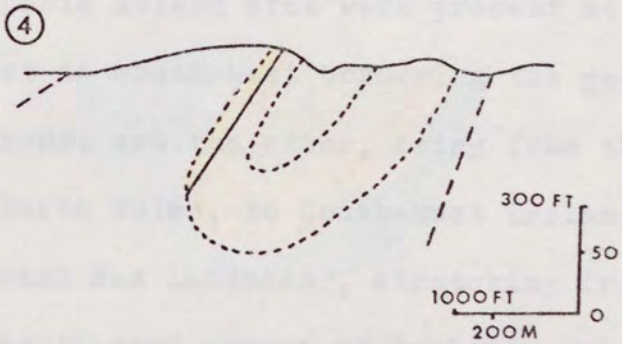

(1) SECTION THROUGH THE CENTRAL PART OF PARYS MOUNTAIN (AFTER GREENLY 1919)

(2) SECTION THROUGH THE WESTERN END OF PARYS MOUNTAIN (AFTER GREENLY 1919)

(3) SECTION THROUGH THE CENTRAL PART OF PARYS MOUNTAIN (AFTER MANNING 1959)

(4) SECTION THROUGH THE CENTRAL PART OF PARYS MOUNTAIN (CURRENT INTERPRETATION··· cf. WHEATLEY, 1971)

SILURIAN SLATE

SILICEOUS SINTER

DACITE

ORDOVICIAN SLATE

RHYOLITE

PRECAMBRIAN MONA COMPLEX

an extrusive volcanic origin for the "felsite", and structure of the mountain was re-interpreted as being a simple overturned syncline (Fig.4-4). These latest interpretations are based on petrographic, structural, and stratigraphic information collected from cores from the exploration programmes, carried out by Northgate Exploration of Canada between 1961 and 1962, and by Canadian Industrial Gas and Oil Limited and various partners, during the period 1966 to 1970.

1.2 Interpretations of the Geological History of Parys Mountain

In the Lower Palaeozoic, the British and Irish basins of deposition, in which Parys Mountain is situated, formed a major branch of the Caledonian Geosyncline, whose margins were the North-West Highlands of Scotland and the western edges of the English Midland Platform (Williams, 1969; Wheatley, 1971b). Williams (1969) suggested that two volcanic island arcs were present at this time: one, trending north-east to south-west bordering the geosyncline along the Southern Uplands; and the other, lying from the English Lake District through North Wales, to South-East Ireland (Fig.5). The existence of an "Irish Sea Landmass", stretching from the Anglesey region to the extreme south-east corner of Ireland, was postulated by Jones (1938), and was accepted by several later authors in their interpretations of the geological history of the area (Brenchley, 1969; Rast, 1969; Williams, 1969; Fitton and Hughes, 1970; Wheatley, 1971a,b). Brenchley (1969) suggested that, in mid-Caradocian time, this Irish Sea Landmass was a belt of active uplift separating the Welsh basin from the other depositional basins of the Caledonian Geosyncline.

Williams (1969) and Wheatley (1971b) interpreted the deposi-

FIGURE 5
EARLY CARADOCIAN PALEOGEOGRAPHY
AFTER ALWYN WILLIAMS

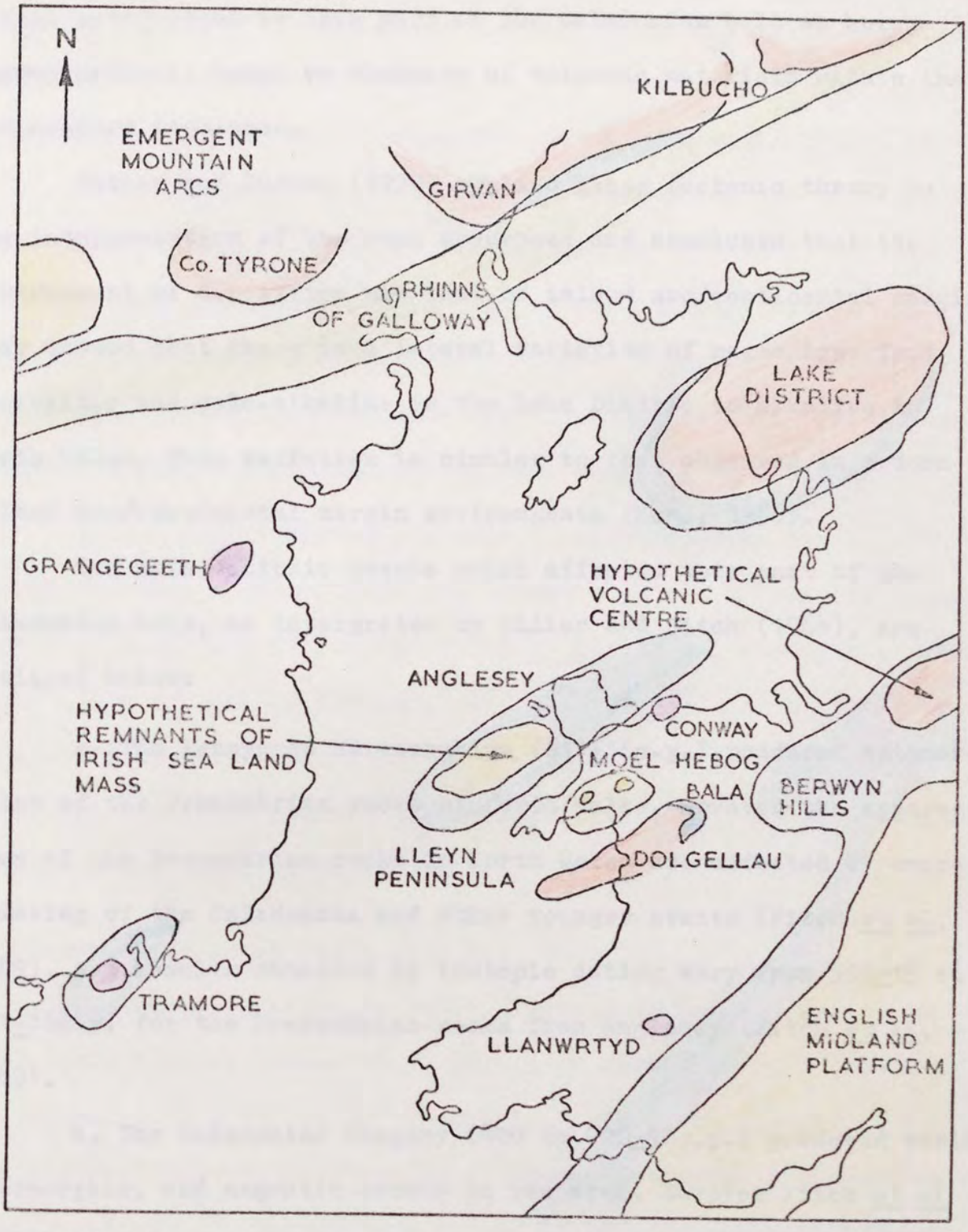

tional environment in this part of the Caledonian belt as being eugeosynclinal, based on abudance of volcanic materials within the sedimentary sequences.

Fitton and Hughes (1970) applied plate tectonic theory to the interpretation of the rock sequences and concluded that the environment of deposition was that of island arc/continental margin. They showed that there is a lateral variation of magma type from tholeiitic and calc-alkaline in the Lake District to alkaline in North Wales. This variation is similar to that observed in modern island arc/continental margin environments (Kuno, 1966).

The main tectonic events which affected this part of the Caledonian belt, as interpreted by Miller and Fitch (1964), are outlined below:

a. The Penmynydd metamorphism (611±16m.y.) produced metamorphism of the Precambrian rocks of North Wales. However the apparent ages of the Precambrian rocks in North Wales are affected by overprinting of the Caledonian and other younger events (Fitch et al, 1969), and results obtained by isotopic dating vary from 595±15 to 611±16m.y. for the Precambrian rocks from Anglesey (Fitch et al, 1969).

b. The Caledonian Orogeny (400 to 420±10m.y.) produced various metamorphic, and magmatic events in the area. However Fitch et al (1969) showed that the Caledonian events in North Wales have a possible subsidiary maximum around 440m.y. ago and, the last major Caledonian event was dated around 390±10m.y.

c. The Variscan Orogeny (325±5 to±295 5m.y.) produced some basic magmatism, metasomatism, and mineralisation. The age of the Variscan event at Parys Mountain measured using K-Ar method on a

silicified ignimbrite, is 294±10m.y. (Fitch and Miller, 1964). This determination is directly comparable with the Pb age of 300±40m.y. obtained from Pb-Zn ore of Parys Mountain by Moorbath (1962). Fitch et al. (1969) suggested that Variscan mineralization was the last important metasomatic event at Parys Mountain. Wheatley (1971a,b) surmised that the mineralization was of a pulsatory nature, spanning the period from 440 to 150m.y. ago. He also suggested that homogenization and crustal contamination may have obscured the true isotopic ratios and that the mineralization is probably Caledonian in age.

d. A swarm of Tertiary alkali olivine dolerite dykes, with a WNW trend, were intruded into the Precambrian and Palaeozoic rocks across Anglesey and Snowdonia (Fitch et al., 1969). The ages of these rocks measured by K-Ar methods, vary from 55.7±3.2 to 61.6±1.4m.y. in rocks from Snowdonia, and from 48.5±0.7 to 62±3m.y. in rocks from Anglesey (Port Dafarch and Gwydryn) (Fitch et al., 1969). These dykes are not found at Parys Mountain.

1.3 Mineralization at Parys Mountain

The mineralization at Parys Mountain is present mainly in the acidic igneous rocks, which have been described most commonly as "felsite". The origin of the mineralization was thought to be epigenetic, produced by deposition from hydrothermal fluids, with some modifications formed as a result of various metasomatic processes. This interpretation was largely based on the identification of the "felsite" in the area as being an intrusive igneous body (Greenly, 1919; Manning, 1959; Derry, 1961). Magmatic processes occurring during the Caledonian and Variscan orogenies were believed

to have produced the mineralization (Fitch et al, 1969; Wheatley, 1971a,b).

Wheatley (1971b) studied the genesis of the ores and discovered that a metal zoning is present in the area. This zoning has an axial belt of pyritic zones and the main copper deposits, bodered by an area with lead-zinc mineralization. The pyritic zones have a close association with the acidic volcanic sequences and commonly postdate them. Wheatley (1971a,b) suggested that these minerals were deposited in a marine environment, possibly during diagenesis. Later, migrating, hydrothermal metal-rich chloride fluids were thought to have resulted in the formation of the major copper deposits stratigraphically associated with the pyritic zones. The complex lead-zinc mineralization was thought to result from reaction between the minerals of the pyritic zones and the final fraction of the hydrothermal fluids. The presence of crosscutting vein-type, fissure infilling, mineralization was interpreted to have resulted from pulsatory metasomatic processes associated with even later structural deformations (Variscan).

The mineral deposits at Parys Mountain have been compared with those at Avoca (South eastern Ireland), and Coniston (Lake District) in that they all have a similar age, and have directly comparable tectonic and stratigraphic positions (Williams, 1969; Fitton and Hughes, 1970; Wheatley, 1971a,b).

1.4 Mining and Exploration History

The mineral deposits at Parys Mountain probably were first mined by the Romans; however, the main mining operations were carried out during the period 1762 to 1885 when Parys Mountain was the largest

copper producer in Europe. Recorded figures on the quantities of metal produced show that a production of some 3000 tons of metallic copper per annum was reached by 1773. After 1885 production dropped and soon afterwards stopped mainly because of a falling off of the grade of the ore at the same time as copper prices decreased.

Attempts were made to re-open the mine in 1920, and again between 1955 and 1958, but failed because significant quantities of new ore were not found above the former working level (250m below surface in the western part of the area, and 200m at the east end).

In 1961 Northgate Exploration of Canada, formed a subsidiary company, Anglesey Copper Mines (Parys Mountain Mines, U.K.) Limited of Toronto, Canada to explore the property. This company drilled a series of eleven, inclined, exploratory, diamond drill holes, the deepest of which is some 500m (DDH. M10), to the north of the old mine(Fig.6A).This drilling programme was abandoned at the end of 1962 because assay results showed that the mineralization found was not of an economic grade. In 1966 Canadian Industrial Gas and Oil Limited took over the property and extended Northgate's drilling programme. This company, in conjunction with various partners, has actively explored the area since that time. One partner, Intermine Limited of Toronto, carried out an extensive exploration programme, including diamond drilling, induced potential (I.P.) surveys, and a geochemical soil survey but relinquished the property at the end of 1973. A new partner, Cominco Limited of Canada, started an exploration programme, at the beginning of 1974, and at the same time Amax Inc. began exploration of the Rhosmynach area, just east of Parys Mountain (Fig.1).

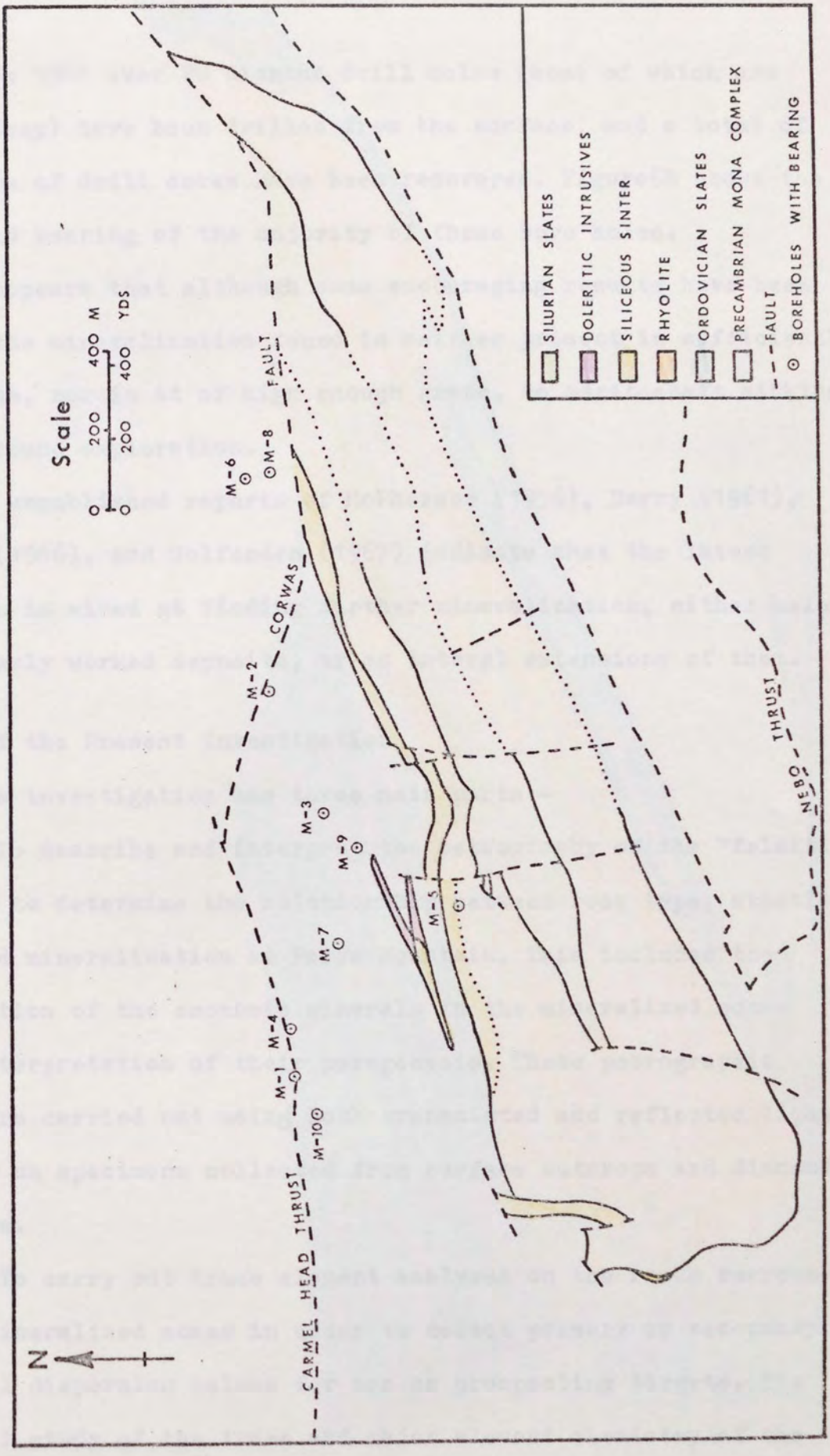

FIGURE 6A SKETCH MAP TO SHOW THE POSITION OF DIAMOND DRILL HOLE DRILLED DURING 1961 AND 1962

Since 1961 over 70 diamond drill holes (some of which are over 600m deep) have been drilled from the surface, and a total of some 25,000m of drill cores have been recovered. Figure6B shows the location and bearing of the majority of these bore holes.

It appears that although some encouraging results have been obtained, the mineralization found is neither present in sufficiently large volume, nor is it of high enough grade, to merit shaft sinking and underground exploration.

The unpublished reports of McPherson (1956), Derry (1961), Schindler (1966), and Wolfenden (1967) indicate that the latest exploration is aimed at finding further mineralization, either below the previously worked deposits, or as lateral extensions of them.

1.5 Aims of the Present Investigation

This investigation has three main parts:-

1) To describe and interpret the petrography of the "felsitic" rocks, and to determine the relationship between rock type, stratigraphy, and mineralization at Parys Mountain. This includes the identification of the economic minerals in the mineralized zones and the interpretation of their paragenesis. These petrographic studies were carried out using both transmitted and reflected light microscopy on specimens collected from surface outcrops and diamond drill cores.

2) To carry out trace element analyses on the rocks surrounding the mineralized zones in order to detect primary or secondary geochemical dispersion haloes for use as prospecting targets. The geochemical study of the trace and major element chemistry of the

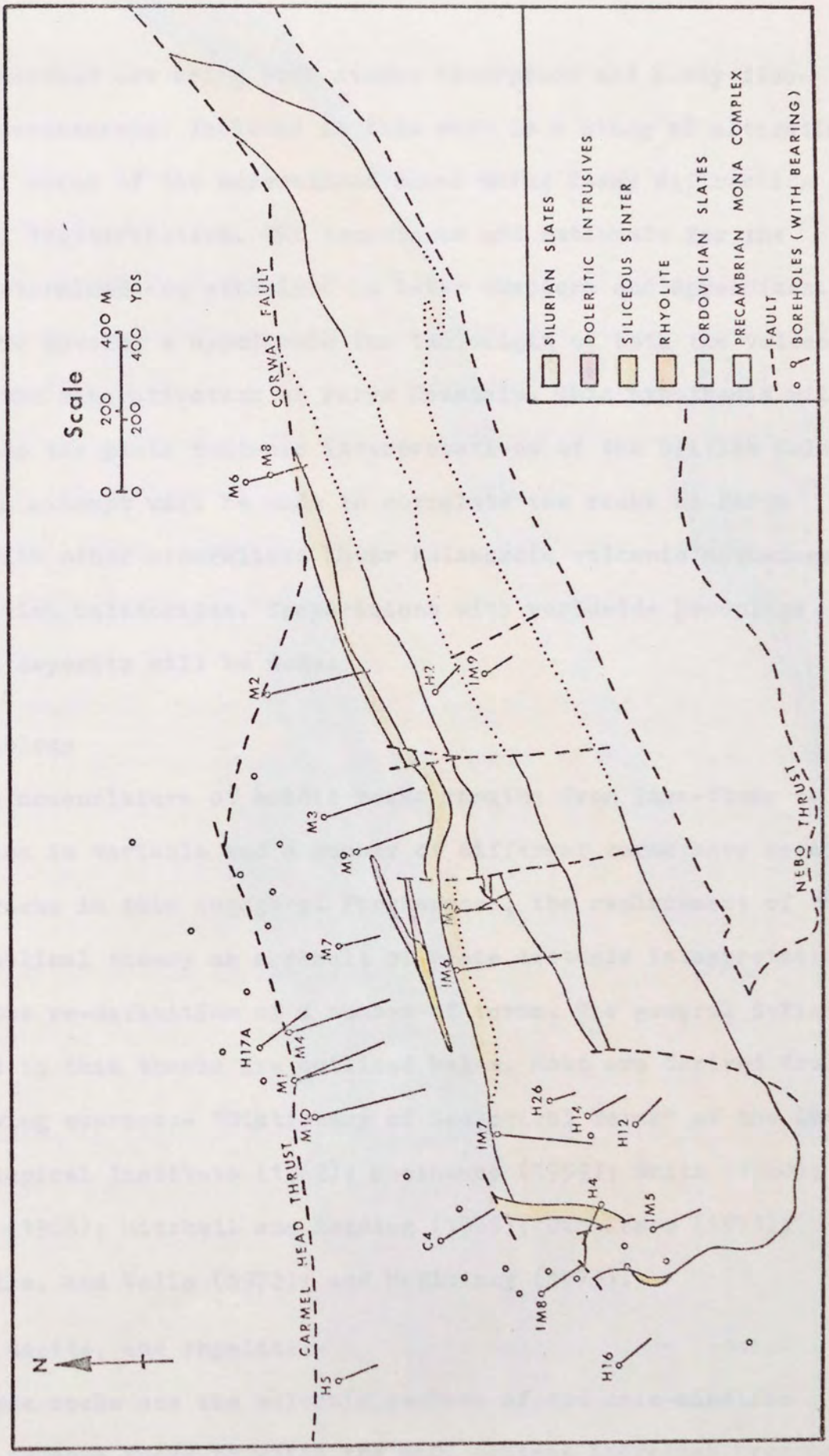

FIGURE 6B SKETCH MAP TO SHOW POSITION (WITH BEARING) OF DIAMOND DRILL HOLES

rocks was carried out using both Atomic Absorption and X-ray fluorescence spectroscopy. Included in this work is a study of alteration of the wall rocks of the mineralized zones using X-ray diffraction for mineral identification. The techniques and rationale for the elements determined are explained in later chapters and appendices.

3) To develop a hypothesis for the origin of both the volcanic rocks and the mineralization at Parys Mountain. This hypothesis will be fitted to the plate tectonic interpretations of the British Caledonides. An attempt will be made to correlate the rocks at Parys Mountain with other mineralized Lower Palaeozoic volcanic sequences in the British Caledonides. Comparisions with worldwide groupings of mineral deposits will be made.

1.6 Terminology

The nomenclature of acidic rocks ranging from lava-flows to pyroclastics is variable and a number of different terms have been used for rocks in this catagory. Furthermore, the replacement of the old geosynclinal theory as a result of plate tectonic interpretations requires the re-definition of a number of terms. The general definitions used in this thesis are outlined below. Most are derived from the following sources:- "Dictionary of Geological Terms" of the American Geological Institute (1962); Moorhouse (1959); Smith (1960); Vlodavetz (1966); Mitchell and Reading (1969); Dickinson (1971); Hatch, Wells, and Wells (1972); and McElhinny (1973).

Andesite, dacite, and rhyolite

These rocks are the volcanic members of the calc-alkaline series of igneous rocks in which the SiO_2 content increases progres-

sively from andesite to rhyolite, e.g. the free quartz content varies from less than 5 percent in andesite up to some 67 percent in rhyolite. Transitions between the three rock types are found, however some main distinctions are made:-

Andesite contains more than 60 percent felsic minerals, of which less than 5 percent is quartz. Intermediate plagioclase (essentially andesine) is the main feldspar though the composition range is from An_{35} to An_{70}. The most common composition however falls within the andesine range, and this constitutes more than 95 percent of the total feldspar. The mafic minerals are pyroxene (generally hypersthene, diopside, or pigeonite), hornblende, and biotite in various proportions.

The essential minerals of dacite are plagioclase (andesine to oligoclase), quartz, pyroxene or hornblende, or both, with minor biotite and sanidine. All these minerals occur as phenocrysts in a glassy, or finely crystalline, groundmass of alkalic feldspar and silica minerals. The chief distinction between dacite and andesite is silica content, with dacite containing between 63 and 68 percent SiO_2. The high percentage of normative quartz in dacite leads to the early precipitation of modal quartz as phenocrysts and the presence of these is used to distinguish dacite from andesite. The fundamental difference between dacite and rhyolite is the ratio of alkali feldspar to intermediate plagioclase (An_{20} to An_{50}) which is less than 1:3 for dacite, and more than 2:3 for rhyolite.

Rhyolite is defined as an aphanitic volcanic rock, containing over 80 percent felsic minerals, 5 to 67 percent of which is quartz, and 67 to 100 percent of its total feldspar is silicic.

Ash flows

These form as a result of either an avalanche of gas and pyroclastic materials, predominantly volcanic ash, produced by the explosive disintegration of viscous lava in a volcanic crater, or by the explosive emission of gas-charged ash from a fissure, or group of fissures. These rocks range in composition from rhyolite to andesite.

Ignimbrite

The wide use of this term has caused much confusion in that it has been used both in a genetic and a descriptive sense. In general the term is used in such a way that it is synonymous to 'welded tuff'. In this thesis the term 'ignimbrite' is applied to a rock, consisting mainly of fine grained rhyolitic welded tuff. It consists of a groundmass of welded glass particles in which crystals of feldspar, quartz, and, in some instances, hypersthene and hornblende, are embedded. The glass particles are firmly welded, and bent around the crystals. These deposits are believed to result from the eruption of dense clouds of incandescent volcanic glass particles in a semi-molten of viscous state from group of fissures. The ignimbrite of the North Island, New Zealand (Steiner, 1963), and the ignimbrites of Snowdonia, North Wales (Beavon, et al, 1961; Fitch, 1967) are examples of such rocks.

Lithic tuff

Tuffs that consist dominantly of rock fragments are best described as lithic tuff. The fragments may be of previously formed rocks (sedimentary or igneous) through which the volcanism has occurred, or of earlier lavas from the same cone, or of small frag-

ments of nes lava (essential ejecta) that solidify in the vent prior to their ejection by later explosive eruptions.

Welded tuff

A tuff which has been indurated by the combined action of heat retained by the particles, and the enveloping hot gases. As a result, the glass particles are flattened and effectively welded.

Siliceous sinter

Silica deposited from hot springs or volcanic emanations, commonly with a colloform texture, is described as siliceous sinter. The term is used here for a variety of very fine grained, white quartz rocks, in close association with siliceous volcanic rocks.

Granophyric rim

This term is used to describe a fine grained aggregate of quartz and feldspar found around quartz phenocrysts in both rhyolitic and dacitic rocks (Moorhouse, 1970).

Spherulitic rim

The term is used, as defined by Moorhouse (1970), to describe an alteration texture present around some quartz phenocrysts in rhyolitic or dacitic rocks. The 'phenocrysts' are thought to have been formed by recrystallization of spherulites.

Terminology on geosynclines and concepts of continental margins used in this thesis is that used by Mitchell and Reading (1969); Dickinson (1971); and McElhinny (1973).

CHAPTER 2

STRATIGRAPHY

The general stratigraphic sequence is shown in Table 1 and approximate thicknesses of the units are given there. The thicknesses of the Precambrian and Silurian rocks are not known due to tectonic and erosional effects.

2.1 Precambrian

Only the general lithology and outcrop patterns for the Precambrian rocks are described here. For detailed petrology and petrography of these rocks, and descriptions of the sequences comprising the Mona Complex (Table 2), the reader is referred to the works of Greenly (1919) and Shackleton (1969).

The part of the Mona Complex present at Parys Mountain belongs in part to the New Harbour Group, and in part to the Gneissic Group (Greenly, 1919). In this area the New Harbour Group consists of green, mica schists and phyllites. These rocks crop out in the northern part of the area and are thrust over the Ordovician rocks along the Carmel Head and Corwas Thrusts. The Gneissic Group, which consists of both micaceous and granitoid gneisses, and quartzitic gneisses, is present in the southern part of the area. This group has thrust fault contacts with the Ordovician slates (Fig.3) and part occurs within these slates as thrust slices.

There are two main interpretations of the relationship between the two members of the Mona Complex in this area. Greenly (1919) separated the Precambrian rocks into the Bedded Succession

Table 1 General stratigraphic sequence at Parys Mountain.

Age	Lithology	Thickness (m)
Silurian	Dark grey to black slates	?
– – – – – – – – – – – –	? unconformity ?	– – – – – – – – – – – – – –
Ordovician	Rhyolitic volcanic rocks	200
	Grey to greenish grey slates	600
— — — — — — — — —	thrust	— — — — — — — — — — — —
Precambrian	Chlorite schists, micaceous and granitoid gneisses, quartzitic gneisses	?

Table 2 Comparision of interpretations of Mona Complex succession proposed by Greenly (1919) and Shackleton (1969).

	Greenly	Shackleton
Top	Holyhead Quartzite	Fydlyn Felsitic Group
	South Stack Series*	Gwna Group
	New Harbour Group	Skerries Group
	Skerries Group	New Harbour Group
	Gwna Group	Rhoscolyn Beds
	Fydlyn Felsitic Beds	Holyhead Quartzite
Base	Gneissic Group@	South Stack Beds

* Includes Rhoscolyn Beds of Shackleton's succession.

@ Rocks of this group are considered by Shackleton to be the high grade metamorphic products of Gwna Group.

(comprised of six main groups), and the Gneissic Group. His stratigraphic sequence was based on a study of the fragments contained in the rocks of each group, e.g. the Holyhead Quartzite contains grains of jasper which he identified as being derived from the Gwna Group. Shackleton (1969) remapped these rocks and evidence from graded bedding, current bedding, pillow shapes, etc., showed that the 'way up' of the stratigraphic sequence is the reverse of that proposed by Greenly (1919). Shackleton (1969) considered the Gneissic Group to be the high grade metamorphic equivalent of the Gwna Group. He proposed a new member for the sequence, the Rhoscolyn Beds, which was included in South Stack Beds by Greenly (1919). The two proposed successions for the Mona Complex are shown in Table 2. For details of the evidence used to make these interpretations the reader is referred to the original works.

Shackleton's (1969) proposed sequence is accepted for purposes of this thesis, thus the gneissic rocks in the southern part of the Parys Mountain area are classed as belonging to the Gwna Group. They are considered to be younger than the micaceous schists and phyllites of the New Harbour Group exposed in the northern part of the area.

2.2 Ordovician

The Ordovician rocks of Parys Mountain were described differently by various workers:- Greenly (1919), Manning (1959), Bates (1964,1966), Schindler (1966), Hawkins (1966), and Wheatley (1971 a,b) called them 'shales'; Evans (1878) and Ramsay (1881) - 'slaty shales'; Derry (1961) and Wolfenden (1967) - 'slates'. These rocks are called 'slates' in this thesis because they possess a well-developed slaty cleavage.

The main area of outcrops of the slates are on the northern, western, and southern slopes of the mountain (Fig.3). Those on the northern and western slopes vary in colour from grey, greenish grey to dark grey. Bedding is rarely seen, but, where present, is parallel to cleavage, which is well developed. Graptolites belonging to the lower part of the Didymograptus bifidus zone have been found, and this indicates that the rocks are Lower Ordovician in age (Greenly, 1919; Bates, 1964,1966). Contacts with the Mona Complex are faulted (Carmel Head Thrust and Corwas Fault).

Hawkins (1966) used lithological evidence, from eleven inclined bore holes drilled during 1961 and 1962 on the northern part of the area (Fig.6), to subdivide the Ordovician into three. Those forming his lower-most division are grey, thinly layered and micaceous. They are approximately 400m thick and have some thin layers of sedimentary breccia in the lower 200m. The breccia layers are generally thinly bedded (6mm to 15cm), but in some instances individual beds are as thick as 20m. These rocks contain angular fragments (up to 4cm) of pale green phyllite and quartzite (from the Mona Complex), and in a few specimens slate fragments are present.

The middle division is approximately 210m thick, poorly bedded, and consists of grey to greenish grey, well cleaved, slates. These are paler grey in colour, less micaceous, than those of the lower division.

The upper-most division is approximately 100m thick, and consists of poorly bedded black pyritic slates, with individual beds up to 30cm thick. The pyrite is present as numerous, small (0.5 to 2mm), euhedral crystals.

The stratigraphical relationship between the three divisions is not easily defined as only the middle division occurs as surface outcrops. Hawkins (1966) interpreted the relationship between the first two divisions, from drill core evidence, as being geographical as the slates of the lower division were found only in the three most westerly bore holes (M1, M4 and M10). The breccia beds of the lower division are not found in the other bore holes (M2, M3, M7, and M9) to the east. The projections of bedding planes of the rocks of the lower division eastwards allow the interpretation that the breccia beds could be present north of the surface position of these easterly bore holes, thus placed the middle division slates stratigraphically above the lower division. Hawkins (1966) also suggested that the slates in the lower 120m of the M10 bore hole (which are stratigraphically higher than those in the upper parts of the bore hole as it was drilled up the sequence) which have no interlayered breccia beds, though different in colour, are probably the lateral equivalent of the middle division slates.

The majority of the black slates of the upper division have

been silicified and are interlayered with the overlying rhyolitic rocks.

This three fold division was checked with cores from the later bore holes (C4, H17A, H34, H35, and IM8) and found to be generally acceptable, except that the breccia beds in the lower division are interpreted here as beds of lithic tuffs (see page 38)

The slates on the southern slope were first considered to be Silurian (Greenly, 1919; Manning, 1959) on the basis of identification of some poorly-preserved graptolites as monograptids. Bates (1964) re-examined these fossils and identified them as didymograptids thus these rocks are Ordovician rather than Silurian. Uncontrovertible evidence for the age of these rocks is not available, however the weight current opinion is that they are Ordovician (Wheatley, 1971a,b). Their relationship with the three divisions of the Ordovician slates on the northern and western slopes is not discernible.

2.3 Silurian

The Silurian slates crop out in the central part of the mountain, and their outcrop area is enclosed by that of the volcanic rocks (Fig.3). These rocks yield remains of monograptids (Wolfenden, 1967) which confirm their Silurian age. An arbitrary division into two parts is made on the basis of the presence or absence of silicification. This division is used merely for descriptive convenience as no evidence for a stratigraphic subdivision was found. The majority of the non-silicified rocks occur on the southern side of the area, and the silicified ones crop out on the northern side, close to the contacts with the volcanic rocks.

The non-silicified slates are very fine grained and vary in colour between dark grey and intense black. The dominant feature of the rocks is a well-developed slaty cleavage which has almost obliterated original bedding planes (Wolfenden, 1967). Bedding is recognized on the basis of some colour layering, and the presence of some few thin (6mm to 2cm) layers of siltstone.

The silicified slates are extremely hard, fine grained, homogeneous, cherty or flinty rocks varying between light and dark grey in colour. They break with a subconchoidal fracture, and cleavage is detected only where silicification is not well developed.

The contact between the Silurian slates and the underlying volcanic rocks does not crop out and Silurian slates are not encountered in the diamond drill holes on the northern side of the area (M6, M8, M2, M3, M9, and M5 - Fig.6) which indicates that they are not present at depth there. The contact between the Silurian slates and the volcanic rocks was encountered in bore hole H2 (Fig.6)

and there it is sharp. This contact is believed to be an unconformity as interlayering is absent, and some fragments of volcanic materials are present in the slates.

CHAPTER 3

IGNEOUS ROCKS

3.1 Volcanic Rocks

3.1.1 Introduction and General Succession

The volcanic rocks crop out in two east-north-easterly trending, subparallel, bands. These bands meet at the western end of the mountain, enclose the outcrop area of the Silurian slates (Fig.3), and to the east they are truncated by the Corwas Fault. The volcanic rocks are the most resistant to erosion in the area, consequently their outcrops form the upper ridges of the mountain. Contacts between the volcanic rocks and the Silurian slates are sharp, and probably unconformable, as shown in Figure 7A. Contacts between the volcanic rocks and the Ordovician slates are gradational, and interlayering between the two is seen both in outcrop and in drill cores. The interlayering generally occurs over a vertical distance of between 20 to 30m. The distance being measured from where volcanic rocks first appear to where Ordovician slates are absent. In this transition zone the Ordovician slates form thin layers, commonly less than 1m thick, in the volcanic rocks (Fig.7B). In some few instances the interlayering extends to 100m (Fig.7C). The Ordovician slate layers in this thicker zone are up to 5m thick and they become progressively thinner upwards (down to less than 1m thick) until the sequence is composed entirely of volcanic rocks (Fig.7D).

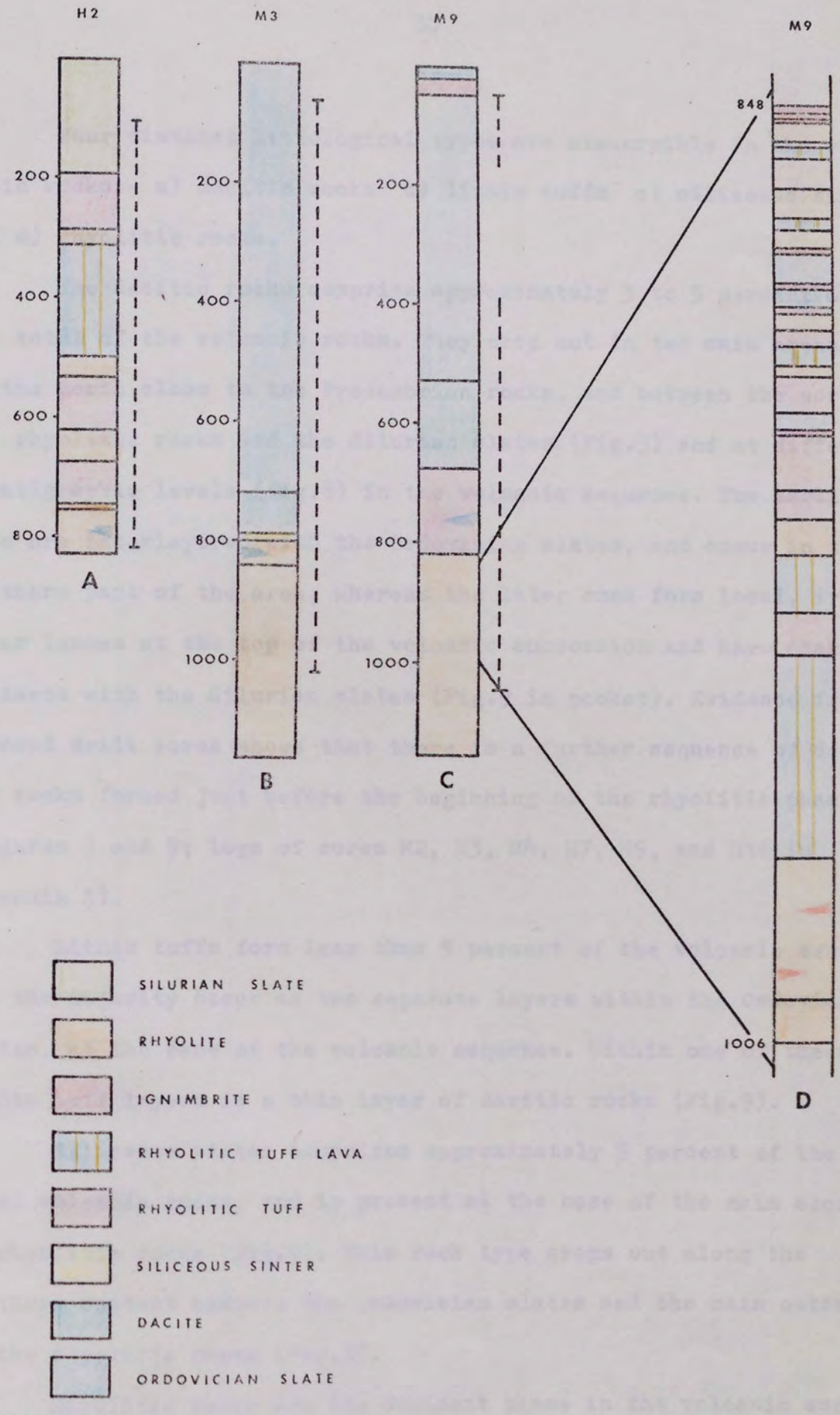

FIGURE 7

Sections from boreholes to illustrate contacts between Silurian slates and rhyolitic rocks (A) and between Ordovician slates and rhyolitic rocks (B, C, and D)

Four distinct lithological types are discernible in the volcanic rocks:- a) dacitic rocks b) lithic tuffs c) siliceous sinter and d) rhyolitic rocks.

The dacitic rocks comprise approximately 3 to 5 percent of the total of the volcanic rocks. They crop out in two main areas in the north close to the Precambrian rocks, and between the northern rhyolitic rocks and the Silurian slates (Fig.3) and at different stratigraphic levels (Fig.8) in the volcanic sequence. The earlier ones are interlayered with the Ordovician slates, and occur in the northern part of the area, whereas the later ones form local, irregular lenses at the top of the volcanic succession and have sharp contacts with the Silurian slates (Fig.9 in pocket). Evidence from diamond drill cores shows that there is a further sequence of dacitic rocks formed just before the beginning of the rhyolitic phase (Figures 3 and 9; logs of cores M2, M3, M4, M7, M9, and M16 in Appendix A).

Lithic tuffs form less than 5 percent of the volcanic sequence, and the majority occur as two separate layers within the Ordovician slates, at the base of the volcanic sequence. Within one of these lithic tuff layers is a thin layer of dacitic rocks (Fig.9).

Siliceous sinter comprises approximately 5 percent of the total volcanic rocks, and is present at the base of the main sequence of rhyolitic rocks (Fig.9). This rock type crops out along the northern contact between the Ordovician slates and the main outcrops of the rhyolitic rocks (Fig.3).

Rhyolitic rocks are the dominant phase in the volcanic succession comprising some 90 percent of the total.

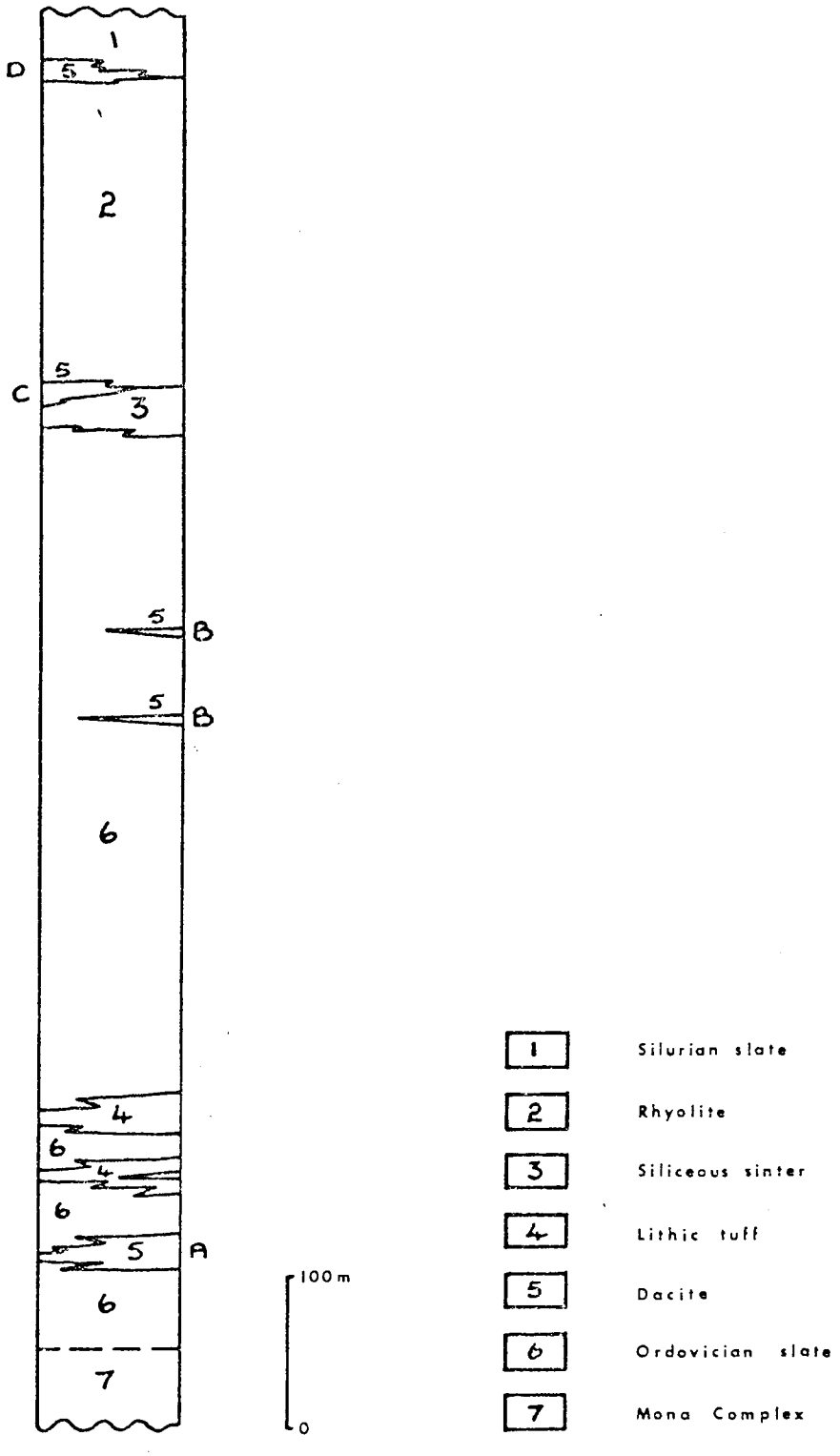

Figure 8 General stratigraphic sequence at Parys Mountain

Evidence from diamond drill cores indicates that variations in composition, as well as lateral variations in thickness, are common in all the volcanic rock types. A simplified stratigraphic table for the area showing the overall sequence, and the contact relationships between the volcanic rocks and the Ordovician and Silurian metasedimentary rocks is shown in Figure 8. This shows the two main parts of the volcanic succession are separated by and occur within the Ordovician sediments.

3.1.2 Dacitic Rocks

The dacitic rocks are divided into four groups (Dacites A, B, C, and D) on the basis of their age. The groups are mineralogically similar and exhibit two main textural types:- porphyritic and aphanitic. Because of this the petrographic descriptions are grouped as one although an introduction to each of the groups is given.

Dacite A is the oldest and occurs interbedded within the Ordovician slates (Fig.3). The porphyritic-type is predominant and comprises some 80 percent of these rocks. The aphanitic-type is dominant in Dacite B where it occurs as thin interlayers in the Ordovician slate sequence. The rocks of Dacite C form a discontinuous layer between the siliceous sinter and the rhyolitic rocks (Fig.3). In this group the aphanitic-type is predominant and the porphyritic-type is very uncommon. The rocks comprising Dacite D occur locally at the top of the volcanic succession. The aphanitic-type is dominant (over 90 percent) in this group, although some thin layers of the porphyritic-type are present.

The porphyritic-type dacite varies in colour from light to dark green, with some tinges of grey, on fresh surfaces. Weathered surfaces are most commonly yellowish or brownish grey. The phenocrysts are dominantly of quartz and plagioclase feldspar. In some specimens phenocrysts either of clinopyroxene or hornblende are present. The phenocrysts vary in size from less than 1mm up to 1cm and may form up to 50 percent of the rock (Plates 1A and 1B). Overall approximately 60 percent of the phenocrysts are of quartz and between 25 and 30 percent are of plagioclase feldspar. Pyroxenes and hornblendes are equally abundant and comprise the rest of the phenocrysts, although both are not necessarily present together.

The phenocrysts of plagioclase feldspar are commonly well formed although some, particularly the larger ones, are commonly corroded and are replaced by quartz, sericite, and chlorite (Plates 1C and 1D). In some specimens where replacement is incomplete, complex twinning can be distinguished (Plates 1D, 1E, and 1F). Compositional determination on combined Carlsbad-Albite twins in the plagioclase phenocrysts show them to be of calcic andesine (An_{46} to An_{48}).

Quartz phenocrysts are commonly round, have granophyric rims (Plates 1C, 1D, and 1E), and some have corroded boundaries (Plate 1F). It should be noted that some quartz phenocrysts are multigranular aggregates with subround boundaries. It has been suggested that such multigranular quartzes may be xenocrysts (Moorhouse, 1959; Steiner, 1963).

The groundmass is very fine grained (less than 0.1mm) and consists of a mosaic of quartz, plagioclase feldspar, and the seri-

PLATE 1

General appearance of Porphyritic Dacites in Hand Specimens.

A : From borehole H38 at 678 feet depth, field of view 7x8cm.

B : From borehole H34 at 35 feet depth, field of view 5x6cm.

Both plates illustrate the sizes and shapes of phenocrysts of quartz, plagioclase feldspar, and mafic minerals. Alteration of the plagioclase, and the rounding of the quartz phenocrysts are illustrated.

Photomicrographs of porphyritic Dacites.

C,D,E: From borehole H36A at 1061 feet depth, field of view 5.83x6.67mm

C : plane polarized light (P.P.L.)

D : x-nicols of C

E : x-nicols

F : From borehole H34 at 35 feet depth, field of view 5.83x6.67mm, x-nicols.

Quartz phenocrysts show granophyric reaction rims and corroded grain boundaries. Some of the large plagioclase phenocrysts show almost complete alteration, and others show complex twinning.

PLATE 1

A

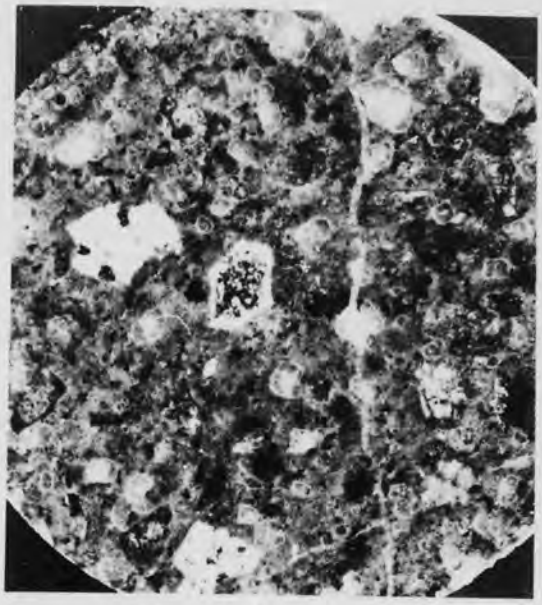

B

C

D

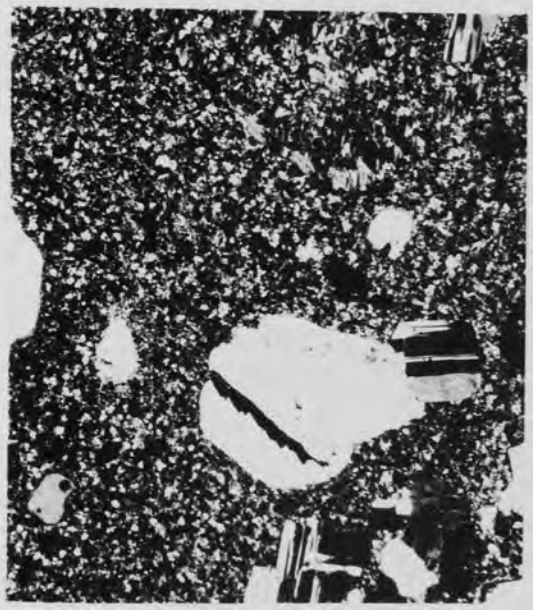

E

F

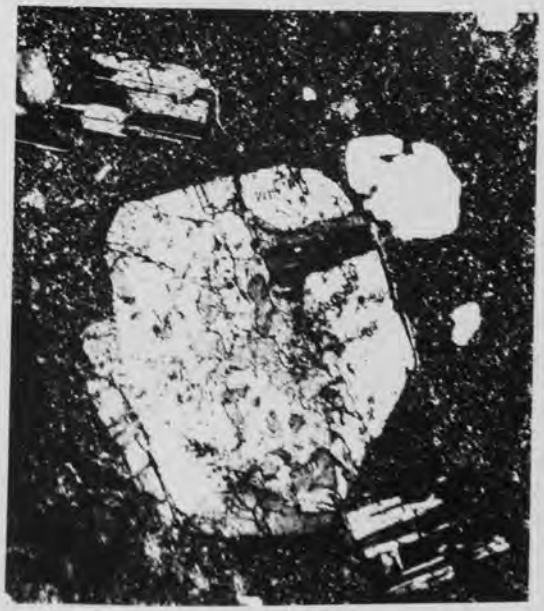

citic alteration products of feldspar. Glass, or its replacement products, is almost always present in the matrix. In some specimens the matrix consists largely of tiny spherulites (0.2mm) (Plate 1C).

The aphanitic-type dacites generally appear to be homogeneous, and vary in colour from greyish green to dark green. In some specimens, spherulitic textures and amygdales are visible in hand specimen (Plates 2A, and 2B). These features show up as round white and dark spots varying in diameter from less than 1mm to 3mm, set in greenish matrix.

In thin section these rocks are seen to consist of lath-shaped plagioclase feldspar (An_{10} to An_{30}), in a fine grained aggregate of quartz, and ferromagnesian minerals which are almost totally replaced by chlorite, calcite, and haematite. Plagioclase comprises up to 45 percent of the rock; quartz is approximately 25 to 30 percent; and mafic minerals, and their alteration products, make up the rest. The spherulitic textures, seen in hand specimen, are represented by subround quartz pseudomorphs with spherulitic rims (Plate 2C). Some specimens are intensely altered, and consist of irregular quartz grains in a matrix of chlorite and carbonate minerals (Plate 2D).

Some of the aphanitic-dacites in type B, especially those found in H16, contain numerous particles of glassy material (more than 50 percent), which give the rock welded (Plate 2E) and flow-like textures (Plates 2F and 3A). In thin section the glass particles are seen to have been replaced by quartz, chlorite, and carbonates. These appear as irregular patches surrounded by a matrix consisting of quartz aggregates and lath-shaped plagioclase feldspars

PLATE 2

General Appearance of Aphanitic Dacites in Hand Specimens

A : From borehole H29 at 175 feet depth, field of view 5x6cm
B : From borehole H35 at 304 feet depth, field of view 7x8cm

Both plates illustrate the common spherulitic textures, in which somespherulites are replaced by quartz and chlorite. The white spots are spherulites replaced by quartz, and dark spots are those replaced by chlorite.

Photomicrographs of Aphanitic Dacites

C : From borehole H38 at 706.7 feet depth, field of view 2.33x2.67mm, P.P.L.

Spherulite replaced by quartz appears as a subround quartz grain, with a spherulitic reaction rim, set in a matrix of chlorite and carbonates.

D : From borehole H32 at 917 feet depth, field of view 2.33x2.67mm, P.P.L.

Intensively altered aphanitic dacite. Round and irregular white quartz aggregates are enclosed in a matrix of chlorite (grey) and carbonates (dark).

General Appearance of Aphanitic Dacites, with Welded and Flow-like Textures, in Hand Specimens

E : From borehole H16 at 395 feet depth, field of view 5x6cm

Subround glass particles, showing welded textures, replaced by quartz (white spots), and chlorite (dark spots).

F : From borehole H16 at 402 feet depth, field of view 4x5cm

A flow-like texture noticeable through fibrous chlorite aggregates (dark) in dacitic groundmass (grey). White patches are of secondary carbonate.

PLATE 2

A

B

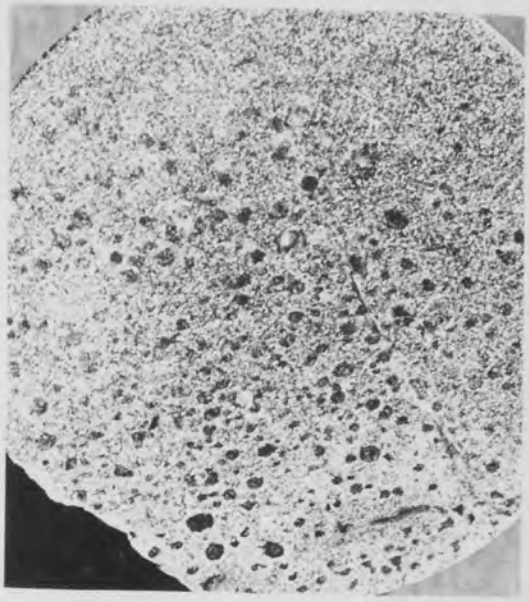

C

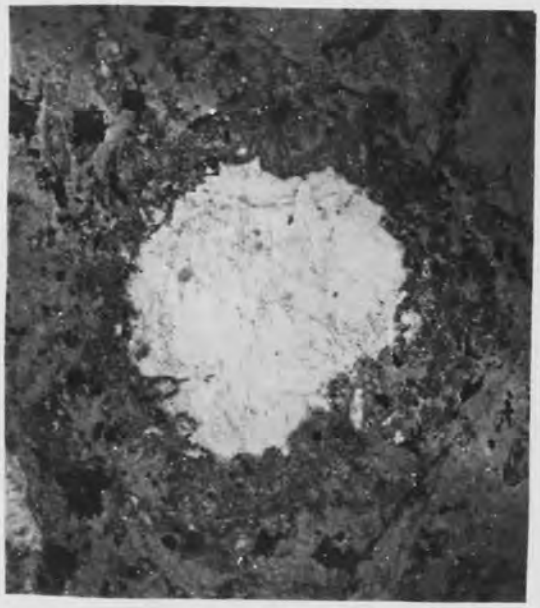

D

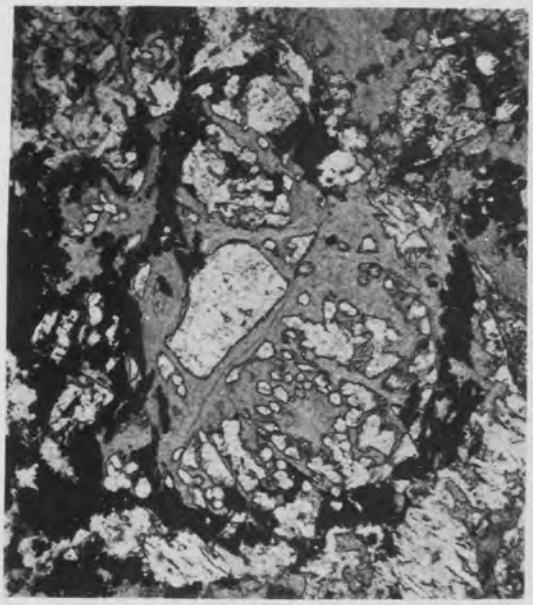

E

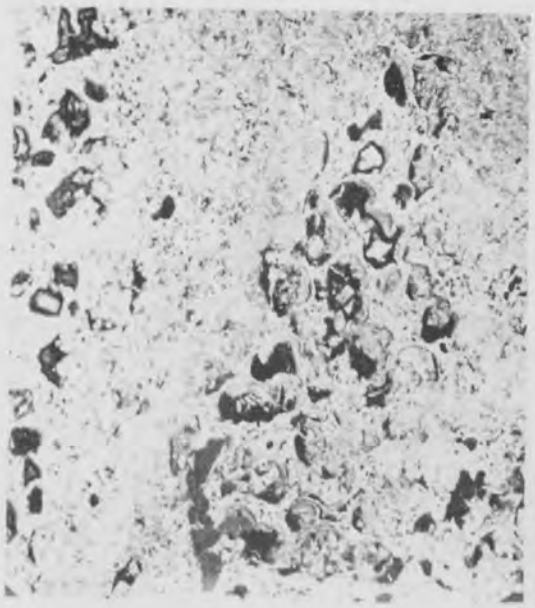

F

PLATE 3

Flow-like Texture in Hand Specimen of Aphanitic Dacite

A : From borehole H16 at 412.8 feet depth, field of view 5x6cm

Flow-like texture in aphanitic dacite, with colour layering ranging through light grey, grey, and greenish grey.

Photomicrographs of Aphanitic Dacites with Welded and Flow-like Textures.

B : From borehole H16 at 395 feet depth, field of view 5.83x6.67mm, P.P.L.

Replaced subround glass particles, seen in hand specimen (Plate 2E), appear as irregular patches in a matrix of lath-shaped plagioclase feldspar and quartz aggregates. These patches are of chlorite, with minute quartz crystallites around their edges, though some also contain fragments of the matrix material.

C : From borehole H16 at 402.8 feet depth, field of view 2.33x2.67mm, P.P.L.

Flow-like texture illustrated by irregular layers of chlorite with lath-shaped plagiocalse feldspar and fine grained quartz aggregates.

D : From borehole H16 at 412.1 feet depth, field of view 2.33x2.67mm, P.P.L.

Perlitic cracks in glassy groundmass of aphanitic dacite.

E : From borehole H16 at 412.1 feet depth, field of view 2.33x2.67mm, P.P.L.

Partly replaced plagioclase phenocryst in a glassy perlitic groundmass.

F : From borehole H16 at 385 feet depth, field of view 5.83x6.67mm, P.P.L.

Subround amygdales, filled with chlorite and quartz, in a quartzo-feldspathic groundmass.

PLATE 3

A

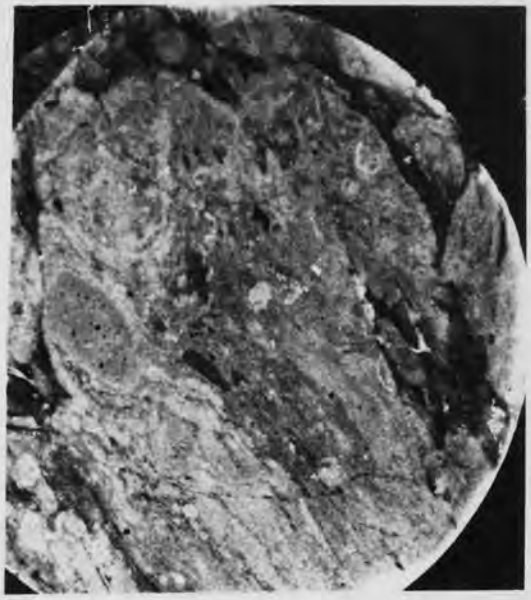

B

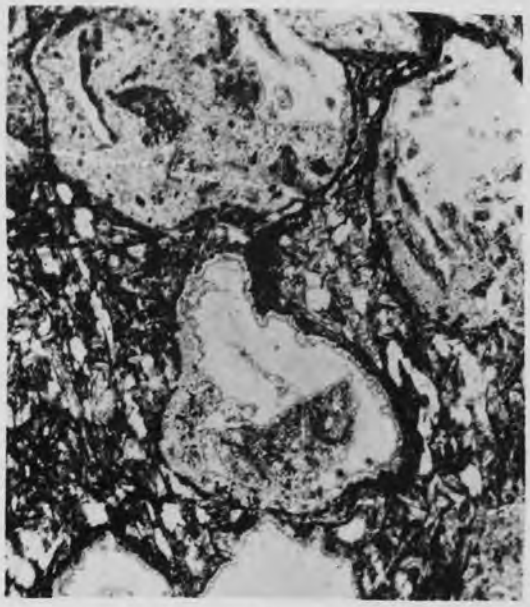

C

D

E

F

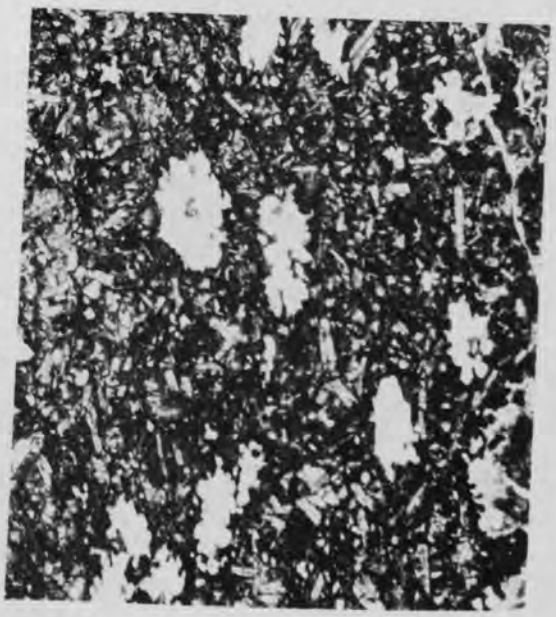

(Plate 3B). The flow-like textures, which are recognizable in hand specimen through grey, green, and dark green colour layering, appear in thin section as irregular interlayers of chlorite and aligned lath-shaped feldspars (Plate 3C). Perlitic crack textures are common in these rocks (Plate 3D), and in some few instances, corroded phenocrysts of plagiocalse feldspar (An_{35-40}) are present embedded in a perlitic matrix of feldspathic and glassy materials (Plate 3E). Amygdales, infilled with chlorite and quartz, are also present (Plate 3F).

3.1.3 Lithic Tuffs

These rocks form two separate layers, each approximately 25m thick, interlayered with the Ordovician slates (Fig.8). The thickness of both layers decrease with depth from the surface, i.e. lateral thinning (Fig.9). They are readily distinguished from other volcanic rocks in that they have agglomeratic textures and are made up of lithic fragments (Plates 4A and 4B).

In hand specimen the overall colour of these rocks ranges from pale grey to dark greenish grey, and the fragments are of various colours including white, grey, dark grey, greenish black, green, or yellow to reddish brown. Fragments form between 60 and 75 percent of the rocks, vary in size from less than 1mm to 4cm in diameter, and vary in shape from angular to subrounded. They consist of various rock types, including the Mona Complex (40 to 50 percent), Ordovician slates, dacitic rocks, and other volcanic materials with very fine grained and glassy textures. The matrix of the lithic tuffs consists of more finely grained lithic fragments (less than 0.1mm) and glass particles.

In thin section the variations in composition and texture of the lithic fragments are more pronounced. Schistose metamorphic fragments, clastic metasedimentary rocks, and the crystalline textures of the dacitic rocks, are readily recognizable. Approximately 10 percent of the fragments consist of broken quartz and feldspar (commonly plagioclase An_{30-50}) crystals, which vary in size from less than 0.1mm up to 2mm. Plates 4C, 4D, 4E, and 4F, show typical textures of the lithic tuffs as seen in thin section.

The mineralogy, and proportions of minerals, of the groundmass is not easily discernible due to the very fine grain-size. Aggregates of quartz, sericite, glass particles, and in some instances chloritic minerals, are present in greatly varying proportions in the groundmass.

3.1.4 Siliceous Sinter

The main part of this rock occurs as an irregular layer directly beneath Dacite C and some parts of its base are interlayered with the Ordovician slates although in general the contacts are sharp. It has a sharp contact with Dacite C, and where this rock is absent the contact with the rhyolitic rocks is sharp (Fig. 8 and 9).

On fresh surfaces the siliceous sinter varies in colour from white to pale grey, or pale yellow, and consists almost entirely of quartz. It has a cherty appearance, and colloform layering is present in many specimens.

In thin section these rocks are seen to consist of up to 80 percent anhedral quartzes as an interlocking, fine grained, mosaic with very fine grained aggregates of sericite and chlorite.

PLATE 4

General Appearance of Lithic Tuffs in Hand Specimen

A : From borehole H25 at 80 feet depth, field of view 5x6cm
B : From borehole M1B at 416 feet depth, field of view 7x8cm

Both plates illustrate typical lithic fragmental textures. The fragments are of various sizes and shapes set in a very fine grained matrix.

Photomicrographs of Lithic Tuffs

C,D: From borehole H25 at 80 feet depth, field of view 5.83x6.67mm, P.P.L.

Both plates illustrate the variation in composition, size, shape, and texture of the lithic fragments.

E : From borehole H25 at 80 feet depth, field of view 2.33x2.67mm, x-nicols
F : From borehole M10 at 249 feet depth, field of view 5.83x6.67mm, x-nicols

Both plates illustrate the occurrence of plagioclase feldspar and quartz crystal fragments embedded in a very fine grained matrix of quartz, sericite, and chlorite.

PLATE 4

A

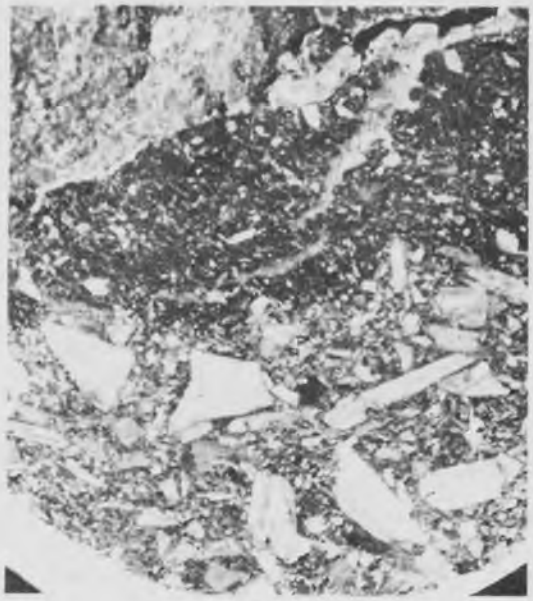

B

C

D

E

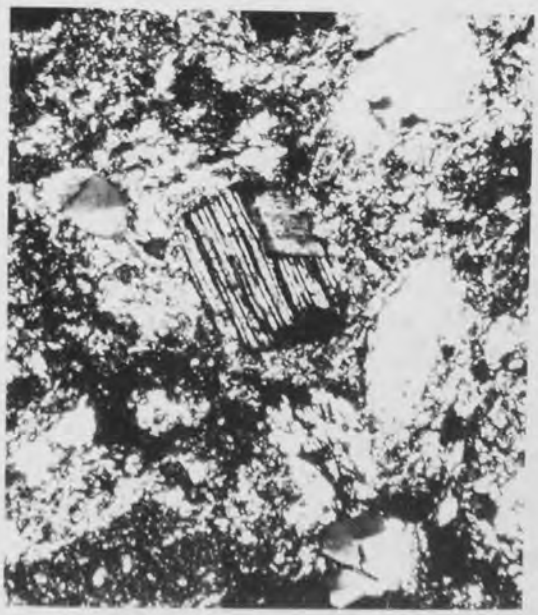

F

Colloform layering is present (Plates 5A, B, and C), as are euhedral quartz grains, which have grown in cavities, and many show overgrowths (Plate 5D).

3.1.5 Rhyolitic Rocks

The rhyolitic rocks form the major part of the volcanic succession, and occur on the map (Fig.3) as two subparallel bands, approximately 150 to 200m wide separating the Ordovician and Silurian slates. The lower contact, with the Ordovician slates, is gradational and interlayered, while the upper contact, with Silurian slates, is sharp. These contacts are best seen in drill cores although they are exposed in outcrop in a number of places. The contact with the siliceous sinter was described in the previous section.

The rhyolitic rocks are divided into the following four types on the basis of texture:- 1) rhyolitic tuffs 2) ignimbrites 3) rhyolitic tuff-lavas and 4) rhyolitic lavas. All of these types are interlayered with each other in the sequence and have varying thicknesses (Fig.7D). The estimated proportions of the four types are as follows:- rhyolitic tuff - 15 to 20 percent; ignimbrite - 15 percent; rhyolitic tuff-lava 30 percent; and rhyolitic lava - 35 to 40 percent.

Description of the various types is made on the order of occurrence of the majority of each type in the stratigraphic sequence.

The rhyolitic tuffs are most abundant in the lower part of the rhyolitic group, and commonly show interlayering with the Ordovician slates (Plates 5E and F). They consist largely of crystal tuffs (approximately 75 percent) and the rest are lithic tuffs.

In hand specimen they vary in colour from pale to dark grey. Fragmental texturs are not easily distinguished due to the small size (commonly less than 1mm) of the fragments. Only those hand specimens containing fragments of Ordovician slates are easily recognizable as having a fragmental texture. Some thin (1-3mm) layering is present though this is also difficult to detect because of the similar compositions of the layers.

Crystal fragments occur in some 75 percent of the rhyolitic tuffs and comprise 20 percent (Plate 6B) to 75 percent (Plate 6C) of the rocks. These rocks are thus rhyolitic crystal tuffs. Between 70 and 80 percent of the crystal fragments are of quartz, with the rest being of sodic plagioclase (An_{10}). The crystal fragments are angular in shape, and vary in size from less than 0.1mm to 3mm, of which the size 0.5mm to 1mm is the most common. A flow-like texture is present in some specimens (Plate 6D) and is seen as orientation of the crystal fragments, and alignment of chlorite and sericite in the matrix.

Fragmental textures are readily seen in some specimens where fragments of other rhyolitic rocks (both pyroclastic and lava-types) are present. In some few specimens, fragments of dacitic rocks are present particularly in specimens which occur at higher levels in the rhyolitic sequence. Fragments of Ordovician slates are very common (Plate 6A), and comprise some 60 percent of the fragments in specimens from borehole IM9.

The groundmass consists largely of fine granular aggregates of quartz and plagioclase feldspar, along with sericite and chlorite, which are the alteration products of feldspar. Glass fragments are

PLATE 5

Photomicrographs of Siliceous Sinter

A,B : From borehole M2 at 627 feet depth, field of view 2.33x2.67mm, A - P.P.L. ; B - x-nicols

C : From borehole M2 at 752 feet depth, field of view 2.33x2.67mm, P.P.L.

All three plates show colloform layering texture of siliceous sinter and illustrate the alignment of quartz crystals in cavities.

D : From borehole M29 at 649 feet depth, field of view 5.83x6.67mm, P.P.L.

Alignment of inclusions illustrate overgrowth on well-formed crystals of quartz, lining cavity walls.

Interlayering of Rhyolitic Tuffs and Ordovician Slates as Seen in Hand Specimen

E,F : From borehole M29 at 650 feet depth, field of view 5x6cm

Both plates illustrate the occurrence of rhyolitic rock materials (white) in the Ordovician slates (black).

PLATE 5

A

B

C

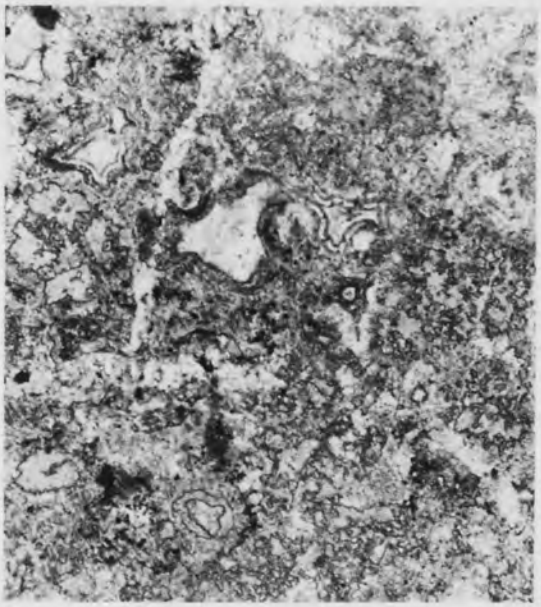

D

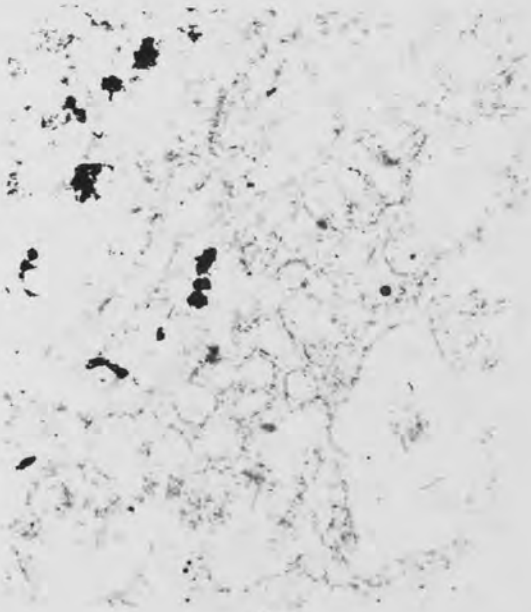

E

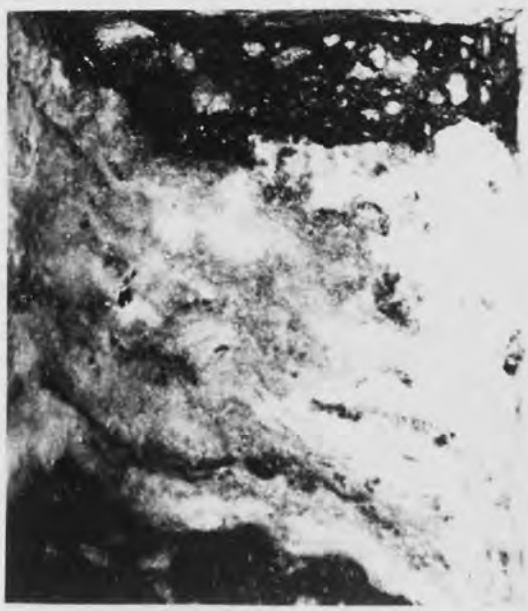

F

PLATE 6

Photomicrographs of Rhyolitic Tuffs

A : From borehole IM9 at 197 feet depth, field of view 5.83x6.67mm, P.P.L.

Fragment of Ordovician slate in rhyolitic tuff.

B : From borehole IM5 at 59 feet depth, field of view 5.83x6.67mm, P.P.L.

Subround crystal fragments of quartz in rhyolitic tuff. Large patches of material have a texture indicative of recrystallized glass and are partly replaced by chlorite.

C : From borehole H29 at 650 feet depth, field of view 5.83x6.67mm, P.P.L.

Angular quartz crystal fragments in rhyolitic tuff.

D : From borehole M5 at 189 feet depth, field of view 2.33x2.67mm, P.P.L.

Angular quartz crystal fragments in a sericite and chlorite rich matrix. A flow-like texture is present.

General Appearance of Rhyolitic Ignimbrite in Hand Specimen

E : From borehole H14 at 464 feet depth, field of view 5x6cm.

Perlitic cracks and spherulitic textures. Replacement of the spherulites by chlorite (dark) and quartz (white) is present.

Photomicrograph of Ignimbritic Rhyolite

F : From borehole H14 at 464 feet depth, field of view 5.83x6.67mm, P.P.L.

Perlitic cracks in ignimbrite. Glassy material partly replaced by chlorite (dark). Recrystallization of the glass is represented by quartz-rich aggregates.

PLATE 6

A

B

C

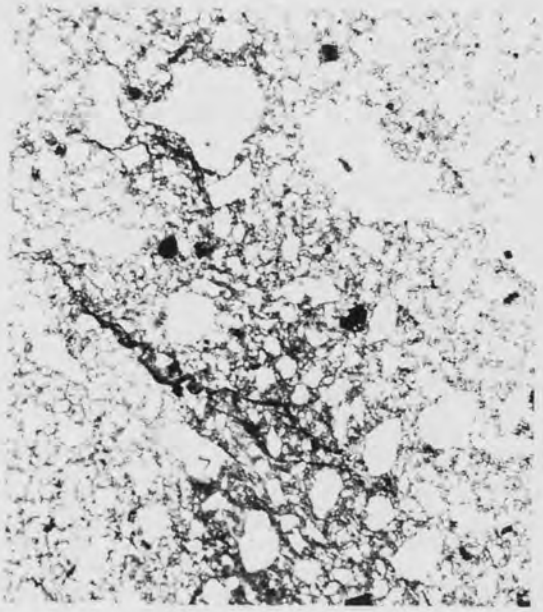

D

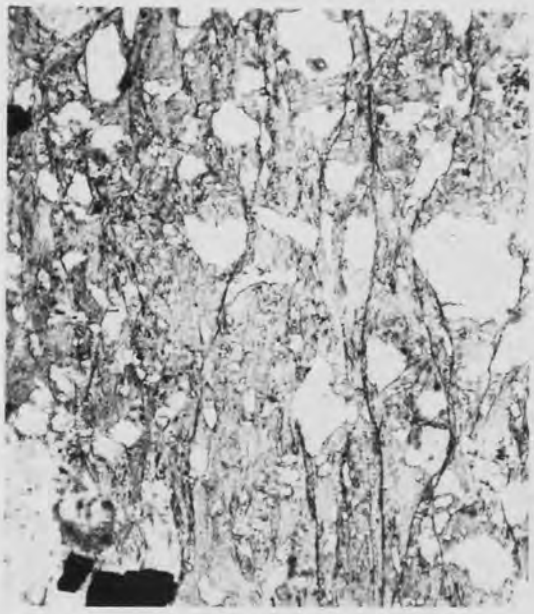

E

F

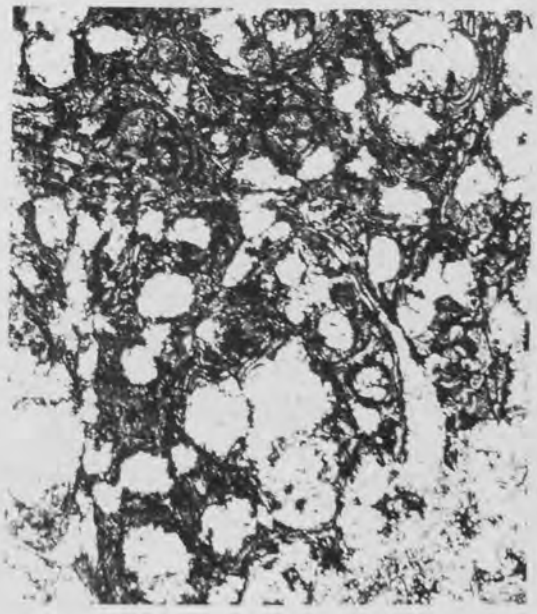

present in the matrix of a number of specimens. These vary in size from less than 0.1mm to 1mm and have cuspidate shapes.

The main sequence of ignimbritic rocks occur directly above the rhyolitic tuffs. In hand specimen these vary in colour from greenish grey to dark grey, with spherulites appearing as white and dark green irregular spots up to 2mm in diameter. The original glassy nature of parts, if not all, of these rocks is indicated by the very common occurrence of spherulites and perlitic cracks (Plate 6E). Glass shards and spherulites are commonly replaced by quartz, carbonates, and chlorite. Where glass is dominant (more than 80 percent) in the rocks they could be classed as rhyolitic pitchstones. Such rocks form some 10 percent of the total of the ignimbritic rocks.

In thin section those rocks which appear to be rhyolitic pitchstones have very well developed perlitic cracks and spherulites (Plates 6F and 7) some parts of which have been replaced and recrystallized. The majority of the ignimbritic rocks contain lesser quantities of glass than the pitchstones; however, perlitic and spherulitic textures are still prominent. Fragments of quartz crystals and, in some instances, of plagioclase feldspar (An_{30-50}) are common and form up to 15 percent of the rocks.

In the less glassy parts of the rocks (less than 40 percent of glass), spherulites are common (Plates 8A, B, and C) and many are aligned with layering (Plate 8B). The typical radiating appearance of the spherulites is still preserved in many specimens (Plate 8C), although in others recrystallization and replacement has destroyed this feature. This is particularly evident where strong

PLATE 7

Photomicrographs of Ignimbritic Rhyolite

A,B : From borehole H14 at 464 feet depth, field of view 5.83x6.67mm,
A : P.P.L. , B : x-nicols.

C : From borehole H14 at 318 feet depth, field of view 2.37x2.67mm,
x-nicols.

D-F : From borehole H14 at 548 feet depth;
D : Field of view 5.83x6.67mm, P.P.L.
E : Field of view 2.33x2.67mm, P.P.L.
F : Field of view 2.33x2.67mm, x-nicols

All plates illustrate perlitic cracks and spherulitic textures. Various degrees of replacement and recrystallization are illustrated. Replacement of glass by chlorite (dark) and quartz aggregates are well developed in A and B, and comparatively less so in C and D. In E and F replacement of glass by quartz is pronounced.

PLATE 7

A

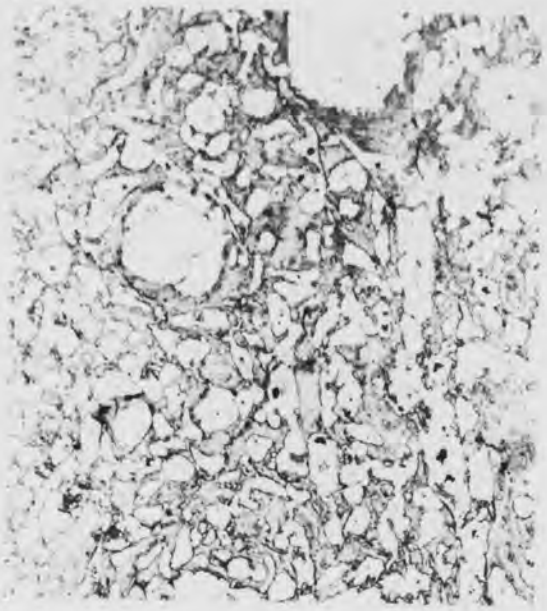

B

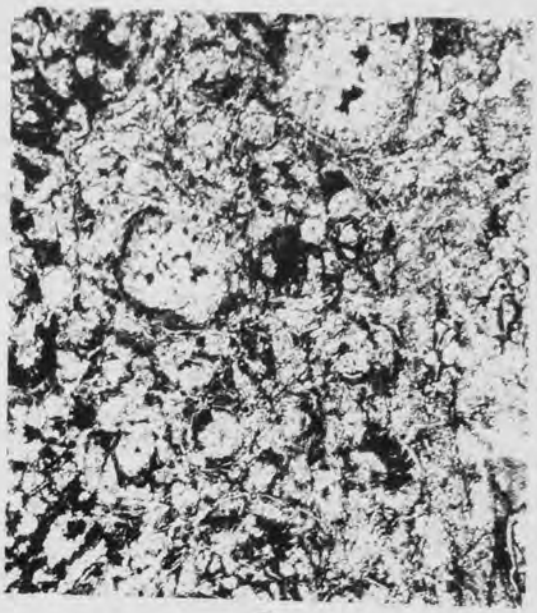

C

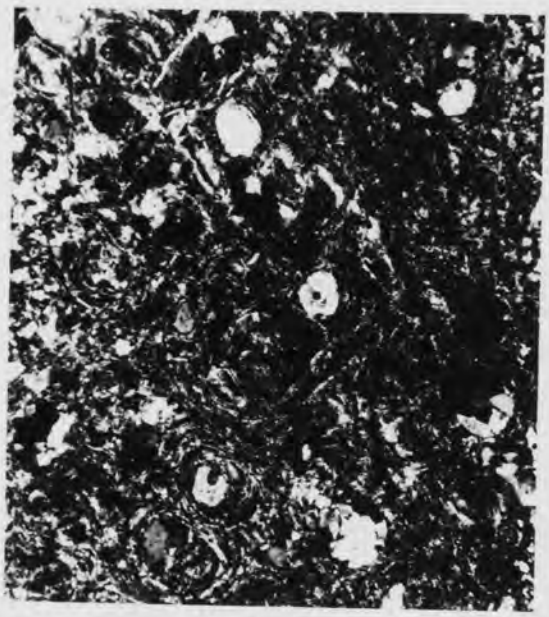

D

E

F

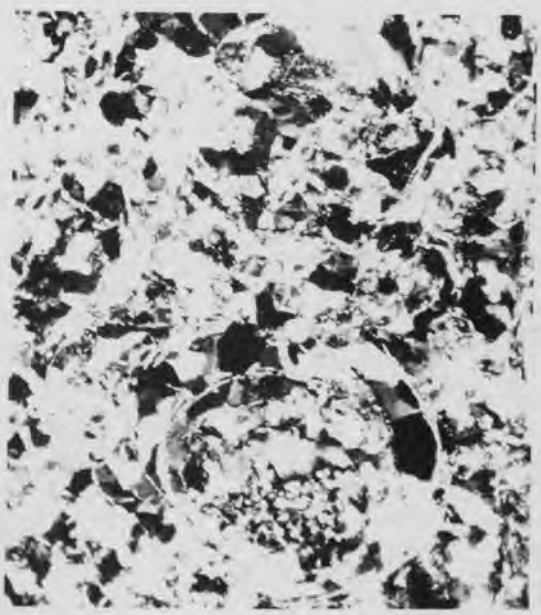

PLATE 8

Photomicrographs of Ignimbritic Rocks

A,B : From borehole H14 at 285 feet depth;
A : Field of view 2.33x2.67mm, P.P.L.
B : Field of view 5.83x6.67mm, P.P.L.

Spherulites in rocks with less than 40 percent glass. Some spherulites are replaced by quartz, and others exhibit radiating textures. In B the spherulites aligned with the layering.

C : From borehole H14 at 421 feet depth, field of view 0.58x0.67mm, x-nicols.

Typical radiating appearance of spherulite.

D : From borehole H14 at 318 feet depth, field of view 4.67x5.33mm, P.P.L.

Perlitic cracks in glassy groundmass with a small amount of chlorite replacement.

E,F : From borehole H14 at 395 feet depth;
E : Field of view 5.83x6.67mm, P.P.L.
F : Field of view 2.33x2.67mm, P.P.L.

Quartz overgrowths on spherulites. The former outlines of the spherulites are distinguished by the presence of aligned inclusions.

PLATE 8

A

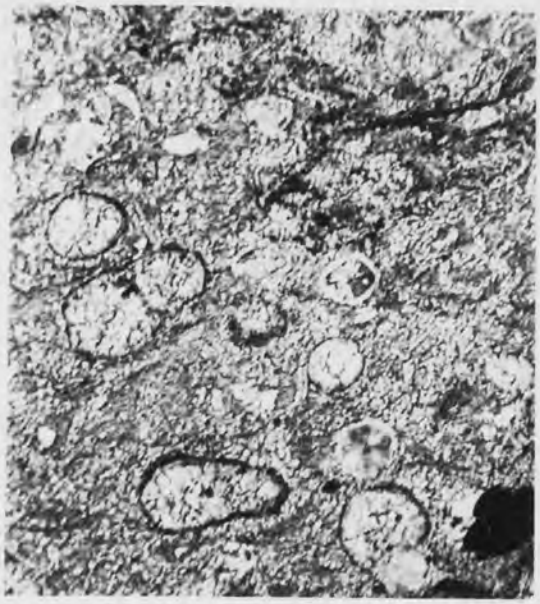

B

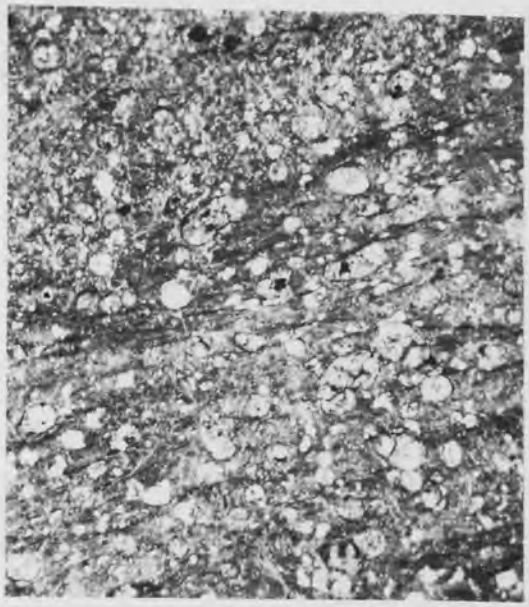

C

D

E

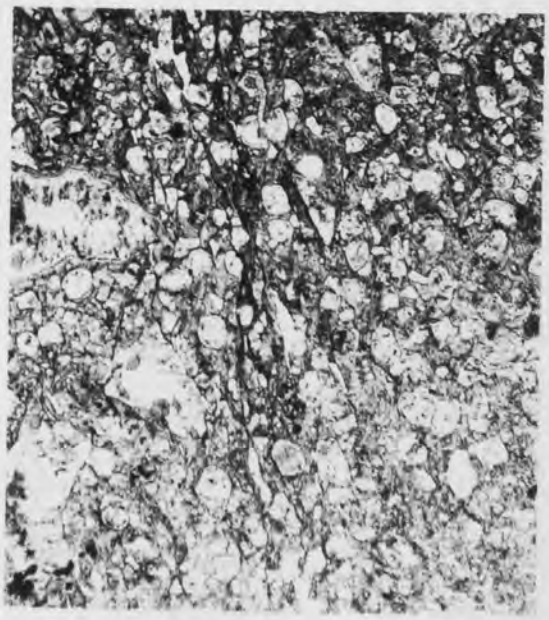

F

devitrification and replacement by chlorite of the groundmass has occurred (Plate 8D). In some specimens quartz overgrowths are present, particularly where recrystallization and replacement effects are most pronounced. In these the original outlines of spherulites beneath the overgrowths are picked out by the concentric alignment of inclusions in quartz grains (Plates 8E, F, and 9A). The matrix of these rocks consists of fibrous aggregates of sericite and chlorite bent around the quartz crystals and spherulites (Plate 9A). Some few specimens of the ignimbritic rocks consist predominantly of large glassy fragments enclosed in a fine grained rhyolitic matrix. In these rocks many of the glass fragments are bent and are aligned with the bedding (Plate 9B).

The majority of the rhyolitic tuff-lavas occur stratigraphically above the ignimbritic rocks. The overall colour ranges from a medium to a greenish grey, and they appear heterogeneous due to the presence of both fragmental and flow layering textures (Plate 9C). Fragments in these rocks are commonly subround, vary in size from 1mm up to 1cm, and comprise some 75 percent of the rock. The fragments are of both rhyolitic material, and crystals of quartz and plagioclase feldspar in the proportions of 1:4. Layering is present and is seen as alternations of thin (2mm to 1cm) layers of pale grey, dark grey, and greenish grey rhyolitic materials.

In thin section the fragments are seen to be lensoid with long axes parallel with layering. They consist of broken quartz and plagioclase (An_{35}) crystals, rhyolitic lava, rhyolitic tuff, glass, and rhyolitic tuff-lava (Plates 9D and F; 10A, B, and C). The

PLATE 9

Photomicrographs of Rhyolitic Ignimbrites

A : From borehole H14 at 395 feet depth, field of view 1.46x1.67mm, P.P.L.

Fibrous aggregates of sericite and chlorite, in matrix of ignimbrite, bent around recrystallized spherulites.

B : From borehole IM9 at 200.5 feet depth, field of view 5.83x6.67mm, P.P.L.

Bent and aligned glass fragments along bedding.

General Appearance of Rhyolitic Tuff-lava in Hand Specimen

C : From borehole H15 at 275 feet depth, field of view 5.5x6.5cm.

Flow-like and fragmental textures.

Photomicrographs of Rhyolitic Tuff-lava

D : From borehole IM9 at 153 feet depth, field of view 5.83x6.67mm, P.P.L.

Quartz crystals and rhyolitic fragments aligned with flow layering.

E,F : From borehole IM9 at 100 feet depth, field of view 5.83x6.67mm, E : P.P.L. , F : x-nicols.

Glass fragments with perlitic cracks in rhyolitic tuff-lava.

PLATE 9

A

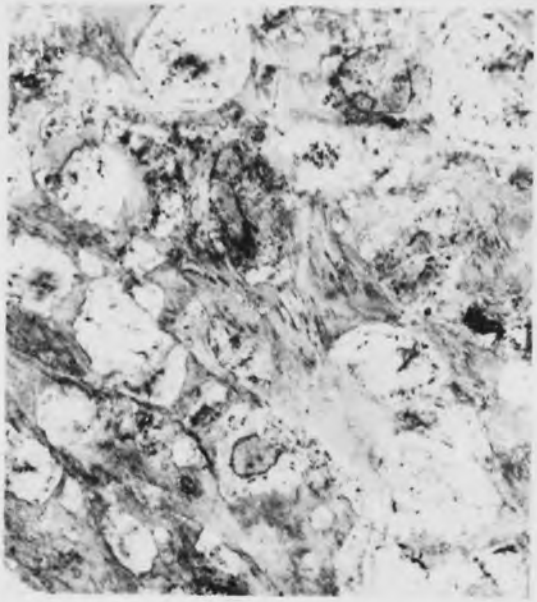

B

C

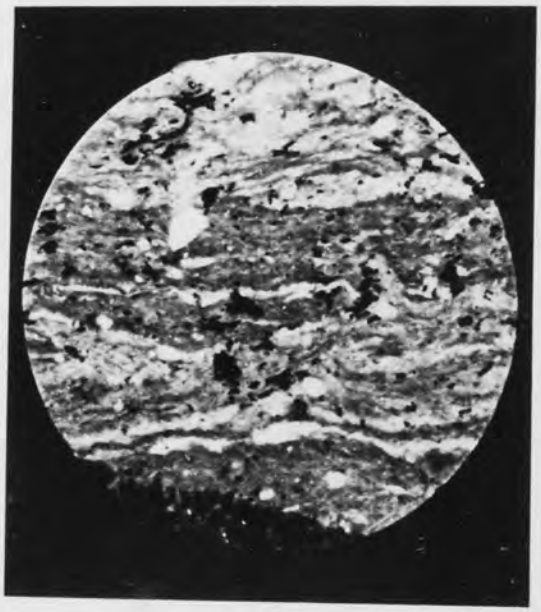

D

E

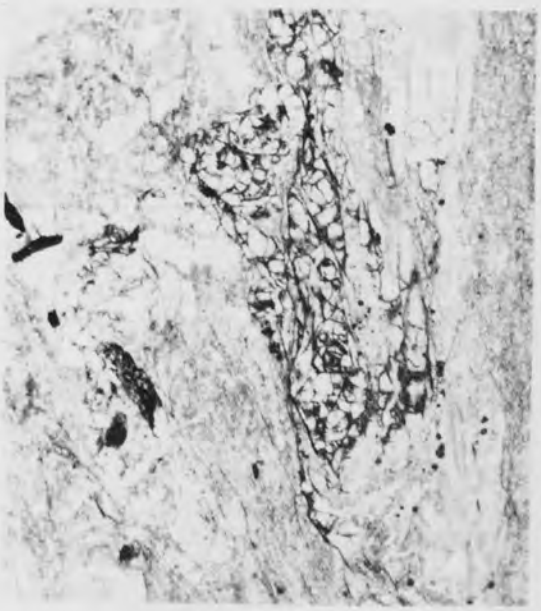

F

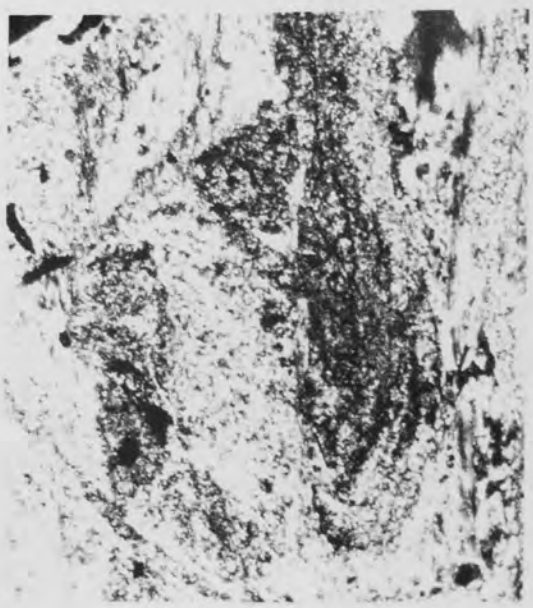

groundmass consists of a fine aggregate of quartz and sodic plagioclase (An_{10-15}), with some sericite, chlorite, and devitrified glass. The glass occurs as particles which are commonly aligned and appear to be bent around fragments in the rocks.

Rhyolitic lava type rocks predominate at the top of the rhyolitic group. These are homogeneous, very fine grained, massive, rocks with a cherty appearance, and range in colour from pale greenish grey to dark grey. Layering is not seen in these rocks.

In thin section the majority of the rocks are seen to consist of an interlocking mosaic of fine grained quartz and feldspar (commonly K-feldspar), with interstitial sericite, and,in some specimens, carbonate. Some few examples of layering are seen (Plate 10D) and are deformed. Amygdales and spherulites are present in many specimens. The amygdales are infilled with quartz, and chlorite (Plate 10E), and the spherulites are replaced by these minerals.

3.2 Intrusive Rocks

These rocks occur as a number of thin, irregularly distributed, generlly conformable, sheets (8 to 17m thick) within the sedimentary-volcanic succession (Fig.3). They are doleritic in composition and intrude all rocks except the Silurian slates. They vary in colour from medium to dark green, and are fine grained homogeneous rocks. White to yellowish-green, irregular, thin veins of carbonate, and of quartz are common in these rocks.

In thin section they are seen to be commonly highly altered and to consist of up to 50 percent fine grained chlorite aggregates,

PLATE 10

Photomicrographs of Rhyolitic Tuff-lava

A : From borehole IM9 at 51 feet depth, field of view 5.83x6.67mm, P.P.L.

B : From borehole IM9 at 100 feet depth, field of view 5.83x6.67mm, P.P.L.

Both plates illustrate the alignment of quartz fragments with layering in rhyolitic tuff-lava. More quartz fragments and less sericite and chlorite matrix materials are present in A.

C : From borehole IM9 at 119.5 feet depth, field of view 5.83x6.67mm, P.P.L.

Shearing textures in rhyolitic tuff-lava. Quartz fragments are aligned inside large spindle-shaped rock fragments.

Photomicrographs of Rhyolitic Lava

D : From borehole H25 at 657 feet depth, field of view 5.83x6.67mm, P.P.L.

Deformed layering in rhyolitic lava.

E : From borehole IM7 at 93 feet depth, field of view 5.83x6.67mm, P.P.L.

Amygdales in rhyolitic lava infilled with chlorite and quartz.

F : From borehole IM6 at 1240 feet depth, field of view 5.83x6.67mm, x-nicols.

Recrystallized spherulites in rhyolitic lava.

PLATE 10

A

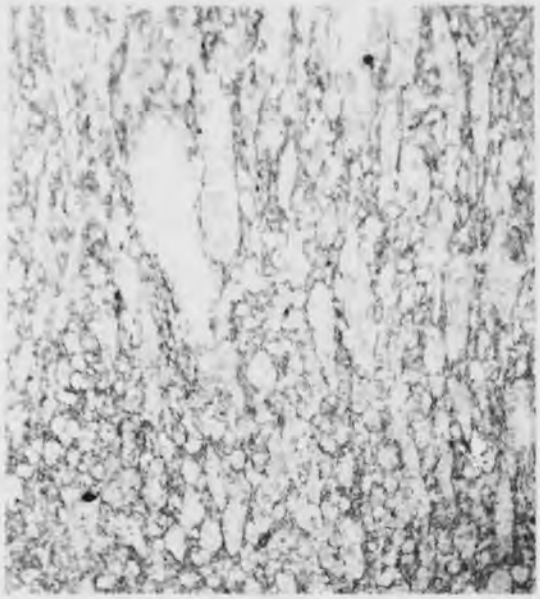

B

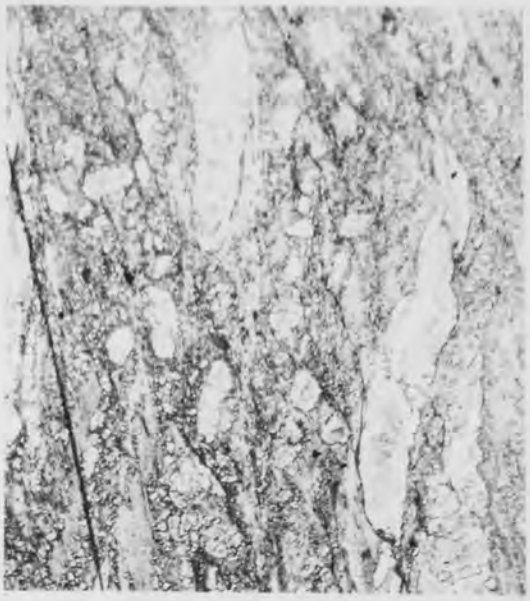

C

D

E

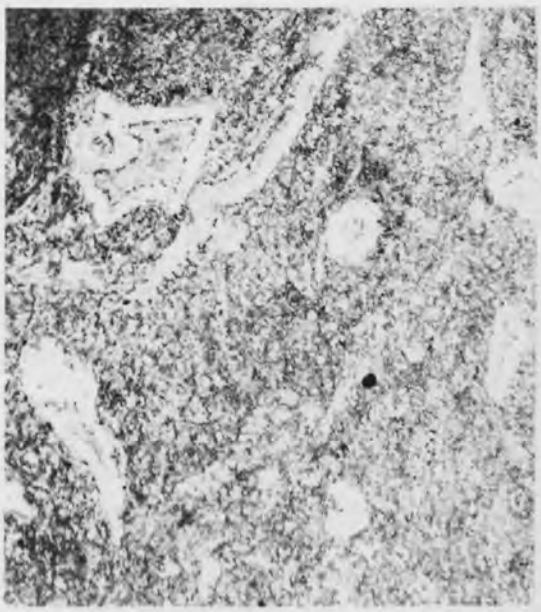

F

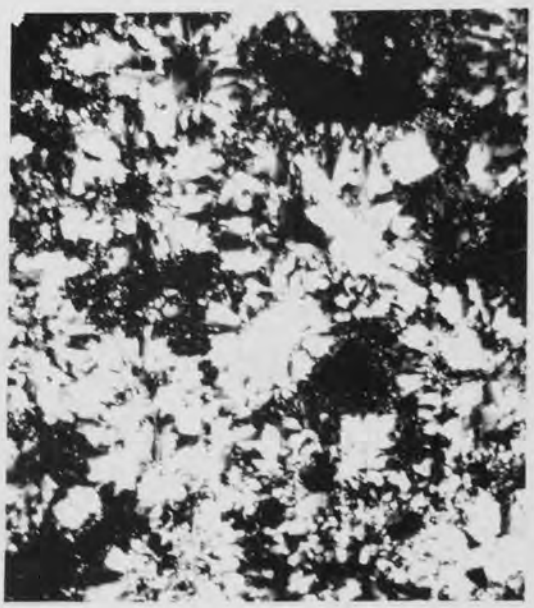

approximately 25 percent carbonate, and equal quantities of plagioclase feldspar (An_{50-70}), sericite, quartz, and acicular aggregates of iron oxide (Plate 11A). In some instances the iron oxide aggregates comprise some 40 percent of the rock (Plate 11B). The rocks are silicified and because of this the quartz content is commonly as high as 40 percent . Where alteration is less prevalent a doleritic texture is present with plagioclases, up to 0.1x1mm, and granular and tabular grains of clinopyroxene (commonly augite) (Plate 11C). In these rocks there is a considerable quantity of secondary chlorite, carbonates, quartz, sericite and iron oxide aggregates still present. Pseudomorphs of serpentine after pyroxene are common as is the occurrence of chlorite in small radiating aggregates (up to 0.1mm), and in irregular veinlets.

A shear foliation is present in some specimens. Others contain tension gashes, with varied orientations,filled with carbonate. Other specimens have talc developed along the fractures, and the rock on either side of these fractures appears whitened for distances up to 0.5cm.

PLATE 11

Photomicrographs of Dolerites

A : From borehole IM5 at 178 feet depth, field of view 5.83x6.67mm, P.P.L.

Comparision between intensely altered parts (top left corner, and right hand side of the plate), and less altered dolerite. Chlorite is prominent in the intensely altered parts, and has almost completely replaced the primary minerals. Most primary minerals, such as plagioclase feldspar and pyroxene, are still preserved in the other part. Carbonates and acicular iron oxide aggregates are scattered throughout the specimen.

B : From borehole H45A at 192 feet depth, field of view 2.33x2.67mm, P.P.L.

Altered dolerite with chlorite and acicular iron oxide as the major alteration products of the mafic minerals. Carbonates, quartz, and sericite are present as secondary minerals though the overall doleritic texture is preserved.

C : From borehole H45A at 149 feet depth, field of view 2.33x2.67mm, P.P.L.

Slightly altered dolerite with a doleritic texture of lath-shaped plagioclase (light colour) and clinopyroxene (augite). Chlorite (grey patches) and iron oxide (black), are present as replacements of the pyroxene.

PLATE 11

A

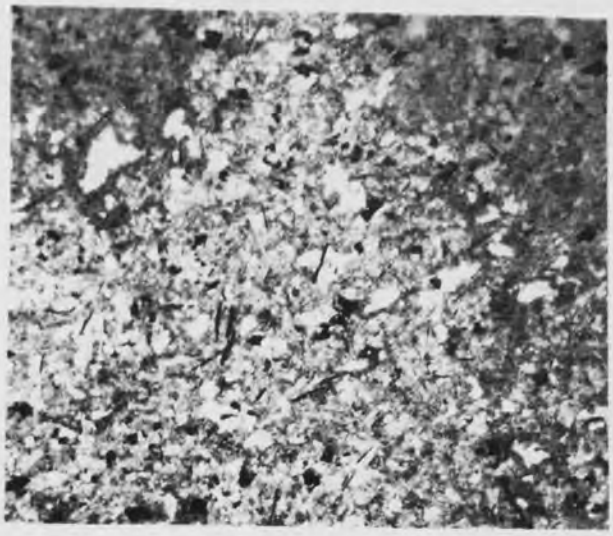

B

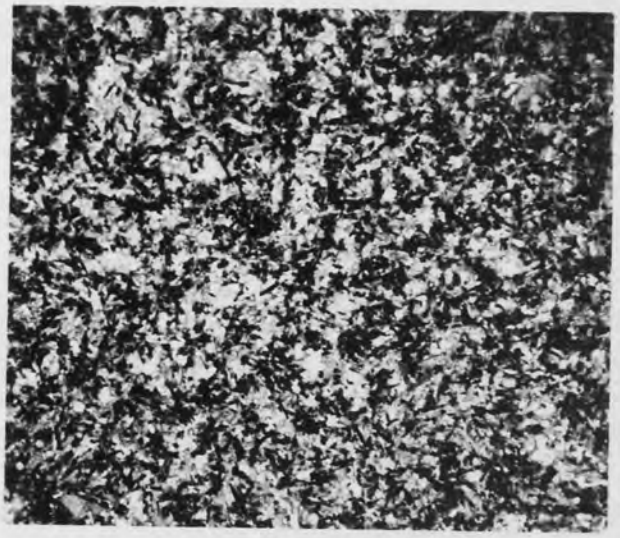

C

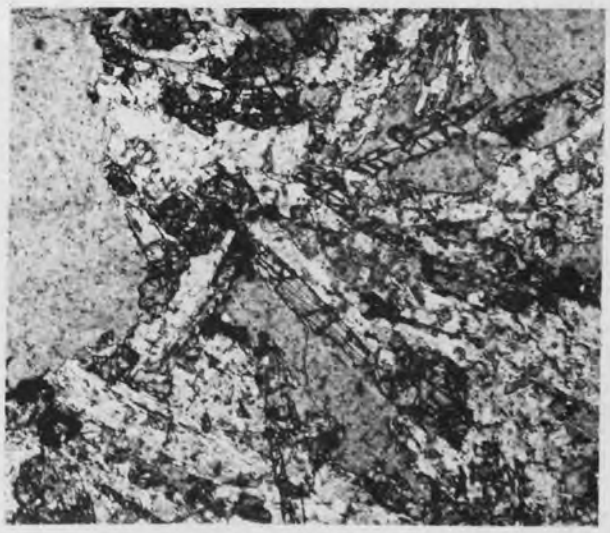

CHAPTER 4

STRUCTURAL GEOLOGY

4.1 Introduction

The interpretation of the 'felsite' of Parys Mountain as a sill-like intrusion (Greenly, 1919), or as a two pronged dyke (Manning, 1959), in conjunction with the scarcity of faunal evidence in the 'southern slates', resulted in a dispute over the major structure of the area. Greenly (1919) suggested that Parys Mountain consisted of two overturned synclines, with an intervening complementary anticline (Figures 4-1 and 4-2). Manning (1959) interpreted the structure as a single syncline overturned to the north (Fig. 4-3). These interpretations were based on the identification of the 'southern slates' as Silurian.

A re-examination of the fossil and structural evidence in the Hillside Opencast allowed Bates (1964) to determine that the 'southern slates' are Ordovician in age. In addition, Hawkins (1966) concluded that the 'felsite' was a complex mixture of silicified sedimentary rocks, rhyolitic intrusions, and tuffs. The results of these works, and that of Wheatley (1971a,b) allowed the major structure at Parys Mountain to be re-interpreted as a single syncline (Fig. 4-4). All evidence collected in the present study, including the logs of some 60 diamond drill holes, also favours the single syncline interpretation (Fig. 4-4).

Bates (1964) stated that the majority of the structures in the Parys Mountain area fall into two categories. These are Caledonian

structures and post-Caledonian structures.

4.2 The Caledonian Structures.

According to Bates (1964) the principal stresses associated with this orogeny at Parys Mountain were orientated at 160° to 340° and six phases of Caledonian deformation were identified. These phases were looked for and verified in the present study, and are described below in their order of formation.

a) Folding Phase.

A major isoclinal syncline is present at Parys Mountain within the rhyolite outcrops. This syncline has an axial trend of 050°, and has minor folds with similarly trending axes associated with it in the Silurian slates of the Great Opencast. The fold axis plunges at an angle of some 20° towards the north east. This north easterly plunge of the fold axis is indicated by the outcrop pattern of the major syncline (Fig.3). Both cleavage and bedding are parallel with a strike which varies between 045° and 070°, and dips ranging from 40° to 60° in a north westerly direction.

b) Reverse Fault Phase.

The production of high angle reverse faults, followed and accompanied the main folding, and the development of its associated cleavages. These faults result from the same compressional Caledonian stresses, which produced the folds and cleavages.

c) Igneous Activity and Metasomatic Phase.

A subsequent period of relative relaxation of pressure gave

rise to the formation of quartz veining and silicification at Parys Mountain. The doleritic intrusions of the area also were emplaced at this time. However, as these intrusions cut all rocks except the Silurian slates, and have been subjected to the same alteration as their host rocks, they probably predate the Caledonian orogeny. A late Ordovician age, similar to the other basic intrusives in other parts of North Wales (Fitch, et al, 1969), is thought to be most likely for these intrusions. The silicification was developed during the Caledonian orogeny as it has extensively affected the rhyolites, parts of the Silurian slates, and is cut by later faults (Bates, 1964).

d) Thrust Phase.

Thrusting resulted from the re-imposition of compressional forces. The thrust planes strike parallel to both the cleavage and bedding, and dip to the north-north-west at angles between 30° and 60°. In the Great Opencast thrust planes are clearly exposed in the Silurian slates where they bring silicified rocks against unsilicified ones. The Carmel Head Thrust and the Nebo Thrust both belong to this phase.

e) Metasomatic Mineralization Phase.

Relief of horizontal compression followed episodes a)to d) and normal faulting occurred. Planes of weakness in the rocks, e.g. faults, cleavage, and bedding became the locations for quartz veining and some mineralization.

The veining was later than the silicification and the reverse faults as it transected both silicified rocks and the fault planes.

Two types of veins are present;an earlier mineralized type, and a later non-mineralized type. The mineralized veins have two directional maxima. One trends at 055° and dips steeply to the north-north-west parallel to bedding, cleavage, and earlier reverse fault planes. The second is horizontal and is subordinate to the first.

Bates (1964) suggested that both the Carreg-y-doll, and the White Rock Formation, are large quartz veins formed during this phase. However, petrographic evidence (section 3.1.4 of Chapter 3), and the folded pattern of these rocks (Fig.9), indicate that these formations are more likely siliceous sinters formed contemporaneously with the volcanic rocks. This interpretation is discussed in detail in Chapter 7 on petrogenesis.

f) Wrench Faulting Phase.

The last phase of the Caledonian orogeny at Parys Mountain is represented by two large wrench faults :- the Carreg-y-doll Cross Course, and the Great Cross Course. The former has a small sinistral movement, strikes at 020° and dips 70° to 80° to the west, and the later has a dextral movement, strikes at 150°, and dips 80° to the north east. Both faults cut and displace the Carreg-y-doll Lode, and have post-Caledonian mineralized veins associated with them.

4.3 Post-Caledonian Structures.

The major post-Caledonian structural episodes are represented by mineralized hydrothermal veins and normal faults (Bates, 1964). These faults trend parallel to the cleavage and bedding, and dip at high angles (70° to 80°) to the north west. Bates (1964) suggested

that these faults may be re-activated reverse faults of the earlier compressional phase (d). Examples of these structures are the White Rock Fault, the Foel-Newydd Fault (Fig.3), and the North Discovery and the Morfa-du Lodes. Nevertheless the interpretation of the ore genesis in the present study regards the hydrothermal activity of this phase as having only a minor contribution to the formation of the ore lodes in the area, and the main episodes of the ore formation are of syngenetic origin (see Chapter 8 on ore genesis).

The above structural interpretation is largely based on information collected from old mining plans and previous works. At present time much of the evidence is no longer visible as the old opencast mining operations either removed information, or the old mine dumps have covered up the exposures. A detailed structural study may be possible, using information from diamond drill cores but this is beyond the scope of the present study.

CHAPTER 5

MINERALIZATION

5.1 General Characteristics of the Ore Bodies.

At Parys Mountain the mineralized belt extends some 1500m in length and is approximately 400m wide, and mining has been carried out down to depths of over 300m. The belt trends between 060° and 070°, following the strike of the enclosing beds. The mineralization is generally concentrated on both sides of the northern outcrops of the rhyolitic rocks. It is found both in the rhyolitic bodies and the rocks in contact with them, e.g. the siliceous sinter, parts of the Ordovician slates in the north, and the northern parts of the Silurian slates on the south side (Fig.10).

Four types of ores were distinguished at Parys Mountain by Wolfenden (1967) and this subdivision is accepted and outlined below:-

1) Copper Ore.

Pyrite, chalcopyrite, with a little sphalerite and galena were the main ore minerals, with quartz as the main gangue. The average copper content varied between 1.5 and 2.5 percent (Wolfenden, 1967). This ore occurred mainly within the northern rhyolite, close to its northern and southern contacts, and in parts of the northern Ordovician slates. It was also abundant in the siliceous sinter.

2) Bluestone Ore.

This was an intimate mixture of argentiferous galena, and

Figure 10 Sketch geological plan with cross sections to show location of ore lodes. (after Manning, 1959).

Facing page 60

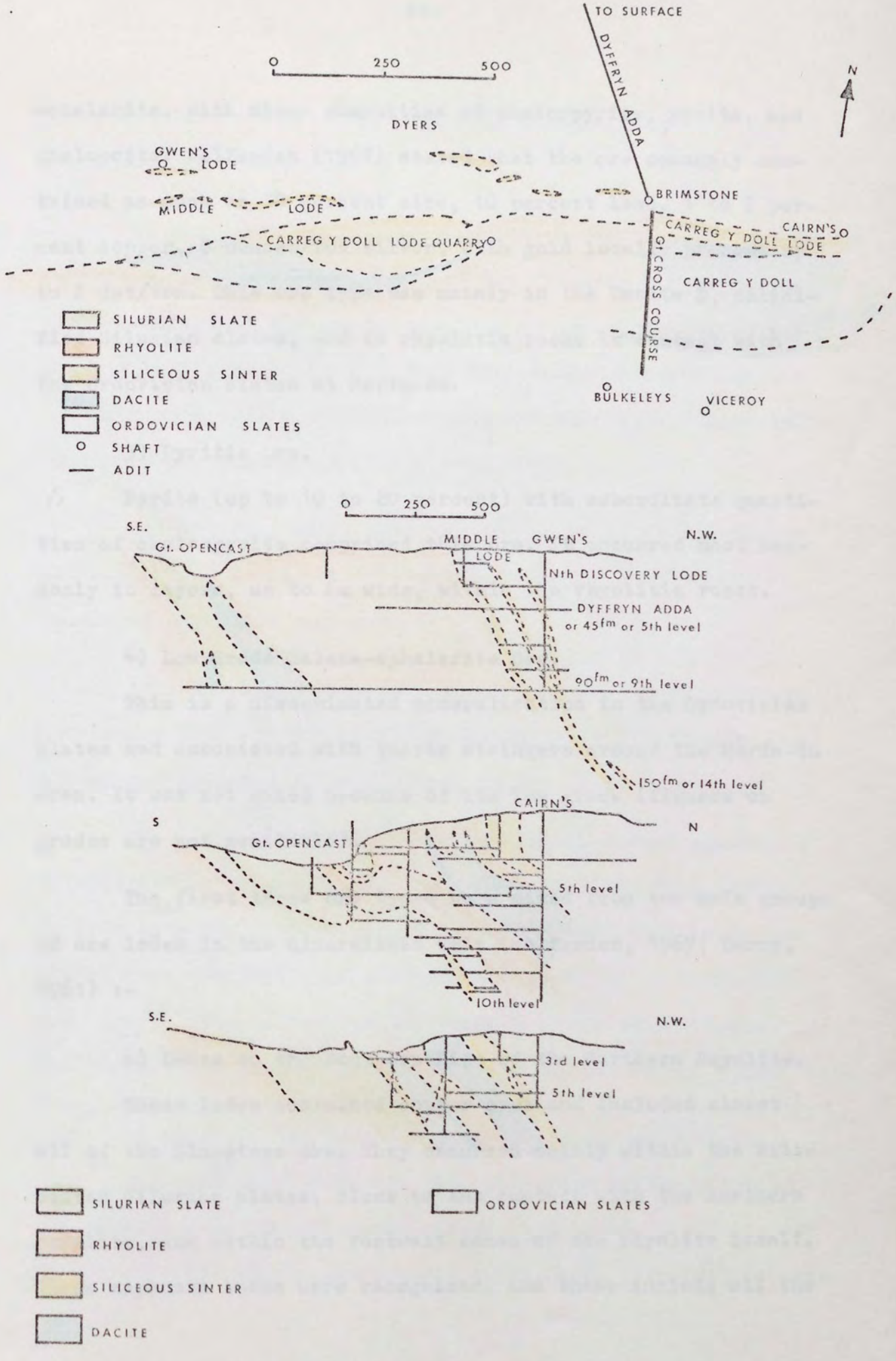
TO SURFACE
DYFFRYN ADDA
0 250 500
N
DYERS
GWEN'S
LODE
MIDDLE
LODE
BRIMSTONE
CARREG Y DOLL LODE QUARRY
CARREG Y DOLL
CAIRN'S
LODE
Gt CROSS COURSE
CARREG Y DOLL
BULKELEYS
VICEROY
SILURIAN SLATE
RHYOLITE
SILICEOUS SINTER
DACITE
ORDOVICIAN SLATES
SHAFT
ADIT
0 250 500
S.E.
N.W.
Gt. OPENCAST
MIDDLE
LODE
GWEN'S
Nth DISCOVERY LODE
DYFFRYN ADDA
or 45fm or 5th level
90fm or 9th level
150fm or 14th level
S
N
CAIRN'S
Gt. OPENCAST
5th level
10th level
S.E.
N.W.
3rd level
5th level
SILURIAN SLATE
RHYOLITE
SILICEOUS SINTER
DACITE
ORDOVICIAN SLATES

Figure 10

sphalerite, with minor quantities of chalcopyrite, pyrite, and chalcocite. Wolfenden (1967) stated that the ore commonly contained as much as 30 percent zinc, 10 percent lead, 1 to 2 percent copper, 8 ounces/ton silver, with gold locally present up to 2 dwt/ton. This ore type was mainly in the Dacite D, silicified Silurian slates, and in rhyolitic rocks in contact with the Ordovician slates at Morfa-du.

3) Pyritic Ore.

Pyrite (up to 10 to 20 percent) with subordinate quantities of chalcopyrite comprised this ore. It occurred most commonly in layers, up to 6m wide, within the rhyolitic rocks.

4) Low Grade Galena-sphalerite Ore.

This is a disseminated mineralization in the Ordovician slates and associated with quartz stringers around the Morfa-du area. It was not mined because of its low grade (figures on grades are not available).

The first three ore types were mined from two main groups of ore lodes in the mineralized belt (Wolfenden, 1967; Derry, 1961) :-

a) Lodes on the Southern Side of the Northern Rhyolite.

These lodes contained copper ores and included almost all of the Bluestone ore. They occurred mainly within the silicified Silurian slates, close to the contact with the northern rhyolite, and within the footwall zones of the rhyolite itself. Three separate lodes were recognized, and these include all the

veins and lenses previously worked by opencast methods. From north to south these were :-

i) The Great or Opencast Lode which was mined in the two opencasts, the Great Opencast, and the Hillside Opencast. The ore was mainly of the Copper ore type though some of the Bluestone type was present. This lode was contained mainly in the northern part of the silicified Silurian slates, but extended to the nearby northern rhyolite (Fig.10).

ii) The Clay Shaft Lode was in the silicified Silurian slates, had an average width of 16m, and consisted mainly of lenses of Bluestone type ore.

iii) The Black Rock Lode which contained both Bluestone and Copper ores. It was confined within the silicified Silurian slates and appeared to be a branch of the Great Lode.

The above three lodes were originally worked separately by underground mining, until the roof collapsed, then working by open pits was developed. Underground stoping was later continued from the bottom of the pit to a depth of approximately 60m. Derry (1961) estimated the tonnage of the ores mined, from the three lodes in the opencasts, to be approximately 1.5×10^6 tons.

b) Lodes on the Northern Side of the Northern Rhyolite.

These lodes were within the Ordovician slates north of the rhyolite, in the siliceous sinter, and in the northern part of the rhyolite itself. In general these lodes were both tabular

and vein type ores, and were generally conformable with the cleavage in the rocks. Both ore types were mined. Six lodes were distinguished :- the Golden Venture Lode, the Carreg-y-doll Lode, the Charlotte Lode, the Middle Lode, the South Branch Lode, and the North Discovery Lode. The first named lode was within the rhyolite, the next two in the siliceous sinter, and the last three in the Ordovician slates (Fig.10). The total tonnage mined from these six lodes was estimated by Derry (1961) to be 10.2×10^5 tons. The North Discovery Lode was the richest and contained some 17×10^4 tons of ore.

Wheatley (1971a) divided the mineralization, seen in the recent drill cores at Parys Mountain, into four groups on the basis of the mineralogy of the economic minerals and their host rocks, or matrix. His division is presented in Table 3.

5.2 General Description of Ore Minerals.

In the present study 73 polished specimens were examined by reflected light microscopy. The ore minerals present in the mineralized zones were divided into two main groups (primary and secondary) from a reflected light study of 73 polished specimens.

Primary minerals are those deposited in the original ore-forming episode, either syngenetically or epigenetically. These include the main sulphide minerals characteristic of the deposits at Parys Mountain, e.g. pyrite, chalcopyrite, sphalerite, and galena. Minor quantities of other primary minerals are present including rutile, marcasite, native bismuth, bismuthinite

Table 3 The economic minerals and their associated host rocks in the four mineralization types of Parys Mountain as proposed by Wheatley (1971a).

Mineralization type	Host rock or matrix	Mineralogy		Example
		Major	Minor	
Pyritic zone	Black shale (Ordovician slates)*	Pyrite Chalcopyrite	Pyrrhotite Sphalerite Galena	Disseminated in shale units
Siliceous zone	Shales and tuffs (silicified) (Silurian slates and rhyolitic tuffs + siliceous sinter)*	Pyrite Chalcopyrite Sphalerite Galena	Pyrrhotite Tetrahedrite Bismuthinite Native Bismuth	Carreg-y-doll Lode, Golden Venture Lode, Charlotte Lode, North Discovery Lode, North and South Branch Lodes
Lead-Zinc zone	Shales and tuffs (Silurian slates and rhyolitic tuffs)*	Sphalerite Galena Pyrite Chalcopyrite	Tetrahedrite Bournonite	Morfa-du and Black Rock Lodes, Clay Shaft Lode (Bluestone)
Veins	Shales, tuffs, and lavas (slates rhyolites and siliceous sinter)*	Galena Sphalerite Chalcopyrite	Tetrahedrite	Great Cross Course, Carreg-y-doll Cross Course

* Nomenclature developed in this thesis.

bismuth sulphosalts, arsenopyrite, pyrrhotite, tetrahedrite, tennantite, and bournonite. Secondary minerals are those formed in later stages, either from alteration, e.g. through oxidation, or through supergene deposition. These include haematite, covellite, bornite, siderite, chlorite, sericite, and carbonate minerals. Quartz is the main gangue mineral, and is both primary and secondary.

Most of the above minerals are described in detail in the following section, in terms of their reflected light properties, although some are just generally referred to.

In addition to the minerals already mentioned, a number of secondary minerals are reported to be present by Greenly (1919), and Wheatley (1971a), i.e. native silver, native gold, native sulphur, chalcocite, cuprite, malachite, melaconite or tenorite (CuO), chalcanthite ($CuSO_4.5H_2O$), melanterite ($FeSO_4.7H_2O$), minium (Pb_3O_4), anglesite, selenite, asbestos, barite, limonite, goethite, leucoxene, and gypsum. However, since all the polished specimens examined in this study are from borehole samples, the minerals of the oxidation and enrichment zones, such as those above, were not commonly seen.

Primary Minerals.

5.2.1 Rutile.

This mineral is widespread in the Ordovician slates, the dacitic rocks (Dacites D and C), and parts of the rhyolitic tuffs. It is associated commonly with euhedral pyrite grains, and occurs

as subhedral grains (Plate 12A), lath-shaped grains (Plate 12B), or irregular aggregates (Plate 12C), embedded in the rock matrix. The grain sizes vary between 0.005 and 0.5mm. Rutile is absent in those parts of the ore where the matrix is of quartz, or carbonate minerals. Rutile is grey in colour, slightly lighter than that of sphalerite, and always shows strong internal reflections. Twinning is common and replacement of rutile by chalcopyrite is seen (Plate 12A).

Rutile is one of the earliest minerals of the paragenetic sequence at Parys Mountain, possibly pre-dating the first generation of pyrite. This mineral was probably previously identified as leucoxene, and thought to be a late mineral (Wheatley, 1971a).

5.2.2 Pyrite.

Pyrite is the most abundant, and the most widespread sulphide at Parys Mountain. It constitutes approximately 50 percent of total sulphide, and is very common in each ore type, except the low grade galena and sphalerite ore. In this ore it is present only in minor quantities and was seen only in a few specimens. Pyrite commonly occurs as disseminated idiomorphic crystals, up to 1mm in diameter, in every rock type except those of the Mona Complex.

Textural observations allow the interpretation that there are three generations of pyrite present in the rocks at Parys Mountain. The oldest generation, pyrite 1, is characterized by zoned euhedral to subhedral grains, associated with rutile. This pyrite is disseminated in the Ordovician slates and the dacitic

PLATE 12

Photomicrographs of Rutile and Pyritohedral Pyrite.

A : From borehole H43A at 1845 feet depth, field of view 0.29x0.33mm, air.

Rutile (R) partly replaced by chalcopyrite (cp) in matrix of dacitic rocks.

B : From borehole H43A at 1845 feet depth, field of view 1.46x1.67mm, air.

Columnar (or lath-shaped) crystals of rutile associated with pyrite (not in the plate) in dacitic rock matrix.

C : From borehole H43A at 1855 feet depth, field of view 0.29x0.33mm, air.

Irregular aggregates of rutile (R) in dacite. The irregularity is due to replacement by minerals in the matrix. Chalcopyrite (cp) is present.

D : From borehole M9 at 731 feet depth, field of view 1.46x1.67mm, air.

Pyritohedral pyrite crystals (py) associated with a string of rutile (R) aggregates, in dacite. Bending in rutile string is probably caused by later growth of pyrite grains. Note fracturing of one of the pyrites.

E : From borehole IM6 at 1044 feet depth, field of view 1.46x1.67mm, air.

Pyritohedral pyrite crystals in matrix of Ordovician slate, some crystals (top left corner) show corrosion effects.

F : From borehole M9 at 731 feet depth, field of view 1.46x1.67mm, air.

Various forms of pyritohedral pyrite in dacite.

PLATE 12

A

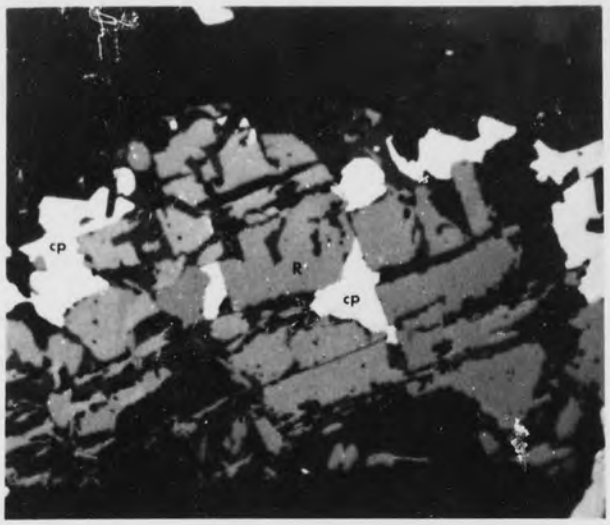

B

C

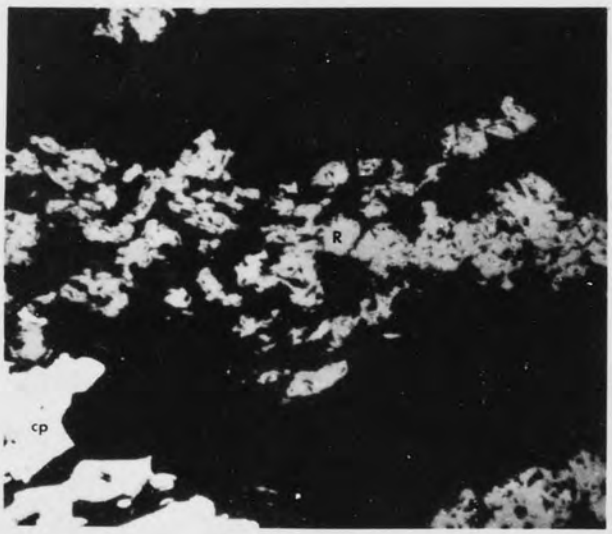

D

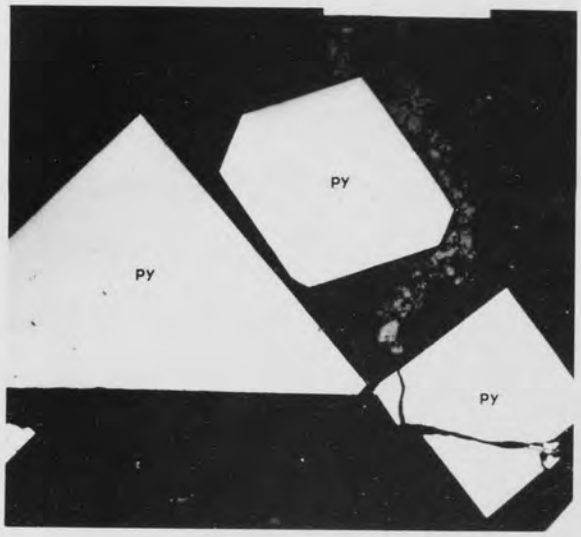

E

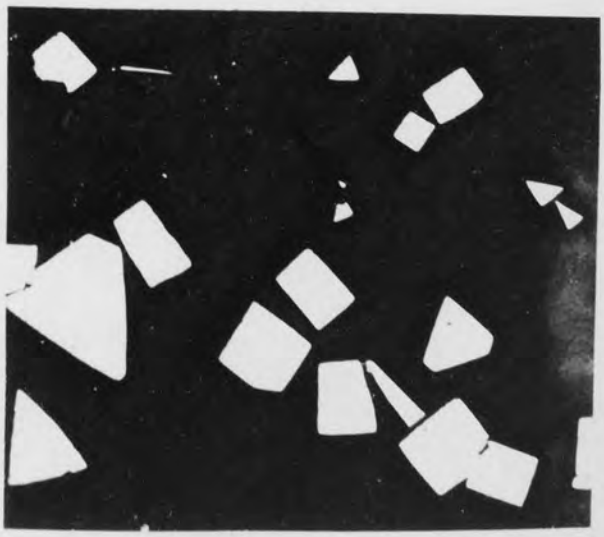

F

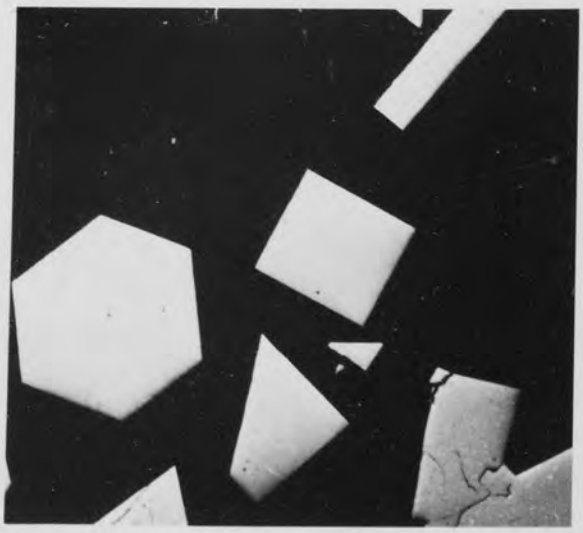

rocks. The second generation, pyrite 2, occurs as framboids and aggregates with colloform textures. It is commonly found associated with euhedral and subhedral pyrite 1 grains in both the rhyolitic rocks and siliceous sinter. The youngest generation of pyrite, pyrite 3, is associated with the quartz veinlets which penetrate all the rock types.

The pyrite of Parys Mountain commonly shows slightly anisotropy. Schneiderhohn (in Ramdohr, 1969) suggested that anisotropy in pyrite is probably accounted for the presence of arsenic. This is possibly applicable at Parys Mountain since arsenopyrite is commonly associated with pyrite. However, anisotropism was also found in pyrite free of arsenic (Ramdohr, 1969). The other possibility is that the anisotropic effects are due to the presence of inclusions in the pyrite grains, which are too small for identification, since anisotropism is only observed where inclusions are present.

Four primary forms of pyrite are recognized :- euhedral, anhedral, framboidal, and colloform. Secondary fabrics, such as overgrowths, crystal corrosion, replacements, and cataclastic features are also present. The various pyrite fabrics are illustrated in Plates 12 to 25, and descriptions of each type are given below.

5.2.2.1 Euhedral Pyrite.

Pyrite shows strong tendencies to euhedral crystallization (Ramdohr, 1969), and in an environment in which it can grow freely cubic or pyritohedral crystals are common (Plates

12D, 12E, and 12F). The euhedral pyrite is generally disseminated, and is closely associated with rutile (Plate 12D). Hawkins (1966) and Wheatley (1971) stated that pyritohedral pyrite is present only in the Ordovician slates, but in this study it was also found, associated with rutile, in the dacitic rocks (Dacite C and Dacite D), and in parts of the rhyolitic tuff where rutile is present. The grain size of euhedral pyrite varies from 0.02mm to 1mm though the most common size is around 0.2mm. Zoning, secondary overgrowth, and crystal corrosion are common phenomena affecting the euhedral pyrites and each of these fabrics is described in later sections.

5.2.2.2 Anhedral pyrite

Anhedral pyrite is much less abundant than euhedral pyrite, and is largely confined to the rhyolitic rocks and the siliceous sinter. It is classified as a primary form of pyrite because its form is preserved and is recognizable through the alignments of inclusions, or colour zoning, resulting from secondary overgrowths (Plate 13A).

Anhedral pyrite commonly forms layers (up to 4mm thick), or clusters (up to 5mm in diameter) in the rhyolitic rocks, and the siliceous sinter. Individual grains vary in size from 0.01 mm to 2mm. The general appearance of this pyrite is illustrated in Plates 13B and 13C.

5.2.2.3 Framboidal pyrite

The framboidal pyrite has a concentric shell-like, or atoll-like, forms, or the form described by Ramdohr (1969) as small cockades. It is present mainly in mineralized specimens from the

PLATE 13

Photomicrographs of Anhedral and Framboidal Pyrite.

A : From borehole M10 at 1608 feet depth, field of view 0.09x0.11mm, oil immersion.

Primary anhedral grains of pyrite (py), with colour zoning due to secondary overgrowths. Aligned inclusions outline the primary grain boundaries.

B : From borehole H14 at 265 feet depth, field of view 1.46x1.67mm, air.

Cluster of anhedral pyrites, partly replaced by quartz.

C : From borehole H43A at 1850 feet depth, field of view 1.46x1.67mm, air.

Anhedral pyrite grains, partly replaced by quartz.

D : From borehole C4 at 960 feet depth, field of view 0.15x0.17mm, oil immersion.

Framboidal pyrites, showing composite pyrite microcrysts.

E : From borehole M10 at 1608 feet depth, field of view 0.09x0.11mm, oil immersion.

Framboidal pyrites, partly replaced by quartz. Note variation in size of the framboids.

F : From borehole H4 at 474 feet depth, field of view 0.37x0.42mm, air.

Cluster of recrystallized pyrite framboids. The outer zone is due to overgrowths.

PLATE 13

A

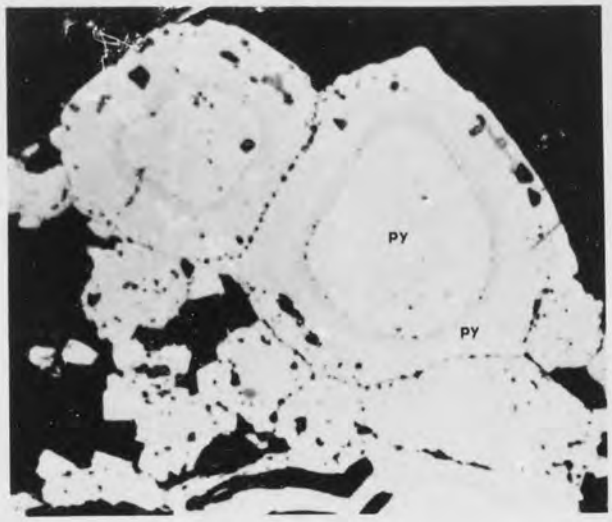

B

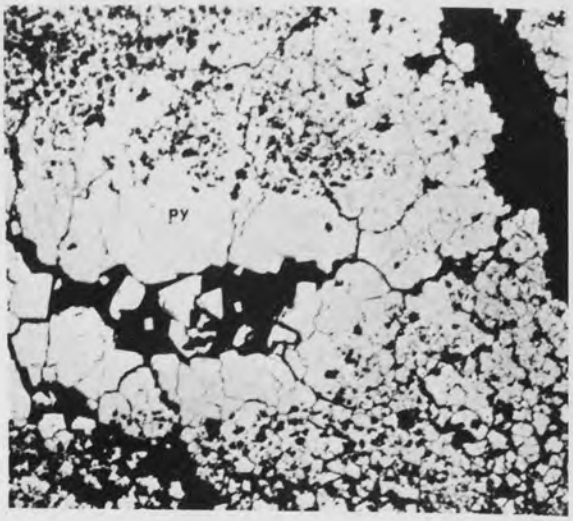

C

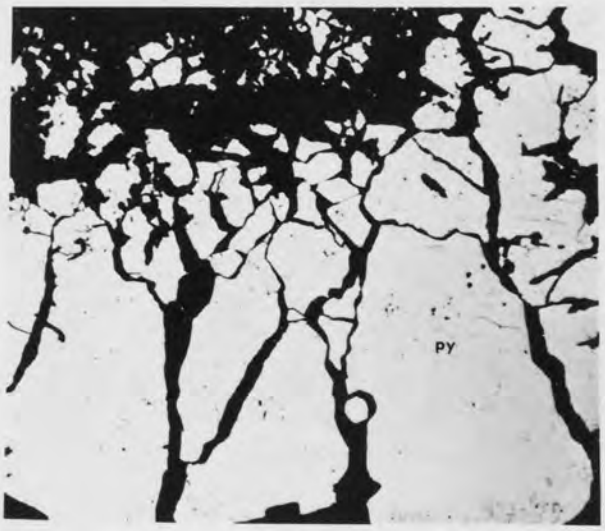

D

E

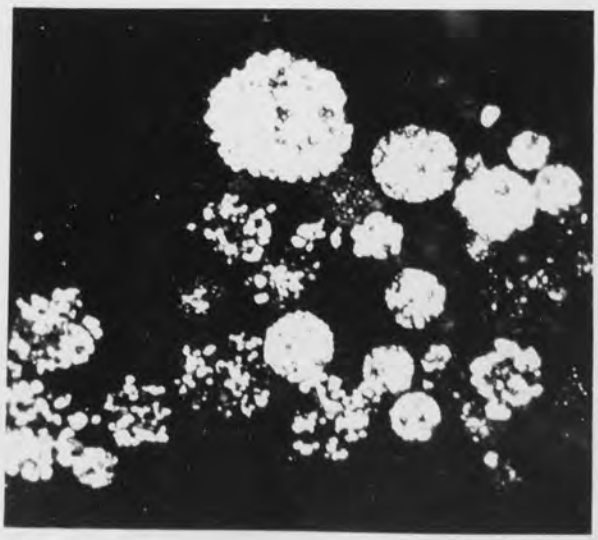

F

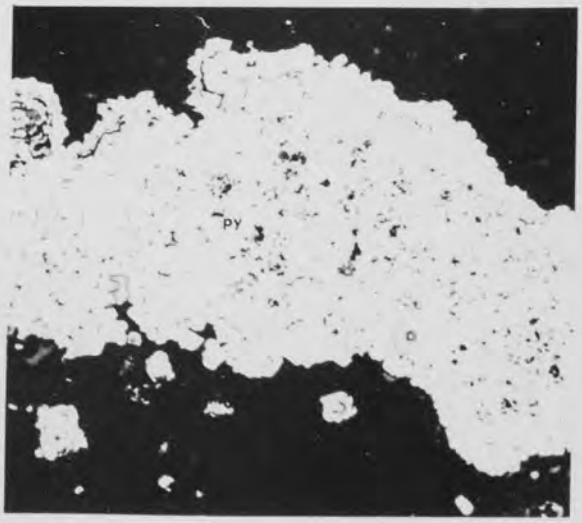

PLATE 14

Photomicrographs of Framboidal Pyrite.

A : From borehole M10 at 1540 feet depth, field of view 0.15x0.17mm, oil immersion.

Framboidal pyrite (py) showing a radiating texture produced by recrystallization.

B : From borehole M10 at 1608 feet depth, field of view 0.15x0.17mm, oil immersion.

Cluster of framboidal pyrites, associated with some euhedral pyrite crystals. Some framboids are partly replaced by quartz and show atoll-like textures.

C : From borehole H16 at 367.4 feet depth, field of view 1.46x1.67mm, transmitted light, plane polarized light.

Cluster of framboidal pyrites (black) in which recrystallization, or secondary overgrowths, have affected the outer part of the cluster. The inner part has been partly replaced by quartz (white) producing atoll-like textures.

D,E,F : From borehole H4 at 474 feet depth, field of view 0.37x0.42 mm, air.

D : Cluster of recrystallized framboidal pyrites (py) with secondary overgrowths, which has been partly replaced by galena (gn) and sphalerite (sl).

E : Framboidal pyrite grains (py), after recrystallization, some are replaced by galena (gn) (those on the left hand side of the photograph), and later galena has filled the spaces between the framboids. Sphalerite (sl) is also present in this section.

F : Cluster of framboidal pyrites, showing selective replacement by galena (gn) producing rings of galena in the framboids. Sphalerite (sl) has filled some spaces between the framboidal grains.

PLATE 14

A

B

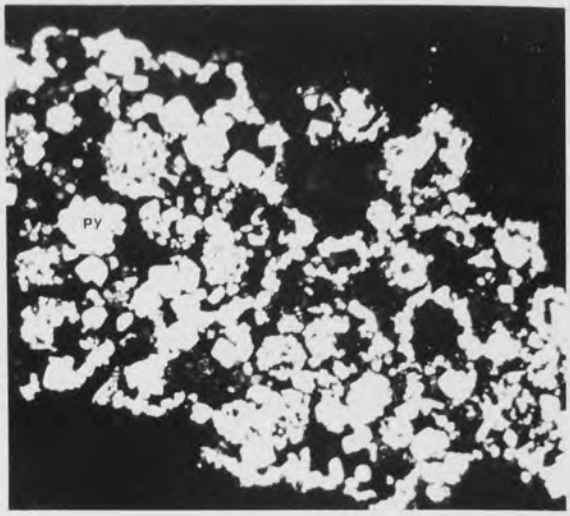

C

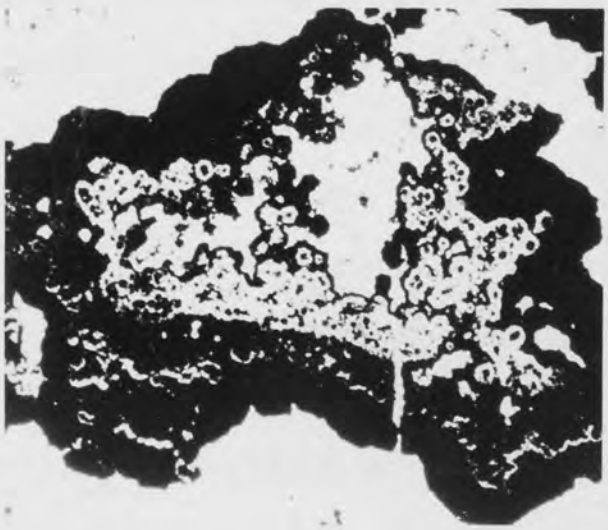

D

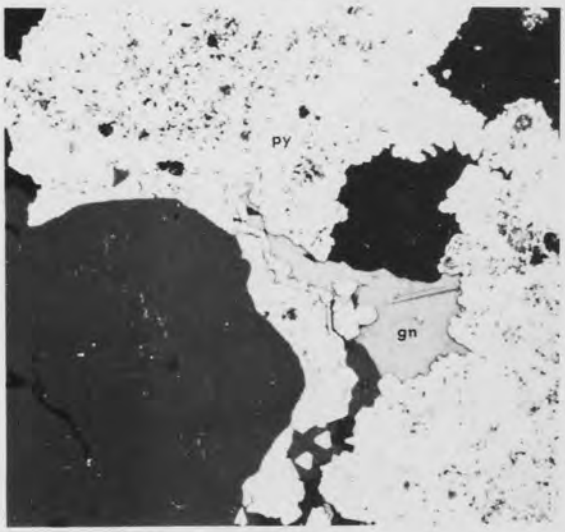

E

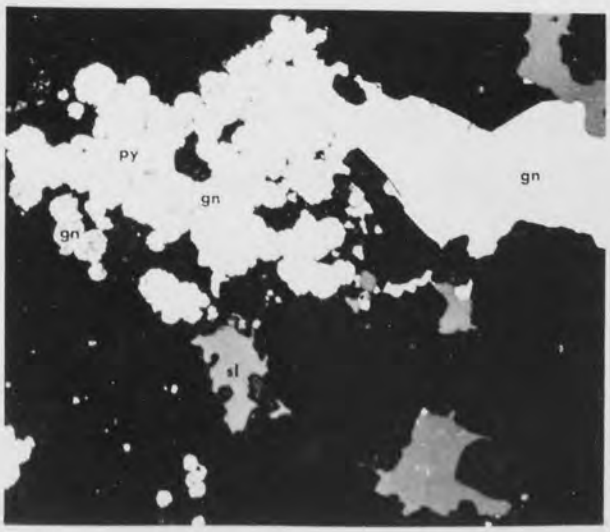

F

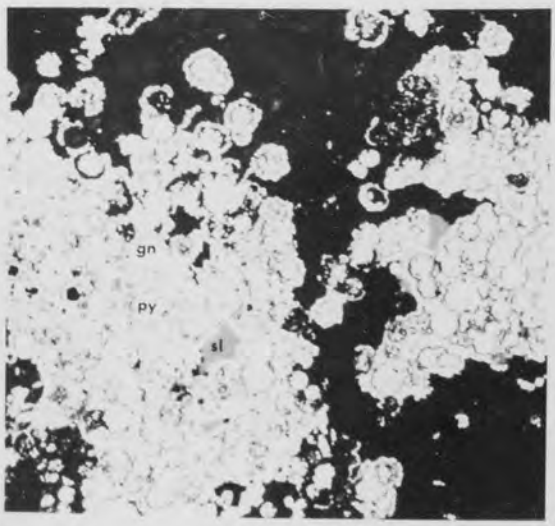

siliceous sinter. The size of the framboids varies from 0.005 up to 0.02mm and the most common size is 0.009mm. It occurs as spherical masses made up of pyrite microcrysts about 0.001mm in size (Plates 13D and E). The framboids occur as clusters, over which secondary overgrowths are commonly developed, producing a mass of pyrite studded with inclusions (Plate 13F). Secondary overgrowths developed over a single framboidal grain, produce a pseudo-radiating form, consisting of tabular pyrite crystals growing outward from the centre of the original framboid (Plate 14A). Framboids also form clusters accompanied by euhedral pyrite grains (Plate 14B). When framboidal clusters are not closely packed,and secondary overgrowths are not developed, replacement by quartz, produces atoll-like, or cockade textures (Plate 14C). A similar texture is observed in a cluster of framboids which has developed secondary overgrowths, and has later been replaced by other sulphide minerals such as galena, sphalerite, and chalcopyrite. When secondary overgrowths are well developed in the framboids, replacement by other sulphides is restricted and only develops either along the edge of the cluster (Plate 14D), or filling the interstices between the framboids (Plate 14E). Where secondary overgrowths and/or recrystallization are poorly developed the framboids are commonly partly or almost totally replaced by galena (Plates 14F and 15A). When either or both secondary overgrowths and recrystallization are not well developed, replacements by other sulphides produce textures similar to quartz replacements, e.g. the atoll-like texture of framboidal pyrite with chalcopyrite (Plates 15B, C, and D), and with sphalerite (Plates 15E and F).

PLATE 15

Photomicrographs of Framboidal Pyrite.

A : From borehole M4 at 474 feet depth, field of view 0.09x0.11mm, oil immersion.

Cluster of framboidal pyrites (py), almost completely replaced by galena (gn).

B,C : From borehole M10 at 1548 feet depth, field of view 0.15x0.17 mm, oil immersion.

B : Chalcopyrite (cp) replacing cores of framboidal pyrite grains (py).

C : Atoll-like textures in chalcopyrite (cp) matrix, produced by replacement of framboids (py) by chalcopyrite. Black is gangue.

D,E : From borehole M10 at 1584 feet depth, field of view 0.37x0.42 mm, oil immersion.

D : Chalcopyrite (cp) replacing and pseudomorphing a pyrite (py) cluster. Galena (gn) is also present in the specimen.

E : Sphalerite (sl) replacing the core of a pyrite framboid (py) with chalcopyrite (cp) partly enclosing the framboidal grain.

F : From borehole M10 at 1584 feet depth, field of view 0.15x0.17mm, oil immersion.

Atoll-like textures of pyrite (py) in sphalerite matrix.

PLATE 15

A

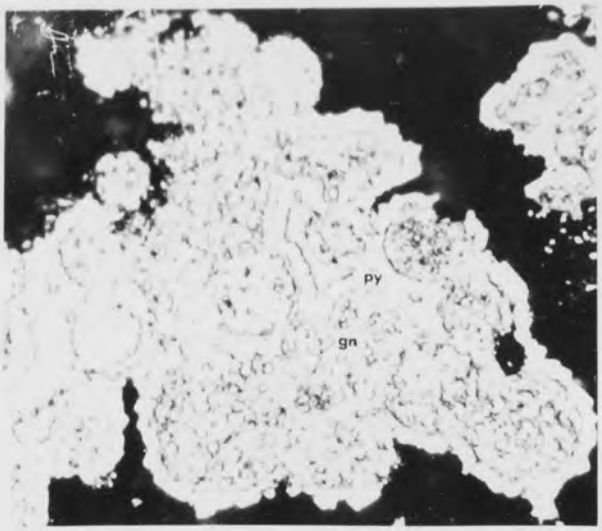

B

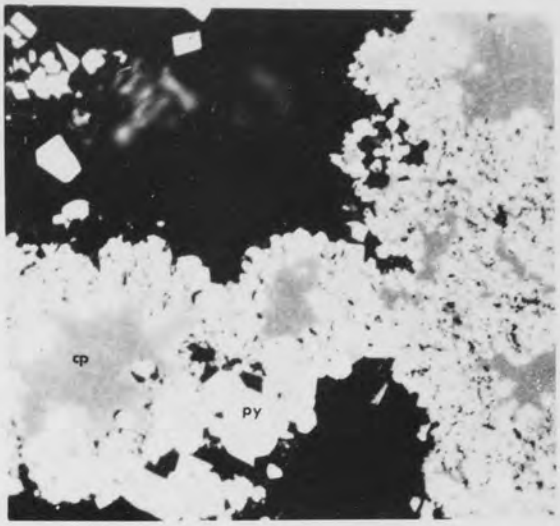

C

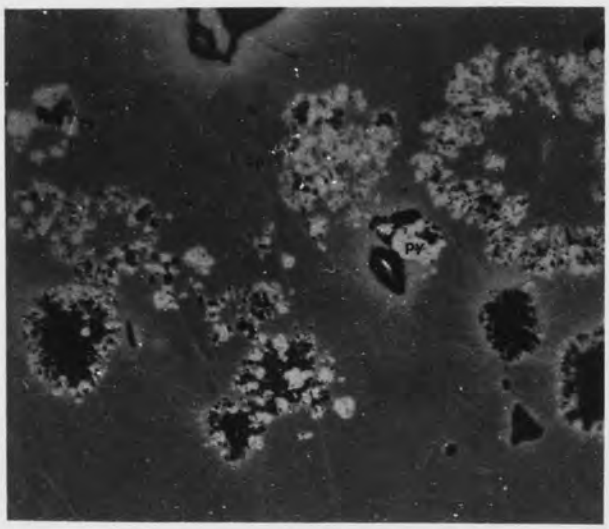

D

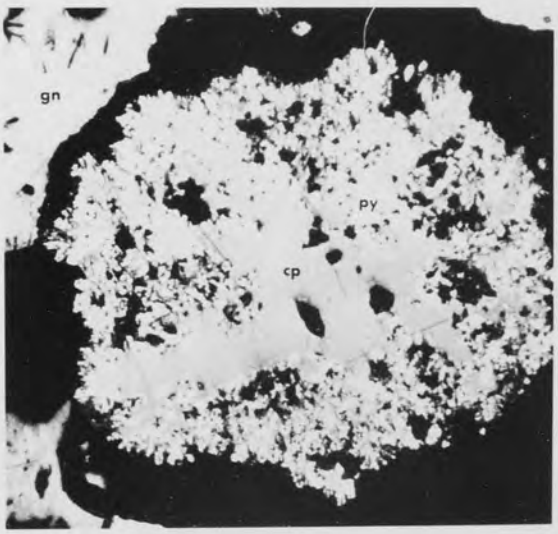

E

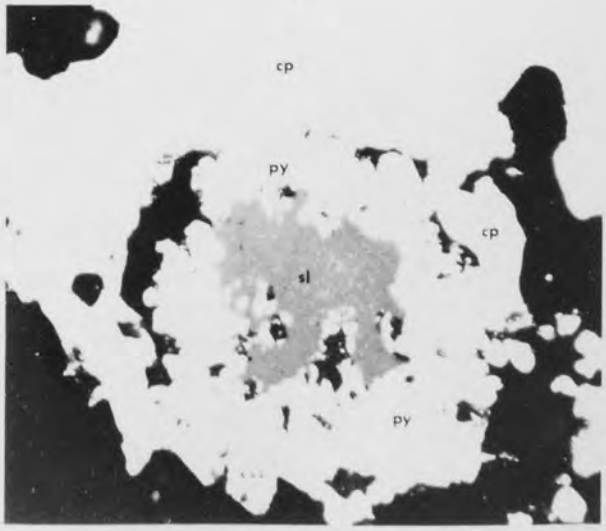

F

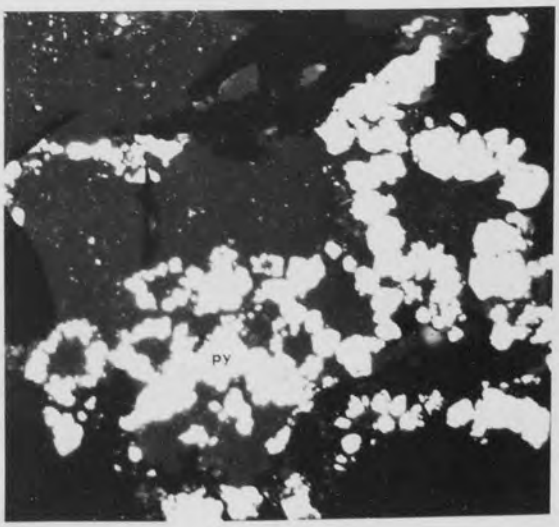

PLATE 16

Photomicrographs of Colloform Pyrite.

A,B,C,D : From borehole IM9 at 102 feet depth, field of view 1.46x 1.67mm, air.

General appearance of colloform pyrites.

E,F : From borehole IM9 at 102 feet depth, field of view 0.15x 0.17mm, oil immersion.

E : Radiating form of colloform pyrite, showing broken outer layers.

F : Secondary overgrowths of pyrite over an original radiating form of colloform pyrite. Note the tabular crystals of pyrite aligned in a radial manner.

PLATE 16

A

B

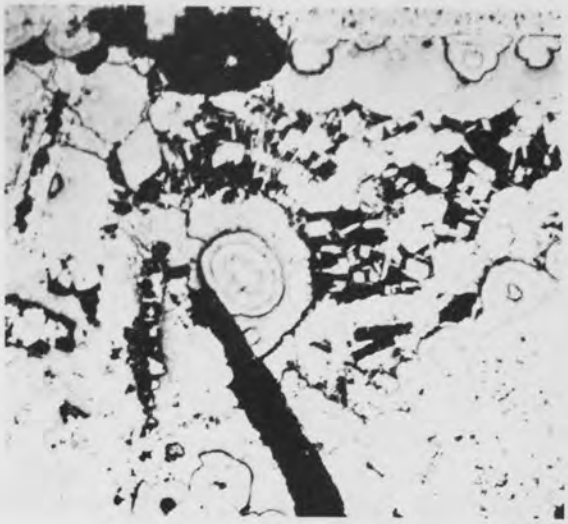

C

D

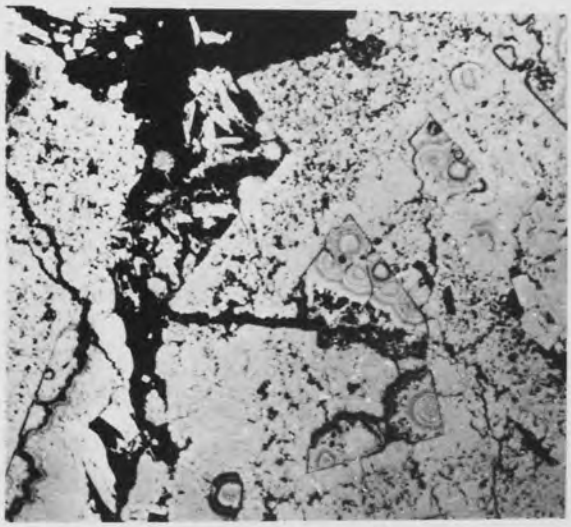

E

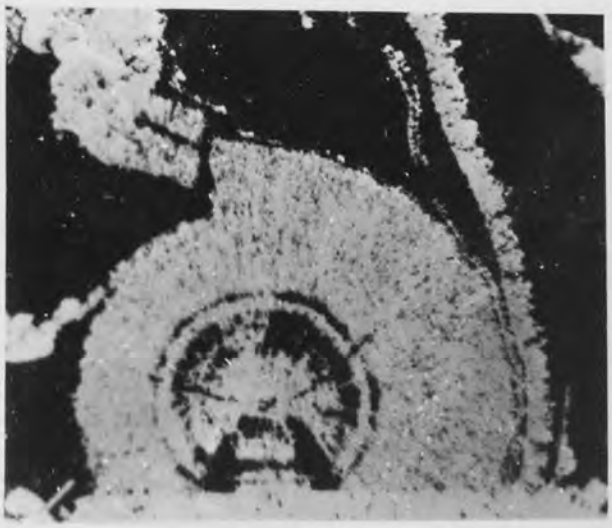

F

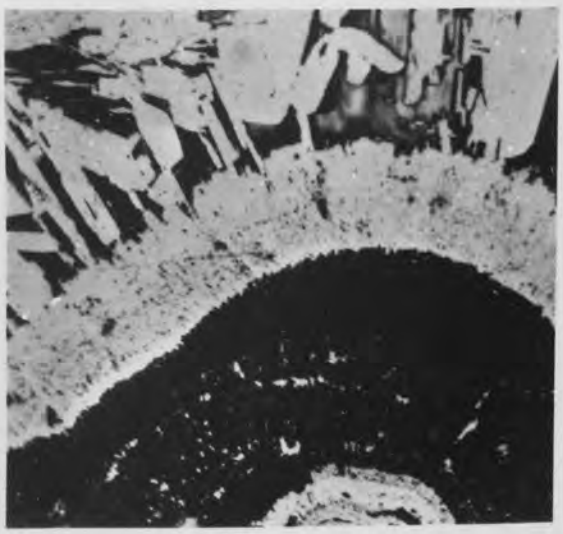

Wheatley (1971a) made a size distribution analysis of apparent framboidal pyrite diameters which gave a maxima at 0.0068mm. He also measured the size variation of the microcrysts in the framboids and showed it to range from 0.0005 to 0.002mm. These sizes and distributions agree with measurements made in the present study.

5.2.2.4 Colloform Pyrite.

Colloform pyrite is probably the result of colloidal precipitation (Ramdohr, 1969) and commonly has botryoidal, concentrically layered, radiating, or rhythmically layered forms. The term 'colloform', as used here, also includes the forms of pyrite identified by Ramdohr (1969) as melnikovite pyrite. Wheatley (1971a) stated that colloform textures, resulting from overgrowths on crystalline pyrite are common and described the presence of melnikovite pyrite but did not give any examples. However, in the present study colloform pyrite was found only in some specimens of mineralized rhyolitic rocks (IM9 at 47ft and IM9 at 102ft), and siliceous sinter (M10 at 1608ft), although it is likely that colloform pyrite is common in the mineralized zones within these rhyolitic rocks and the siliceous sinter. Although it was found in only a few specimens, a number of colloform fabrics are well-developed, especially in a specimen from borehole IM9 at a depth of 102 feet. In this specimen textures similar to those described as melnikovite pyrite by Ramdohr (1969) are present. The botryoidal and concentrically layered textures are illustrated in Plates 16A, B, C, and D. Plate 16E shows a pyrite with a radiating form in which the outer layers are fractured, and this was probably followed by quartz replacement. Plate 16F shows

overgrowths of pyrite on an originally radiating form, in which later pyrite crystals are also aligned in a radiating manner. Rhythmically-layered forms are also present (Plates 17A and B) as are secondary overgrowths with subhedral pyrite grains aligned concentrically around a colloform pyrite core (Plate 17C). In some specimens the rhythmically-layered pyrite is developed over clusters of pyrite crystals (Plates 17D, E, and F).

The three different ages of pyrite is seen in these specimens. The youngest (pyrite 3) is that of overgrowths on, and replacements of, the colloform pyrite (Plates 18A, B, and C). The oldest is represented by crystalline clusters of pyrite grains (pyrite 1) overgrown by colloform pyrite (Plates 18D and E), which represents the second formation (pyrite 2).

The layering in the colloform pyrite is picked out by colour differences, and by the presence of inclusions. Generally, two types of pyrite form the layering, one is bright yellow and inclusion-free, and the other is brownish yellow with numerous inclusions (Plate 18F). The alternating (rhythmic) deposition of the two forms produces the layering effects.

5.2.2.5 Secondary Overgrowths.

At Parys Mountain secondary overgrowths of pyrite are very common, and are associated with all forms of primary pyrite. As previously mentioned, pyrite is strongly idiomorphic, and this is also true of the overgrowths. These textures are illustrated in Plates 19A and B, where secondary overgrowths are developed over primary euhedral pyrite grains. Plate 19A shows primary, cubic,

PLATE 17

Photomicrographs of Colloform Pyrite.

A : From borehole IM9 at 102 feet depth, field of view 0.37x0.42 mm, air.

Colloform pyrite, showing concentric colour layering.

B : From borehole IM9 at 102 feet depth, field of view 0.15x0.17 mm, oil immersion.

Colloform pyrite, showing concentric form of rhythmic layering.

C : From borehole IM9 at 102 feet depth, field of view 0.29x0.33 mm, air.

Secondary overgrowths of subhedral pyrite grains aligned concentrically around a colloform pyrite core.

D,E,F : From borehole IM9 at 102 feet depth, field of view :

D : 1.46x1.67mm , air.

E : 0.37x0.42mm , air.

F : 0.15x0.17mm , oil immersion.

Development of various forms of rhythmic layering of colloform pyrite over pyrite 1.

PLATE 17

A

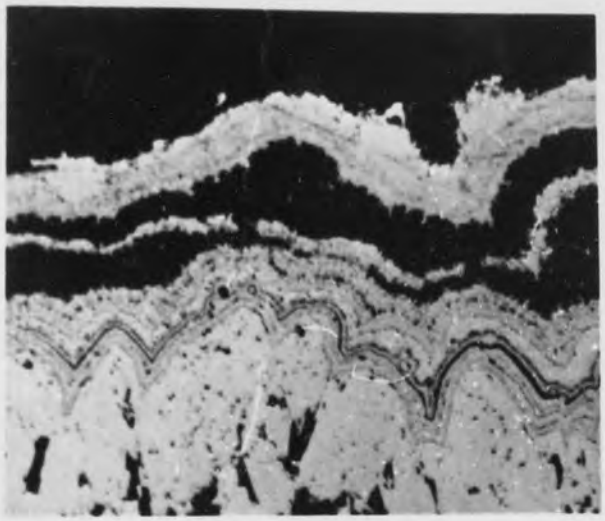

B

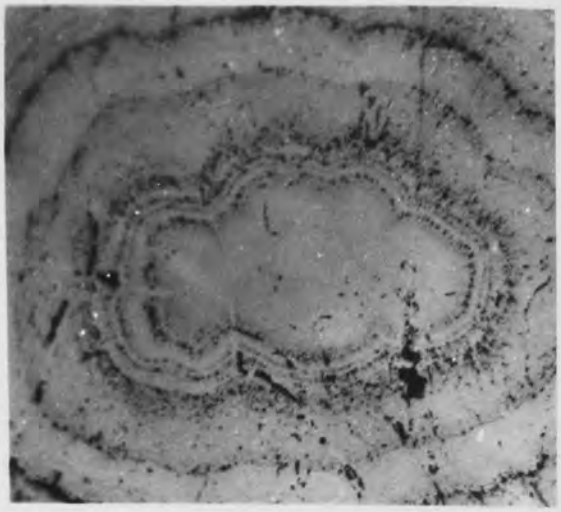

C

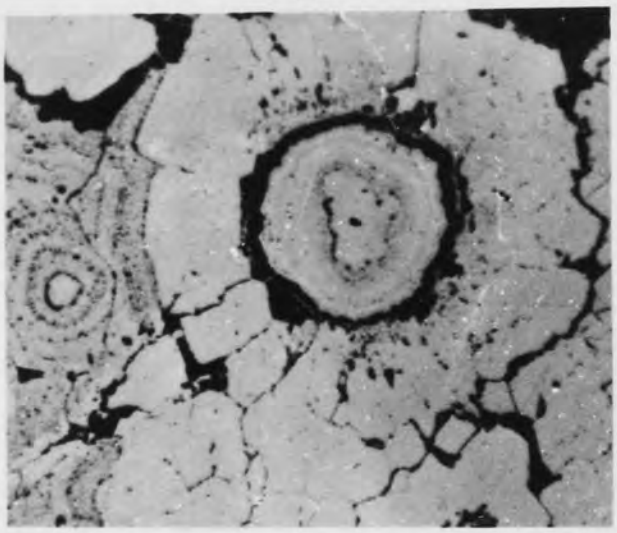

D

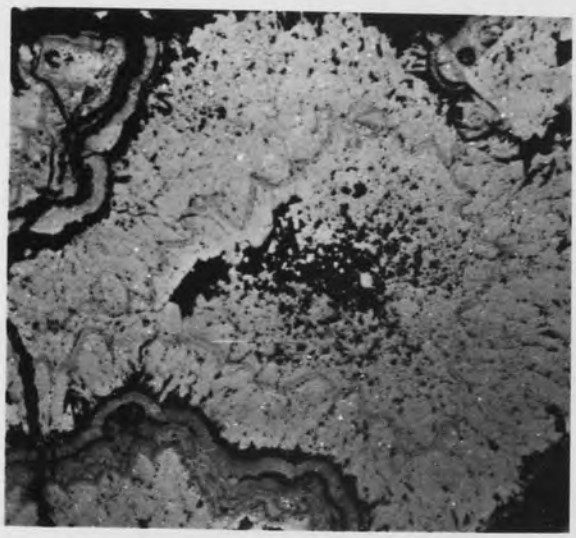

E

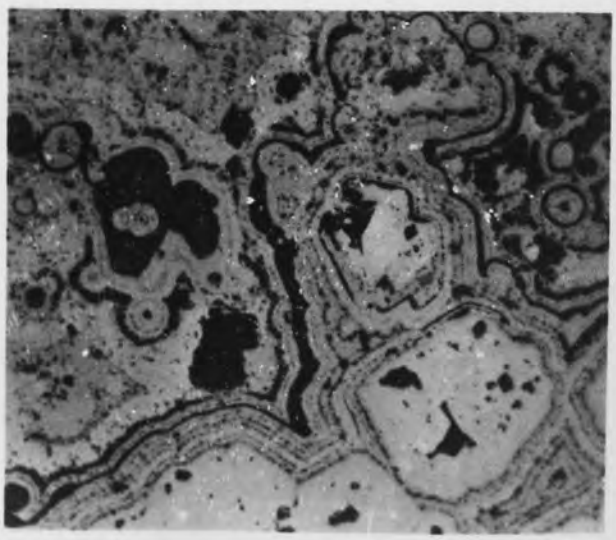

F

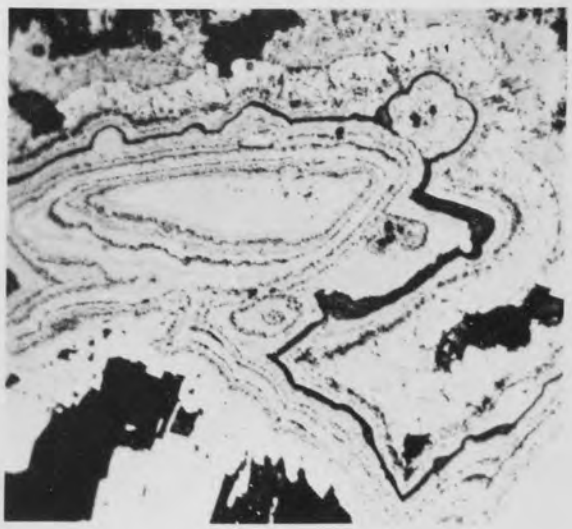

PLATE 18

Photomicrographs of Colloform Pyrite.

A,B : From borehole IM9 at 102 feet depth, field of view 0.15x0.17 mm, oil immersion.

A : Replacement of colloform pyrite by later pyrite.

B : A fragment of colloform pyrite being partly replaced (1) and overgrown (2) by later pyrite.

C : From borehole IM9 at 102 feet depth, field of view 0.29x0.33 mm, air.

Overgrowths of younger pyrite on fragments of colloform pyrite.

D,E : From borehole IM9 at 102 feet depth, field of view :
D : 0.37x0.42mm, air.
E : 0.73x0.83mm, air.

Colloform pyrite overgrown on older pyrite (1), and later a younger pyrite (2) has replaced both the colloform and the earlier pyrite.

F : From borehole IM9 at 102 feet depth, field of view 0.15x0.17 mm, oil immersion.

Two phases of pyrite 2, the one on the left is bright yellow and inclusion-free, the other, on the right, is brownish yellow and contains numerous inclusions (gangue). Marcasite (M) is also present in the plate.

PLATE 18

A

B

C

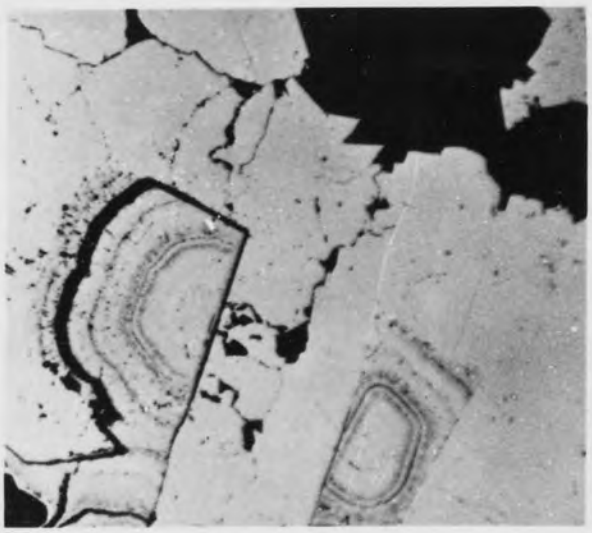

D

E

F

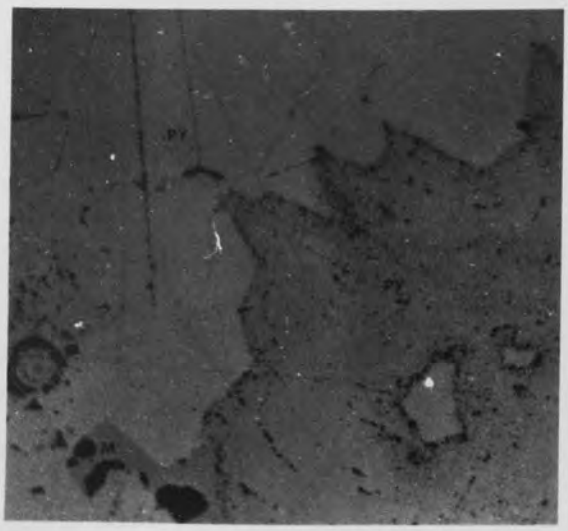

euhedral pyrite, in which colour zoning is present, and a secondary overgrowth forms an incomplete six-sided crystal outline over the original crystal. Secondary overgrowth forms with more or less cubic crystal outline superimposed over primary cubic grains, but with a different orientation (Plate 19B). Primary pyrite grains are also commonly recognizable through the alignment of inclusions, and by the occurrence of aligned galena and chalcopyrite grains replacing the pyrite. Where secondary overgrowths are developed over several closely packed grains of primary pyrite, a massive patch of pyrite is formed.

Secondary overgrowths of pyrite produce textures other than euhedral crystal outlines, if the environment was not favourable for free growth. This is exemplified by Plates 19C and D, where secondary overgrowths formed as 'spongy' pyrite over a primary euhedral pyrite grain. This is probably due to the depositional temperature which, if low (less than 100°C) would precipitate pyrite rapidly from the ore solutions thus not produce a euhedral form. Another explanation is that the primary pyrite grains were embedded in a fine grained sediment (for example shale, or, in this instance, tuffaceous rhyolite), and subsequently, the secondary overgrowths were developed during later diagenetic processes in the sediment. Intergrowths of pyrite and sedimentary particles would then produce the spongy pyrite.

When the supply of 'FeS_2' in the ore solution is limited, secondary overgrowths tend to develop on a preferred part of the primary grain, e.g. faces which have a particular orientation (Plate 19E); or along the edges or corners of the primary grains, which were most exposed to the solution (Plate 20A). In some instances

PLATE 19

Photomicrographs of Secondary Overgrowths in Pyrite.

A : From borehole M10 at 1540 feet depth, field of view 0.15x0.17 mm, oil immersion.

Secondary overgrowths on a formerly cubic pyrite crystal producing an incomplete six-sided crystal. A haematite (h) inclusion, and indications of replacement by galena (gn) and chalcopyrite (cp) are present.

B : From borehole H4 at 474 feet depth, field of view 0.73x0.83mm, air.

Secondary overgrowths on a euhedral pyrite (py). The primary crystal form is observed through alignment of gangue inclusions, and selective replacement by galena (gn). Chalcopyrite (cp), and sphalerite (sl) are present in the overgrowths.

C,D : From borehole IM9 at 365.3 feet depth, field of view 0.15x0.17mm, oil immersion.

Secondary overgrowths on euhedral pyrite grains (py) by 'spongy' pyrite. Chalcopyrite (cp) is present as inclusions in euhedral pyrite grains.

E : From borehole M10 at 1540 feet depth, field of view 0.15x0.17 mm, oil immersion.

Secondary overgrowths of pyrite (py) along a preferred direction, east-west of the plate. Haematite (h), and chalcopyrite (cp) are present as inclusions.

PLATE 19

A

B

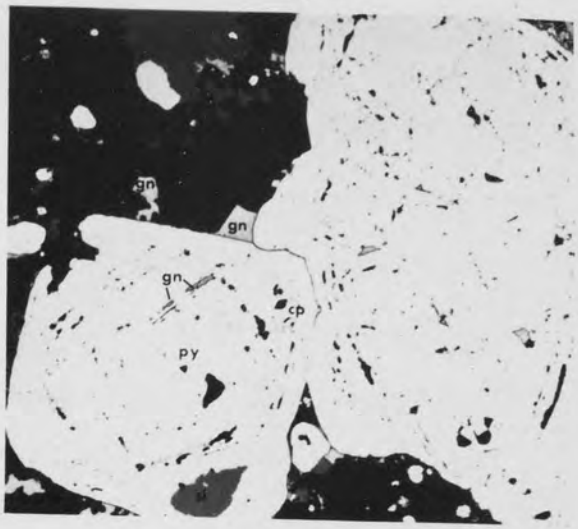

C

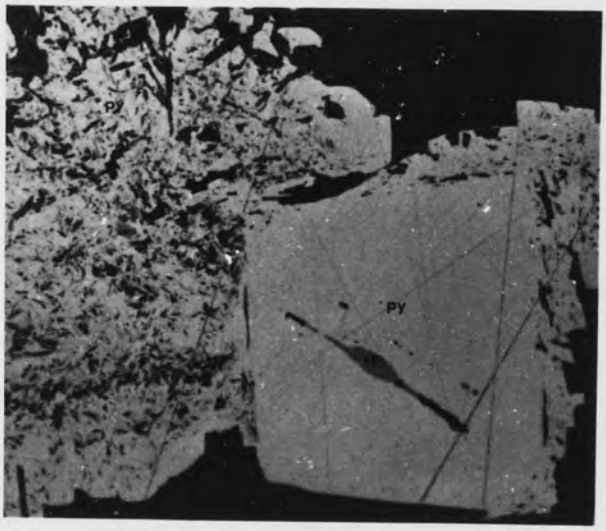

D

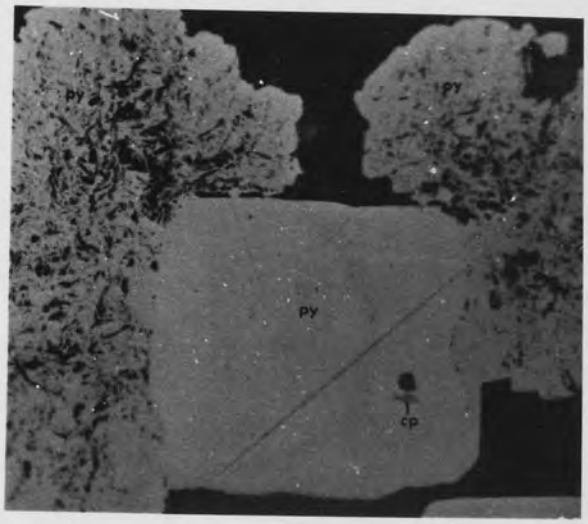

E

skeletal crystals of pyrite are formed (Plate 20B) (Ramdohr, 1969).

In some instances secondary overgrowths form euhedral outlines over framboidal pyrite grains (Plate 20C). Growth is away from the core of the framboid, which is, sometimes left unfilled and acts as a preferred site for later replacement by other minerals, e.g. chalcopyrite (Plate 20D). If the cores are filled, subsequent replacement occurs between the original grain and the overgrowth (Plate 20E).

Secondary overgrowths are commonly defined by colour layering in the pyrite grains and in some instances the primary crystal form is clearly seen (Plate 20F). More complicated overgrowths occur where inclusions in the pyrite grains have an irregular alignment, probably along original grain boundaries (Plate 21A). Euhedral overgrowths of pyrite over original euhedral grains of other minerals are common, e.g. overgrowths over quartz (Plate 21B).

5.2.2.6 Crystal Corrosion.

Corroded pyrite grains are commonly due to alteration of the host rocks by barren hydrothermal solutions. Primary euhedral pyrites in the dacitic rocks and slates are commonly corroded around their boundaries (Plates 21C and E). Other grains are corroded on the inside (Plate 21D).

Corrosion along edges of massive pyrite grains produces spongy pyrite (Plates 22A and B). The spongy pyrite which is developed along grain boundaries, hence can be distinguished from that produced as a result of secondary overgrowths (cf. Plates 19C and D) which is spongy throughout.

PLATE 20

Photomicrographs of Secondary Overgrowths and Recrystallization of Pyrite.

A : From borehole IM9 at 47 feet depth, field of view 0.04x0.05mm, oil immersion.

Incomplete secondary overgrowths on a euhedral pyrite crystal along sides, and one corner of the crystal.

B : From borehole IM9 at 102 feet depth, field of view 0.15x0.17mm, oil immersion.

Skeletal pyrite produced by secondary overgrowths on quartz and/or recrystallization of pyrite.

C : From borehole IM9 at 47 feet depth, field of view 0.37x0.42mm, air.

Secondary overgrowths on recrystallized framboidal pyrite.

D : From borehole M10 at 1630 feet depth, field of view 0.09x0.11mm, oil immersion.

Secondary overgrowths on a framboidal pyrite grain (py). Chalcopyrite (cp) has replaced the core, and some of the outer part of the framboid.

E : From borehole IM6 at 745 feet depth, field of view 1.46x1.67mm, air.

Primary framboids, with overgrowths and recrystallization, which have been selectively replaced by gangue to produce a shell-like texture.

F : From borehole IM9 at 102 feet depth, field of view 0.09x0.11mm, oil immersion.

Aligned inclusions and colour layering, in two overgrown pyrite (py) grains, indicating former crystal outlines. Marcasite (M) is present in the pyrite grains.

Facing page 82

PLATE 20

A

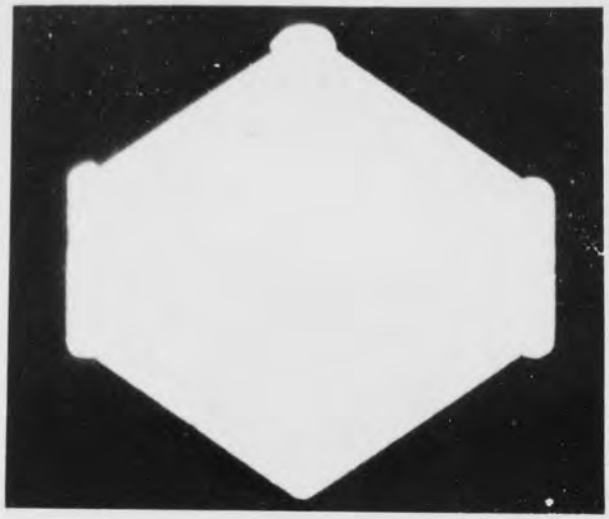

B

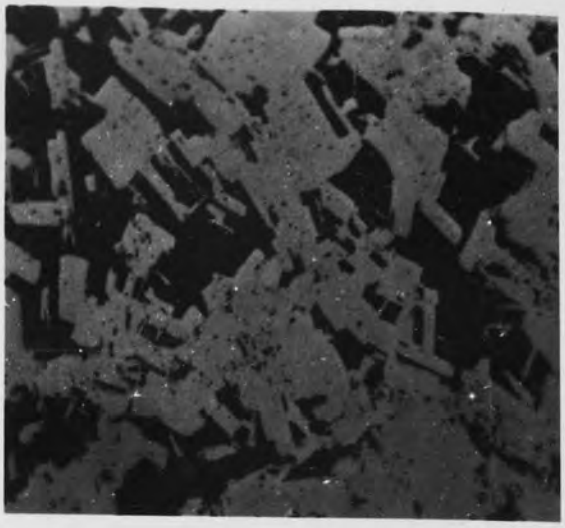

C

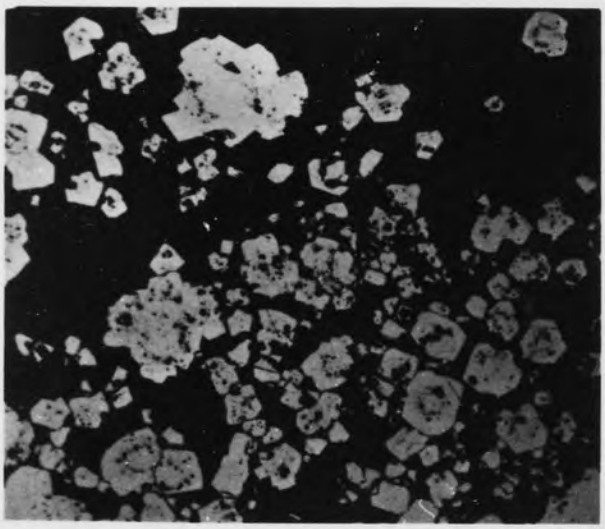

D

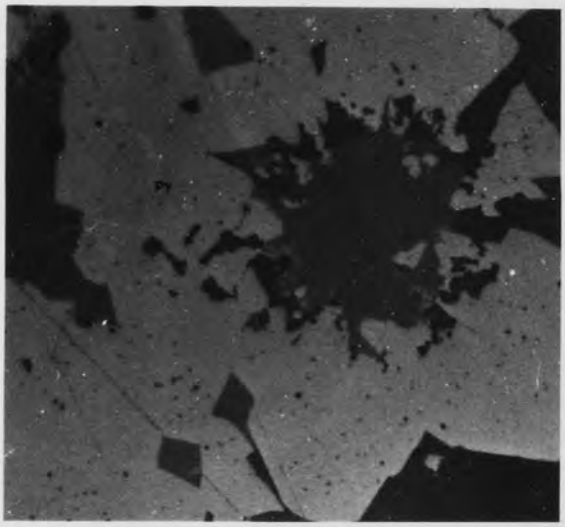

E

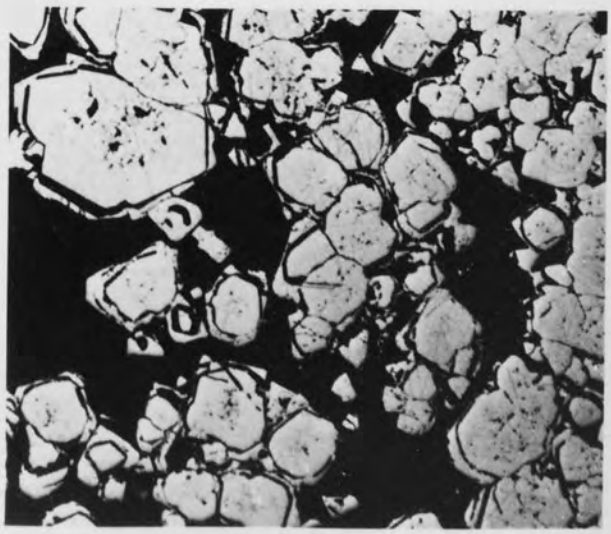

F

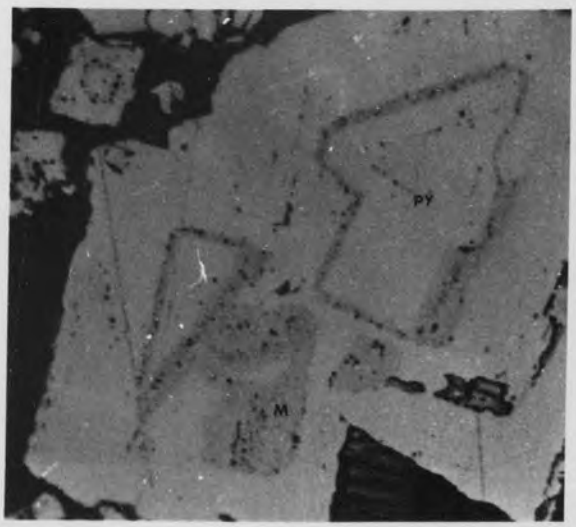

PLATE 21

Photomicrographs of Secondary Overgrowths and Corrosion in Pyrite.

A : From borehole IM9 at 47 feet depth, field of view 0.15x0.17mm, oil immersion.

Complex of overgrowths on formerly anhedral pyrite grains. Primary grain boundaries are marked by a concentration of aligned inclusions of gangue minerals.

B : From borehole IM9 at 47 feet depth, field of view 0.47x0.53mm, air.

Euhedral secondary overgrowths of pyrite (py) over earlier quartz crystals.

C : From borehole H43A at 1832 feet depth, field of view 1.46x1.67mm, air.

Corrosion of formerly euhedral pyrites (py) in dacitic rock matrix.

D : From borehole H43A at 1850 feet depth, field of view 1.17x1.33mm, air.

Corrosion affecting the inner part of formerly euhedral pyrite (py) grains, in dacitic rock matrix.

E : From borehole C4 at 755 feet depth, field of view 1.17x1.33mm, air.

Corroded euhedral pyrite (py) grain in slate, cut by a later carbonate vein.

PLATE 21

A

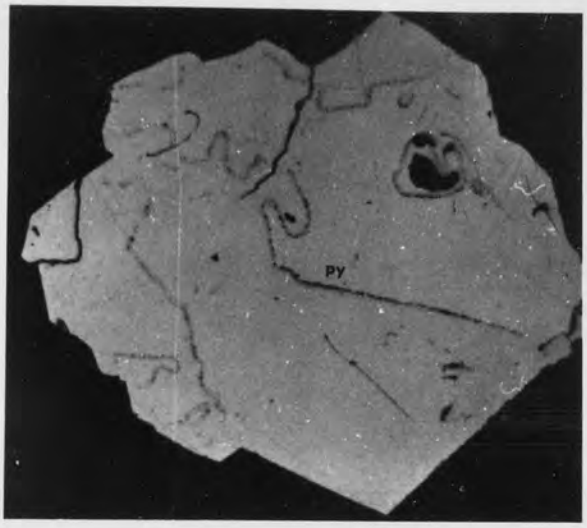

B

C

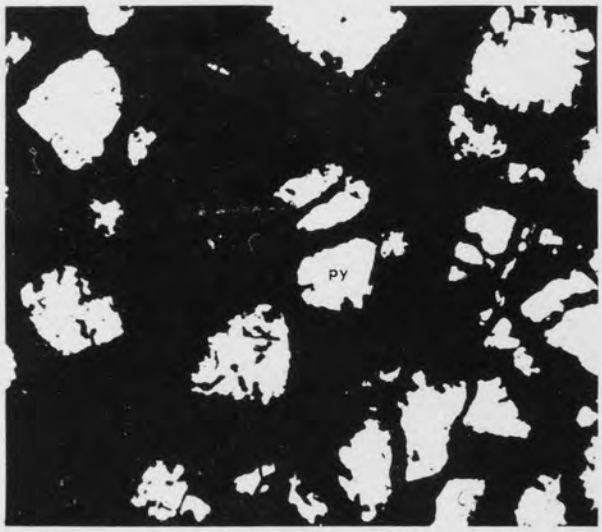

D

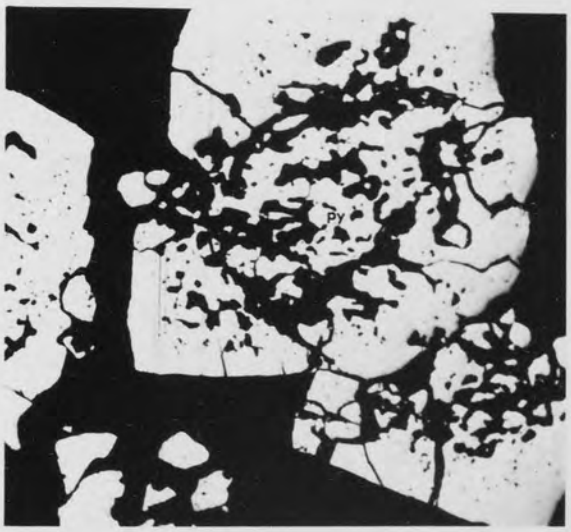

E

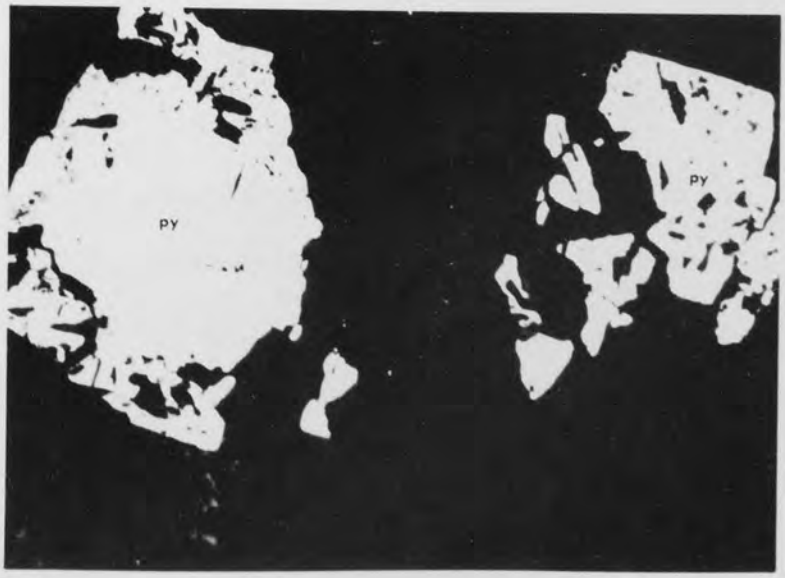

Irregular grain outlines due to corrosion are present in both pyrite 1 (Plates 21C, D, and E) and pyrite 2 (Plates 22A, B, C, and D). The matrix containing such grains is very varied, e.g. dacitic rocks (Plates 21C and D), Ordovician slates (Plate 21E), quartz (Plates 22A, B, and C), and sulphides (Plate 22D). Wheatley (1971a) described pyrites with corroded grain boundaries but found them only in a sulphide matrix.

5.2.2.7 Zoning.

Zoning is regarded as a texture resulting from, either changes in depositional conditions in a system from which the minerals being precipitated show solid solution, or variations in the chemical concentration of a component of the depositing solution, for a monomineralic system ('pure substances'). interruption of growth, and periodic changes in deposition of porous and dense bands, and deposition of sucessive bands with and without inclusions of foreign minerals can also produce zoning effects (Ramdohr, 1969). Like secondary overgrowths, zoning can be recognized from aligned inclusions, colour and reflectivity variations, and differences in hardness. Generally zoning is an indication of rapid growth at low temperatures from impure solutions (Ramdohr, 1969).

Zoning is very common, especially in pyrite 1. It is detected either by a use of the features described above (Plates 22E and F, 23A, B, C, and D), or through occurrence of selective replacement of the pyrite by later minerals, commonly chalcopyrite, galena, and sphalerite (Plates 23E and F). It is especially well seen after etching.

PLATE 22

Photomicrographs of Corrosion and Zoning in Pyrite.

A : From borehole IM6 at 1179 feet depth, field of view 1.46x1.67 mm, air.

Corrosion of pyrite (py) producing spongy pyrite around grain boundaries. Chalcopyrite (cp) is present as inclusions in pyrite grain.

B : From borehole IM6 at 1179 feet depth, field of view 0.37x0.42 mm, air.

Higher magnification of Plate A to show the general appearance of spongy pyrite.

C : From borehole H43A at 1832 feet depth, field of view 0.29x0.33mm, air.

Corroded pyrite (py) grain in quartz matrix.

D : From borehole M10 at 1548 feet depth, field of view 0.11x0.13mm, oil immersion.

Corroded pyrite (py) grain in sphalerite (dark grey) matrix, gangue is black. Galena (gn) is present as inclusions in both pyrite and sphalerite.

E,F : From borehole IM9 at 47 feet depth, field of view 0.09x0.11mm, oil immersion.

Colour zoning in euhedral pyrite, resulting from secondary overgrowths.

PLATE 22

A

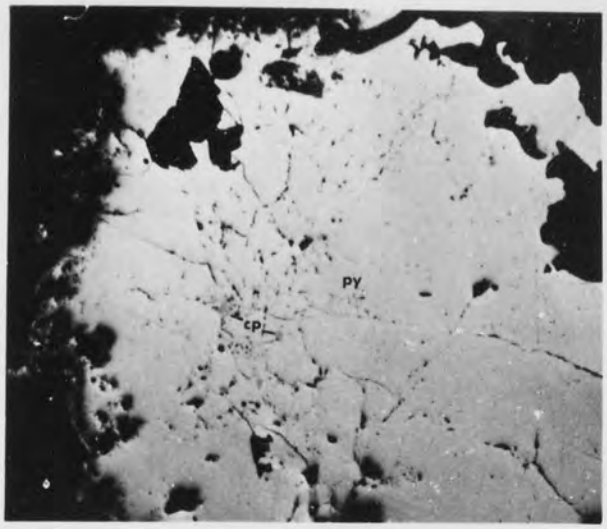

B

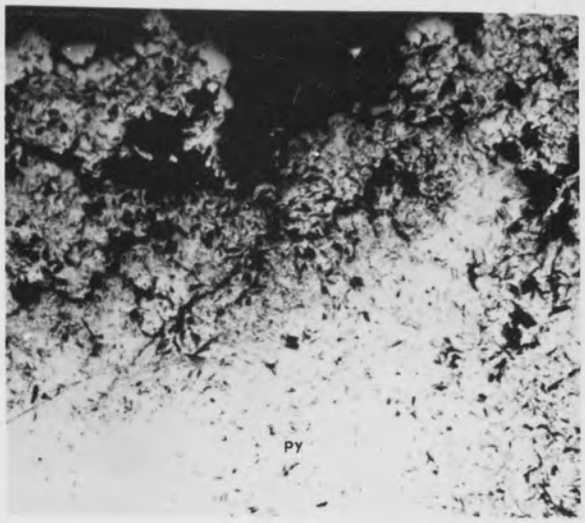

C

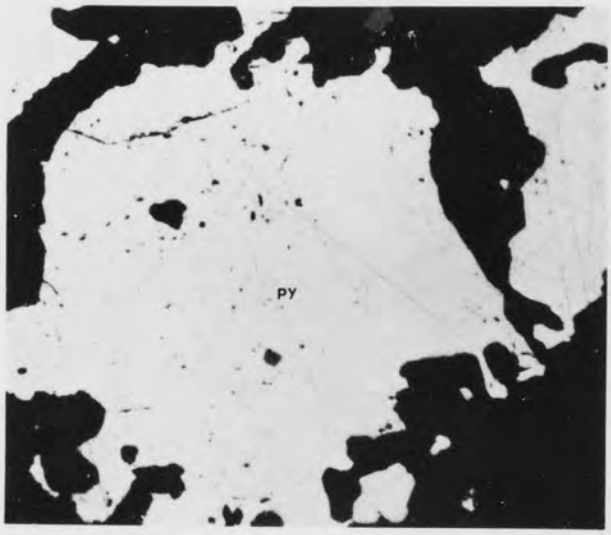

D

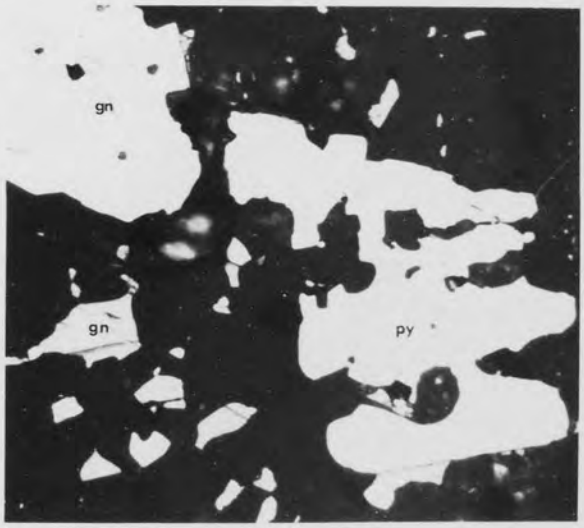

E

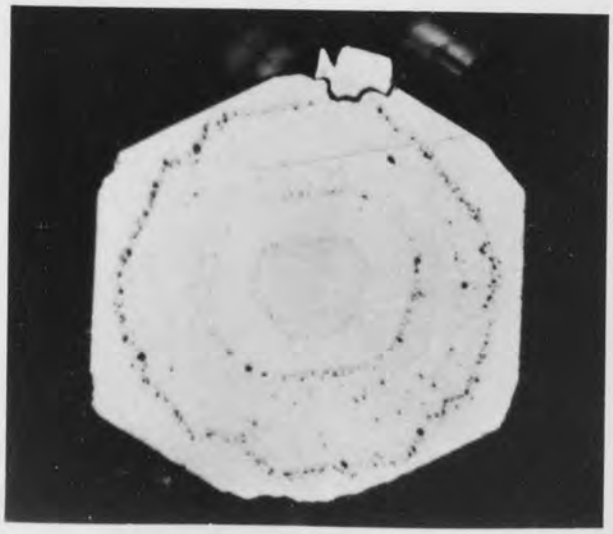

F

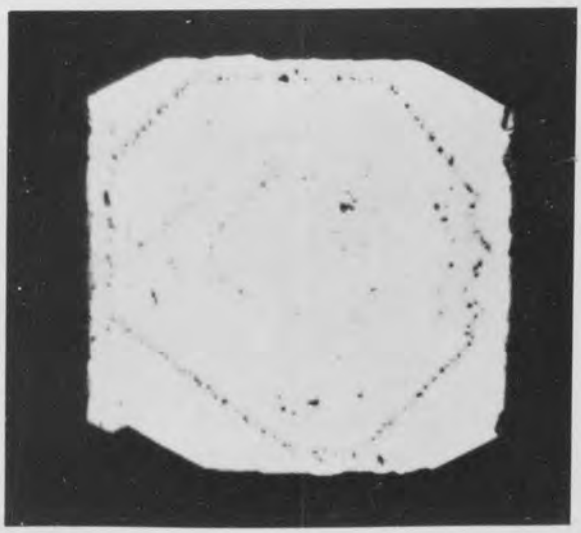

PLATE 23

Photomicrographs of Zoning in Pyrite.

A : From borehole C4 at 920 feet depth, field of view 1.46x1.67 mm, air.

Zoning in euhedral pyrite grains.

B : From borehole IM9 at 102 feet depth, field of view 0.37x0.42 mm, air.

Concentric zoning in colloform pyrites.

C,D : From borehole IM9 at 102 feet depth, field of view 0.09x0.11 mm, oil immersion.

Colour zoning in pyrites (py) with marcasite (M) cores.

E : From borehole H4 at 460 feet depth, field of view 0.37x0.42 mm, air.

Zoning in euhedral pyrite (py) grains with selective replacement by galena (gn). Chalcopyrite (cp) and sphalerite (sl) are also present as later development.

F : From borehole H4 at 460 feet depth, field of view 0.11x0.13 mm, oil immersion.

Selective replacement of euhedral pyrite (py) grains by galena (gn), and chalcopyrite (cp) outlining zoning.

PLATE 23

A

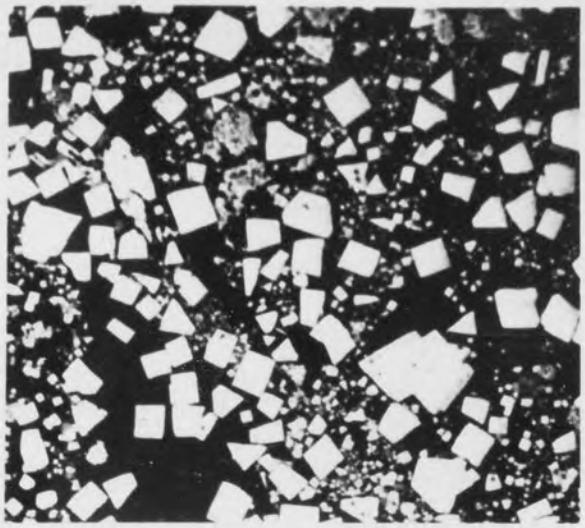

B

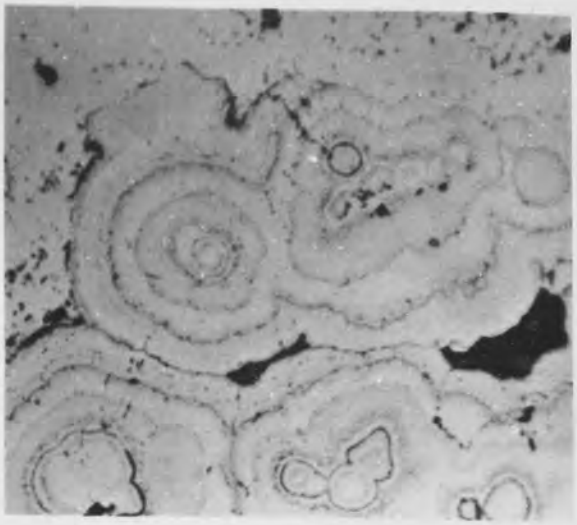

C

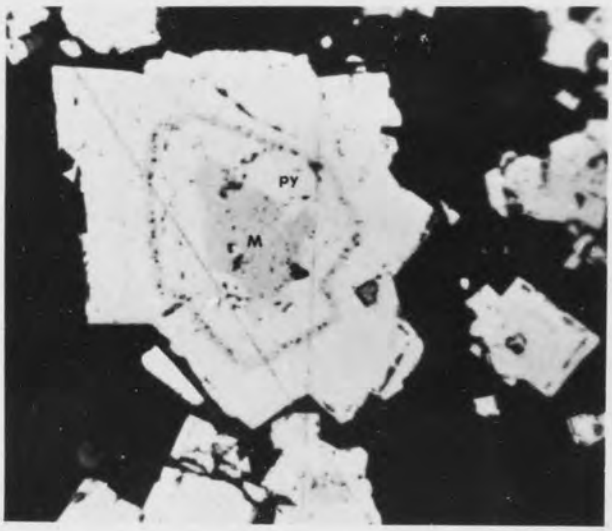

D

E

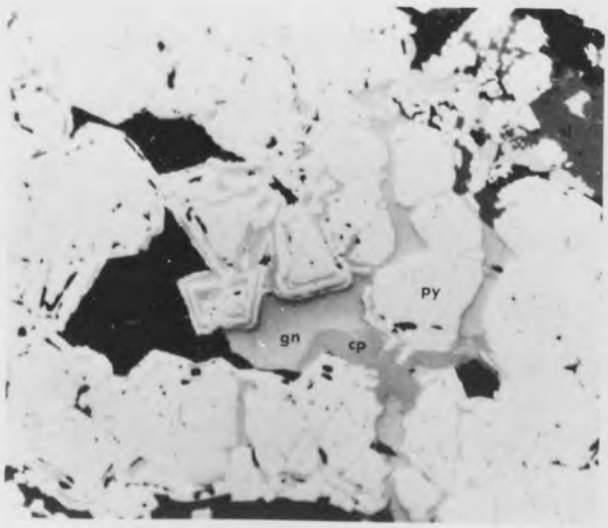

F

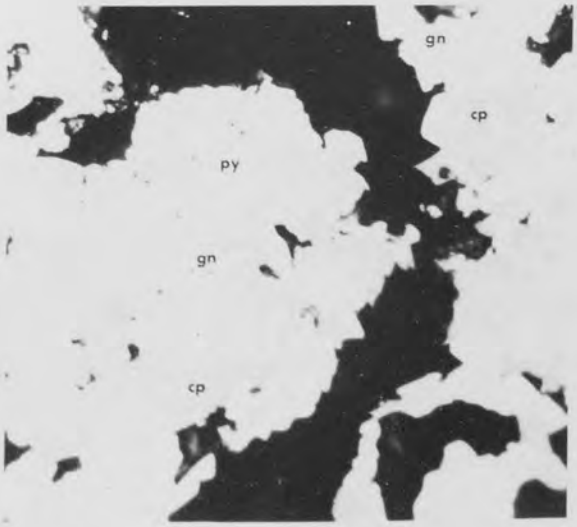

The zoning in pyrite at Parys Mountain is not developed in individual isolated grains but all pyrites in the same specimen show similar zoning, i.e. if zoning in a specimen is of the colour zoning type, or inclusion zoning type, then every grain in that specimen exhibits the same feature, and to the same degree.

Wheatley (1971a) recognized zoning in pyrite at Parys Mountain, but did not describe it, and stated that zoning is not as common as in the similar ores of Avoca.

5.2.2.8 Idioblastic and Poikilitic Textures.

These textures are formed during recrystallization of ore mixtures (Ramdohr, 1969), and result in the formation of euhedral crystals of pyrite (idioblasts) in a matrix of other sulphides, such as galena, chalcopyrite, or sphalerite. The pyrite idioblasts commonly contain inclusions of galena. In some instances chalcopyrite occurs as poikilitic intergrowths, giving the pyrite a poikilitic, or idioblastic sieve, texture (Plate 24A). This texture is not common, and is found only in the Bluestone ore type, and in some parts of the copper ore in the rhyolitic rocks and siliceous sinter. This texture has not previously been reported.

5.2.2.9 Cataclastic Textures.

Cataclastic textures occur in a number of specimens, where the pyrite is present as broken grains with numerous fractures filled with later sulphides (Plate 24B and C). Wheatley (1971a) stated that this texture was rare, and suggested that many of them were pseudo-cataclastic only occurring adjacent to fractures. In the specimens looked at in this study these textures were common,

especially in pyrite grains larger than 0.5mm. They are present where fractures are absent as well as adjacent to fractures. This is especially true of specimens from the rhyolitic tuffs. This texture also occurs in some euhedral, (pyritohedral) pyrite 1, grains, where the shattered grains have a matrix of Ordovician slate, or dacitic rock, and are associated with later unbroken euhedral grains (Plates 24D, E, and F).

5.2.2.10 Special Fabrics.

Pyrite forms pseudomorphs in some specimens where it partly replaces original crystals of unknown composition (Plate 25A), and spherulites in thr rhyolitic rocks, where it appears as a radiating mass (Plate 25B). Pyrite 'flame', or slump textures of fine grained pyrite, embedded in a matrix of rhyolitic tuff (Plate 25C) are considered to be early depositional forms of pyrite, probably of sedimentary (diagenetic) origin.

The youngest generation of pyrite, pyrite 3, which is closely associated with quartz veins, does not show secondary fabrics, such as overgrowths, colloform layering, zoning, and replacement. It is commonly present as euhedral to subhedral grains of 0.01 to 0.02mm size range, in veinlets, or stringers, and forms a maximum of 10 percent of the total pyrite in the rocks.

5.2.3 Marcasite.

Marcasite is probably the first mineral in paragenetic sequence, as it is replaced by the earliest generation of pyrite (pyrite 1). As stated by Ramdohr (1969), marcasite is easily altered

PLATE 24

Photomicrographs of Poikilitic Texture and Cataclastic Texture in Pyrite

A : From borehole M10 at 1548 feet depth, field of view 0.37x0.42mm, air.

Poikilitic texture in a pyrite (py) idioblast intergrown with galena (gn), chalcopyrite (cp), and sphalerite (sl). The tiny inclusion spots in the pyrite are of galena.

B : From borehole H43A at 1847 feet depth, field of view 1.46x1.67mm, air.

Cataclastic pyrite (py) with chalcopyrite (cp) infilling along cracks and cleavage planes.

C : From borehole H14 at 265 feet depth, field of view 1.46x1.67 mm, air.

Cataclastic pyrite (py) cemented by chalcopyrite (cp).

D : From borehole IM9 at 365.3 feet depth, field of view 1.46x1.67mm, air.

Shattered pyrite (py) grains in a quartz matrix. The unbroken pyrite grains and the chalcopyrite (cp) are of a later generation.

E,F : From borehole M9 at 731 feet depth, field of view 1.46x1.67mm, air.

Cataclastic pyritohedral pyrite grains in dacitic rock. In plate E chalcopyrite (cp), and sphalerite (sl) have cemented parts of the broken grains.

PLATE 24

A

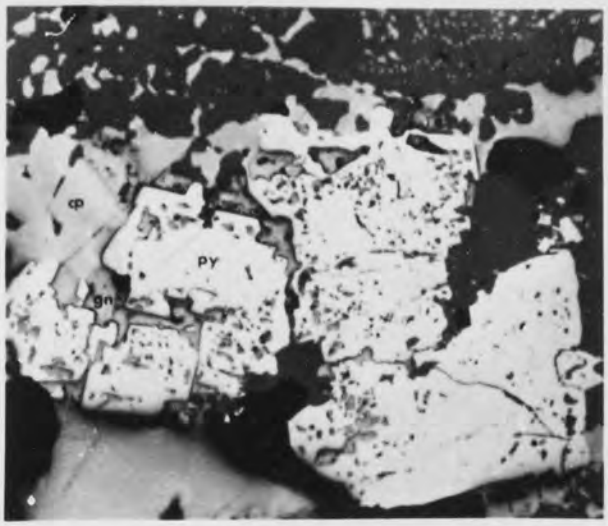

B

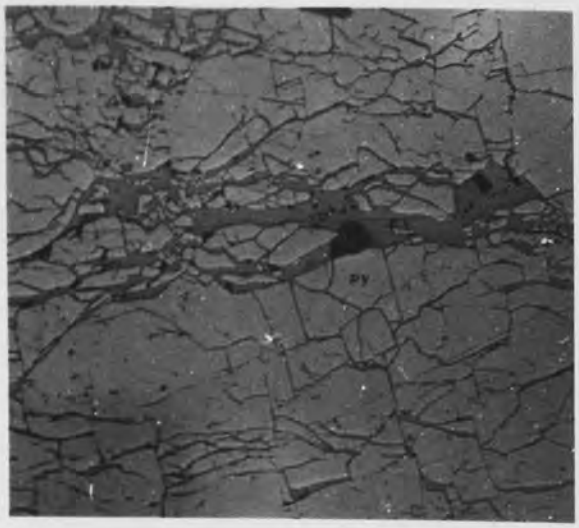

C

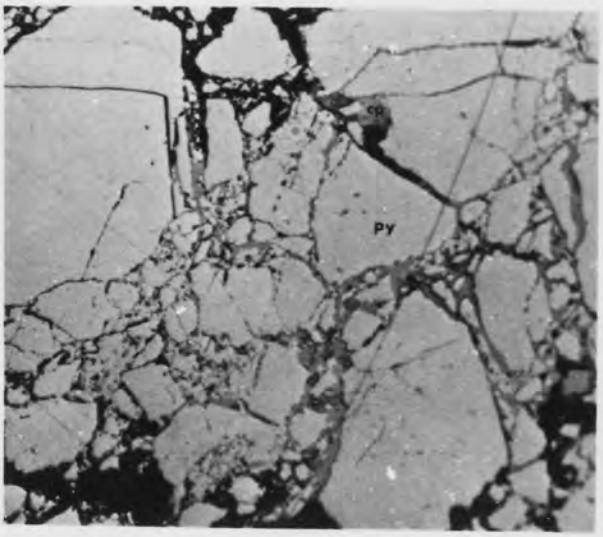

D

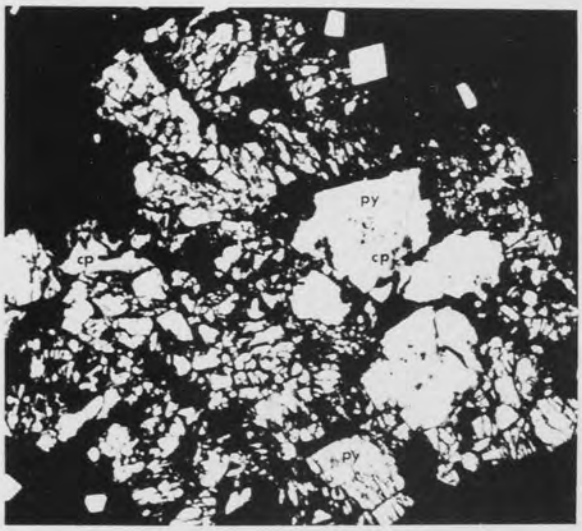

E

F

PLATE 25

Photomicrographs of Special Fabrics of Pyrite.

A : From borehole IM9 at 47 feet depth, field of view 0.23x0.27mm, air.

Pyrite pseudomorphing an earlier incomplete euhedral crystal. The original composition of the crystal is not known.

B : From borehole IM9 at 47 feet depth, field of view 0.47x0.53mm, air.

Pyrite pseudomorph of a spherulite in rhyolitic tuff.

C : From borehole IM9 at 365.3 feet depth, field of view 0.73x0.83mm, air.

Pyrite 'flame' or slump texture. The fine grained pyrite is probably of sedimentary origin. Chalcopyrite (cp) and a later pyrite (py) are also present.

PLATE 25

A

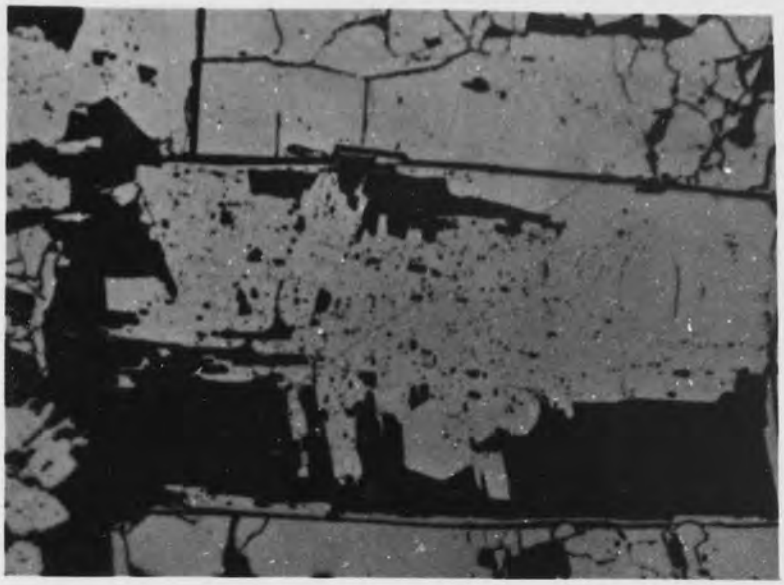

B

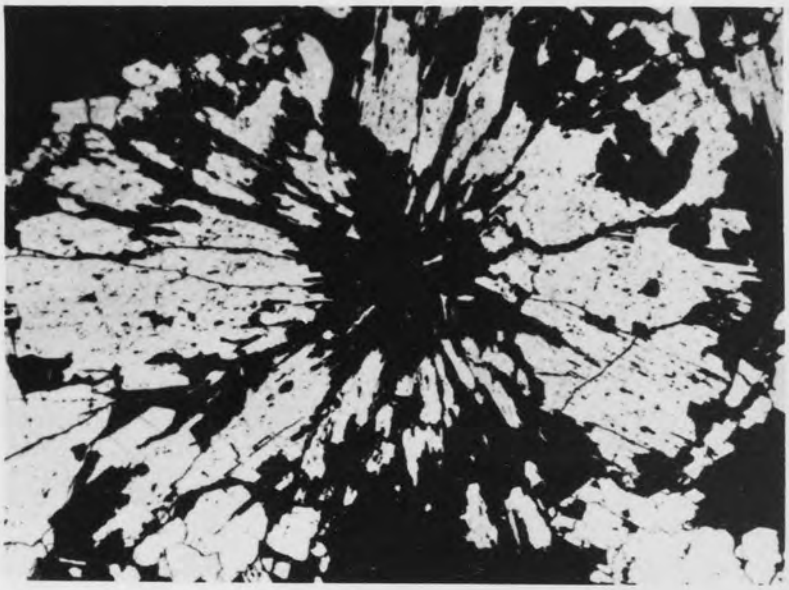

C

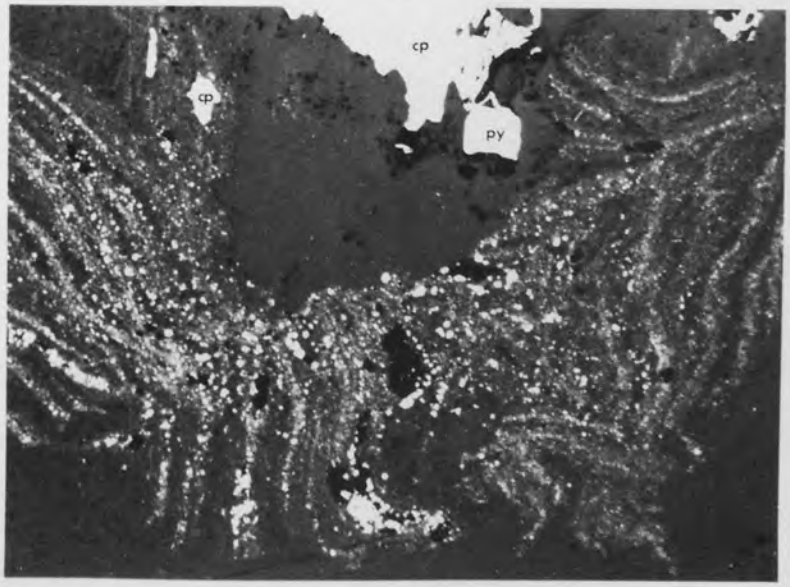

to, or replaced by, pyrite. In the specimens studied marcasite is present only in a small quantities probably due to this replacement. It is found only inside grains, or masses, of the older pyrite, as euhedral (Plates 20F, 23C and D), or subhedral grains (Plates 26A, B, and C), with a size range of 0.001 to 0.04mm. Its general colour is yellow with a greenish tint which is very pronounced against the brassy yellow colour of pyrite. Bireflectance and anisotropy is strong in this mineral (Plates 26A and B). Replacement of marcasite by chalcopyrite is also seen in a few specimens (Plate 26D). The occurrence of this mineral was not noted by Wheatley (1971a), probably because of its low abundance.

5.2.4 Pyrrhotite.

Pyrrhotite is widespread but is present only in a very small quantities. It commonly is light yellow in colour with tints of pink or brown, but in some instances it is brownish yellow probably due to oxidation effects (Ramdohr, 1969). Pleochroism is rarely observed but anisotropy is quite strong and is readily recognized when the nicols are partly crossed.

In many specimens pyrrhotite has a close association with pyrite of the older generation (pyrite 1) where it occurs as small (up to 0.36mm), subround blebs in the pyrite (Plate 26E). It also occurs as apparent intergrowths with chalcopyrite (Plate 26F). This texture probably results from the replacement of pyrrhotite by chalcopyrite, as chalcopyrite commonly replaces most minerals at Parys Mountain. Unmixing of primary ores to produce such a texture, is unlikely, because it would require an environment of

PLATE 26

Photomicrographs of Marcasite and Pyrrhotite.

A,B,C : From borehole IM9 at 102 feet depth, oil immersion, field of view :-

A : 0.09x0.11mm
Remnants of marcasite (M) replaced by pyrite (py).

B : 0.15x0.17mm
X-nicols of Plate B at lower magnification showing the anisotropy of marcasite.

C : 0.09x0.11mm
Remnant marcasite (M) after replacement by pyrite (py).

D : From borehole M10 at 1548 feet depth, field of view 0.15x0.17mm, oil immersion.

Pyrite (py) replacing marcasite (M) (slightly darker than pyrite). Chalcopyrite (cp) has later replaced both marcasite and pyrite.

E,F : From borehole M10 at 1521 feet depth, field of view 0.15x0.17mm, oil immersion.

Pyrrhotite (po) blebs in pyrite (py) grain. Chalcopyrite (cp) has replaced part of pyrrhotite.

PLATE 26

A

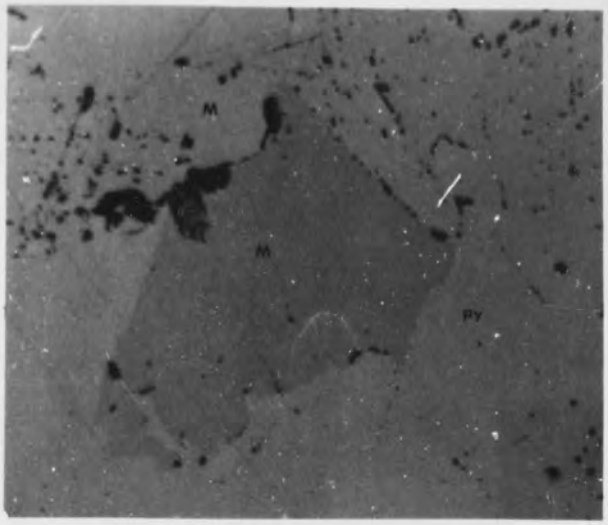

B

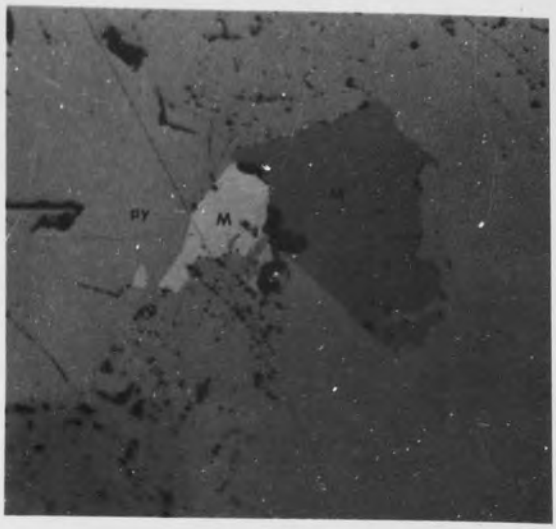

C

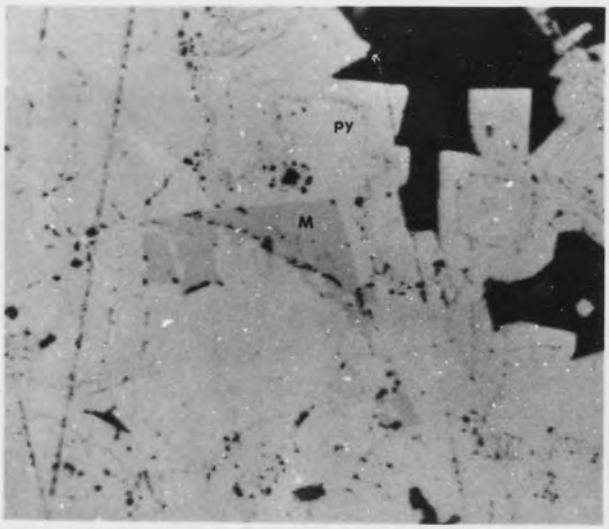

D

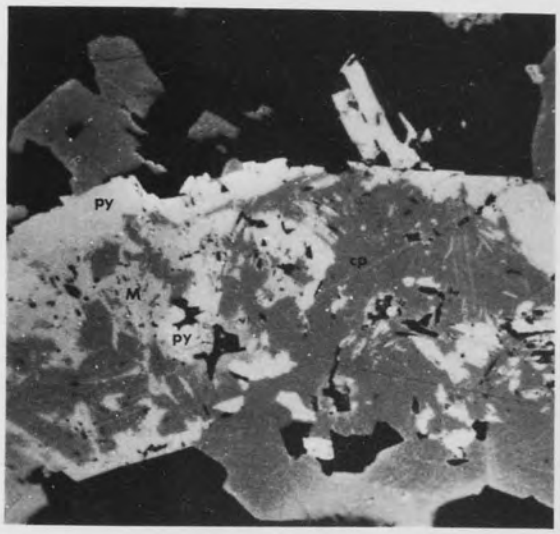

E

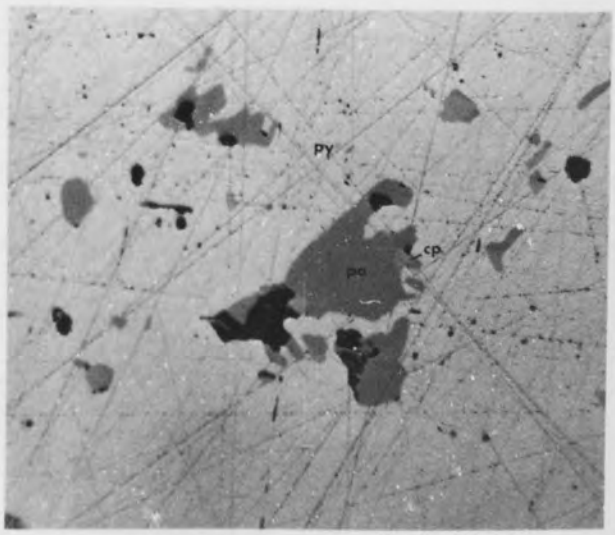

F

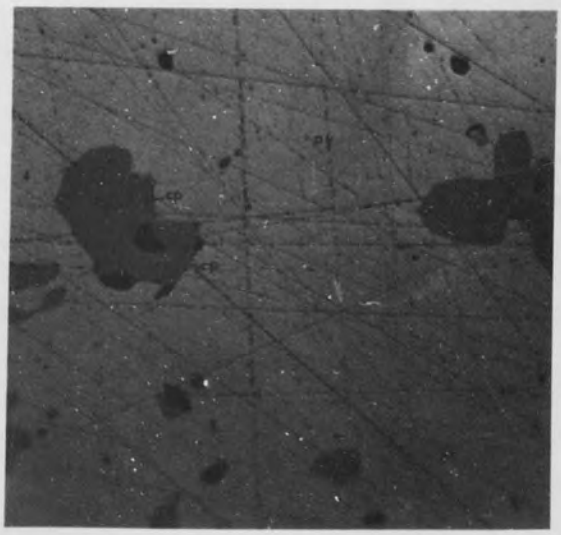

deposition of 'exceptionally' high temperature (Ramdohr, 1969). The occurrence of inclusion blebs of pyrrhotite in pyrite grains is thus evidence against unmixing. Pyrrhotite has a similar position to the older generation of pyrite, pyrite 1, in the paragenetic sequence, i.e. it is one of the first formed primary ore minerals.

5.2.5 Arsenopyrite

Like pyrite,arsenopyrite shows strong tendencies to euhedral crystallization (Ramdohr, 1969). The euhedral grains vary in size from 0.005 to 0.1mm. Optically they are distinctly anisotropic, white or pale yellow in colour, and zoning and mimetic twinning are present in some specimens. An association between arsenopyrite and bismuthinite, the tetrahedrite group minerals, and/or framboidal pyrite is present.

At Parys Mountain, arsenopyrite is present as euhedral crystals, showing typical pseudorhombic, or columnar forms (Plates 27A and B). This mineral is common in the Bluestone ore type, and in parts of the Copper ore from the siliceous sinter, and the northern part of the rhyolitic rocks. Euhedral grains of arsenopyrite are commonly present both in groups, or vein-like clusters, in a quartz matrix, and enclosed by later sulphides such as chalcopyrite, galena, and sphalerite (Plates 27C and D).

In a previous study of the Parys Mountain mineralization (Wheatley, 1971a) arsenopyrite was not recognized, but its presence was recognized in the Avoca deposits which have a similar mineralogy and origin.

5.2.6 Chalcopyrite

Chalcopyrite is the second most common sulphide at Parys Mountain, after pyrite. Its exact abundance cannot be determined, due to the previous mining operations, but is roughly estimated at 30 percent of the total sulphide. It is very widestread and is present in every ore type in varying proportions; being most abundant in the Copper ore and the Bluestone ore, and least abundant in the Galena-Sphalerite ore.

Chalcopyrite is commonly present as an allotriomorphic mass (Plate 27E) and its grain size, as revealed by etching, varies from 0.02 to 0.2mm (Wheatley, 1971a). Optically chalcopyrite is weakly anisotropic, and both lamellar and polysynthetic twinning are present in this mineral. Wheatley (1971a) suggested that the twinning was probably developed from crystallization within a stressed environment. This explanation seems the most reasonable and fits the information gained in the present study.

Various fabrics of chalcopyrite are present, including mutual intergrowths with sphalerite and galena, particularly in the Bluestone ore type (Plate 27E); layers up to 5mm thick interlayered with layers of pyrite and sphalerite; fillings of open spaces between pyrite grains, or cementing broken pyrite grains (Plates 27F and 28A); intergrowths with tennantite (Plates 28B and C); replacing framboidal and other pyrite grains (Plates 28D, 29A and B); exsolution bodies in sphalerite grains; as isolated masses; and filling spaces between quartz grains in the rock matrix. A fabric of chalcopyrite intergrowths with fibrous minerals, probably sericite and/or chlorite, in the matrix of dacitic rocks, is present

PLATE 27

Photomicrographs of Arsenopyrite and Chalcopyrite.

A : From borehole M10 at 1608 feet depth, field of view 0.15x0.17 mm, oil immersion.

Arsenopyrite crystals (ap) in quartz matrix.

B : From borehole M10 at 1599 feet depth, field of view 0.15x0.17 mm, oil immersion.

Arsenopyrite (ap) and pyrite (py) crystals in chalcopyrite (cp) matrix. Galena (gn) has replaced parts of arsenopyrite grains.

C : From borehole M10 at 1548 feet depth, field of view 0.37x0.42mm, air.

Arsenopyrite (ap) (euhedral crystals) in matrix of chalcopyrite (cp), sphalerite (sl), and gangue (black). Pyrite (py) grains are present.

D : From borehole M10 at 1548 feet depth, field of view 0.15x0.17 mm, oil immersion.

Euhedral crystals of arsenopyrite (ap) in matrix of quartz (black) and sphalerite (very dark grey).

E : From borehole H4 at 474 feet depth, field of view 1.46x1.67mm, air.

Allotriomorphic grains of chalcopyrite (cp), intergrown with galena (gn) and sphalerite (sl) in Bluestone ore type. Pyrite (py) grains are present. Note the exsolution of chalcopyrite in the sphalerite in the top right hand corner of the plate.

F : From borehole M10 at 1548 feet depth, field of view 0.15x0.17mm, oil immersion.

Chalcopyrite (cp) and galena (gn) infilling spaces between pyrite (py) grains.

PLATE 27

A

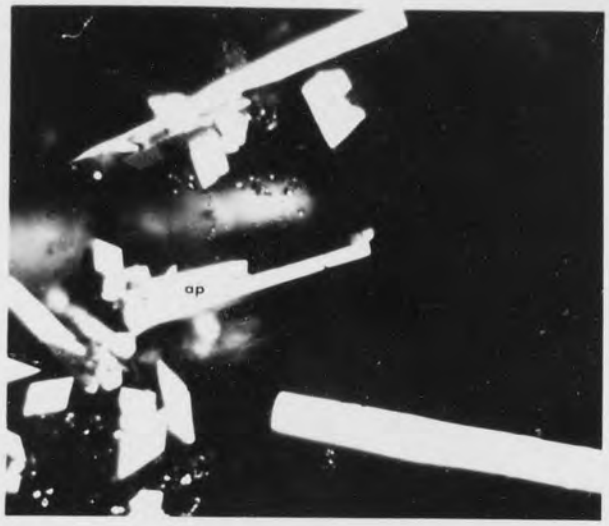

B

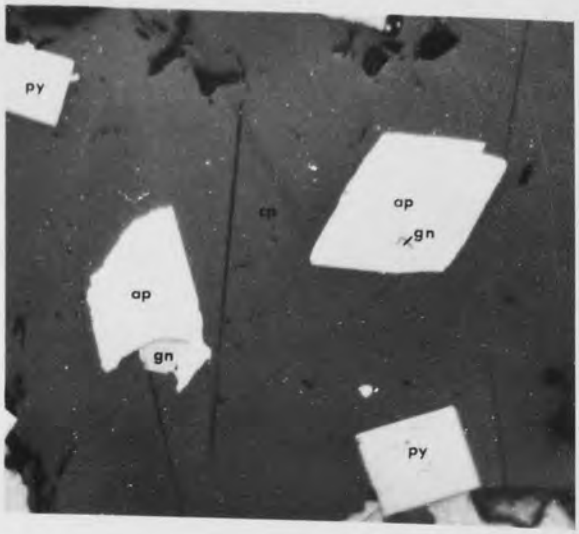

C

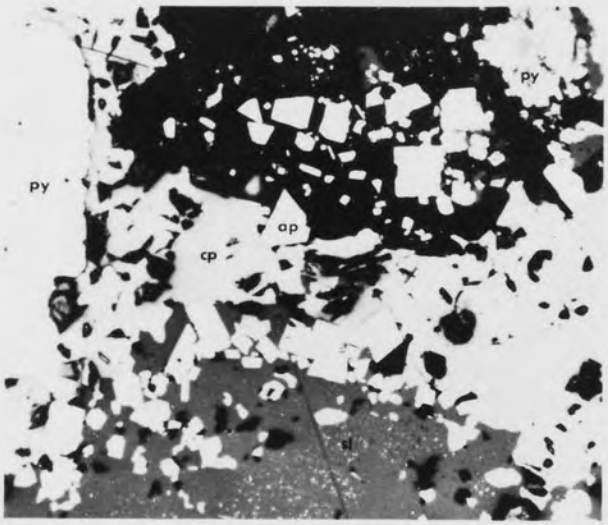

D

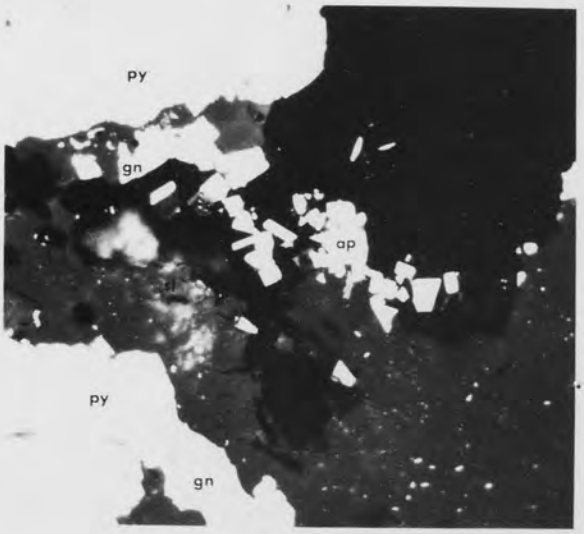

E

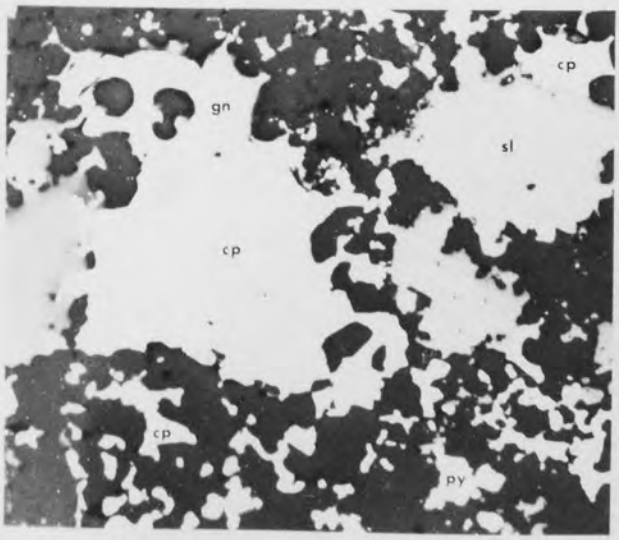

F

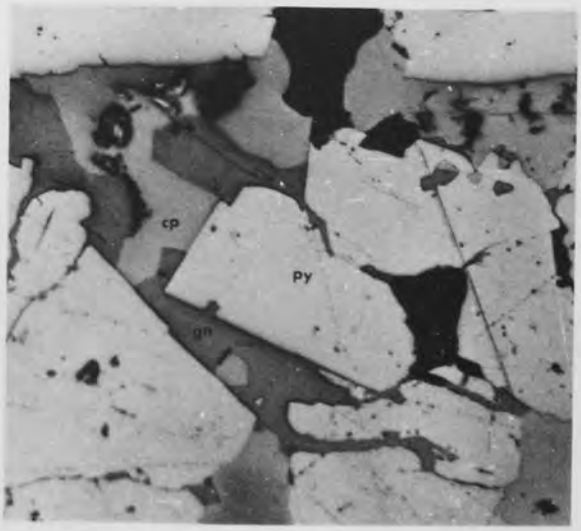

PLATE 28

Photomicrographs of Chalcopyrite.

A : From borehole H43A at 1847 feet depth, field of view 1.46x1.67mm, air.

Chalcopyrite (cp) infilling cracks in fractured pyrite (py) grains.

B : From borehole H14 at 186 feet depth, field of view 0.37x0.42mm, oil immersion.

Intergrowths of chalcopyrite (cp), sphalerite (sl), and tennantite (tn).

C : From borehole IM9 at 364 feet depth, field of view 0.73x0.83mm, air.

Intergrowths between chalcopyrite (cp) and tennantite (tn), enclosing pyrite (py) grains.

D : From borehole H43A at 1855 feet depth, field of view 0.37x0.42mm, air.

Chalcopyrite (cp) replacing the inner part of a pyrite (py) grain.

PLATE 28

A

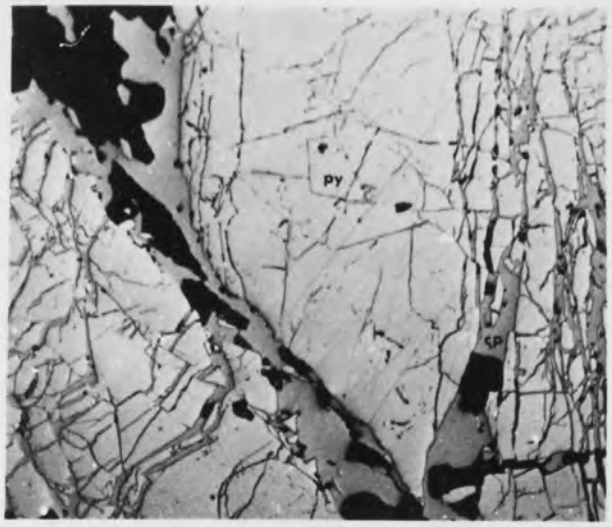

B

C

D

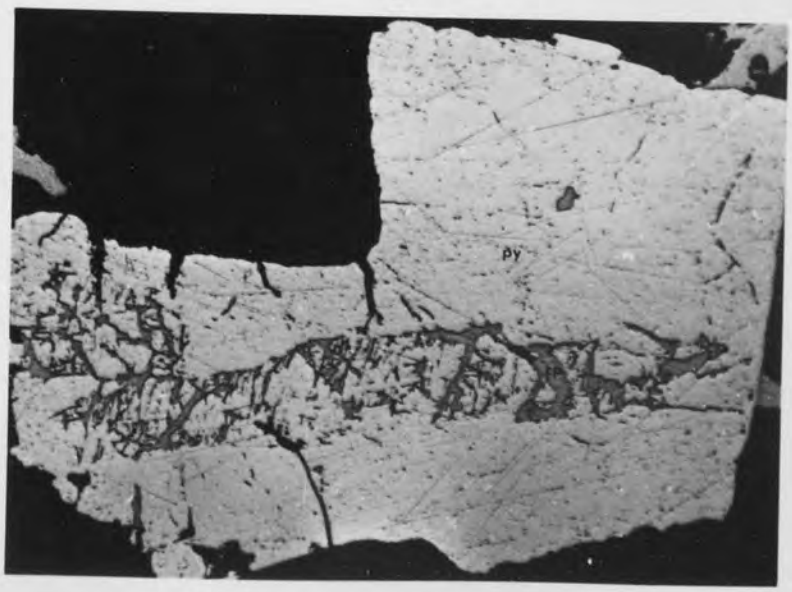

(Plates 29C and D). Another fabric is that identified by Ramdohr (1969, Figs. 20 and 21) as vortices of compression or shearing textures (Plate 29E).

Generally the chalcopyrite grains are inclusion-free, but some inclusion blebs of bismuthinite, native bismuth, tetrahedrite group minerals, and Bi-sulphosalts are present in some specimens.

Chalcopyrite may have been deposited during all stages of ore formation (Ramdohr, 1969) as it has a close association with all the sulphide minerals. However, as is evident from its common association with the late minerals sphalerite and galena, and its replacement relationship with earlier minerals, it, along with sphalerite and galena, probably is strongly represented in the last phase of ore deposition.

Chalcopyrite shows some supergene alteration to covellite and bornite (Plate 29F), but this occurs only in the core specimens from shallow depths.

5.2.7 Sphalerite

Sphalerite is the major sulphide mineral of the Bluestone ore type, and is present in lesser quantities in all other ore types. It constitutes approximately 10 percent of the total sulphide at Parys Mountain. The most common occurrence of sphalerite in the Bluestone ore is as aggregates of irregular grains, and as intimate intergrowths with chalcopyrite, pyrite, and galena (Plates 30A, B, C and D). In the Copper ore, and the Galena-Sphalerite ore, layers of sphalerite, up to 4mm thick, are common, interlayered with chalcopyrite, pyrite, and gangue (mostly quartz) rich layers. Patches of sphalerite with

PLATE 29

Photomicrographs of Chalcopyrite.

A : From borehole M10 at 1584 feet depth, field of view 0.37x0.42mm, air.

Chalcopyrite (cp) and galena (gn) replacing framboidal pyrite (py).

B : From borehole M9 at 731 feet depth, field of view 0.29x0.33mm, air.

Chalcopyrite (cp) replacing and enclosing two framboids and a broken pyrite (py) grain.

C,D,E : From borehole H43A at 1855 feet depth, air.

C : Field of view 1.46x1.67mm

Intergrowths between chalcopyrite (cp) and chlorite and sericite (dark) in matrix of dacite.

D : Field of view 0.37x0.42mm

A higher magnification of the grain boundaries of Plate C.

E : Field of view 1.46x1.67mm

Vortices of compression or shearing textures, produced by intergrowths between chalcopyrite (cp) and sericite or chlorite (black). Pyrite (py) grains with corroded boundaries are present.

F : From borehole H14 at 195 feet depth, field of view 0.15x0.17mm, oil immersion.

Covellite (co) (black with fine branches) and bornite (bn) (grey, enclosed by covellite) occurring as secondary products of chalcopyrite (cp) along cracks. Pyrite (py) is present.

PLATE 29

A

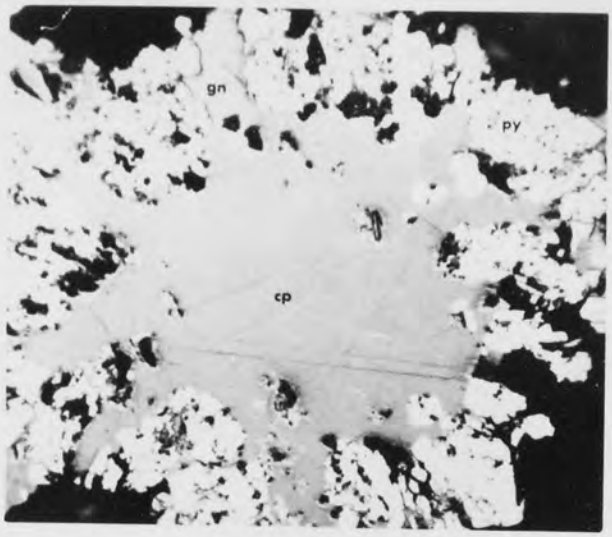

B

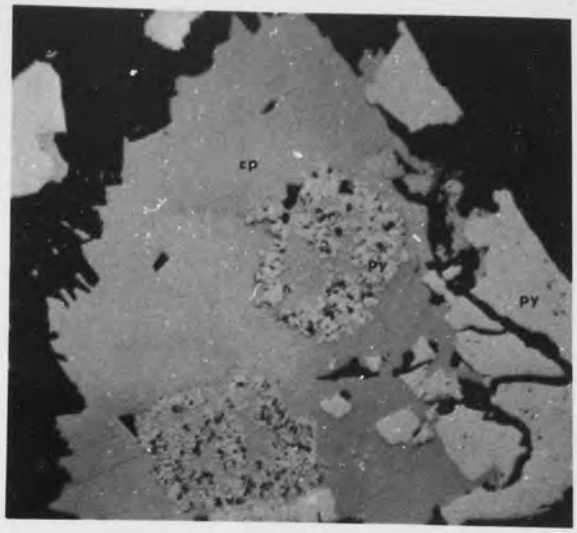

C

D

E

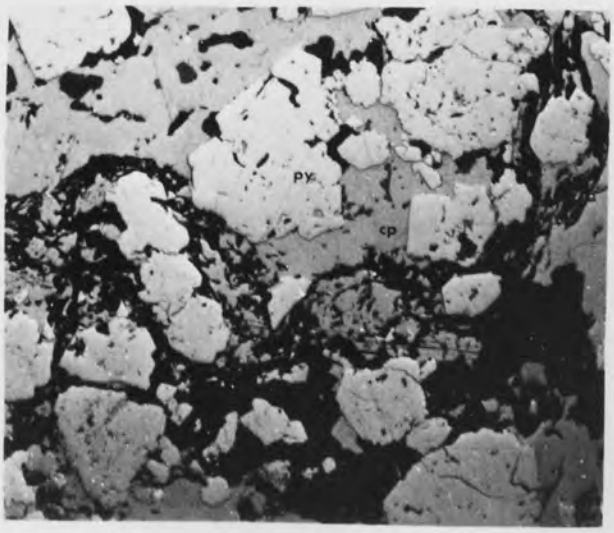

F

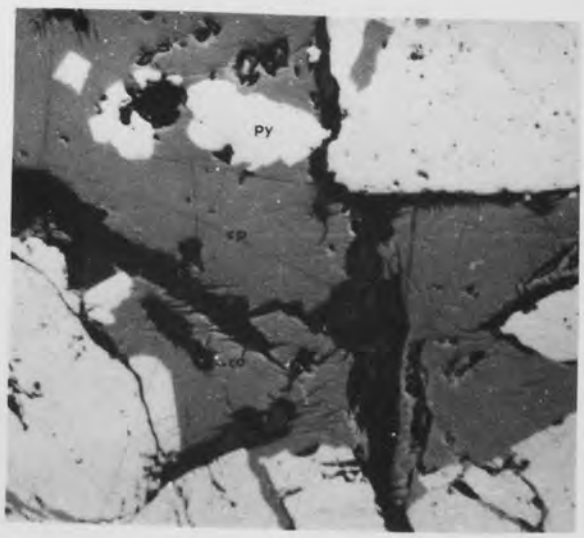

PLATE 30

Photomicrographs of Sphalerite.

A : From borehole H4 at 491 feet depth, field of view 1.46x1.67mm, air.

Intimate intergrowths of sphalerite (sl) (dark grey), galena (gn) (light grey, almost white), chalcopyrite (cp) (white) in Bluestone type ore, enclosing former pyrite (py) grains (white with high relief.

B : From borehole M10 at 1572 feet depth, field of view 0.37x0.42mm, oil immersion.

Intergrowths between sphalerite (sl) (dark) containing chalcopyrite exsolution bodies, and galena (gn).

C : From borehole H4 at 474 feet depth, field of view o.59x0.67mm, air.

Intergrowths between sphalerite (sl) and galena (gn). Sphalerite grain, in the top half of the plate has replaced an earlier pyrite (py). This sphalerite is partly surrounded by later pyrite grains (on the upper right hand side). Galena has filled interstices between pyrite grains (right hand side of the plate).

D : From borehole M10 at 1548 feet depth, field of view 0.29x0.33mm, air.

Intergrowths between sphalerite (sl), chalcopyrite (cp), and bismuthinite (bm). Chalcopyrite exsolution blebs are present in the sphalerite.

E : From borehole H4 at 464 feet depth, field of view 1.46x1.67mm, air.

Sheared texture in sphalerite (grey), similar to that in chalcopyrite (cf. Plate 29E). Galena (gn), chalcopyrite (cp), and numerous pyrite (py) grains are present.

PLATE 30

A

B

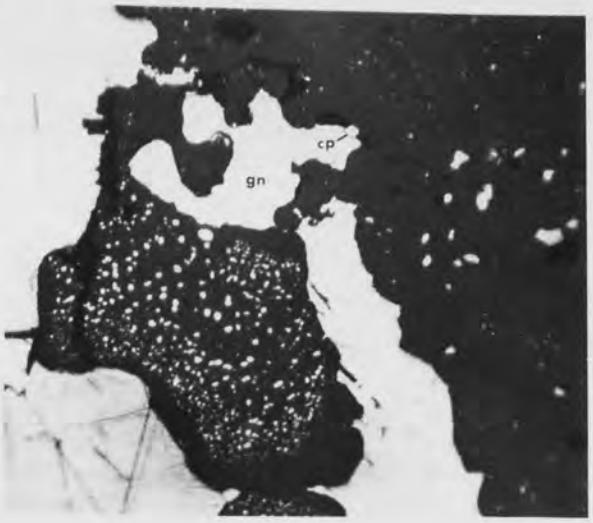

C

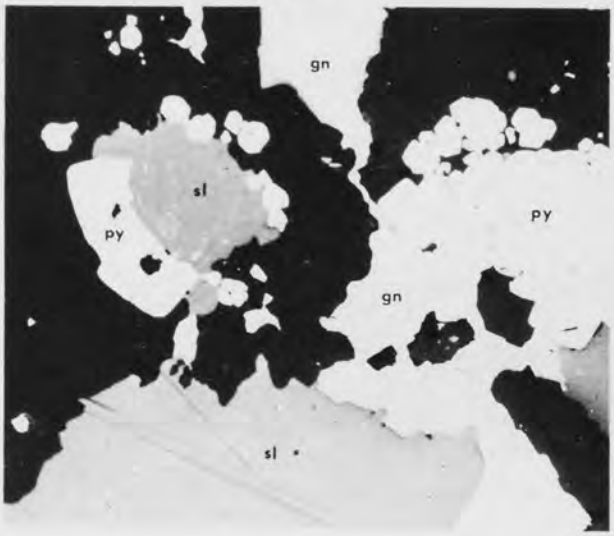

D

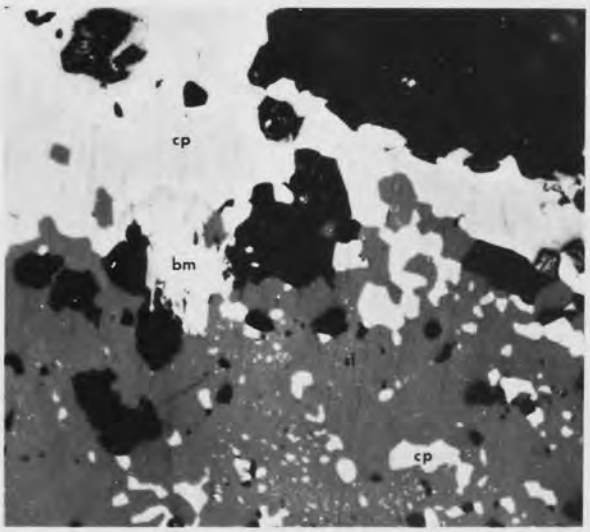

E

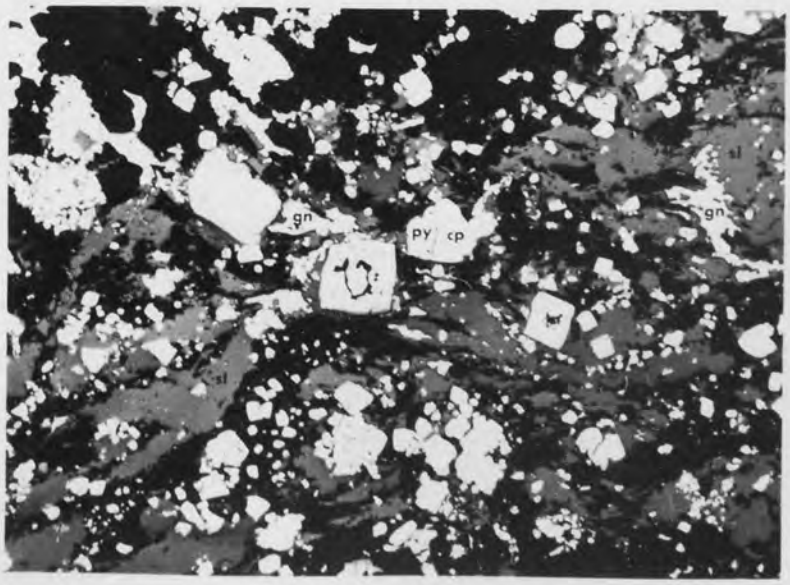

irregular outlines and variable size (up to 1cm) embedded in the gangue matrix are common, and shear textures in sphalerite of the Bluestone ore are present (Plate 30E).

Internal reflections, zoning, and twinning are common in the sphalerite grains. Exsolution of chalcopyrite in the sphalerites is very common. The exsolution patterns are related to zoning, twin planes, and morphology of the grains. On the basis of chalcopyrite exsolution, two generations of sphalerite are recognized:- the older generation, sphalerite 1, contains chalcopyrite exsolution (Plates 31A, B, C, and D); and the younger generation, sphalerite 2 or 'clean' sphalerite, without exsolution (Plates 31E and F). The proportion of sphalerite 1 and 2 is approximately 10:1. Evidence for the age relationship between the two sphalerite is illustrated in Plate 32A, where sphalerite 1 is partly replaced by sphalerite 2. However the gap, or the age difference, between the two generations, is probably small, as both have replaced the older pyrite 1 (Plates 32B and D), and are enclosed by the younger pyrite 3 (Plates 32E and F).

Exsolution bodies of chalcopyrite in sphalerite can be divided into three generations. The earliest phase is represented by round to subround exsolution blebs, with a random orientation, and variable sizes (0.002 to 0.03mm) (Plate 33A). The second generation is represented by very fine grained (less than 0.002mm) blebs of chalcopyrite which are commonly either zonally arranged, or are aligned parallel to the grain boundaries (Plate 33B). The third generation is represented by irregularly shaped exsolution bodies,

PLATE 31

Photomicrographs of Sphalerite.

A : From borehole M10 at 1548 feet depth,
field of view 0.15x0.17mm, oil immersion.

B,C,D : From borehole H4 at 474 feet depth,
B : field of view 0.15x0.17mm, oil immersion.
C : field of view 0.11x0.13mm, oil immersion.
D : field of view 0.29x0.33mm, air.

Various chalcopyrite (1 and 2) exsolution textures in sphalerite 1.

E,F : From borehole H4 at 474 feet depth,
E : field of view 0.73x0.83mm, air.
F : field of view 0.37x0.42mm, air.

Sphalerite 2 or 'clean' sphalerite.

In E earlier chalcopyrite (cp) and pyrite (py) grains are enclosed within the sphalerite mass.

PLATE 31

A

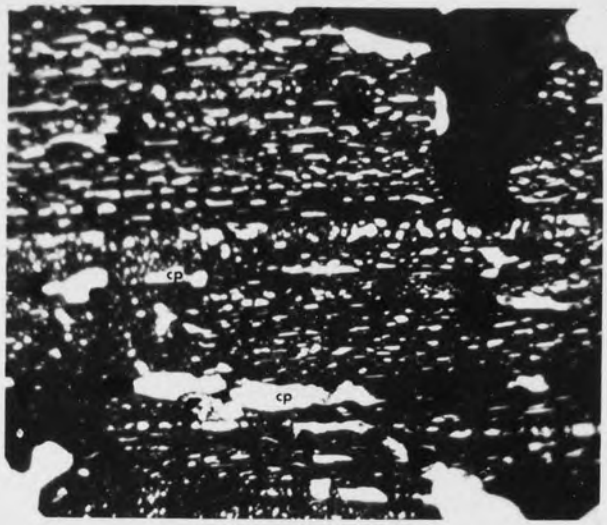

B

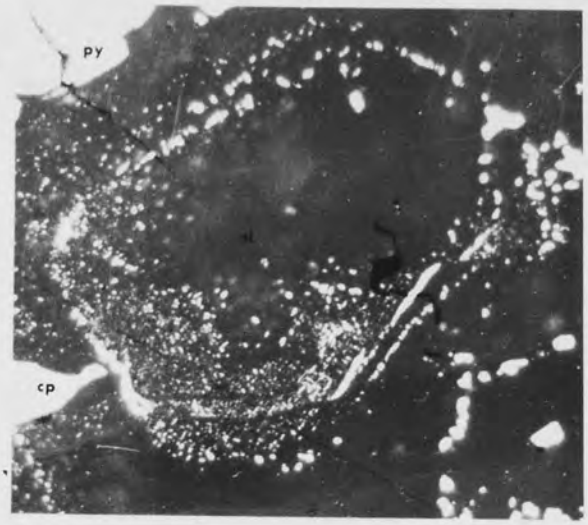

C

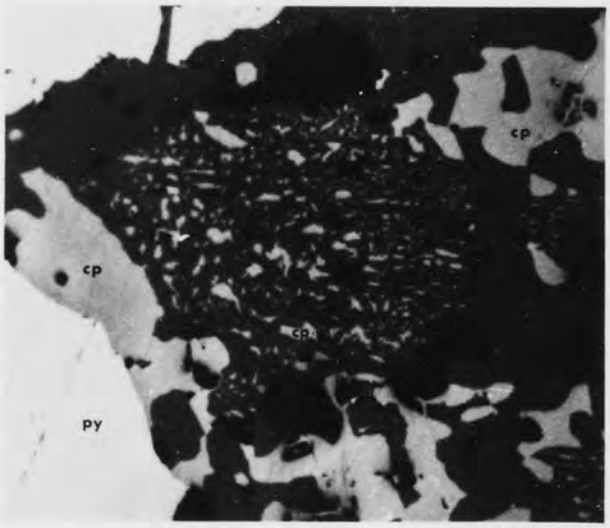

D

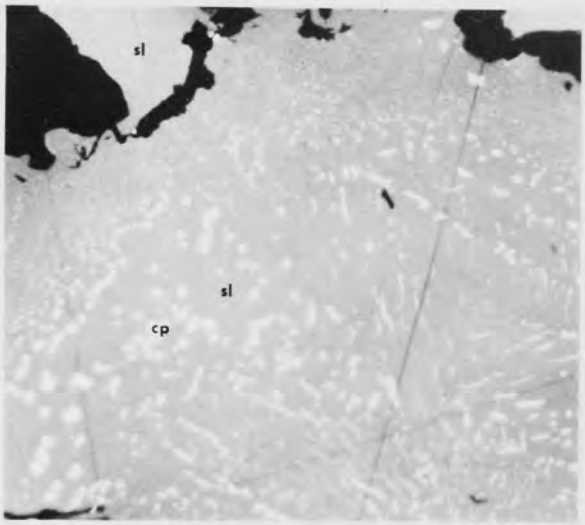

E

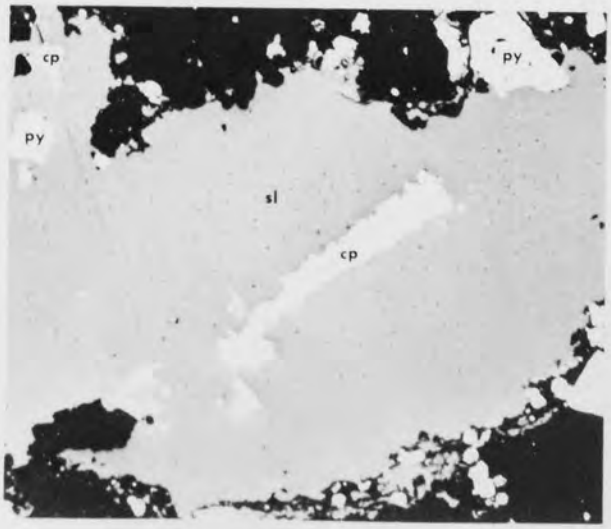

F

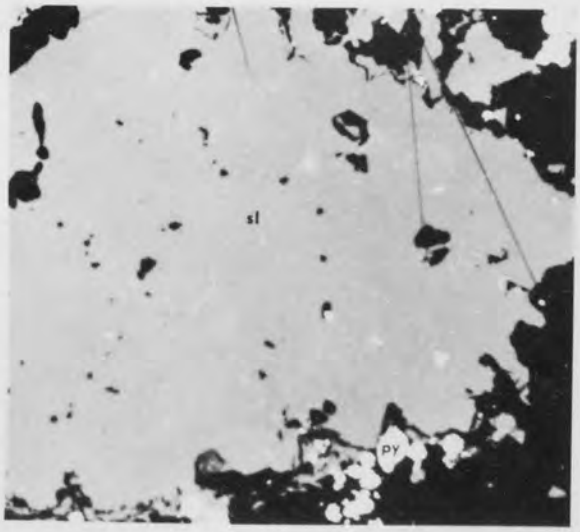

PLATE 32

Photomicrographs of sphalerite.

A : From borehole IM9 at 288 feet depth,
field of view 0.15x0.17mm, oil immersion.

Sphalerite 1 (with chalcopyrite exsolution) replaced partly by sphalerite 2 (without exsolution).

B : From borehole H4 at 474 feet depth,
field of view 0.47x0.53mm, air.

Sphalerite 1 grains partly enclosed by framboidal pyrite (left hand side), and by subhedral pyrite (right hand side).

C : From borehole H4 at 474 feet depth,
field of view 0.37x0.42mm, air.

Sphalerite 2 replacing earlier pyrite (py) grains, which in turn are enclosed by chalcopyrite (cp). Galena (gn) is present.

D : From borehole H4 at 474 feet depth,
field of view 0.73x0.83mm, air.

Sphalerite 1 partly replacing earlier pyrite grains (py). Fractures in the pyrite were previously infilled by galena (gn).

E : From borehole H4 at 474 feet depth,
field of view 0.37x0.42mm, air.

Sphalerite 1 partly enclosed by later pyrites(py).

F : From borehole H4 at 474 feet depth,
field of view 1.46x1.67mm, air.

Sphalerite 2 surrounded by galena(gn), and framboidal pyrites (py).

PLATE 32

A

B

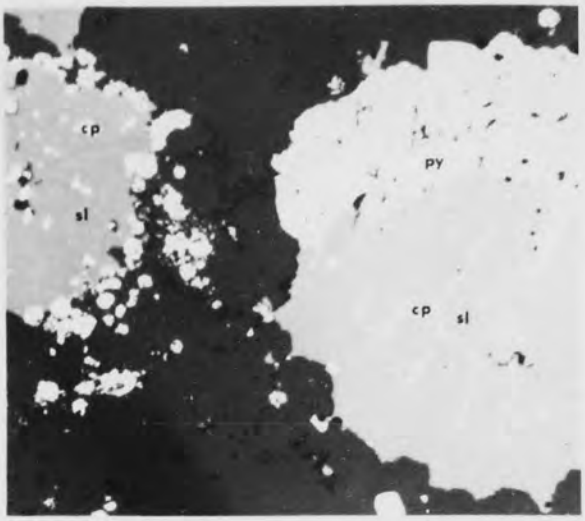

C

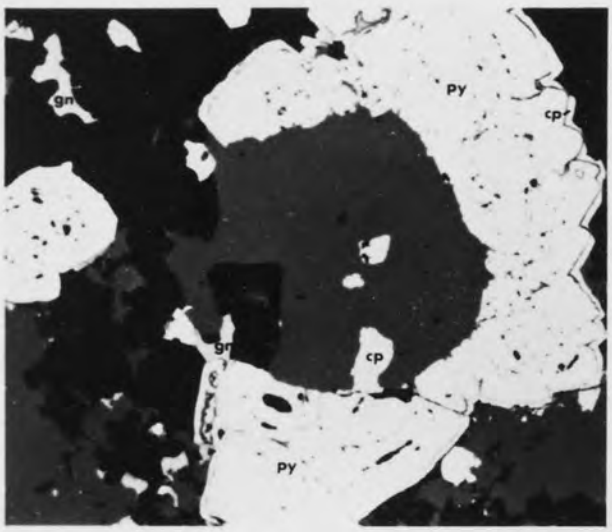

D

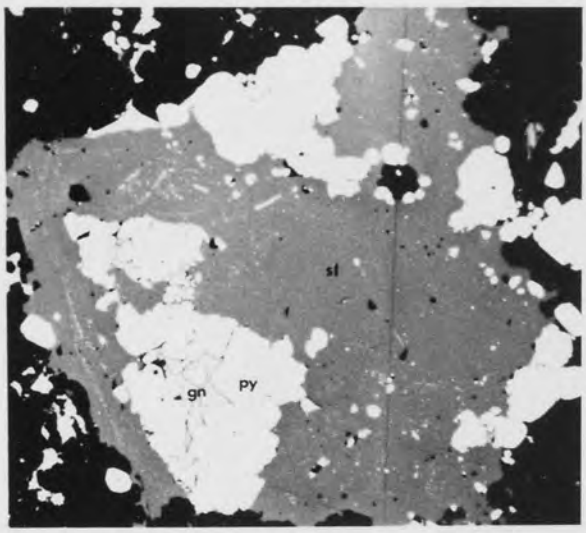

E

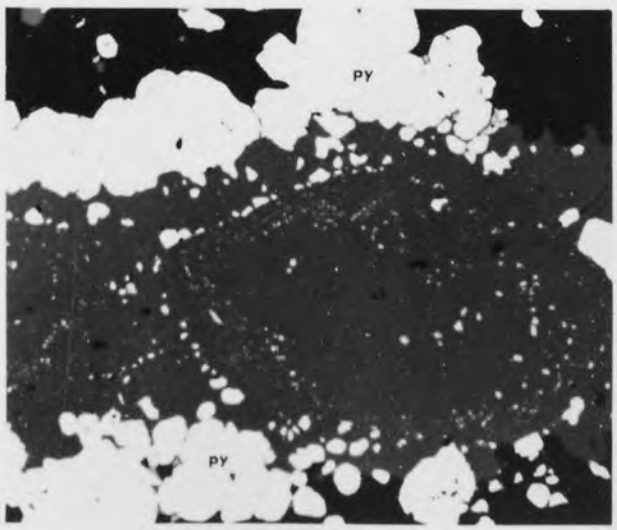

F

PLATE 33

Photomicrographs of Chalcopyrite Exsolution in Sphalerite.

A : From borehole M10 at 1584 feet depth,
field of view 0.15x0.17mm, oil immersion.

Earliest chalcopyrite exsolution bodies in sphalerite 1.

B : From borehole H4 at 474 feet depth,
field of view 0.11x0.13mm, oil immersion.

Second generation of chalcopyrite exsolution bodies in sphalerite 1.

C : From borehole H4 at 460 feet depth,
field of view 0.15x0.17mm, oil immersion.

Round chalcopyrite exsolution bodies of the first generation enclosed by smaller exsolution bodies of the second generation. These in turn are enclosed by the irregular larger bodies of the third generation.

D,E : From borehole M10 at 1584 feet depth,
field of view 0.15x0.17mm, oil immersion.

Sphalerite 1, with chalcopyrite 2 exsolution, enclosed by sphalerite 2 containing chalcopyrite 3 exsolution.

F : From borehole H4 at 474 feet depth,
field of view 0.73x0.83mm, air.

Relationship of chalcopyrite exsolution bodies of 1,2, and 3 generation in sphalerite (cp=chalcopyrite, py=pyrite).

PLATE 33

A

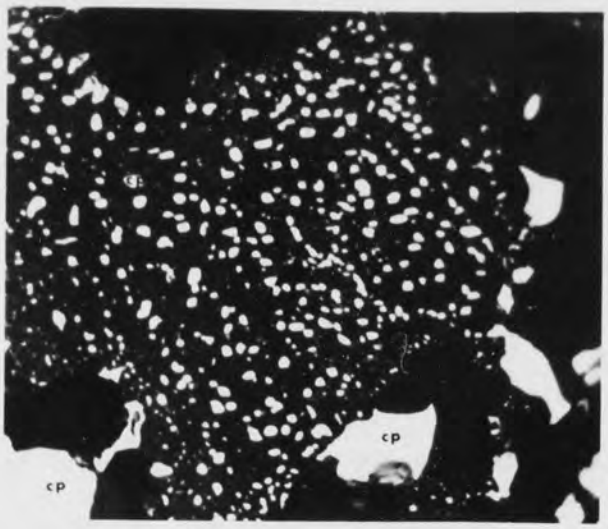

B

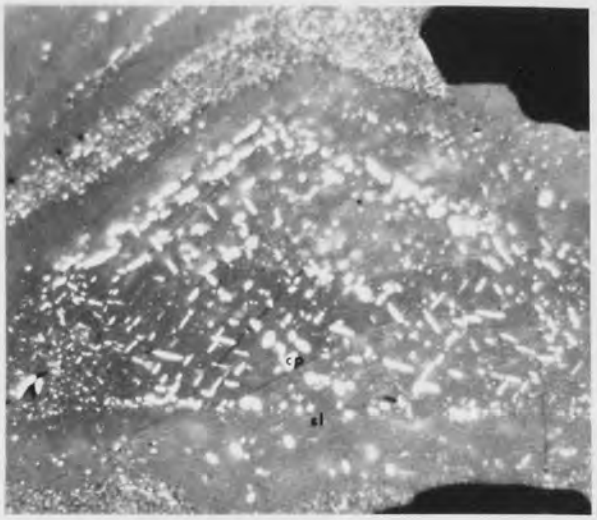

C

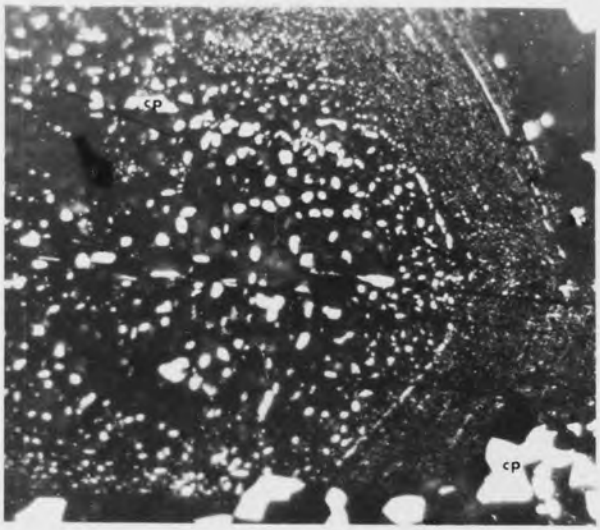

D

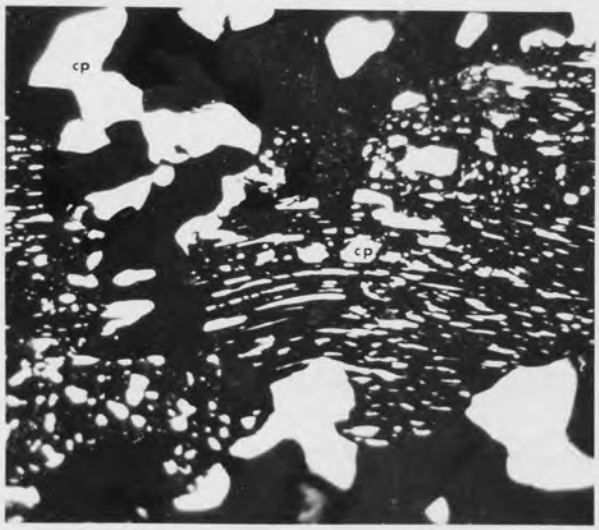

E

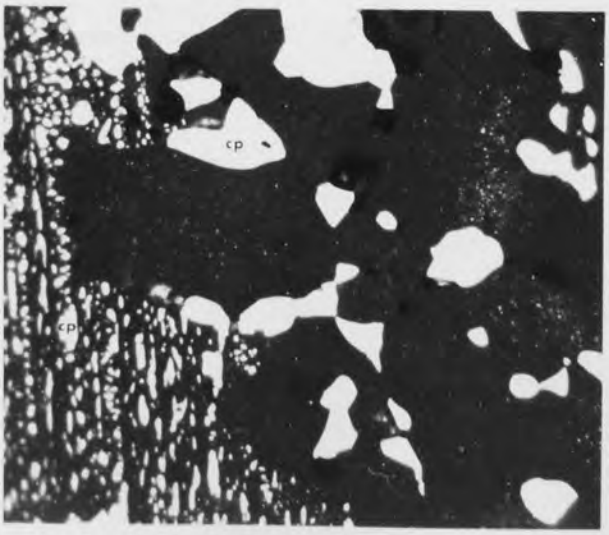

F

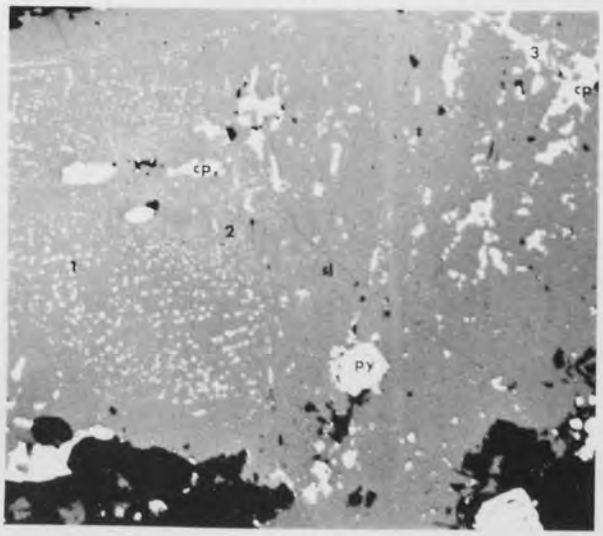

in the size range of 0.01 to 0.06mm, which commonly occur along intergranular boundaries of the sphalerites. Plates 33C, D, E, and F show the relationship between these three generations of exsolution bodies. The various exsolution bodies of chalcopyrite in sphalerite are shown in Plates 35 and 36.

The grain size of sphalerite varies from 0.03 to 0.05mm. This was measured on grains with chalcopyrite exsolution bodies present (Plate 31C), or grains where sphalerites 1 and 2 are close to each other, as in other instances the individual grains could not be distinguished without etching. This is directly comparable with the size range reported by Wheatley (1971a), which was obtained by etching.

The mutual intergrowths between sphalerite, chalcopyrite, and galena, suggest that these minerals have similar paragenetic positions. However, the common occurrence of galena and chalcopyrite, replacing pyrite, and all three minerals subsequently enclosed by sphalerite (Plate 31D), shows that some sphalerite post-date the galena and chalcopyrite. The main phase of crystallization of the three minerals was however essentially contemporaneous. Chalcopyrite + tennantite (Plate 34A), and chalcopyrite + galena (Plate 34B), fill fractures in pyrite grains. These pyrites were subsequently replaced by sphalerite, and the remnants of chalcopyrite, galena, and tennantite, which previously were in the cracks in the pyrites, can still be observed in the sphalerite mass. This is a further indication that the crystallization of sphalerite ended later than that of chalcopyrite, galena, and tennantite.

PLATE 34

Photomicrographs of Sphalerite.

A,B : From borehole IM9 at 288 feet depth,
field of view 0.15x0.17mm, oil immersion.

Sphalerite (dark), with exsolution bodies, replacing and enclosing pyrite (py) grains which have chalcopyrite (cp) + tennantite (tn) (Plate A), and chalcopyrite + galena (gn) (Plate B), infilling fractures. Remnants of the infilling minerals are present in the sphalerite mass.

C : From borehole M10 at 1584 feet depth,
field of view 0.37x0.42mm, oil immersion.

D : From borehole M4 at 456 feet depth,
field of view 0.07x0.11mm, oil immersion.

E,F : From borehole M4 at 456 feet depth,
field of view 0.37x0.42mm, oil immersion.

To illustrate the various exsolution fabrics of chalcopyrite 2 in sphalerite 1.

PLATE 34

A

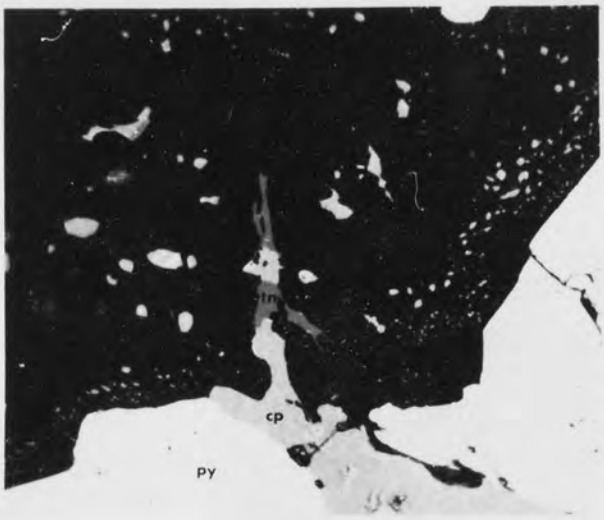

B

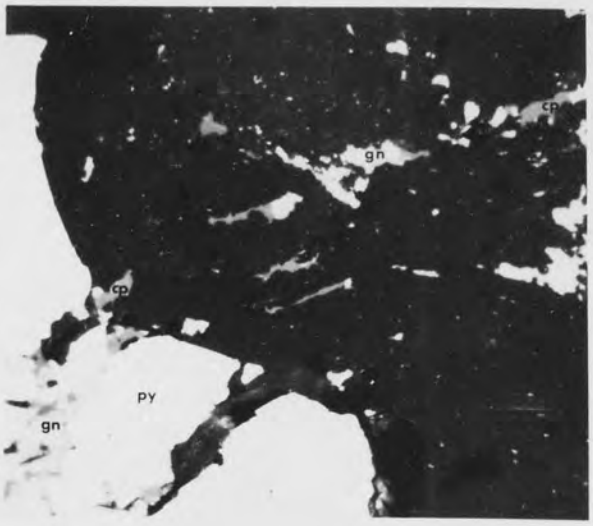

C

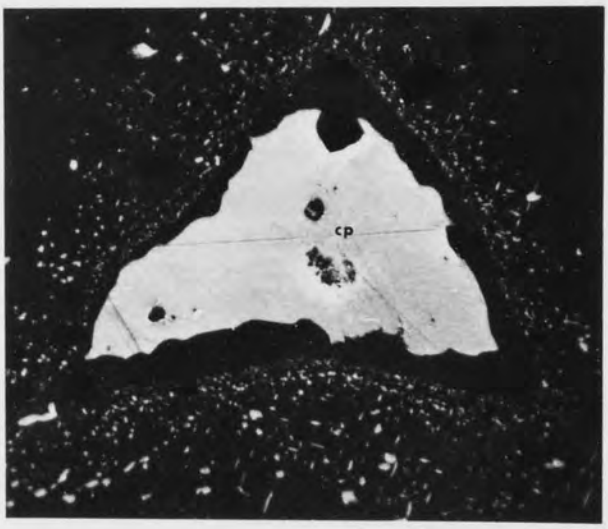

D

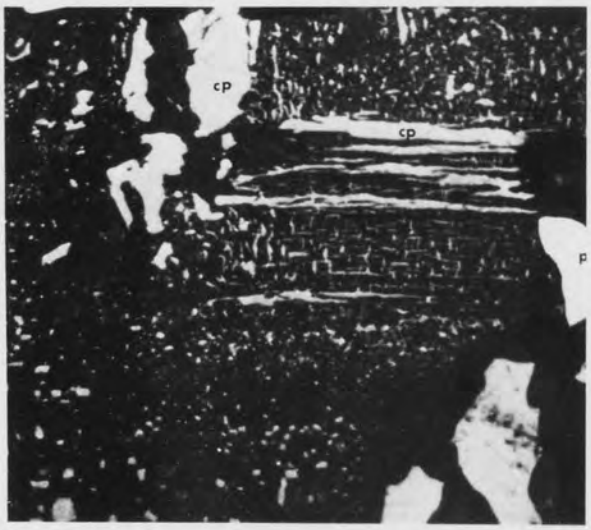

E

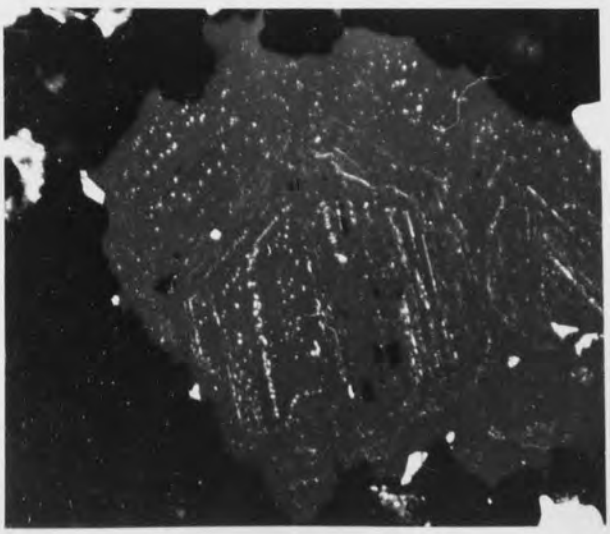

F

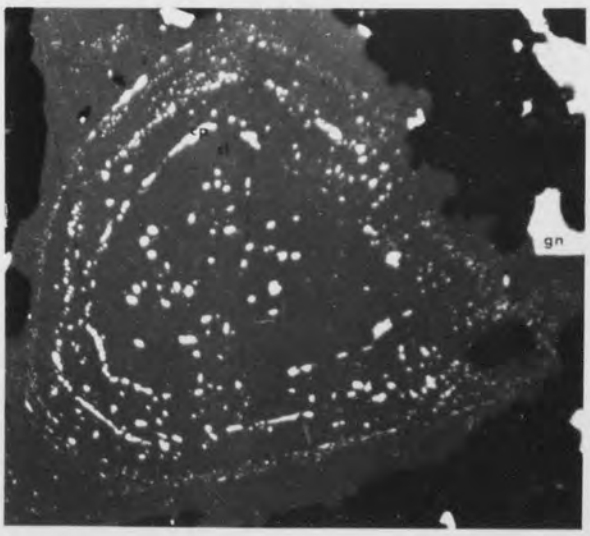

PLATE 35

Photomicrographs of Sphalerite.

A : From borehole M10 at 1589 feet depth,
field of view 0.59x0.67mm, air.

Chalcopyrite 2 exsolution in sphalerite 1, developed near grain boundaries. Earlier pyrite (py), chalcopyrite 1, and later chalcopyrite grains (cp) are present.

B : From borehole IM9 at 283 feet depth,
field of view 0.73x0.83mm, air.

Chalcopyrite 2 exsolution in sphalerite 1, developed along cleavage planes in sphalerite grain. The two veinlets of small euhedral crystals are of arsenopyrite (ap).

C : From borehole M4 at 456 feet depth,
field of view 0.37x0.42mm, oil immersion.

Chalcopyrite 2 exsolution in sphalerite 1, developed along zone boundaries. Earlier grains of chalcopyrite (cp), and pyrite (py) are present.

PLATE 35

A

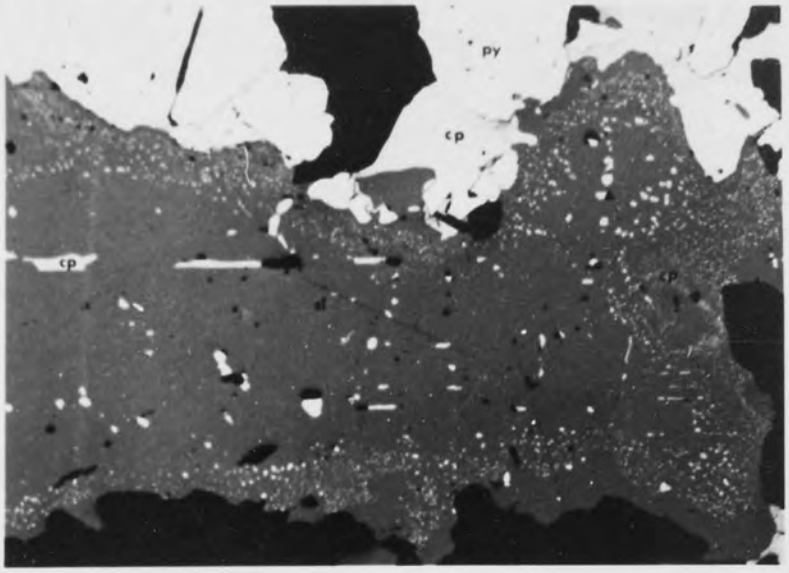

B

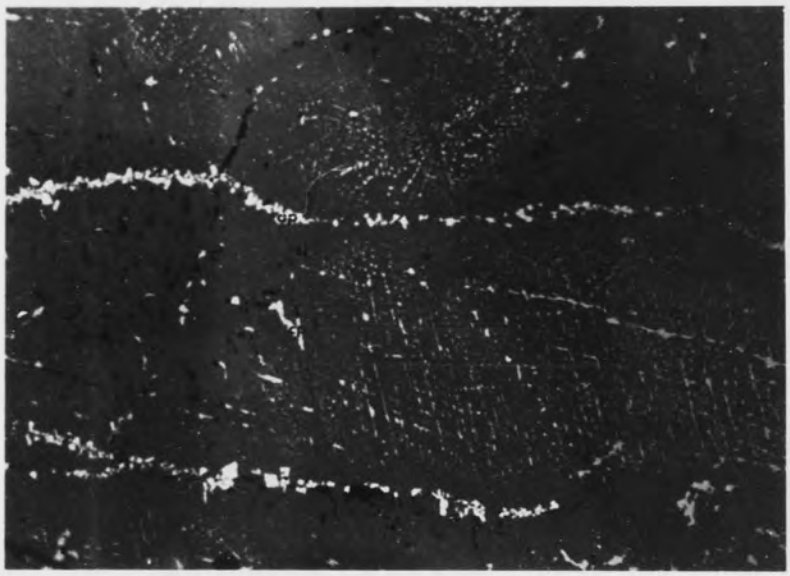

C

PLATE 36

Photomicrographs of Sphalerite.

A,B,C : From borehole H4 at 456 feet depth,
field of view 0.37x0.42mm, oil immersion.

Exsolution bodies of chalcopyrite 2 aligned along zoning in sphalerite 1. Earlier grains of pyrite (py), chalcopyrite (cp), and galena (gn) are present.

PLATE 36

A

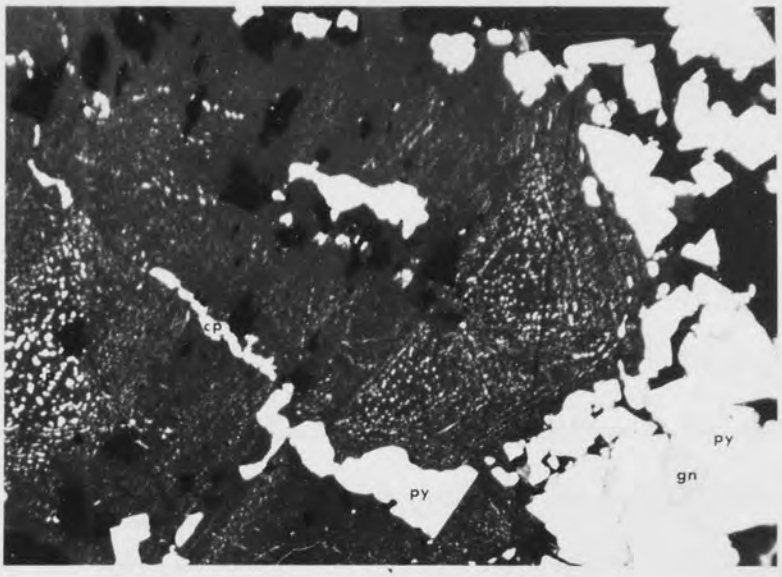

B

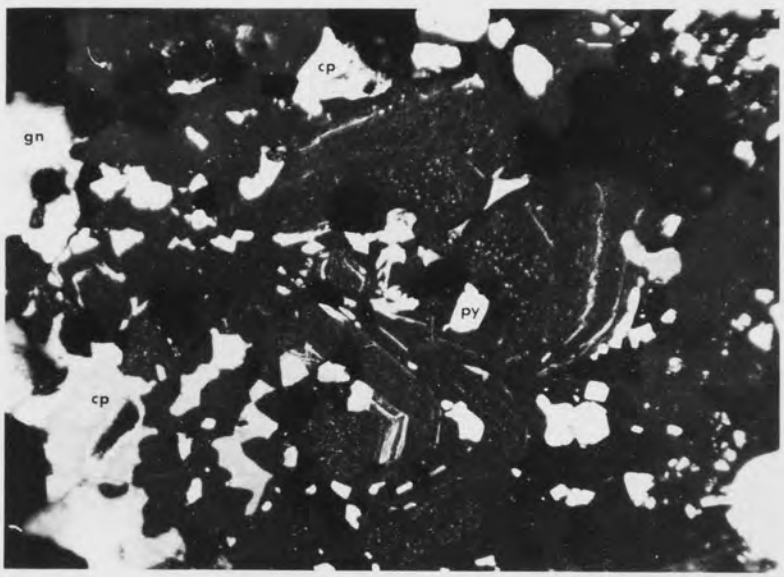

C

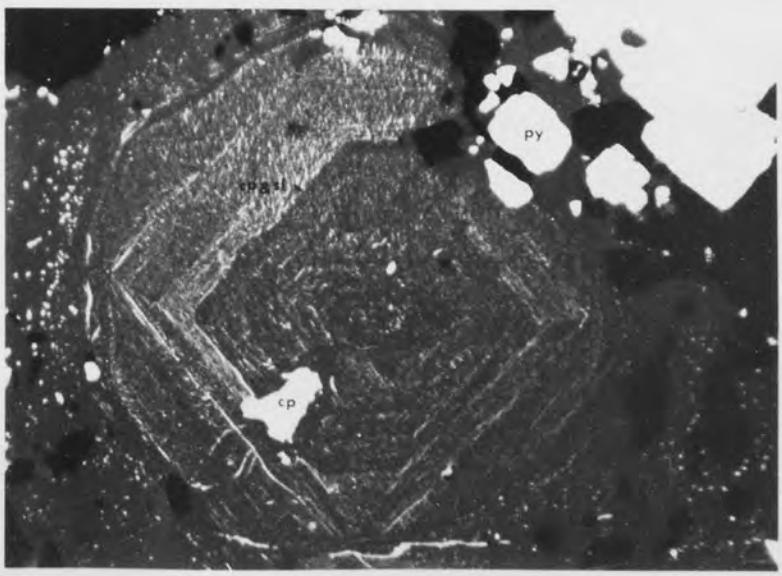

5.2.8 Galena

Galena constitutes approximately 5 percent of the total sulphide at Parys Mountain. It is commonly present in the Bluestone and the Galena-sphalerite ore type, and is comparatively rare in the Copper, and Pyritic-ores. The common occurrence of galena is either as allotriomorphic masses, intimately associated with sphalerite (Plates 37A, B, C, D, and E), such as those in the Bluestone ore, or as granular mosaic masses with irregular outlines embedded in the gangue (commonly quartz) such as those in the Galena-sphalerite ore. The grain size of the galena, measured on etched specimens, varies from 0.05 to 0.3mm (Wheatley, 1971a). In general galena shows the typical triangular polishing pits, and cleavage cracks, are common.

Galena grains, present in the Bluestone ore, commonly contain small inclusions (up to 0.05mm) of tennantite (Plates 37F and 38A), tetrahedrite, and some bismuth sulphosalts, where as those in the other ore types are inclusion-free.

Apart from the common occurrences of galena as described above, it is also present replacing earlier pyrite grains (Plates 15A, 23E and F, and 38A), it also encloses idioblastic pyrite grains (Plates 24A and 37D), or fills the cracks in pyrite. Commonly it is associated with chalcopyrite in filling fractures (Plates 27F and 34B).

The paragenetic position of galena can be placed alongside those of chalcopyrite and sphalerite, although the earliest phase of galena probably pre-dates chalcopyrite and sphalerite. Evidence for this is seen where galena replaces older pyrite grains, and is, in turn, enclosed by chalcopyrite and sphalerite. The last phase of

PLATE 37

Photomicrographs of Galena.

A : From borehole H4 at 474 feet depth,
field of view 0.23x0.27mm, air.

Intergrowths between galena (gn) and sphalerite 2 (sl). Pyrite (py) grains are present (older than both galena and sphalerite.

B,C : From borehole M10 at 1589 feet depth,
B : field of view 0.73x0.83mm, air.
C : field of view 0.37x0.42mm, air.

Intergrowths between galena (gn), chalcopyrite (cp), and sphalerite 1 (with chalcopyrite 1 exsolution).

D : From borehole M10 at 1584 feet depth,
field of view 0.37x0.42mm, oil immersion.

Intergrowths between galena (gn) and sphalerite (almost black) enclosing earlier pyrite (py) grains. The galena is replacing the pyrite grains giving them a corroded outline.

E : From borehole M10 at 1572 feet depth,
field of view 0.37x0.42mm, air.

Galena (gn) infilling fractures in sphalerite 1.

F : From borehole M10 at 1584 feet depth,
field of view 0.15x0.17mm, oil immersion.

Intergrowths between galena (gn) and tennantite (tn) with sphalerite (dark grey).

PLATE 37

A

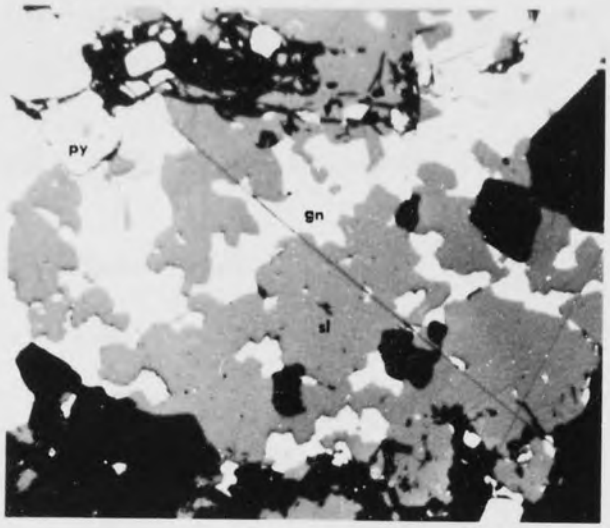

B

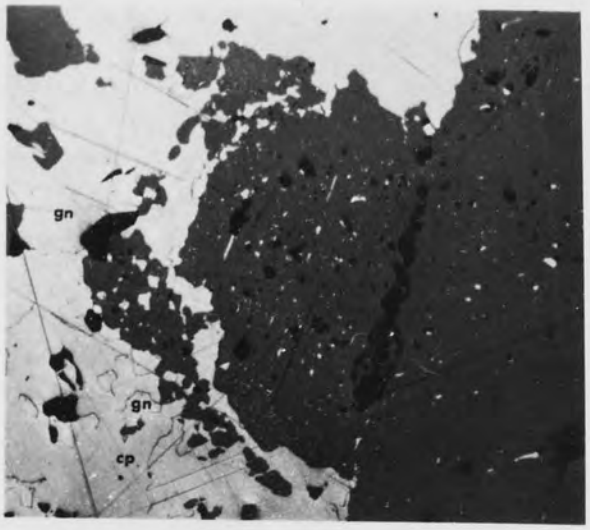

C

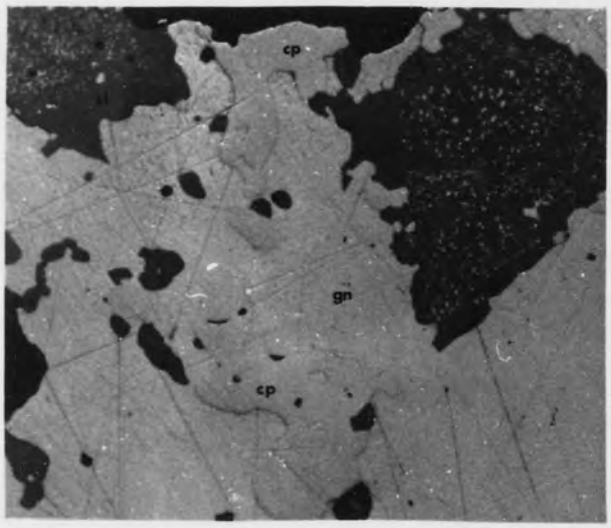

D

E

F

galena ends before that of sphalerite, although its major phase of deposition is contemporaneous with that chalcopyrite and sphalerite.

5.2.9 Tennantite

This mineral occurs mainly in the Bluestone ore type, where it is closely associated with chalcopyrite and galena (Plates 37F and 38A). It is also present in minor quantities in the Copper ore type. It occurs as greenish-grey, irregular grains, with the size-range of 0.01 to 0.15mm. Its common occurrence is as inclusions in, or intergrowths with, chalcopyrite (Plates 28B and C, 38C and D) and galena (Plates 37F, 38A, E and F). These intergrowths occur filling cracks in pyrite grains (Plates 38A, C, and F), and replacing earlier chalcopyrite (Plates 39A, B, and C).

Because of the close association with chalcopyrite and galena, it is probable that the paragenetic position of tennantite is during the early stages of crystallization of these two minerals.

5.2.10 Tetrahedrite

Tetrahedrite is very similar to tennantite in occurrence being commonly associated with chalcopyrite and galena. It is common in the Bluestone ore, and in minor quantities in some specimens of the Copper ore. Tetrahedrite is far less abundant than tennantite, and its grain size rarely exceeds 0.05mm. It is in close association with tennantite, native bismuthinite, and bismuth sulphosalts.

Commonly tetrahedrite occurs as irregular to subround grains, 0.01 to 0.05mm, which are grey with a brownish tint and are isotropic. Tetrahedrite occurs as inclusions, closely associated with bismuth sulphosalts (Plate 39D). It also occurs, associated with tennantite

PLATE 38

Photomicrographs of Galena and Tennantite.

A : From borehole M10 at 1584 feet depth,
field of view 0.15x0.17mm, oil immersion.

Inclusions of tennantite (tn) in galena (gn).

B : From borehole C4 at 813 feet depth,
field of view 0.37x0.42mm, oil immersion.

Galena (gn) replacing cores of two pyrite framboids. Secondary overgrowths of later pyrite are present.

C : From borehole IM9 at 288 feet depth,
field of view 0.11x0.13mm, oil immersion.

Tennantite (tn), intergrowth with chalcopyrite (cp), both of which occur in spaces between pyrite (py) grains.

D : From borehole H14 at 186 feet depth,
field of view 0.37x0.42mm, oil immersion.

Tennantite (tn), with inclusions of older chalcopyrite (cp), enclosed by later chalcopyrite. Earlier pyrite (py) grains are also present.

E : From borehole M10 at 1584 feet depth,
field of view 0.11x0.13mm, oil immersion.

Tennantite (tn), intergrown with galena (gn), and chalcopyrite (cp), filling cracks in pyrite (py) grain.

F : From borehole IM9 at 288 feet depth,
field of view 0.15x0.17mm, oil immersion.

Tennantite (tn), intergrown with galena (gn) and chalcopyrite (cp) replacing pyrite (py) grains.

PLATE 38

A

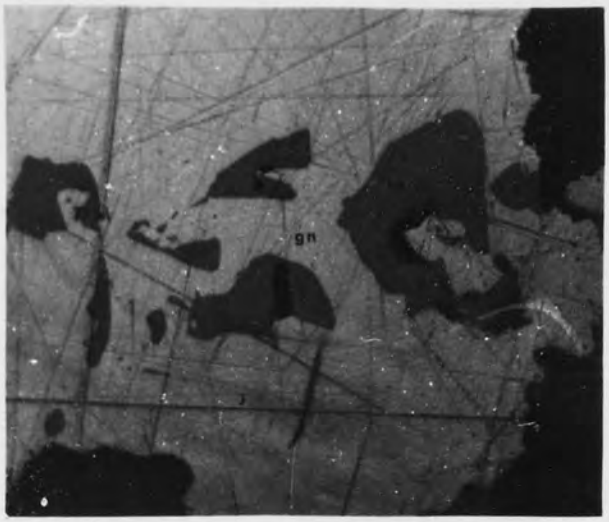

B

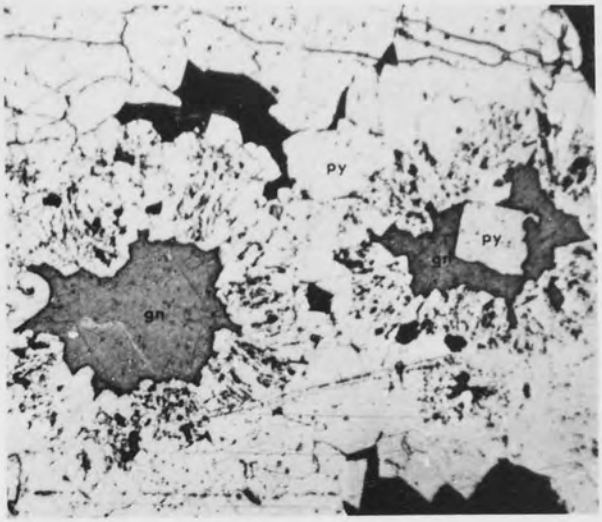

C

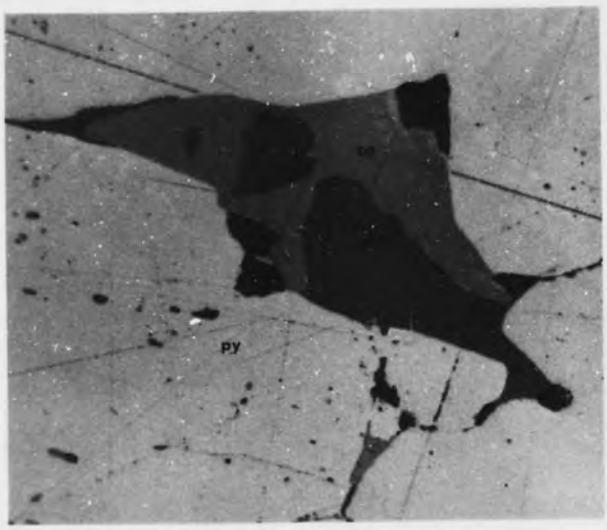

D

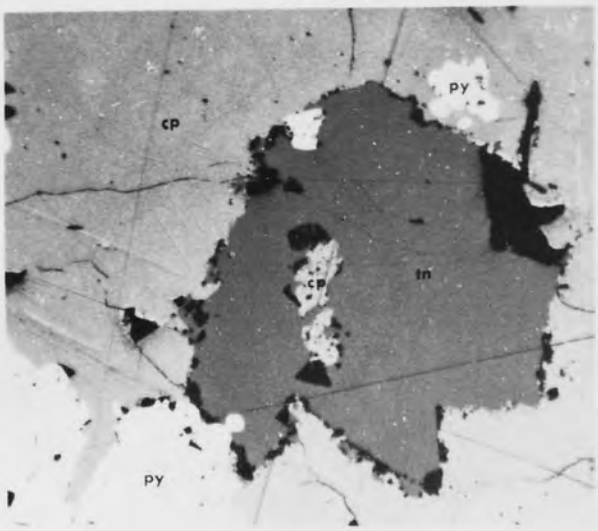

E

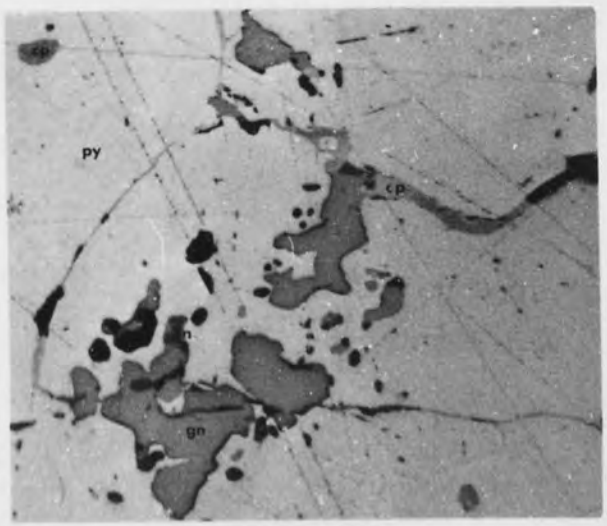

F

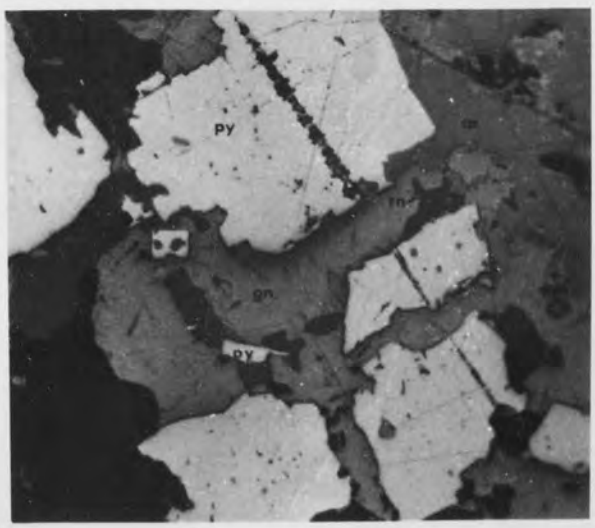

infilling cracks in pyrite (Plate 39F). Native bismuth and bismuthinite are commonly present with these minerals (Plates 39D and F).

Wheatley (1971a) reported the occurrence of tetrahedrite, but not tennantite, at Parys Mountain, and his analyses show that the tetrahedrite is argentian.

5.2.11 Native Bismuth

Native bismuth has a very low hardness and always appears with scratches. The colour is bright creamy white, with shades of pink and yellow. This mineral is present only in minor quantities, and, like the previous two minerals, is found mainly in the Bluestone ore although it is present in some few specimens of the Copper ore. The grain size, in the specimens from the Parys Mountain, is commonly between 0.005 and 0.01mm. It is always in contact with bismuthinite, and is commonly enclosed within, or around the edges of chalcopyrite, galena, and sphalerite masses (Plates 40A, B, and C).

5.2.12 Bismuthinite

Bismuthinite is present mainly in the Bluestone ore, and in some specimens of the Copper ore, and its abundance is approximately the same as that of tennantite. These two minerals are the next most abundant primary ore minerals following pyrite, chalcopyrite, sphalerite and galena.

Bismuthinite commonly occurs as irregular multi-grained patches, which are commonly fibrous with a grain size in the range of 0.005 to 0.02mm. Bismuthinite is white with greenish tint,

PLATE 39

Photomicrographs of Tennantite and Tetrahedrite.

A : From borehole IM6 at 770 feet depth,
field of view 0.15x0.17mm, oil immersion.

Intergrowths between tennantite (tn) and chalcopyrite (cp).

B : From borehole C4 at 960 feet depth,
field of view 0.37x0.42mm, oil immersion.

Tennantite (tn) enclosing framboidal pyrite and subhedral pyrite 2 grains (py). Galena (gn) and chalcopyrite (cp) are present.

C : From borehole H14 at 186 feet depth,
field of view 0.37x0.42mm, oil immersion.

Tennantite (tn) intergrown with chalcopyrite (cp), enclosing sphalerite (sl) and pyrite 2 (py).

D : From borehole M10 at 1584 feet depth,
field of view 0.11x0.13mm, oil immersion.

Tetrahedrite (tt) intergrown with bismuth-sulphosalts (bs) as inclusions in chalcopyrite (cp). Native bismuth (Bi) and bismuthinite (bm) are also present.

E : From borehole M10 at 1584 feet depth,
field of view 0.15x0.17mm, oil immersion.

Tetrahedrite (tt), with tennantite (tn), filling cracks in pyrite 1. Native bismuth (Bi), bismuthinite (bm), and bismuth-sulphosalts (bs) are partly enclosed by, and fill cracks in, pyrite 2.

PLATE 39

A

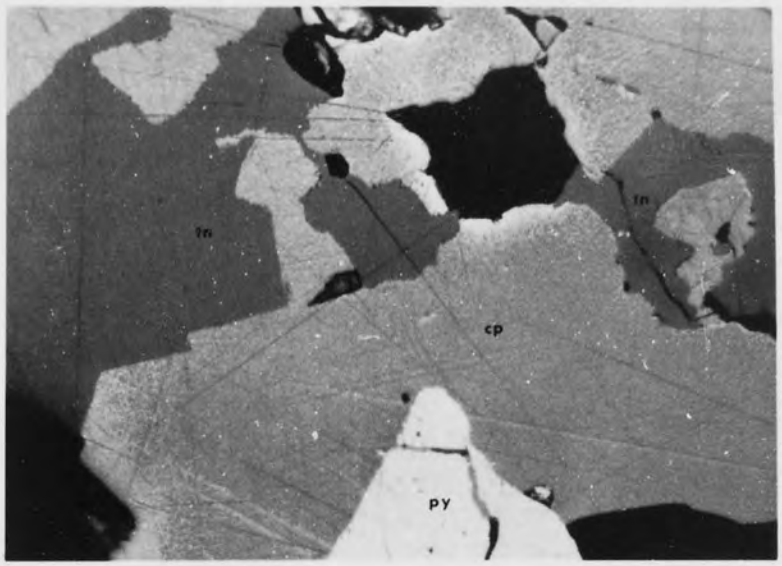

B

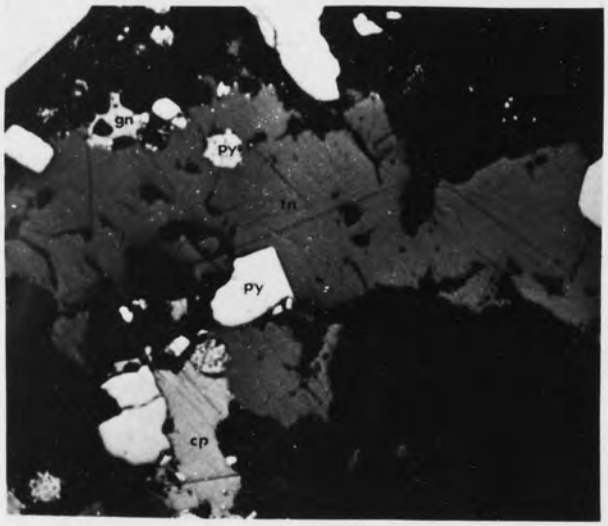

C

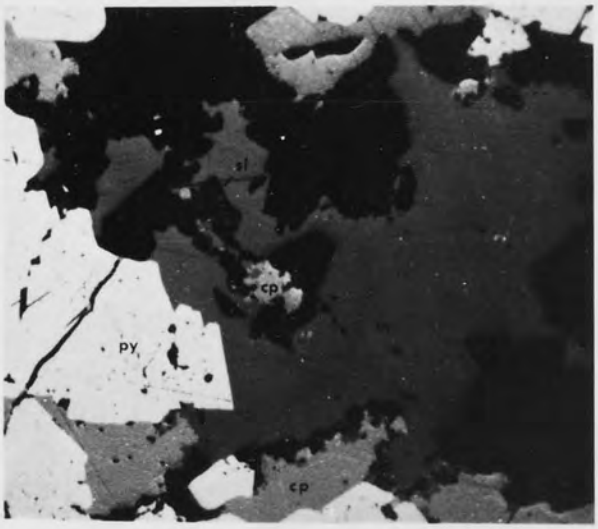

D

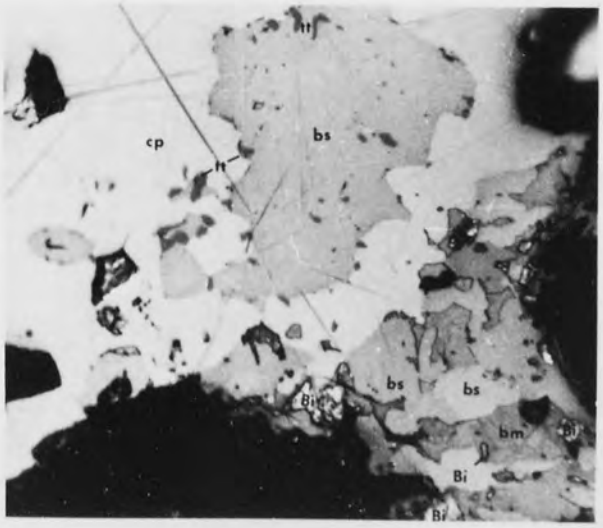

E

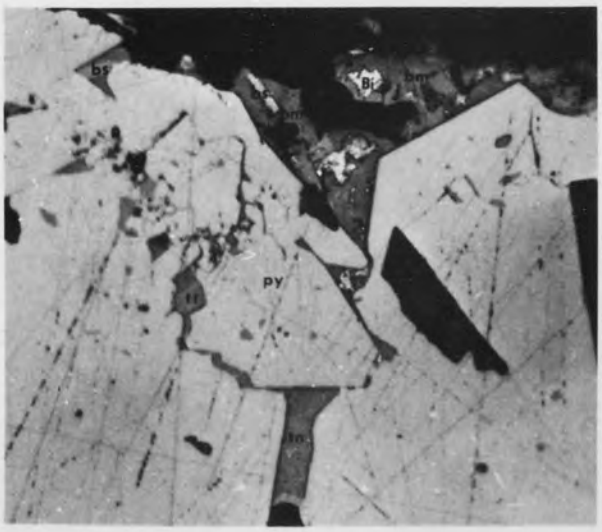

shows a very strong bireflectance, and has strong anisotropy. Individual grains were determined through using these properties. Bismuthinite is closely associated with native bismuth, bismuth sulphosalts, and tetrahedrite, and commonly occurs as inclusions in, or near to the edges of, chalcopyrite, galena, and sphalerite masses (Plates 40A, B, C, D, E, and F).

5.2.13 Bismuth Sulphosalts

This group of minerals occurs in close association with native bismuth, bismuthinite, the tetrahedrite group minerals, chalcopyrite, galena, and sphalerite. Its abundance is slightly less than that of tennantite, and bismuthinite, but it is approximately 4 to 5 times more abundant than native bismuth, tetrahedrite and bournonite. Positive identifications of individual minerals were not made because of the small grain size, up to 0.025mm, and partly because of the lack of diagnostic optical features. Electron probe microanalysis would give positive identifications, but this tool was not available for this study. However, considering their general optical and physical characteristics, together with associations with other minerals, they were grouped together in the bismuth sulphosalt group.

On the basis of their properties in reflected light the bismuth-sulphosalts were divided into two types.

A. Bismuth-sulphosalt 1

This mineral varies in colour from pale yellow with greenish tint, to greenish grey and has a hardness very similar to that of chalcopyrite. It has strong bireflectance, and strong anisotropy

PLATE 40

Photomicrographs of Bismuthinite, Native Bismuth, and Bismuth-Sulphosalts.

A : From borehole M10 at 1548 feet depth,
field of view 0.11x0.13mm, oil immersion.

Intergrowths between native bismuth (Bi), bismuthinite (bm), and bismuth-sulphosalts (bs1 and bs2).

B : From borehole M10 at 1584 feet depth,
field of view 0.09x0.11mm, oil immersion.

Intergrowths between native bismuth (Bi), bismuthinite (bm), and bismuth-sulphosalts (bs), enclosing a chalcopyrite (cp) grain.

C : From borehole M10 at 1584 feet depth,
field of view 0.15x0.17mm, oil immersion.

Native bismuth (Bi), bismuthinite (bm), and bismuth-sulphosalts (bs) inclusions in chalcopyrite (cp).

D : From borehole M10 at 1584 feet depth,
field of view 0.09x0.11mm, oil immersion.

Bismuthinite (bm) and bismuth-sulphosalts (bs) in quartz matrix. Chalcopyrite (cp) is present.

E : From borehole M10 at 1584 feet depth,
field of view 0.15x0.17mm, oil immersion.

Intergrowths between bismuthinite (bm) and bismuth-sulphosalts (bs), enclosing sphalerite 1 which has chalcopyrite 1 (cp) inclusions.

F : From borehole M10 at 1521 feet depth,
field of view 0.23x0.27mm, air.

Intergrowths between chalcopyrite (cp), bismuthinite (bm), tetrahedrite (tt), and sphalerite (sl). Earlier pyrite (py) grains are enclosed and replaced by bismuthinite and chalcopyrite.

Facing page 115

PLATE 40

A

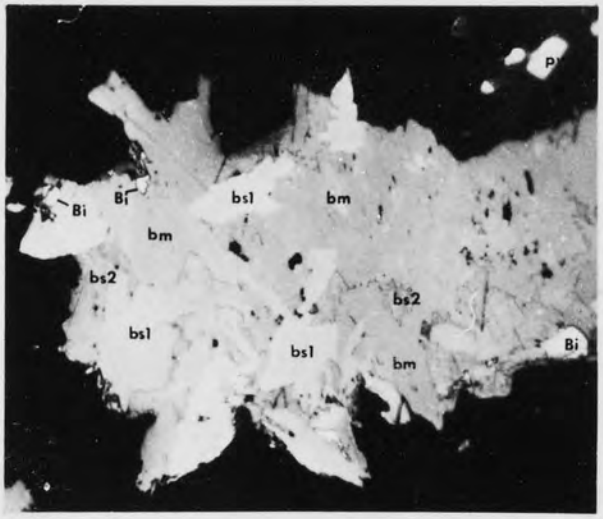

B

C

D

E

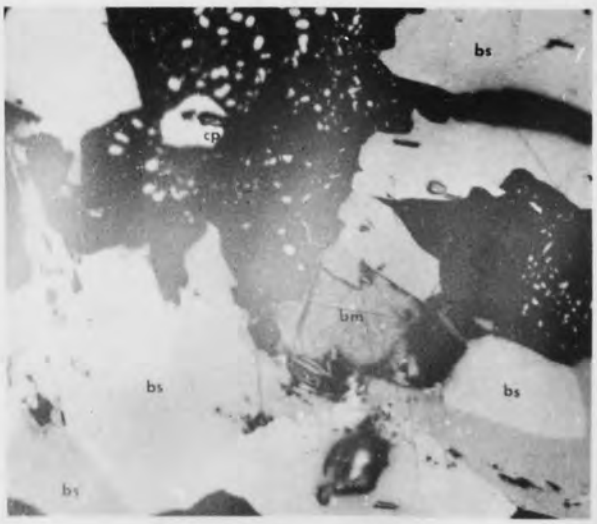

F

through which the shape and size of individual grains can be detected. It commonly occurs as anhedral granular grains in the size range of 0.001 to 0.05mm, and is closely associated with bismuthinite.

B. Bismuth-sulphosalt 2

This mineral is less abundant than 1, the proportion is approximately 1 to 10. Its colour is light grey, or creamy white and is slightly darker than galena. The hardness is a little lower than that of galena, but is higher than native bismuth. Bireflectance and anisotropy are present, but are very weak. Its common occurrence is as fibrous or tabular grains which are generally less than 0.002mm in length

The general appearance of both types of bismuth-sulphosalts, described above, are illustrated in Plates 40A, B, C, D, E, and F, 41A and B, and a comparison between the two is shown in Plate 40A.

5.2.14 Bournonite

This mineral was reported to be present in trace quantities in the Parys Mountain ore bodies by Wheatley (1971a). In this study a mineral whose characteristics fit the description of bournonite, (harder than galena but softer than chalcopyrite, pale greyish white with shades of blue, or green, weakly anisotropic, and always associated with galena, chalcopyrite, tetrahedrite, and bismuth-minerals) is present in some specimens from the Copper and Bluestone ores. However, since the grain size is very small, less than 0.005mm, a positive identification was not made. This mineral is rare, and where found commonly enclosed in chalcopyrite grains.

The paragenetic position of the six minerals, (from tennantite to the bismuth-sulphosalt group), judging from their occurrences, and their close association with chalcopyrite, galena, and sphalerite, is that they were probably contemporaneous with or slightly later than, the main stage of crystallization of the three major sulphides.

Secondary Minerals

5.2.15 Haematite

Haematite is present in trace quantities, as an alteration product of pyrite in all ore types, and occurs as small inclusions (0.02mm) in the pyrite grains (Plates 19C and E). The grains are commonly tabular in shape, and their colour is a blueish grey, or steel grey, with typical red internal reflections.

5.2.16 Covellite

Covellite is present locally in the Copper ore and has a close association with bornite. It forms veinlets, commonly 0.02mm thick, either along cleavage cracks in chalcopyrite grains, or as fibrous penetrative branches into the chalcopyrite mass (Plate 41C), though one euhedral grain (0.001mm) of covellite was observed (Plate 41D). Covellite is blue in various shades, with strong bireflectance. It is anisotropic with striking bright orange or reddish brown colour.

5.2.17 Bornite

Bornite is present in association with covellite in the supergene enriched part of the Copper ore type, and occurs as an alteration of chalcopyrite. It commonly forms euhedral to subhedral grains, in the 0.001 to 0.01mm size-range, and is almost always enclosed by covellite (Plates 41E and F). Its colour is brown with shades of pink, and bireflectance and anisotropy are detectable but are weak.

5.2.18 Siderite

The presence of siderite was not observed in the polished

PLATE 41

Photomicrographs of Bismuth-sulphosalts, Covellite, and Bornite.

A : From borehole M10 at 1521 feet depth,
field of view 0.37x0.42mm, air.

Intergrowths between bismuth-sulphosalts (bs), tennantite (tn), and chalcopyrite (cp).

B : From borehole M10 at 1548 feet depth,
field of view 0.15x0.17mm, oil immersion.

Intergrowths between bismuth-sulphosalts (bs) and chalcopyrite (cp), enclosed by sphalerite (dark).

C : From borehole H14 at 195 feet depth,
field of view 0.15x0.17mm, oil immersion.

Covellite (co) (vein-like with small branches) formed along cracks in chalcopyrite (cp). Sphalerite (sl) grains are present.

D : From borehole H14 at 195 feet depth,
field of view 0.09x0.11mm, oil immersion.

Subhedral grains of covellite (co) at the edges of a chalcopyrite (cp) grain.

E,F : From borehole H14 at 195 feet depth,
field of view 0.15x0.17mm, oil immersion.

Bornite (bn) associated with, and enclosed by, covellite (co) along cracks in chalcopyrite (cp). Grains of pyrite 1 (py) are present.

PLATE 41

A

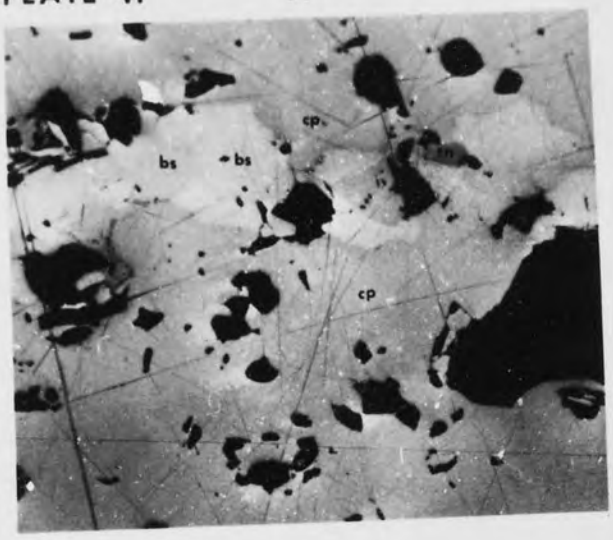

B

C

D

E

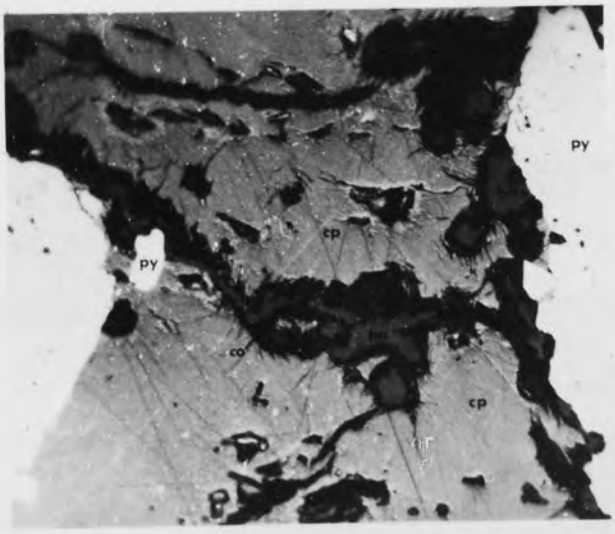

F

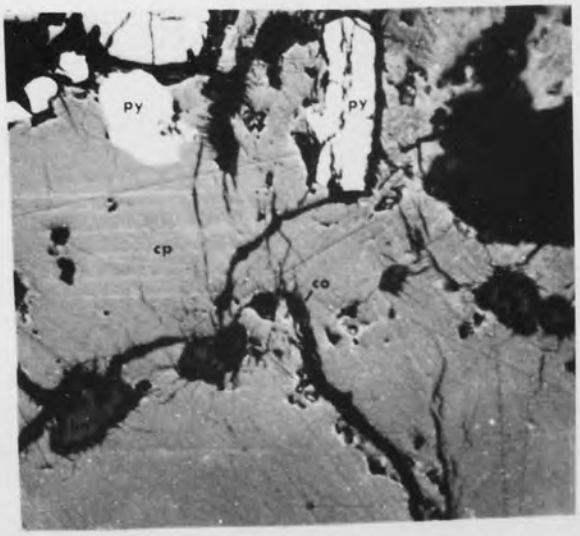

specimens, but was detected in thin section and in hand specimen. Because siderite is present in the altered parts of the rhyolitic tuffs which are the host rocks of Pyritic ore type, and occurs in specimens containing pyrite, its description is given in this section.

Positive identification of siderite was made by x-ray diffraction, and transmitted light microscopy.

Siderite is present commonly as clusters of subspherical grains between 2 to 8mm diameter. In thin section, siderite exhibits a radiating texture, commonly with some haematite and pyrite in the core. Because of its radiating form, and the host rock, siderite is believed to be secondary in origin, and probably replaces spherulites in the rhyolitic tuffaceous sediments.

5.2.19 Gangue Minerals

The major gangue mineral associated with sulphides at Parys Mountain, is quartz, which is present both as a primary and as a secondary mineral. It was probably developed throughout the period of mineralization because the host rocks are commonly silitic, e.g. the siliceous sinter, and the rhyolitic rocks. As a secondary mineral, quartz commonly occurs as veins cutting all the rock types, and most ore types. These late-stage quartz veins are commonly free of sulphides.

The next most abundant gangue minerals are chlorite and sericite, both of which are commonly present as alterations of minerals in the slates, dacitic rocks, and rhyolitic rocks.

Carbonate minerals, mainly calcite, are also present in the gangue in minor quantities. In general carbonate gangue occurs only

in the dacitic and rhyolitic rocks.

The paragenesis of quartz is very extensive, i.e. quartz is formed throughout the paragenetic sequence. Chlorite may be partly primary, especially in those deposits associated with the slates, but the majority is secondary. Sericite and the carbonate minerals are secondary, and the carbonate minerals probably were the latest minerals to be formed.

5.3 Ore Mineral Paragenesis

The paragenetic sequence of the ore minerals at Parys Mountain, is given in Table 4. This interpretation was made on the basis of inter-relationships between the minerals, as well as their relationship to the associated host rocks. Examples of the phenomena used as evidence are replacement fabrics, cross cutting relationships, the enclosure of one mineral by another, the filling of cracks in minerals, the associated minerals, and secondary fabrics such as overgrowths, deformation of mineral grains, and corrosion textures.

The paragenetic position of each mineral has been briefly outlined in the previous section, accompanying their general descriptions. This section will mainly deal with the inter-relationships between the minerals to develop a paragenetic sequence for all the minerals.

The ore minerals at Parys Mountain are divided into two main groups: primary minerals, i.e. those being formed during the original ore forming episode; and secondary minerals, those formed as a consequence of the alteration of pre-existing minerals.

Table 4 Paragenesis of Ore Minerals at Parys Mountain.

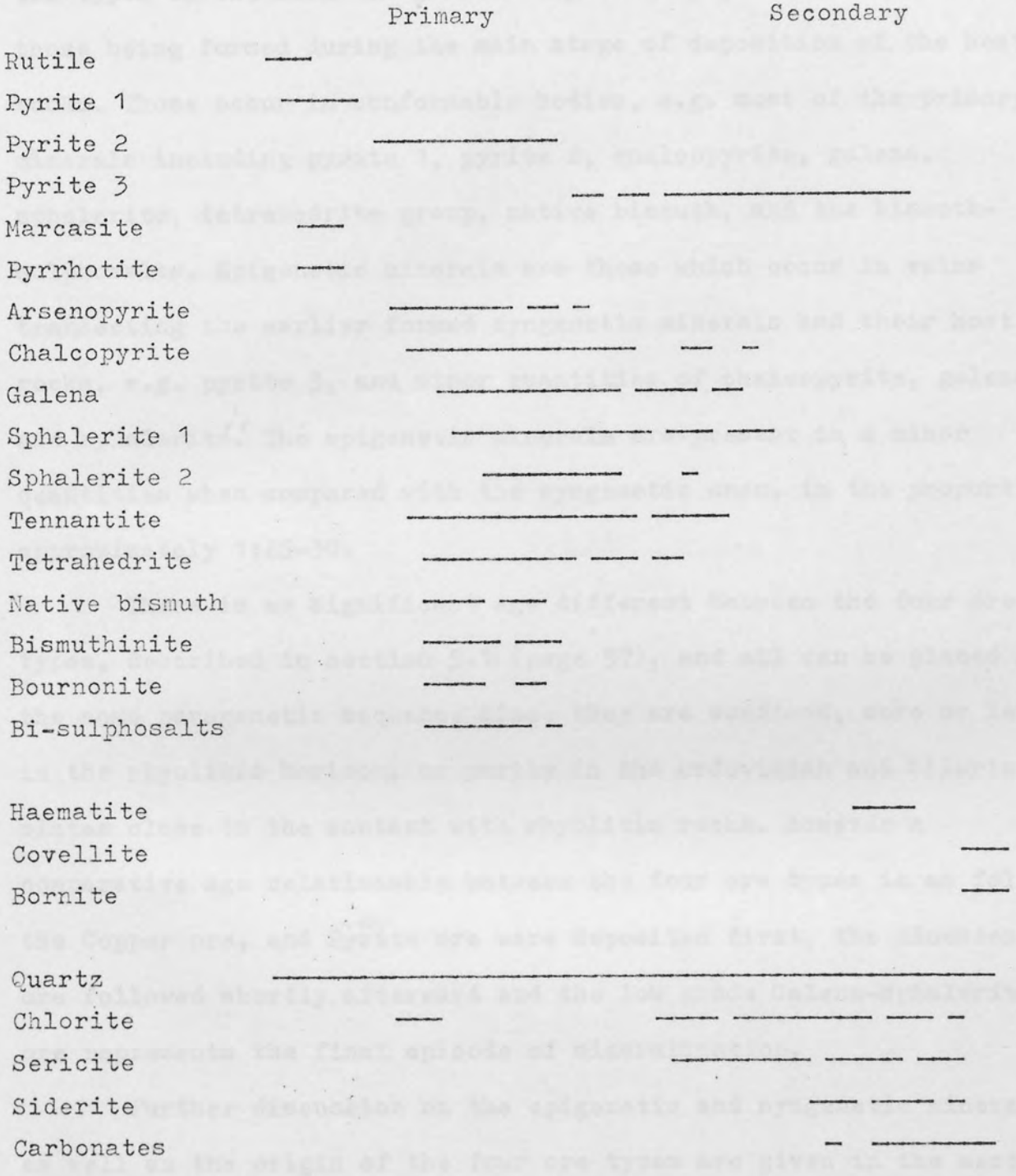

Mineralization at Parys Mountain can also be divided into two types on the basis of genetic aspects; syngenetic minerals are those being formed during the main stage of deposition of the host rocks. Those occur in conformable bodies, e.g. most of the primary minerals including pyrite 1, pyrite 2, chalcopyrite, galena, sphalerite, tetrahedrite group, native bismuth, and the bismuth-sulphosalts. Epigenetic minerals are those which occur in veins transecting the earlier formed syngenetic minerals and their host rocks, e.g. pyrite 3, and minor quantities of chalcopyrite, galena, and sphalerite. The epigenetic minerals are present in a minor quantities when compared with the syngenetic ones, in the proportion approximately 1:25-30.

There is no significant age different between the four ore types, described in section 5.1 (page 57), and all can be placed in the same paragenetic sequence since they are confined, more or less, in the rhyolitic horizon, or partly in the Ordovician and Silurian slates close to the contact with rhyolitic rocks. However a comparative age relationship between the four ore types is as follows: the Copper ore, and Pyrite ore were deposited first, the Bluestone ore followed shortly afterward and the low grade Galena-sphalerite ore represents the final episode of mineralization.

Further discussion on the epigenetic and syngenetic minerals, as well as the origin of the four ore types are given in the section on ore genesis.

5.3.1 Rutile

Rutile is probably the first mineral of the paragenetic

sequence because its host rocks, the Ordovician slates and the dacitic rocks, are the oldest of those containing mineralization, and it is completely absent from the later quartz matrix. The general appearance of rutile also indicates its early formation, as it is replaced both by chlorite or sericite, from the matrix of the host rocks, and by chalcopyrite (Plates 12A, B, and C).

According to Ramdohr (1969) rutlie is a common primary accessory mineral in igneous rocks. It also occurs as detrital grains in sedimentary rocks,or as an alteration product of ilmenite or other titano-ferrous minerals. Rutile formed as an alteration product would be intimately associated with haematite and pyrite (if sulphur is available). Such intergrowths are absent in rutiles from Parys Mountain hence it is likely that this mineral formed either as a primary accessory mineral in the dacitic rocks, or as detrital grains in the Ordovician sediments.

The close association between rutile and pyrite 1, especially the pyritohedral pyrite, is universal in the host rocks. This indicates that these minerals may have been deposited contemporaneously. The occurrence of a string of rutile grains, which has been slightly deformed due to the formation of pyritohedral pyrite (Plate 12D), indicates that this rutile was earlier than pyritohedral pyrite (pyrite 1).

5.3.2 Pyrite 1

This oldest generation of pyrite includes the pyritohedral pyrite, associated with rutile (Plates 12D, E, and F), and those euhedral pyrites exhibiting secondary overgrowths (Plates 19A, B, C, and D), or corrosion (Plates 21C, D, and E). Its paragenesis is

later than rutile, but is earlier than other ore minerals.

The majority of pyritohedral pyrite grains were not affected by shattering or deformation, but cataclastic textures are present in some. Since most later phases do not have cataclastic or shattering effects, it is possible that the cataclastic textures were developed locally, probably after the formation of the pyrites, but prior to the main episode of mineralization.

Euhedral pyrites, with secondary overgrowths and corrosion fabrics, are probably slightly later than the pyritohedral pyrite. They are commonly associated with, and are commonly replaced or enclosed by, later sulphide phases.

The 'pyrite flame' (Plate 25C) is classed as part of the earliest part of pyrite 1 generation because its sedimentary, or slump texture, indicates contemporaneity with the enclosing sediments.

5.3.3 Marcasite

Marcasite is interpreted as being later than the pyritohedral pyrite and contemporaneous with, or earlier than, the later euhedral pyrite 1. This interpretation is made because marcasite occurs only in the cores of, and enclosed by, the euhedral pyrite 1 (Plates 23C and D, 26D and E), and it is absent from the pyritohedral pyrite. Since marcasite commonly changes to pyrite (Ramdohr, 1969), its occurrence within pyrite 1 suggests that it was replaced by the pyrite rather than being deposited contemporaneously with it.

5.3.4 Pyrrhotite

The only occurrence of pyrrhotite is as inclusion blebs in euhedral grains of pyrite 1. Exsolution is extremely rare in pyrite (Ramdohr, 1969), thus the pyrrhotite probably represents the remnants of earlier formed grains replaced by pyrite. The paragenetic position of pyrrhotite thus is approximately the same as that of marcasite, i.e. later than pyritohedral pyrite, but earlier than most of the pyrite 1.

5.3.5 Pyrite 2

The pyrites of the second generation (pyrite 2) include those with framboidal, colloform, and recrystallization fabrics (such as a poikilitic texture), and other textures produced by secondary overgrowths. The paragenetic position of these pyrites is extensive, and they are probably formed throughout the main stage of mineralization at Parys Mountain. This interpretation is based on the extensive association of these pyrites with other ore minerals. However, the beginning of deposition of pyrite 2 must be earlier than that of the major sulphide phases because it is very commonly replaced by them.

5.3.6 Arsenopyrite

Arsenopyrite deposition extends from the beginning of the main stage of mineralization to just before the end. This interpretation is made on the basis of its close association with chalcopyrite, galena, and sphalerite (Plates 27B, C, and D). Arsenopyrite crystals are present in a matrix of these sulphides which are later than the arsenopyrite. Some arsenopyrite is later

than chalcopyrite and sphalerite (Plate 35B) in that it occurs in veinlets which cut through sphalerite grains containing chalcopyrite 2 exsolution.

5.3.7 Chalcopyrite

Chalcopyrite, galena, and sphalerite are commonly intimately intergrown, and they replace each other in various specimens. These three major sulphides are thus probably contemporaneous in deposition which extended over a long period.

Chalcopyrite is associated with almost every other mineral, and it replaces most of the earlier minerals, e.g. rutile (Plate 12A), broken grains of pyritohedral pyrite (Plate 24E), marcasite (Plate 26D), and pyrrhotite (Plates 26E and F). It also replaces pyrite 2, and commonly has intergrowths with the sulphosalts. Its deposition probably began earlier than the other two major sulphide ores (galena and sphalerite), and the sulphosalts, since it is commonly enclosed by them.

5.3.8 Galena

Galena, like chalcopyrite, is extensive in its paragenesis. Its occurrence is similar to that of chalcopyrite, but it is less abundant. Galena does not replace rutile, pyritohedral pyrite, marcasite, or pyrrhotite, but it does enclose chalcopyrite. Because of this it is believed that the deposition of galena began later than that of chalcopyrite, although they are both contemporaneous in their stages of deposition.

5.3.9 Sphalerite

Both sphalerite 1 and sphalerite 2 are discussed together since they have only slightly different age relationships (cf. section 5.3.7). Sphalerite is slightly later than galena in the paragenetic sequence in that it replaces and/or encloses chalcopyrite and galena, both of which fill fractures in pyrite grains (Plates 34A and B). The main stage of deposition of sphalerite is extensive and contemporaneous with that of chalcopyrite and galena. The three stages of chalcopyrite exsolution in sphalerite 1 indicate that the two minerals were deposited from the same ore solution.

5.3.10 Tetrahedrite Group, Native Bismuth, Bismuthinite and Bismuth-sulphosalts.

These minerals are discussed together because they are closely associated. They are commonly associated with chalcopyrite, galena, and sphalerite. Their position in the paragenetic sequence is approximately the same as that of galena. Tennantite is probably the earliest among these minerals, and may also be earlier than some galena because it commonly has intergrowths with chalcopyrite (Plate 23C),and accompanies chalcopyrite filling fractures in pyrite. The common occurrence of these minerals within chalcopyrite, and in some instances, within galena and sphalerite, is used as an indication of their paragenetic position.

5.3.11 Pyrite 3

This is the latest primary sulphide in the paragenetic sequence. The position of pyrite 3 in the sequence is indicated by its association with quartz veins, the almost undeformed character

of these grains, and the fact that it is not replaced by any of the earlier minerals.

5.3.12 Secondary Minerals

Haematite, covellite, and bornite are all very late in the paragenetic sequence since they formed as a result of alteration of pyrite and chalcopyrite. Haematite is probably the earliest and may be earlier than some of the pyrite 3. This interpretation is based on the fact that haematite is present only in pyrite 1 and pyrite 2. Covellite and bornite are contemporaneous, and are the latest in the paragenetic sequence.

5.3.13 Gangue Minerals

Quartz has the most extensive paragenetic position among the minerals present at Parys Mountain and occurs both as a primary and secondary mineral. The earliest episode is associated with deposition of the siliceous sinter, and the rhyolitic rocks. This episode is probably contemporaneous with the euhedral pyrite 1. The latest quartz occurs as veins which either carry pyrite 3, or are barren.

Chlorite is present partly as a primary mineral formed during the deposition and diagenesis of the Ordovician sediments, but the majority formed as a secondary mineral replacing original ferromagnesian minerals.

Sericite, siderite, and the carbonate minerals most commonly are the result of alteration processes in the host rocks. Some carbonates are present as very late stage veinlets and hence are the last formed gangue minerals.

In addition to the microscopic textures of the ores, described in previous sections, many ore textures, observed in hand specimens, are also used in genetic interpretation of the ores. These include colloform layering of pyrite in matrix of quartz and Ordovician sediments (Fig. 11A), stockworks of pyrite and chalcopyrite associated with quartz in Ordovician sediments (Fig.11B), layering of sedimentary inclusions in massive chalcopyrite masses (Fig.11C), interlayering between chalcopyrite, sphalerite, and pyrite, with some galena, in quartz matrix (Fig.11D), fragments of Ordovician sediments,containing pyrite crystals, being cemented by barren quartz (Fig.11E), and folding of pyrite + chalcopyrite layer in quartz matrix (Fig.11F). The interpretation and discussion of these features are made in chapter on ore genesis.

Figure 11 Sketches of Polished Section Specimens to Show Various Macroscopic Textures of the Sulphide Ores.

A : From borehole H43A at 1850 feet depth

Colloform layering of pyrite in quartz matrix and Ordovician slate.

B : From borehole H43A at 1855 feet depth

Chalcopyrite + pyrite stockworks associated with quartz in Ordovician slate.

C : From borehole IM6 at 1392 feet depth

Layering of Ordovician sediment inclusions in massive chalcopyrite.

D : From borehole M10 at 1548 feet depth

Interlayering of chalcopyrite, sphalerite, and pyrite with some galena in quartz matrix.

E : From borehole C4 at 745 feet depth

Fragments of Ordovician slates containing pyrite crystals being cemented by barren quartz.

F : From borehole M10 at 1620 feet depth

Folding of pyrite + chalcopyrite in quartz matrix.

: Pyrite

: Chalcopyrite

: Galena

: Sphalerite

: Quartz

: Slate

Facing page 131

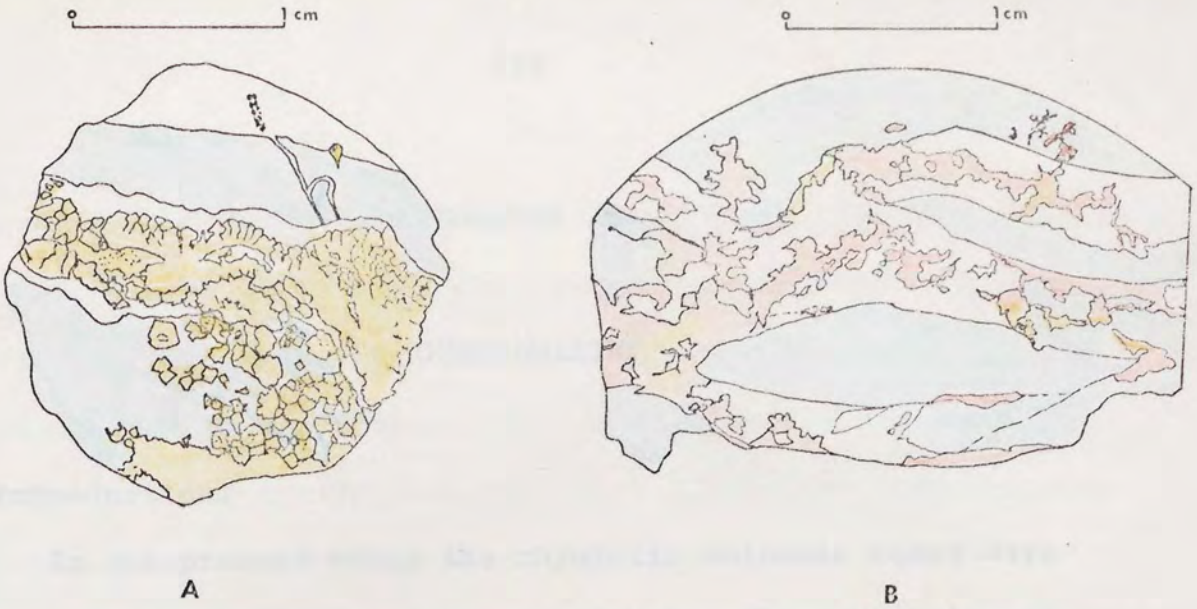

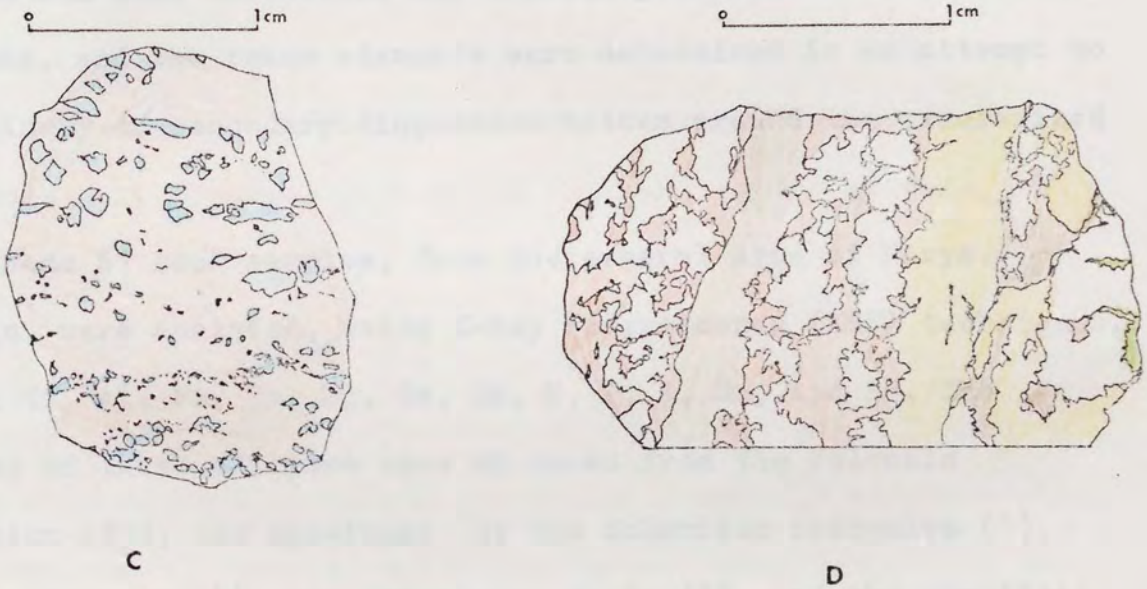

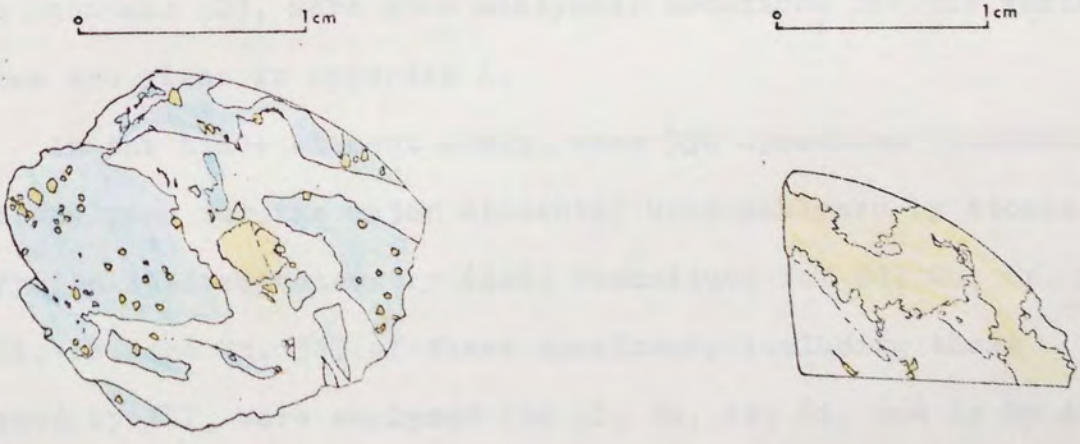

Figure 11

CHAPTER 6

GEOCHEMISTRY

6.1 Introduction.

In the present study the rhyolitic volcanic rocks were analysed for both major and trace elements. The major element analysis was done to outline the overall geochemical variation in the rocks, and the trace elements were determined in an attempt to find primary or secondary dispersion haloes around the mineralized zones.

Some 61 rock samples, from the general area of Parys Mountain, were analysed, using X-ray fluorescence (XRF) techniques, for Si, Ti, Al, Fe, Mn, Mg, Ca, Na, K, P, S, Sr, and Rb. The majority of these analyses were on rocks from the volcanic succession (53), but specimens of the doleritic intrusive (1), the Mona Complex (4), the Ordovician slate (1), and the rhyolitic rocks which crop out in the areas both to the east and west of Parys Mountain (2), were also analysed. Locations for the various samples are given in Appendix A.

In the trace element study, some 350 specimens (including those analysed for the major elements) were analysed by Atomic Absorption Spectrophotometry (AAS) techniques for Cd, Co, Cr, Cu, Hg, Ni, Pb, and Zn. 315 of these specimens, including those analysed by XRF, were analysed for Al, Ba, Fe, Si, and Sr by AAS. This was done to allow comparision of the results obtained from both techniques. Relationships between the concentrations of

different elements and the elements contained in the ore minerals (Cu, Pb, Zn, Fe) were made using computer techniques (see Appendix E for computer programme information). This was done to determine if an association exists between particular elements and anomalous concentrations of ore-metals, e.g. high Si content corresponding to an anomalous ore-metal content may indicate an association between mineralization and silicification. The relationship between the trace element distributions and the petrology and stratigraphy was investigated to determine if anomalous concentrations are present in particular rock types or stratigraphic horizons. The occurrence of any correlation would indicate if the petrologic, stratigraphic, or structural controls apply to the ore bodies.

Cu, Pb, Zn, and Fe were determine in an attempt to discover if primary or secondary dispersion haloes of the ore-metals are present around the mineralized zones. The discovery of anomalous concentrations of these elements has led to the discovery of many ore bodies, e.g. those of New Brunswick and the Gaspe' peninsula in eastern Canada (Hawkes and Webb, 1962), the Adak area of northern Sweden (Nairis, 1971).

The Co:Ni ratio in sulphides has been used to indicate the depositional environment of the ores (Loftus-Hills and Solomon, 1967). These elements are commonly found in pyrites associated with economic sulphide mineral deposits. The reflected light studies of the pyrites show that colour zoning is present in them which may be the result of substitution of either or both these elements in the pyrite lattice.

Cd was determined as it is closely associated with Zn (Rankama and Sahama, 1950), and it may act as "pathfinder element" for Zn.

Cr shows strong association with Ni and Mg in basic rocks; and with Fe and Al in sedimentary cycle (Hawkes and Webb, 1962). Correlation between Cr and either pairs of these elements may be used to determine depositional environment of the rocks.

Ba and Sr are associated with Ca, because of their similar chemical properties, and similarly Rb is closely associated with K (Rankama and Sahama, 1950; Krauskopf, 1967). The abundance and distribution of these elements is useful for comparing the rocks of Parys Mountain with similar rocks in other parts of the Caledonian Geosyncline. Ba also accompanies many Lead-Zinc sulphide ores as barite which is relatively unstable (Hawkes and Webb, 1962) thus may be a useful "pathfinder element"for deposits of Pb and Zn.

Hg is a "pathfinder element" for the base metal sulphide deposits, because of its close association with Sb, As, Se, Ag, Zn, and Pb. It has a low background content in the lithosphere, i.e. less than 0.1ppm in igneous rocks and less than 0.5ppm in sedimentary rocks (Rankama and Sahama, 1950). An anomalously high Hg content in the rocks around the sulphide mineralized zones would constitute a primary halo (Hawkes and Webb, 1962; Kraynov, Volkov, and Korol'kova, 1966).

6.2 Bulk Chemistry.

A description of the techniques used in whole rock chemical analyses, and a complete list of the analyses is given in Appendix D.

The volcanic rocks of Parys Mountain are of the orogenic calc-alkaline type, and the main lines of evidence are listed below:-

1) Wilson et al. (1965) plotted values for both typical oceanic alkaline lavas and typical orogenic calc-alkaline lavas on a Niggli alk-si diagram. This diagram allowed a smooth curve to be drawn separating the two groups of lavas. Values for the volcanic rocks from Parys Mountain, plotted on a similar diagram (Fig.12) all lie within the orogenic calc-alkaline field.

2) The Differentiation Index (D.I.), which is the sum of normative percentages of quartz, orthoclase, albite, nepheline, leucite, and kalsilite (Thornton and Tuttle, 1960), was calculated for the analyses and these indices are listed in Table 12 (Appendix D).

Thornton and Tuttle (1960, p.675) plotted a silica-D.I. diagram for 5000 analyses of igneous rocks and produced contours for silica distribution and two lines separating oversaturated, saturated, and undersaturated rocks. The contours for silica distribution showed two maxima, one at a D.I. of 38 and a silica content of about 52 percent (corresponding to the basalts and gabbros), and the other, a very strong maxima, at a D.I. of 90 and a silica content of 75 percent (corresponding to the granites and rhyolites). The line separating saturated and undersaturated rocks

Aston University

Illustration has been removed for copyright restrictions

Si

Figure 12 Niggli alk-si diagram for the metamorphic and volcanic rocks at Parys Mountain, showing the curve separating the fields of oceanic alkaline and orogenic calc-alkaline rocks (from Wilson et al., 1965).

is drawn from the silica content of albite (at D.I. 100, silica 64.7 percent) to the silica content of anorthite (at D.I. 0, silica 43.2 percent). Rocks whose analyses fall below the line are undersaturated. The line separating saturated and oversaturated rocks is drawn from the silica content of orthoclase (at D.I. 100, silica 69.0 percent) to the silica content of anorthite. Rocks whose analyses fall above this line are oversaturated. The weight percent of silica and D.I. for each of the volcanic rocks from Parys Mountain were plotted on a similar diagram on which the above contours and lines were reproduced (Fig.13). Values for the rhyolitic rocks fall close to the rhyolite maxima of Thornton and Tuttle (1960), i.e. at D.I. 87, and a silica content of 79 percent. The dacitic rocks spread along the trend of rhyodacite and dacite, i.e. between D.I. 72 and silica content of 75 percent, and D.I. 45 and silica content of 62 percent (cf. Thornton and Tuttle, 1960, Fig.10, p.675). All the volcanic rocks of Parys Mountain lie in the oversaturated field, except that for one dacite which falls in the saturated field (Fig.13).

3) Irvine and Baragar (1970, Fig.7, p.538) produced a diagram in which normative colour index (sum of normative olivine, orthopyroxene, clinopyroxene, magnetite, ilmenite, and haematite) was plotted against normative plagioclase composition (100anorthite/(anorthite + albite + 5/3nepheline)) to distinguish various volcanic types. They plotted values for the Thingmuli, Cascades, Mount Wood, Aleutian Islands, Paricutin region, Mexico basalt-andesite-dacite-rhyolite suites, Hawaiian tholeiites, Columbia River tholeiites,

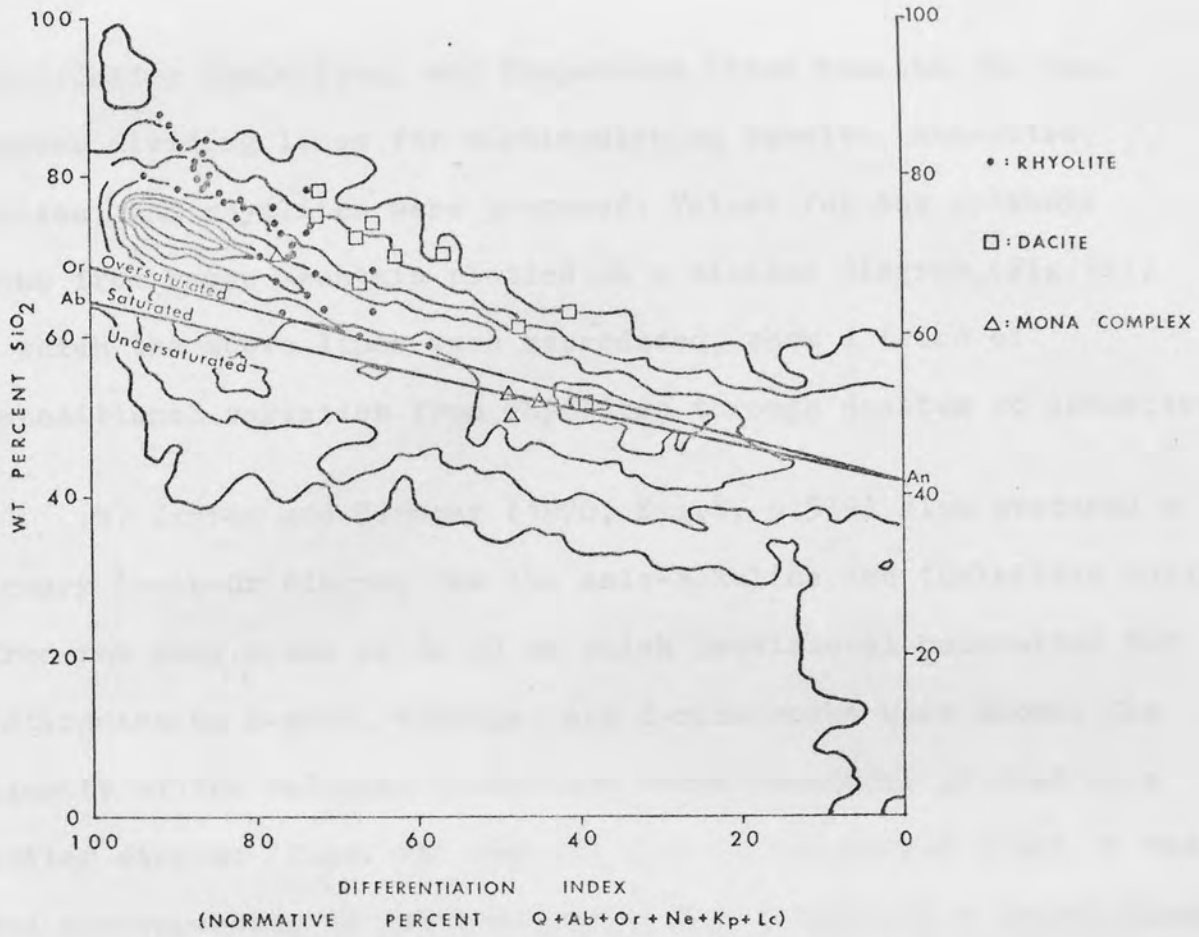

Figure 13 Diagram showing the silica versus differentiation index for the rocks of Parys Mountain, the silica content of normative Or, Ab, and An together with lines separating oversaturated and undersaturated rocks (after Thornton and Tuttle, 1960). The contours represent the frequency distribution of 5000 analyses of igneous rocks. The area between the outermost and the next higher contour contains from 1 to 12 points in a 0.16 percent area, the next area contains from 13 to 25, the next 26 – 38, then 39 – 50, 51 – 75, 76 – 100, and 101 – 125.

Mid-Atlantic tholeiites, and Coppermine River basalts. On this diagram dividing lines for distinguishing basalts, andesites, dacites, and rhyolites were proposed. Values for the volcanic rocks from Parys Mountain plotted on a similar diagram (Fig.14), on which the above lines were reproduced, show a trend of compositional variation from rhyolites through dacites to andesites.

4) Irvine and Baragar (1970, Fig.8, p.539) also produced a ternary An-Ab-Or diagram for the calc-alkaline and tholeiitic suites (from the same areas as in 3) on which provisional boundaries for distinguishing K-poor, average, and K-rich rocks were shown. The majority of the volcanic rocks from Parys Mountain, plotted on a similar diagram (Figs. 15A and B), fall in the K-rich field in the area corresponding to potassic rhyolite and rhyodacite compositions (Fig.15A). It is interesting to note that 28 of the 42 analyses, which fall in the above field, lie in the area which has values for Or of between 90 and 100 percent (Fig.15B). This may reflect the relative abundance of K-feldspar in the groundmass of the rocks.

5) Yoder (1969, p.79) showed variation trends representing the four major rock series(alkaline, tholeiite, island arc calc-alkaline, and continental margin calc-alkaline series) by plotting the analysed values of these rocks on a MgO versus $FeO+Fe_2O_3$ diagram. Values for the volcanic rocks from Parys Mountain were plotted on a similar diagram (Fig.16), using Fe_2O_3 as total Fe, on which the above trends were reproduced. The results show that the majority of the analyses, particularly the rhyolitic rocks, fall in the continental margin calcalkalic series field. However

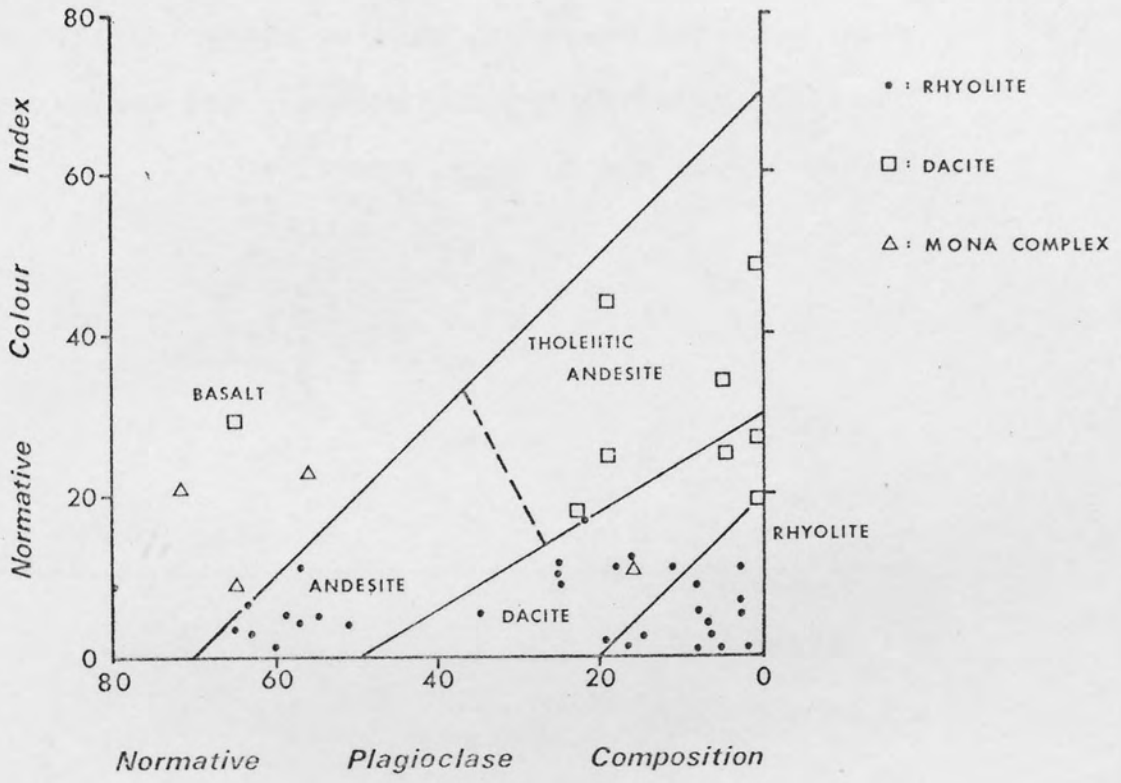

FIGURE 14 Plots of normative colour index versus normative plagioclase composition for the metamorphic and volcanic rocks of Parys Mountain, showing dividing lines for distinguishing basalts, andesites, dacites, and rhyolites (after Irvine and Baragar, 1970).

Figure 15A An-Ab-Or projections of the metamorphic and volcanic rocks of Parys Mountain, showing provisional boundaries for distinguishing K-poor, average, and K-rich rocks (after Irvine and Baragar, 1970).

• : Rhyolite

□ : Dacite

△ : Mona Complex

Figure 15B An-Ab-Or projections of the volcanic rocks of Parys Mountain. The diagram shows the plots which fall in the area enclosed by An_{0-10}, Ab_{0-10}, and Or_{90-100}.

Figure 15 A

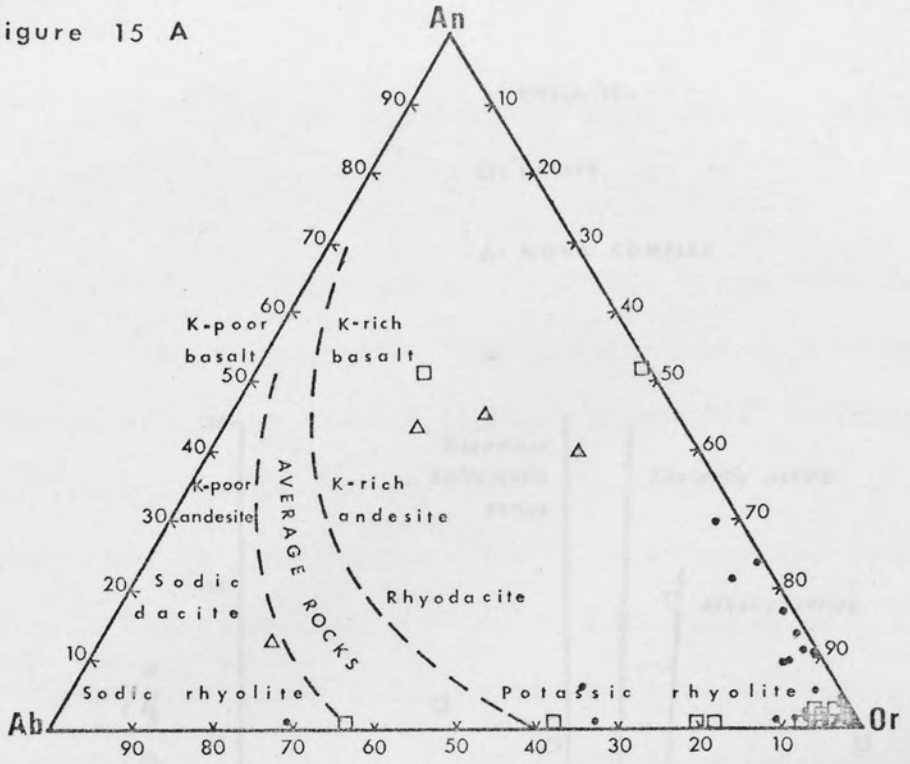

Figure 15 B

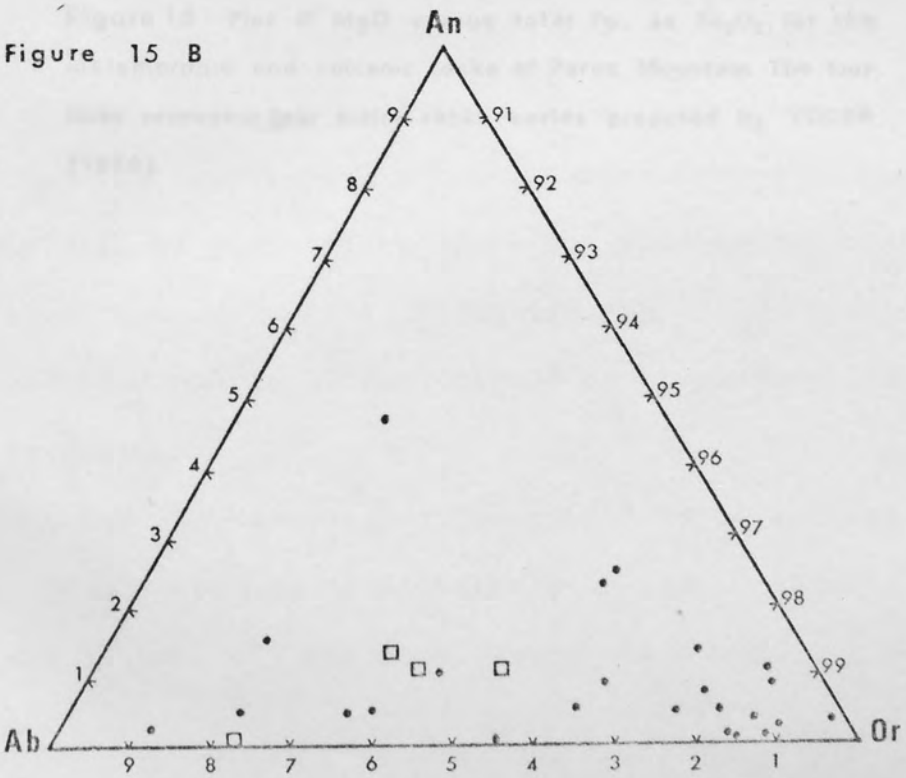

•: RHYOLITE

□: DACITE

△: MONA COMPLEX

Aston University

Content has been removed for copyright reasons

Figure 16 Plot of MgO versus total Fe, as Fe_2O_3, for the metamorphic and volcanic rocks of Parys Mountain. The four lines represent four major rocks series proposed by YODER (1969).

it must be noted that the dacites and Mona Complex rocks show a wide scatter.

6) An A-F-M diagram plotted for the Parys Mountain rocks is illustrated by Fig.17. The line proposed by Irvine and Baragar (1970) which separates tholeiitic and calc-alkaline types, and the differentiation trends for calc-alkaline magmas (after Ringwood, 1974) are shown on the diagram. The majority of the rhyolitic rocks lie in the calc-alkaline field, although only a few lie on Ringwood's calc-alkaline differentiation trends, whereas the dacitic rocks generally lie in the tholeiitic field.

6.3 Discussion of Bulk Chemical Results.

The information presented above indicates that the volcanic rocks of Parys Mountain are calc-alkaline and vary in composition from andesite, through dacite, to rhyolite. The derivation of such magmas may be attributed either to partial melting of the upper part of the crustal lithosphere (oceanic) on a Benioff zone, or to partial melting of the mantle under high load pressures and high water pressures, above such a zone. Magmas formed in this way are characteristic of plate convergence and continental margin/island arc systems (Ringwood, 1974; Miyashiro, 1974). Further discussion of the probable origin of such magmas is given later in the chapter on petrogenesis.

The K-rich character of the rhyolitic rocks (Fig.15A), and the distribution of the dacitic rocks in the tholeiitic field (Figs. 14, 16, and 17) needs further explanation. The variations

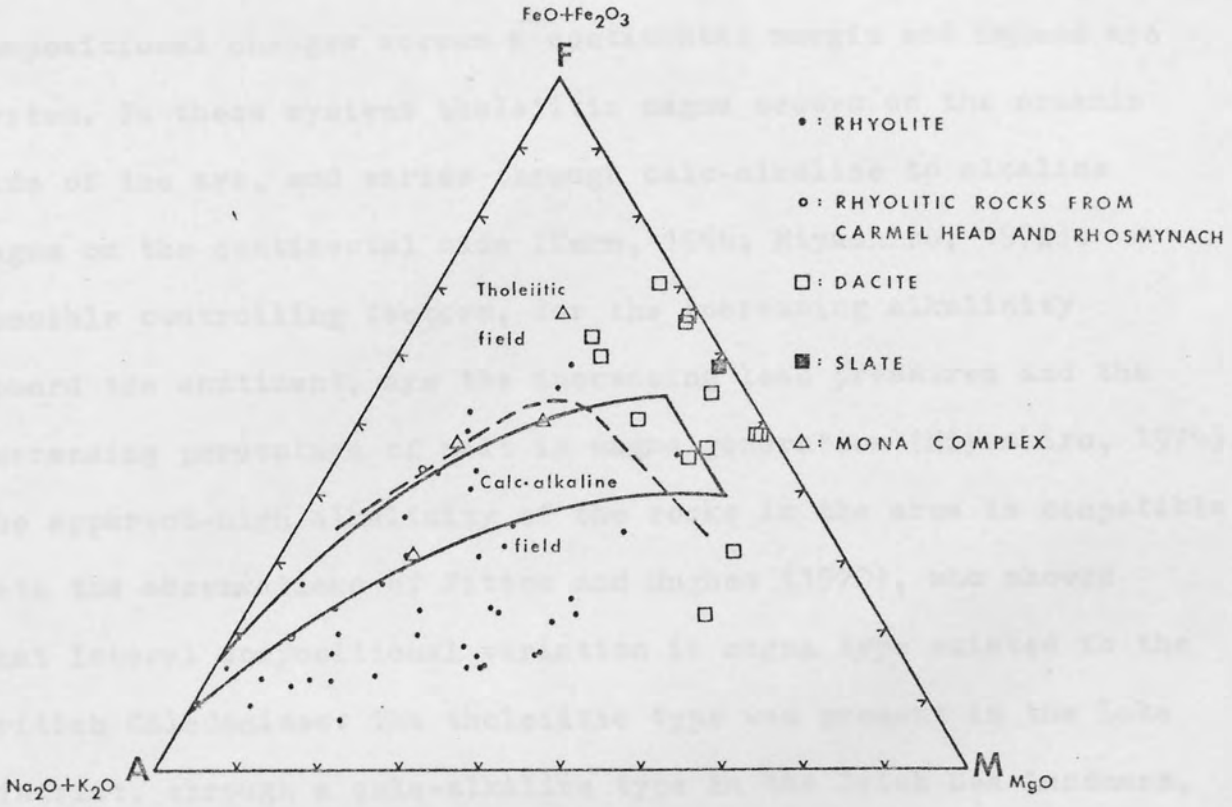

Figure 17 A–F–M diagram for the rocks of Parys Mountain (values in weight percent)

The dashed line serves to separate tholeiitic and calc-alkaline composition (after Irvine and Baragar, 1970). The area enclosed by solid lines is the differentiation trends of the calc-alkaline magmas from the Cascade, Aleutian, and New Zealand calc-alkaline provinces (after Ringwood, 1974).

in alkalinity in the magma types can be ascribed to lateral compositional changes across a continental margin and island arc system. In these systems tholeiitic magma occurs on the oceanic side of the arc, and varies through calc-alkaline to alkaline magma on the continental side (Kuno, 1966; Miyashiro, 1972). Possible controlling factors, for the increasing alkalinity toward the continent, are the increasing load pressures and the decreasing percentage of melt in magma generation (Miyashiro, 1974). The apparent-high alkalinity of the rocks in the area is compatible with the observations of Fitton and Hughes (1970), who showed that lateral compositional variation in magma type existed in the British Caledonides. The tholeiitic type was present in the Lake District, through a calc-alkaline type in the Irish Sea Landmass, to an alkaline type in the Welsh Basin. However a plot of Na_2O + K_2O (as total alkalis) versus SiO_2 (Fig.18A) shows depletion of alkalis with increasing silica content. The alkali depletion is largely due to variations in potassium content since sodium shows a constant trend (Fig.18B), while potassium shows a decreasing trend similar to that of the total alkalis (Fig.18C). This feature may be attributed to increasing silica content due to silicification, while potassium was removed from the rocks, during later metasomatic processes (i.e. the Caledonian and Variscan orogenies).

The occurrence of the dacitic rocks in the tholeiitic field has three possible explanations.

a) In an island arc area, where plate consumption was developed, rapid plate convergence gives rise to volcanic rocks of the tholeiitic trend, whereas slow plate convergence produces

FIGURE 18

Harker diagrams for metamorphic and volcanic rocks of Parys Mountain

A : Plot of percent of total alkali (Na_2O+K_2O) against SiO_2

B : Na_2O vs SiO_2

C : K_2O vs SiO_2

D : MgO vs SiO_2

E : Al_2O_3 vs SiO_2

F : Fe_2O_3 vs SiO_2

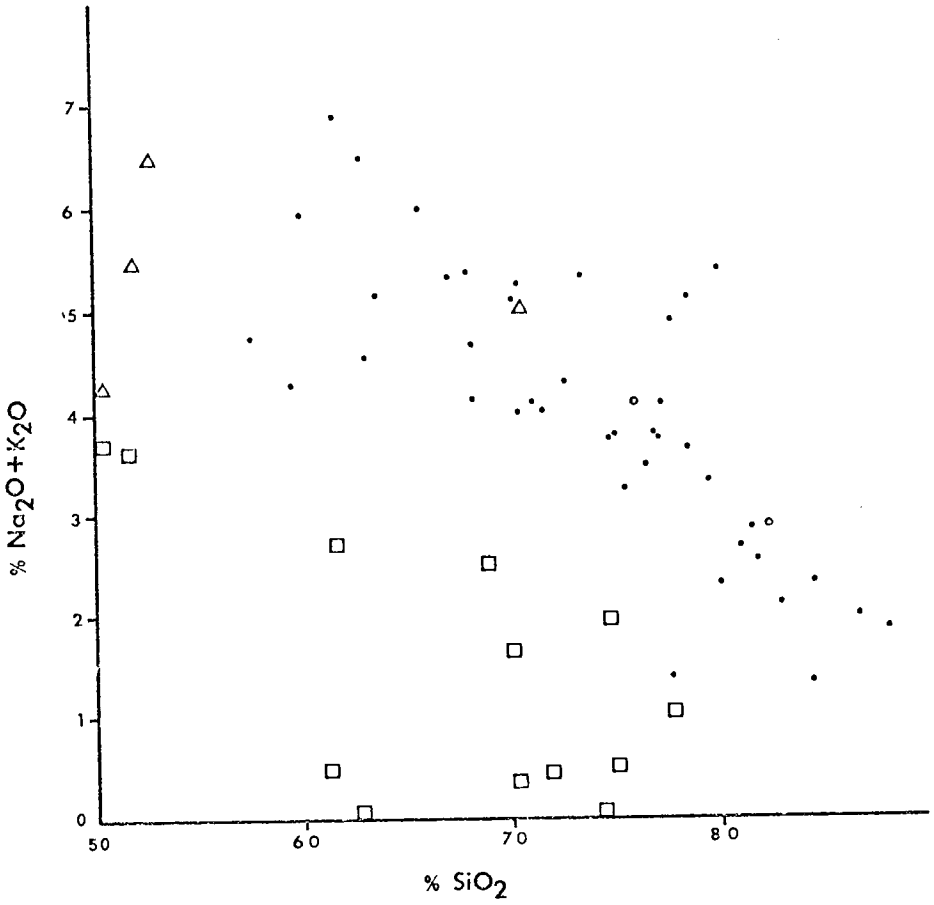

FIGURE 18 A

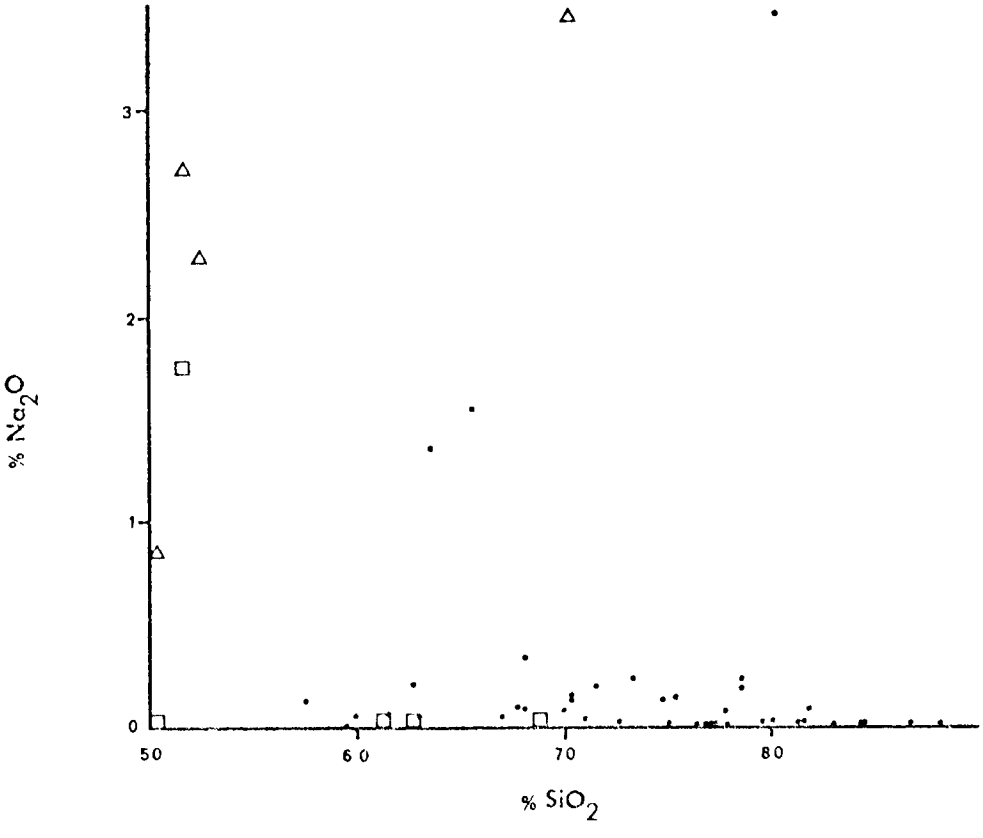

FIGURE 18 B

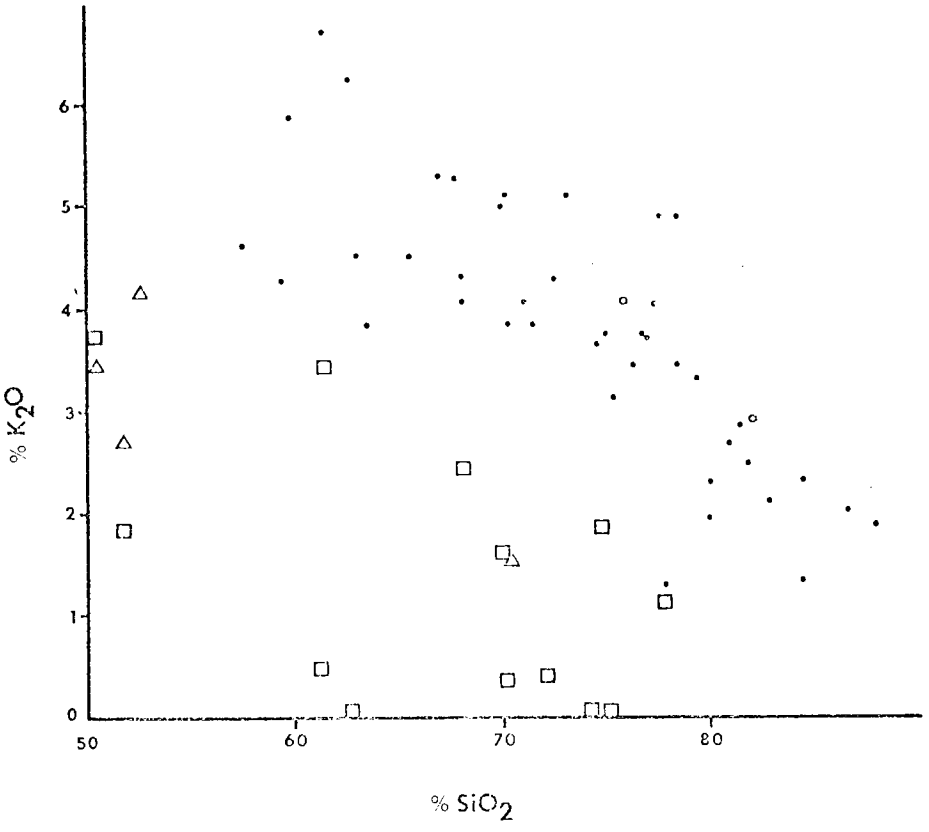

FIGURE 18C

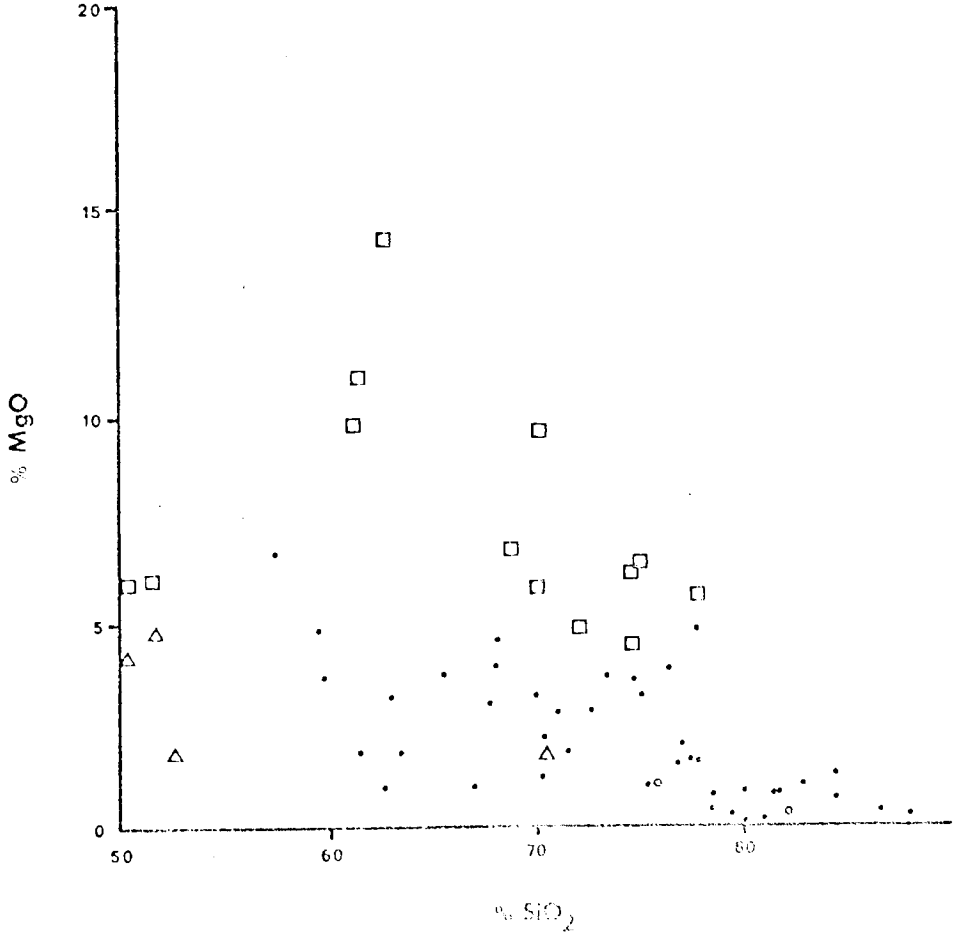

FIGURE 18D

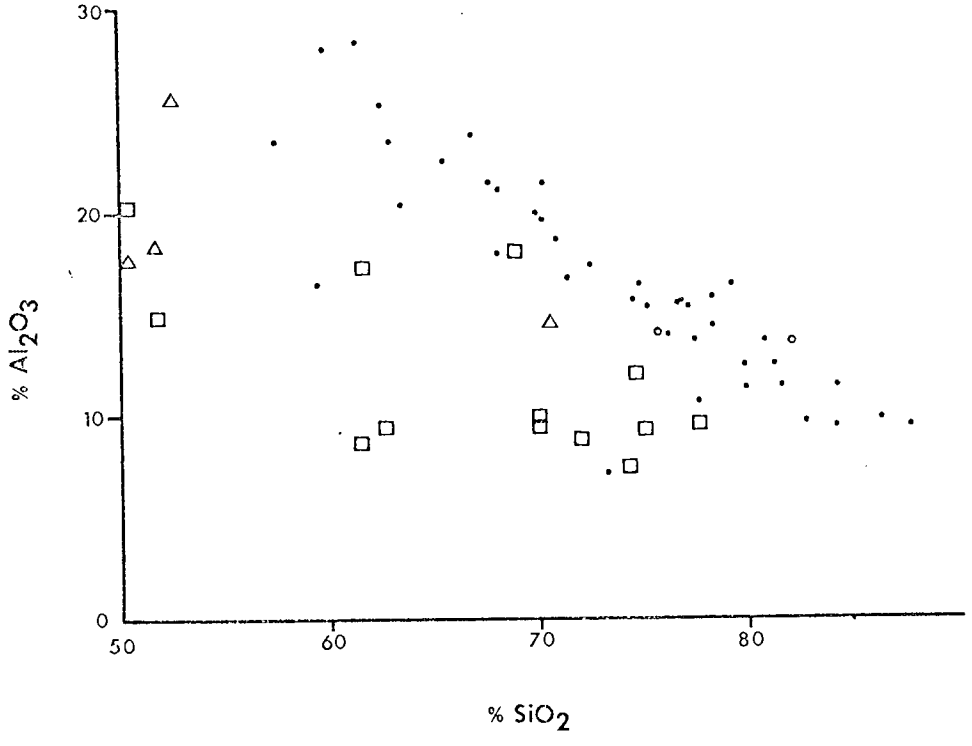

FIGURE 18E

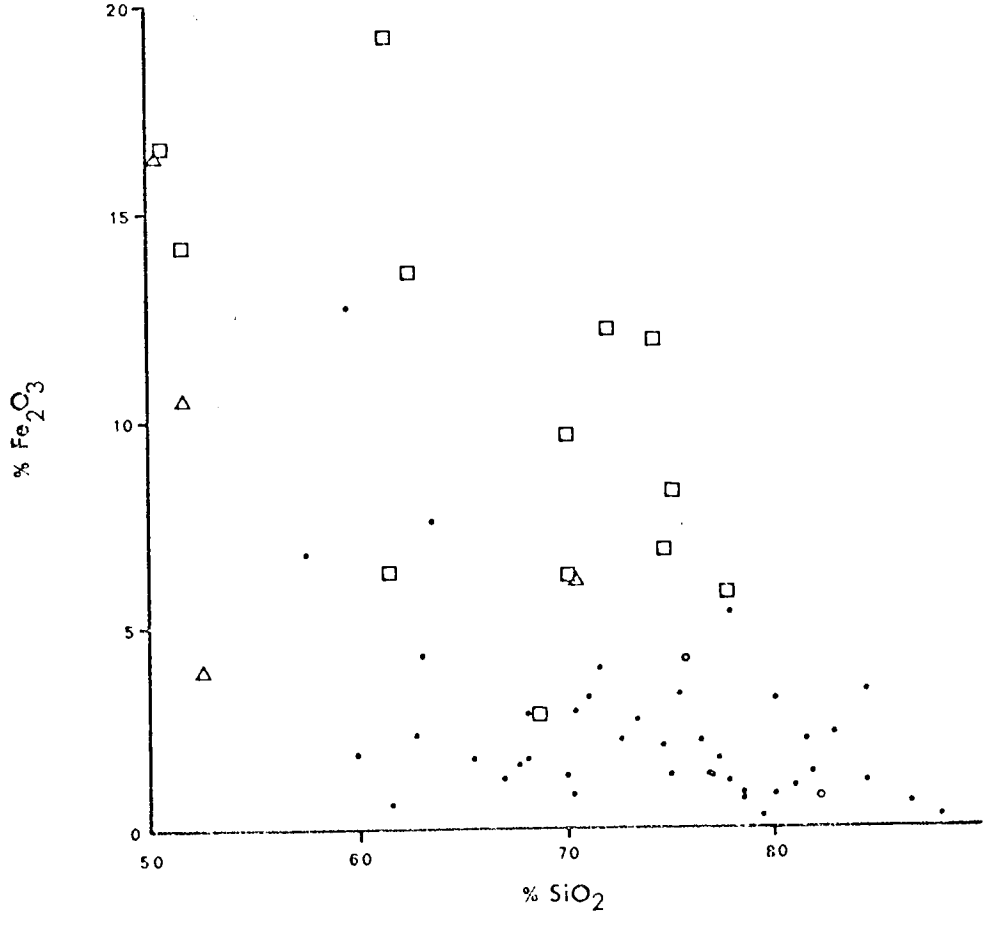

FIGURE 18F

calc-alkaline volcanism (Miyashiro, 1972). This is probably due to the fact that the rate of uprise of magmas above the Benioff zone is controlled by the rate of convergence. A rapidly descending plate would accelerate the rate of ascension of the magmas hence they reach the surface with little or no differentiation. Magmas produced above a plate descending more slowly have more time for differentiation processes to be developed, and the resultant magmas become enriched in silica and are relatively depleted in iron (Mg, Al, and Fe show a depleted trend against Si for the volcanic rocks of Parys Mountain - Figs. 18D, E, and F). The rapid uprise of magma in areas of rapid plate convergence may result from high temperatures produced by frictional heating along the Benioff zone (Oxburgh and Turcotte, 1970). If the magmas of Parys Mountain formed as outlined above, then this part of the island arc system must have been an area where the rate of plate consumption fluctuated.

b) Osborn (1959 and 1962) suggested that both calc-alkaline and tholeiitic trends might be produced from the same basaltic magma system by varying crystallisation conditions, in particular the oxygen pressure. A low oxygen pressure generally results in tholeiitic trend and a high oxygen pressure would activate fractionation processes thus producing a calc-alkaline trend. This explanation requires the presence of a parental basaltic magma and the oxygen pressure differences in the area.

c) Ringwood (1974) proposed that in the early phase of volcanic evolution, in which the location of the volcanoes with

respect to the Benioff zone is shallow (80 to 100km), a tholeiitic phase is produced. In the later phases, magma is produced at greater depths (100 to 150km), giving rise to the calc-alkaline type. This model involves differentiation of magma plus partial melting under different conditions of water pressures (Ringwood, 1974).

Of the three models described above a) and c) are more applicable. Model b) requires the presence of a parental basaltic magma which in this case is not likely since evidence for the presence of such magma is not found (see Chapter 7 on petrogenesis). However model b) can be fitted to both models a) and c) in that the variation in partial pressures of oxygen can be ascribed to water being driven off from the deeper part of the descending lithosphere. Both models a) and c) involve differentiation of magma but from different causes. Model a) is concerned with the rate of plate convergence hence the rate of the uprising magma, and model b) is concerned with the commencing point of the magma (shallow or deep) produced on the descending plate. A more suitable explanation for the magma type at Parys Mountain may be a combination of these two models. This plate tectonic model explains the magma variation in the British Caledonide as a whole.

6.4 Trace Element Chemistry.

Some 350 rock specimens were analysed for Cu, Pb, Zn, Ni, Co, Cd, Cr, Hg, Ba, and Sr using A.A.S., and 61 of the 350 specimens were also analysed by X.R.F. for Rb and S. A description of specimen locations and techniques used is given in Appendices A, B, and C. The analytical results are tabulated in Appendix D.

The trace element study was done to discover if any anomalous concentration (dispersion haloes) are present around the mineralized zones. The distribution of these elements and their intercorrelation, both among themselves and with some major elements (Si, Al, and Fe), were investigated in order to discover if they show dispersion pattern characteristics.

Principal Component Analysis and Factor Analysis was done on the analytical results. This determined the deviations of those elements which had large variance (principal component), and allowed interpretation of their common variation (factor). The analytical data were separated into two sets:- one consisting of 289 samples on which values for 13 elements (Al, Ba, Cd, Co, Cr, Cu, Fe, Hg, Ni, Pb, Si, Sr, and Zn) were determined, and the other consisting of 61 samples with values for 22 elements (the above 13 elements plus Ti, Mn, Mg, Ca, Na, K, P, S, and Rb).

The general characteristics and advantages of Principal Component Analysis and Factor Analysis are described in Appendix E. The correlation matrices of the two data sets (289 and 61 samples) are given in Tables 5A and B, and the statistical data, containing values of means, minimum values, maximum values, and standard deviations for each element, are tabulated in Appendix E (Tables

Table 5a Correlation Matrix of 289 Samples.

	Al	Ba	Cd	Co	Cr	Cu	Fe	Hg	Ni	Pb	Si	Sr	Zn
Al	1.00	.48	-.23	-.33	.29	-.38	.09	-.05	.10	-.27	-.57	.13	-.27
Ba	.48	1.00	-.12	-.17	.04	-.21	-.19	.38	-.05	-.15	-.09	-.01	-.15
Cd	-.23	-.12	1.00	.07	.08	.32	.00	-.01	-.03	.84	-.13	.03	.96
Co	-.33	-.17	.07	1.00	.03	.20	.11	.06	.54	.08	.08	-.08	.07
Cr	.29	.04	.08	.03	1.00	-.02	.30	-.06	.24	.03	-.40	.13	-.07
Cu	-.38	-.21	.32	.20	-.02	1.00	.34	.01	-.02	.38	-.12	.03	.35
Fe	.09	-.19	.00	.11	.30	.34	1.00	-.09	.14	.02	-.67	.13	.02
Hg	-.05	.38	-.01	.06	-.06	.01	-.09	1.00	.02	.01	.08	-.03	-.01
Ni	.10	-.05	-.03	.54	.24	-.02	.14	.02	1.00	-.04	-.19	.06	-.04
Pb	-.27	-.15	.84	.08	.03	.38	.02	.01	-.04	1.00	-.01	.00	.90
Si	-.57	-.09	-.13	.08	-.40	-.12	-.67	.08	-.19	-.01	1.00	-.28	-.12
Sr	.13	-.01	.03	-.03	.13	.03	.13	-.03	.06	.00	-.28	1.00	.03
Zn	-.27	-.15	.96	.07	-.07	.35	.02	-.01	-.04	.90	-.12	.03	1.00

Table 5b Correlation Matrix of 61 Samples

	Si	Ti	Al	Fe	Mn	Mg	Ca	Na	K	P	S
Si	1.00	-.61	-.51	-.69	-.70	-.62	-.48	-.26	-.11	.13	.16
Ti	-.61	1.00	.28	.43	.58	.11	.63	.43	.05	-.06	-.20
Al	-.51	.28	1.00	-.20	.02	-.14	.11	.15	.77	-.05	-.23
Fe	-.69	.43	-.20	1.00	.76	.79	.25	.06	-.52	-.10	-.06
Mn	-.70	.58	.02	.76	1.00	.51	.58	.31	-.26	-.08	-.12
Mg	-.62	.11	-.14	.79	.51	1.00	.06	-.08	-.49	-.12	-.15
Ca	-.48	.63	.11	.25	.58	.06	1.00	.51	.07	-.05	.06
Na	-.26	.43	.15	.06	.31	-.08	.51	1.00	-.07	-.02	-.13
K	-.11	.05	.77	-.53	-.26	-.49	.07	-.07	1.00	-.02	-.03
P	.13	-.06	-.05	-.10	-.08	-.12	-.05	-.02	-.02	1.00	-.09
S	.16	-.20	-.23	-.06	-.12	-.15	.06	-.13	-.03	-.09	1.00
Ba	.00	.06	.35	-.38	-.18	-.24	.08	.20	.46	.08	-.11
Sr	-.20	.26	-.03	.01	.39	-.04	.73	.58	.11	-.05	.14
Rb	.06	-.05	.70	-.64	-.39	-.54	-.05	-.06	.83	.00	-.03
Cu	-.23	.47	.10	.24	.38	.08	-.03	-.08	.05	-.03	-.05
Zn	-.15	-.06	.07	.10	.01	.25	-.11	-.14	.01	-.10	.04
Pb	.24	-.01	-.16	-.13	-.12	-.14	-.07	-.07	-.10	-.02	-.03
Ni	-.64	.82	.33	.43	.60	.24	.46	.35	.05	-.06	-.18
Co	-.05	.21	.02	.01	.05	-.03	.11	.12	-.05	-.06	.07
Cd	-.17	.11	.19	.05	-.03	.16	-.11	-.03	.00	-.08	-.06
Cr	-.33	.57	.13	.31	.41	.16	.02	.01	.01	-.02	-.09
Hg	.08	-.13	-.20	-.12	.01	-.05	.30	.06	.14	-.04	.44

Table 5b continued

	Ba	Sr	Rb	Cu	Zn	Pb	Ni	Co	Cd	Cr	Hg
Si	.00	-.20	.06	-.23	-.15	.24	-.64	-.05	-.17	-.33	.08
Ti	.06	.26	-.05	.47	-.06	-.01	.82	.21	.11	.57	-.13
Al	.35	-.03	.70	.10	.07	-.16	.33	.02	.19	.13	-.20
Fe	-.38	.01	-.64	.24	.10	-.13	.43	.01	.05	.31	-.12
Mn	-.18	.39	-.39	.38	.01	-.12	.60	.05	-.03	.41	.01
Mg	-.24	-.04	-.54	.08	.25	-.14	.24	-.03	.16	.16	-.05
Ca	.08	.73	-.05	-.03	-.11	-.07	.46	.11	-.11	.02	.30
Na	.20	.58	-.06	-.08	-.14	-.07	.35	.12	-.03	.01	.06
K	.46	.11	.83	.05	.01	-.10	.05	-.05	.00	.01	-.14
P	.08	-.05	.00	-.03	-.10	-.02	-.06	-.06	-.08	-.02	-.04
S	-.11	.14	-.03	-.05	.04	-.03	-.18	.07	-.06	-.09	.44
Ba	1.00	.32	.34	.03	-.01	-.14	.17	.08	.16	.11	.37
Sr	.32	1.00	-.03	-.06	-.14	-.05	.21	.05	-.09	-.03	.68
Rb	.34	-.03	1.00	-.07	-.01	-.04	-.03	.04	.00	-.13	-.04
Cu	.03	-.06	-.07	1.00	.03	-.04	.48	.14	.11	.92	-.05
Zn	-.01	-.14	-.01	.03	1.00	.13	.02	.07	.17	.07	.13
Pb	-.14	-.05	-.04	-.04	.13	1.00	-.12	-.17	-.07	-.05	.06
Ni	.17	.21	-.03	.48	.02	-.12	1.00	.17	.34	.60	-.10
Co	.08	.05	.04	.14	.07	-.17	.17	1.00	.14	.18	.01
Cd	.16	-.09	.00	.11	.17	-.07	.34	.14	1.00	.17	-.02
Cr	.11	-.03	-.13	.92	.07	-.05	.60	.18	.17	1.00	-.05
Hg	.37	.68	-.04	-.05	.13	.06	-.10	.01	-.02	-.05	1.00

13A and B). Other statistical analytical data including total variance for principal component analysis, matrix of principal component analysis with list of components, matrix of factor loadings with list of factors, matrix of principal component co-ordinates for boreholes C4, M10, IM9, H17A, IM6, H14, H16, and matrix of factor scores for the above boreholes, are also presented in Appendix E (Tables 14 to 26).

Discussion of Results.

Intercorrelation of the trace elements is based on data from Table 5A (for 289 samples) because of its greater reliability. However correlation with major elements also used data in Table 5B (for 61 samples).

Ba, Sr, and Rb are positively correlated. These also show a positive correlation with Al and K, and a negative correlation with Fe, Mg, and Mn. This is interpreted to show that they are associated with K and Al in feldspars, particularly in the more felsic volcanic rocks of the area (Rankama and Sahama, 1950; Hawkes and Webb, 1962; Krauskopf, 1967).

The positive correlation between Ba and Hg (Table 5A) probably is indicative of remobilization (Rankama and Sahama, 1950), or an association with Pb-Zn sulphide mineralization (Hawkes and Webb, 1962). Both interpretations are applicable at Parys Mountain in that Ba and Hg were primarily associated with Pb-Zn sulphide mineralization of the area, and, being highly mobile elements (Rankama and Sahama, 1950; Hawkes and Webb, 1962), were remobilized by later tectonic deformations.

Cu, Pb, and Zn are positively correlated with each other and with Cd. This is interpreted to indicate that they are associated with the mineralization of the area, though none of them show a positive correlation with S. This probably is because S was determined in only 61 samples, none of which contain ore minerals.

The positive correlation between Cu and Fe probably reflects the presence of Fe in chalcopyrite, whereas the correlation between Pb and Si (Table 5B) may be related to some later Pb-mineralization during silicification.

Positive correlation of Co with Ni may indicate an association with the more basic members of the volcanic sequence of the area, or association with the main sulphide mineralization episode. Association with mineralization is likely to be the more significant since only Ni shows a positive correlation with Ti, Mn, Cr, and Fe (Table 5B). These elements are associated with ferro-magnesian minerals and as the volcanic rocks are quartz-feldspar-rich such a correlation is unlikely.

Cr is the least abundant of the trace elements determined, and its correlation with Fe, Al, and Ni (Table 5A) is thought to be due to the sedimentary cycle (Hawkes and Webb, 1962). Cr probably is present in detrital sediments, derived from older basic rocks, deposited as part of the Ordovician sequence. Its strong correlation with Cu (Table 5B) is either fortuitous or due to their association in the mineralized sedimentary rocks.

Hg shows positive correlation with Ba (Table 5A), and with Sr, S, and Ca (Table 5B). This probably reflects the remobilization of the Hg, in solutions containing sulphate anions (Rankama and Sahama, 1950) associated with later carbonatization of the rocks.

Principal Component Analysis.

The main purpose of this analysis is to determine the linear combinations of variables with large variance, and to consider only the linear combinations (component) of variables that show large values of variations. This is done by considering the eigenvalue or variance of each principal component. This value is given in Table 14, which illustrates total variance for the data set of 289 samples, and it indicates that of the 13 components the first 5 show larger variances and account for 76.38 percent of the total variance. Because of this only these 5 components are considered. The matrix of the 5 components, together with lists of each component, is given in Table 15.

Component No. 1 (Zn, Pb, Cd, Cu)

This component is associated with mineralization since the participating elements are of the major sulphide ores. High Zn, Pb, Cd, and Cu levels, through the negative component co-ordinates (Table 15), lead to negative values. Plots of the co-ordinates of this component (values given in Tables 20 and 25) along boreholes C4, M10, and M17A (Figs. 19A, B, and C) show that the high values correspond to the mineralized zones in C4 and M17A, and extend beyond the mineralized zone (in the siliceous sinter layers) in M10. The higher values occur in the siliceous sinter layers of C4 and

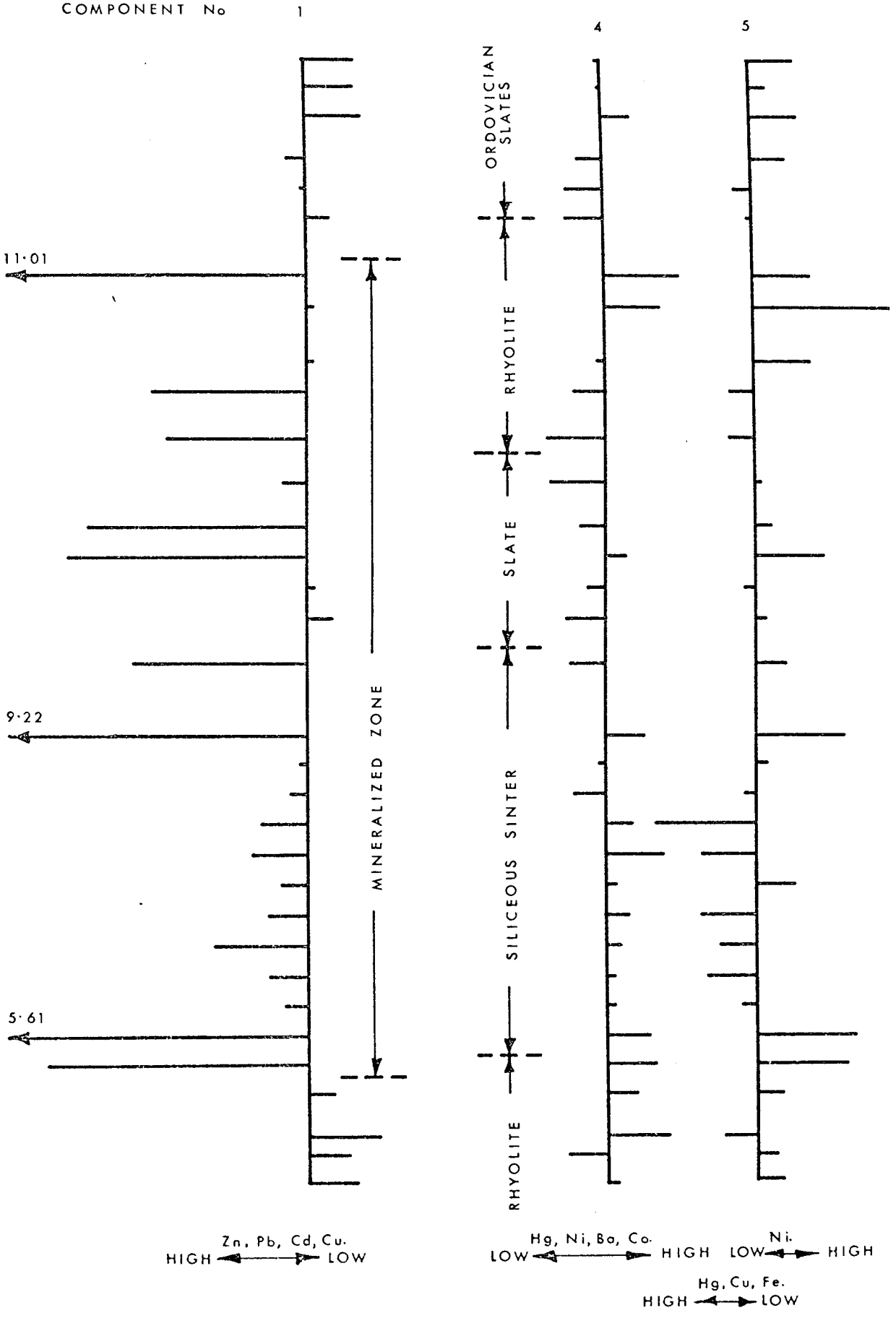

FIGURE 19A PLOTS OF PRINCIPAL COMPONENT CO-ORDINATES ALONG BOREHOLE C4 FROM 700 TO 1078 feet (DEPTH ALONG COVE) (COMPONENTS No 1, 4 and 5.)

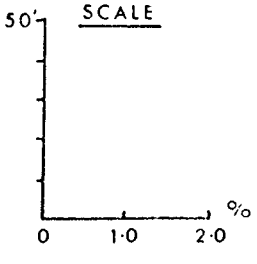

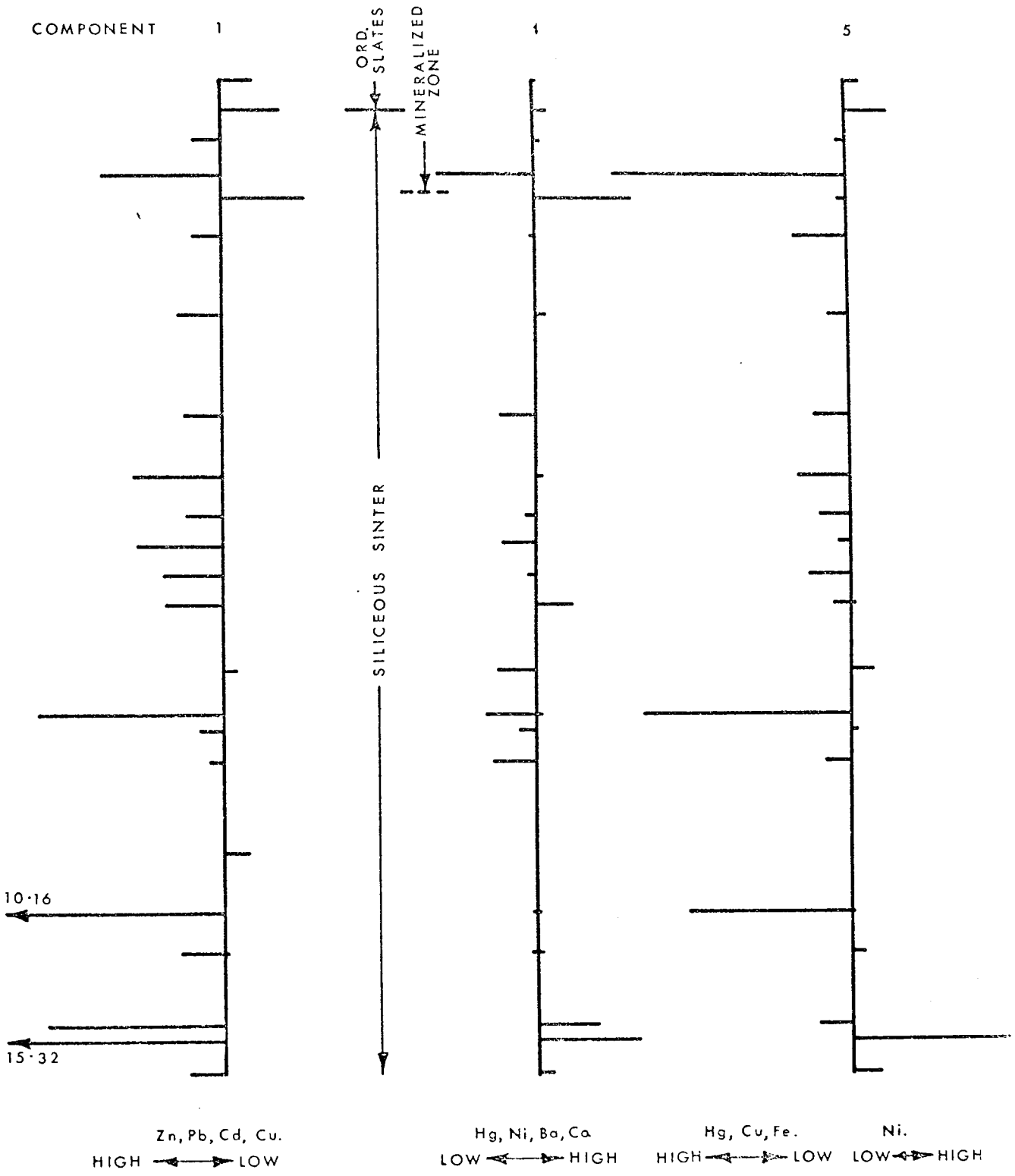

FIGURE 198 PLOTS OF PRINCIPAL COMPONENT CO-ORDINATES ALONG BOREHOLE M10 FROM 700 TO 1078 feet (DEPTH ALONG CORE) (COMPONENTS 1 4 and 5)

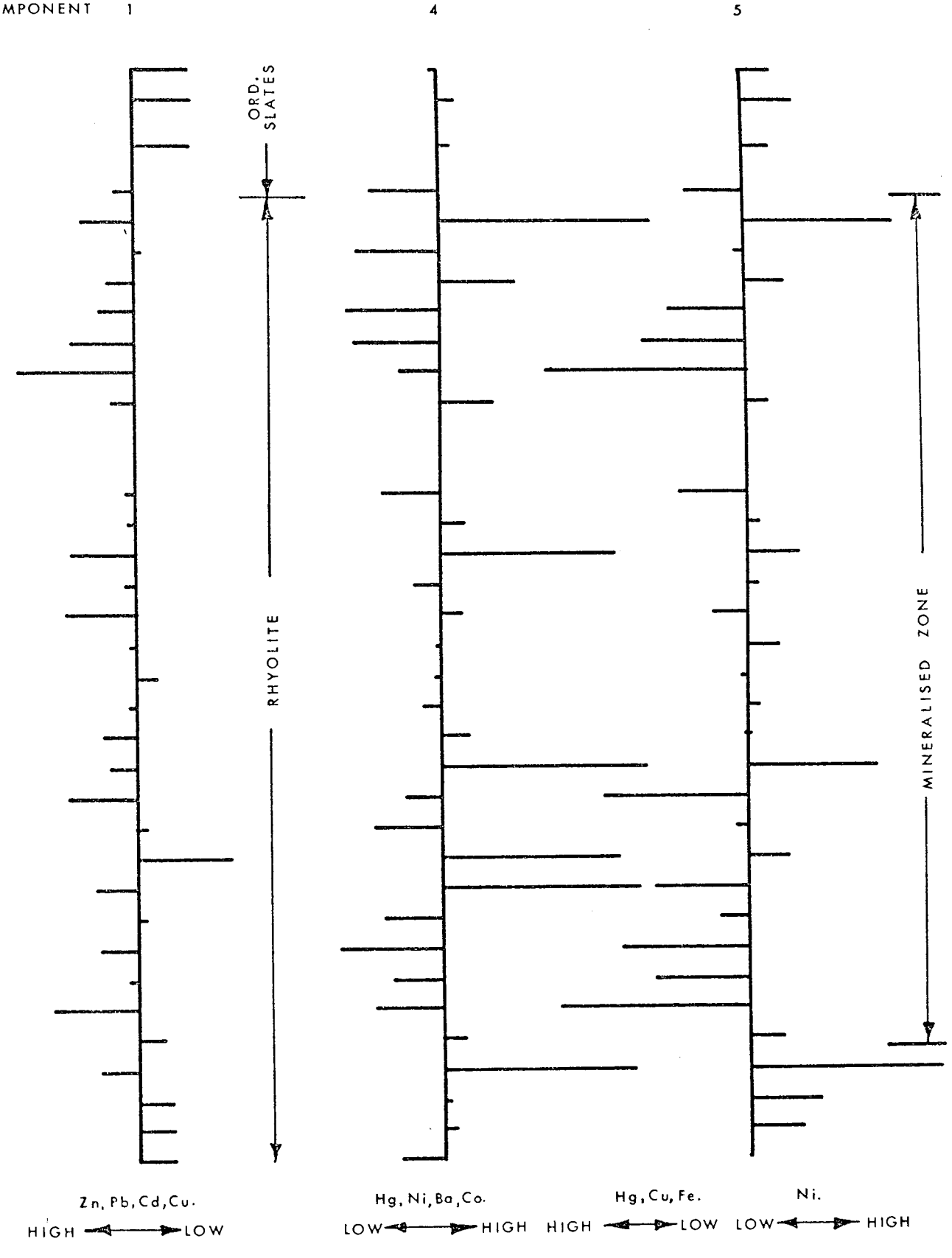

FIGURE 19C PLOTS OF PRINCIPAL COMPONENT CO-ORDINATES ALONG BOREHOLE H17A FROM 700 TO 1078 feet (DEPTH ALONG CORE) (COMPONENT No 1 4 and 5)

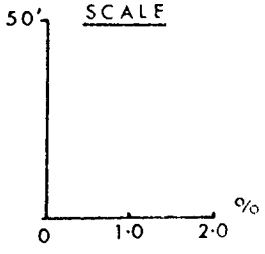

M10. This component is thus closely associated with the siliceous sinter and may reflect the mineralization formed with this rock type. Similar distributions, but with relatively lower values, occur in materials from the other boreholes. These were not plotted but the values are given in Table 25.

Component No. 2 (Fe, Cr, Al vs Si)

This component illustrates the distribution of Fe, Cr, and Al against that of Si. High positive values correspond to high Fe, Cr, and Al levels, whereas high negative values correspond to high Si levels. This component is considered to be lithologically controlled (i.e. Fe, Cr, Al reflect the more basic rocks and Si reflects the acidic ones) and the values can be read from Tables 20 and 25.

Component No. 3 (Ba, Al vs Co, Ni)

This component is thought to reflect the crystallization behaviour of the volcanic rocks. It probably reflects the relationship between felsic minerals (feldspar or other alumino-silicates) containing Ba and Al, and mafic minerals which have Co and Ni in their crystal structures. Positive values correspond to high levels of Ba and Al, and negative values correspond to high levels of Co and Ni. This component was not plotted as it has no relationship to mineralisation, however it does distinguish acidic from more basic rocks.

Component No. 4 (Hg, Ni, Ba, Co)

This component probably reflects the effects of tectonic

deformation on the rocks and the ore mineralization. It indicates either the presence of later hydrothermal processes or the remobilization of these elements. The latter possibility is believed to be more likely since all four elements are highly mobile (Hawkes and Webb, 1962). High positive values correspond to high levels of Hg, Ni, Ba, and Co. Plots of this component along boreholes C4, M10, and M17A (Figs.19A, B, and C) show that in borehole C4 high values are generally in the siliceous sinter part of the mineralized zone, in M10 a few high values are also in the siliceous sinter, and the highest values occur in the mineralized zone of borehole M17A. The component is interpreted to be related to mineralization, though some relationship to the volcanic rocks is probably also present. Values for the other boreholes are listed in Table 25. They were not plotted as they show similar distributions, and the values are generally low.

Component No. 5 (Ni vs Hg, Cu, Fe)

This component mainly reflects the distribution of Hg and to some extent that of Cu, Fe with respect to Ni. High negative values correspond to high levels of Hg, Cu, and Fe with low Ni levels. Plots of this component (Figs.19A, B, and C) show that it is controlled both by mineralization and the volcanic rocks as the higher values occur in the mineralized zones, and are comparable with Component No. 1 where the host rocks are volcanic.

Factor Analysis.

The list of factors and the matrix of factor loadings are

given in Table 16. Of the seven factors listed only three (factors 1 - Zn, Cd, Pb, Cu; 3 - Ba, Al vs Fe, Cu, Co; and 5 - Hg, Ba, Cu) are related to mineralization. Factor 7 (Pb) may be an ore factor but the variance of this factor is too small (i.e. 0.001) to be significant.

Plots of the three factors (1, 3, and 5) along boreholes C4, M10, IM9, and H17A are illustrated in Figs.20, 21, 22, and 23 respectively. These plots were used because most samples were taken from these boreholes and the factor scores in these boreholes (Tables 21, 22, 23, and 24) show good variations. Values for other samples are listed in Table 26 (Appendix E).

Factor 1 (Zn, Cd, Pb, Cu)

High Zn, Cd, Pb, and Cu levels, through the negative factor loadings of these elements (Table 16), lead to negative scores. The highest negative scores are found in the mineralized zone of borehole C4 (Fig.20) and in the siliceous sinter layers of borehole M10 (Fig.21). The factor shows lower values in the mineralized part of boreholes IM9 and H17A (Figs.22 and 23) relative to the values from C4 and M10. The host rocks of IM9 and H17A are rhyolites, and this factor is interpreted to be a mineralization factor particularly related to the siliceous sinter type lithology and depositional environment.

Factor 3 (Ba, Al vs Fe, Cu, Co)

This is also a mineralization factor for which high negative scores correspond to high levels of Fe, Cu, and Co, and low levels of Ba and Al. It has high values in the mineralized zone of borehole

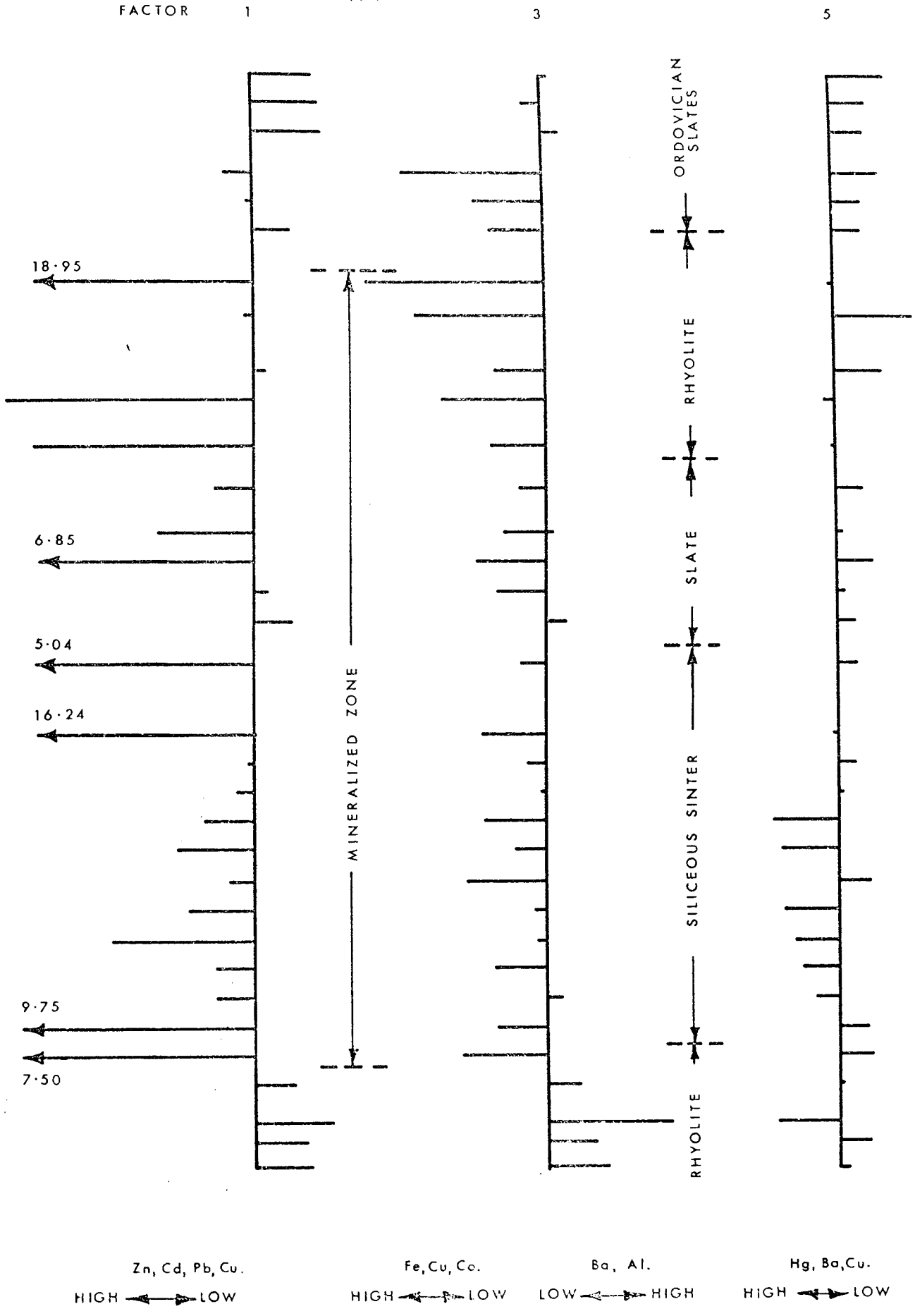

FIGURE 20 PLOTS OF FACTOR SCORES (FACTOR 1, 3 and 5.) ALONG BOREHOLE C4 FROM 700 TO 1078 feet (DEPTH ALONG CORE)

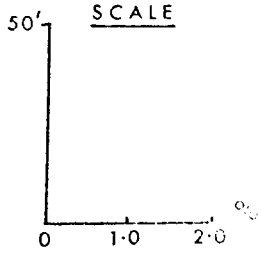

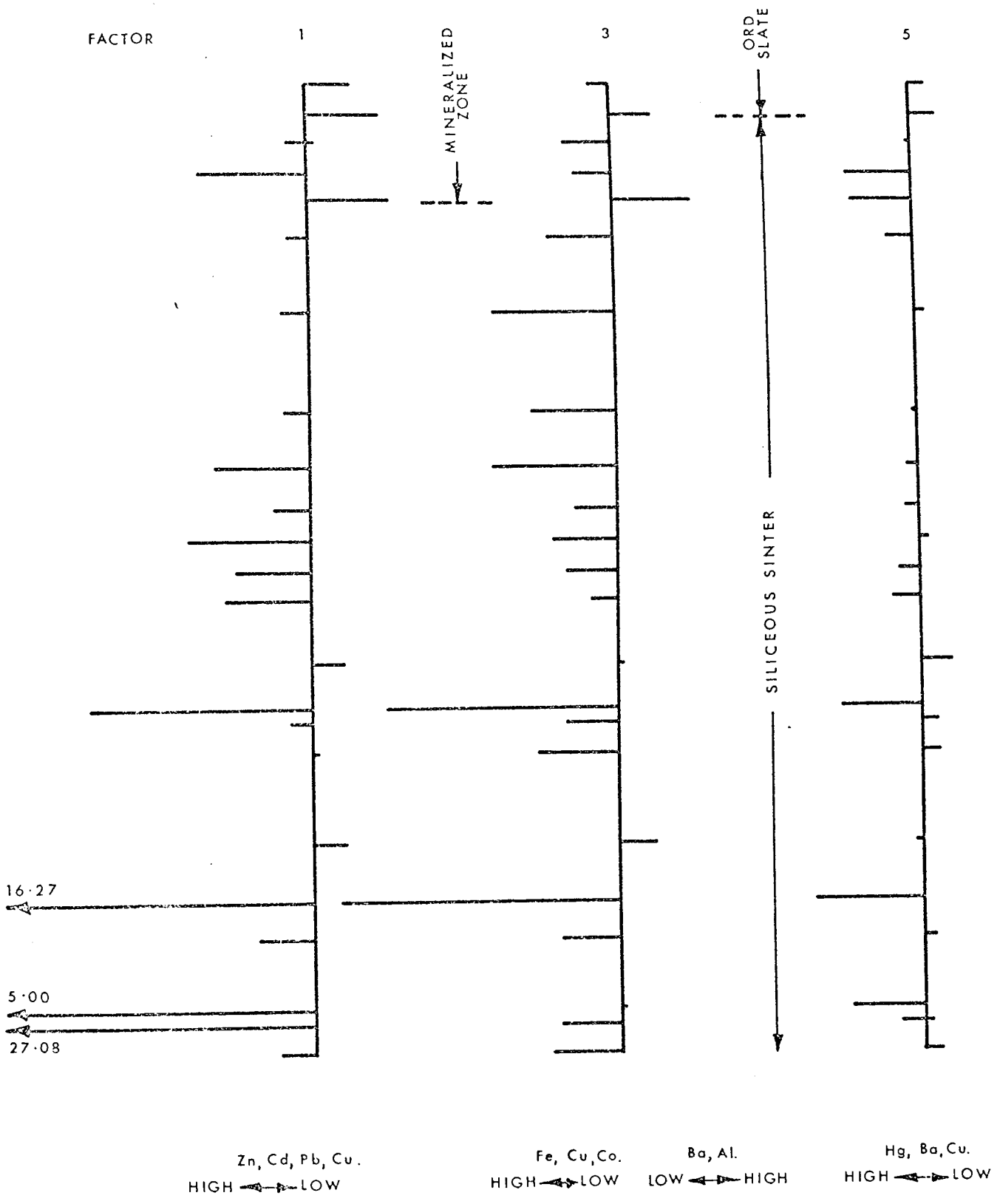

FIGURE 21 PLOTS OF FACTOR SCORES (FACTOR 1, 3 and 5.) ALONG BOREHORE M10 FROM 1279 TO 1599 feet (DEPTH ALONG CORE)

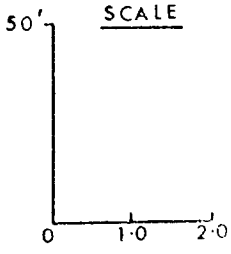

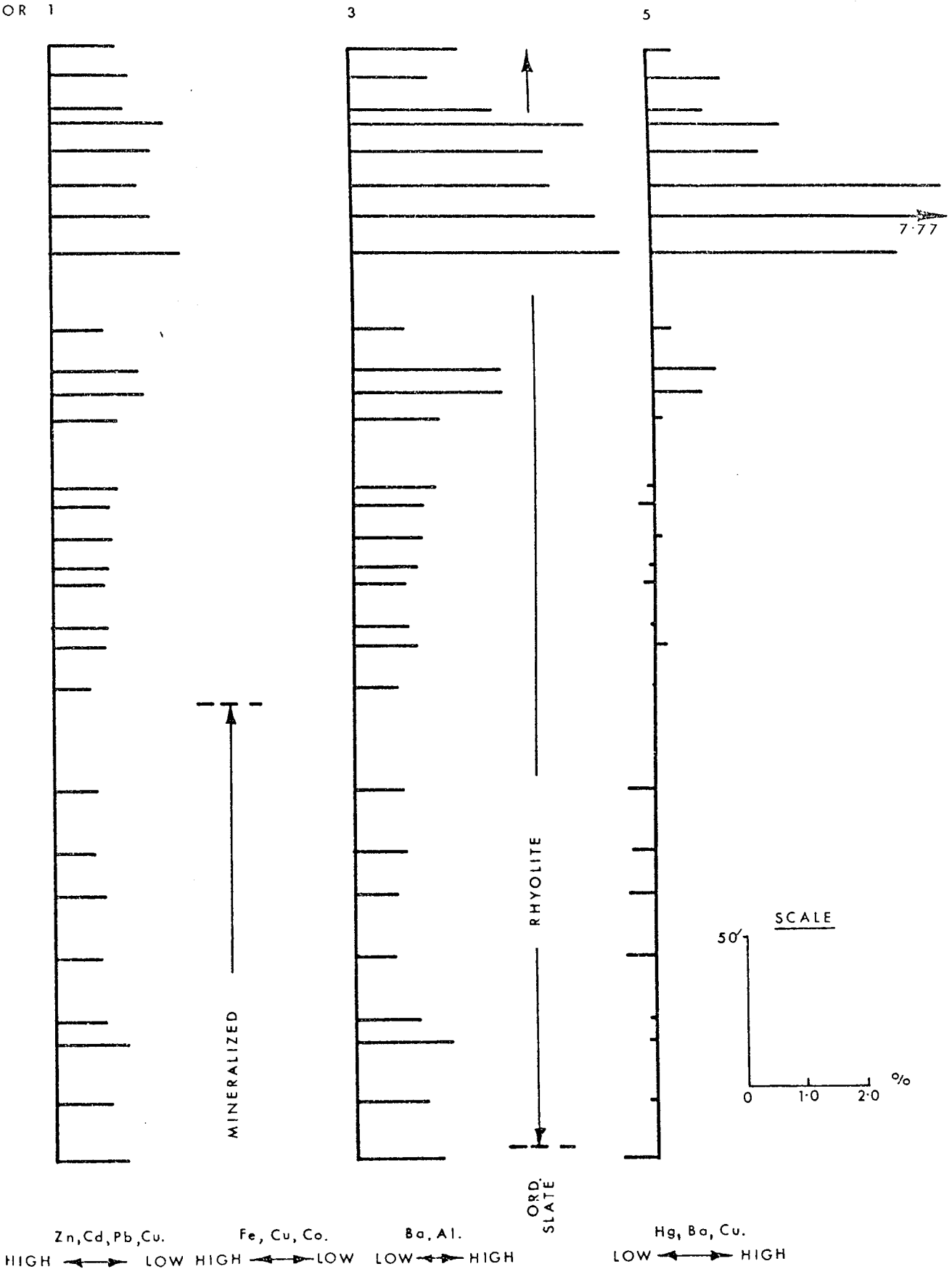

FIGURE 22 PLOTS OF FACTOR SCORES (FACTOR 1, 3 and 5) ALONG BOREHOLE IM9 FROM 51 TO 423 feet (DEPTH ALONG CORE)

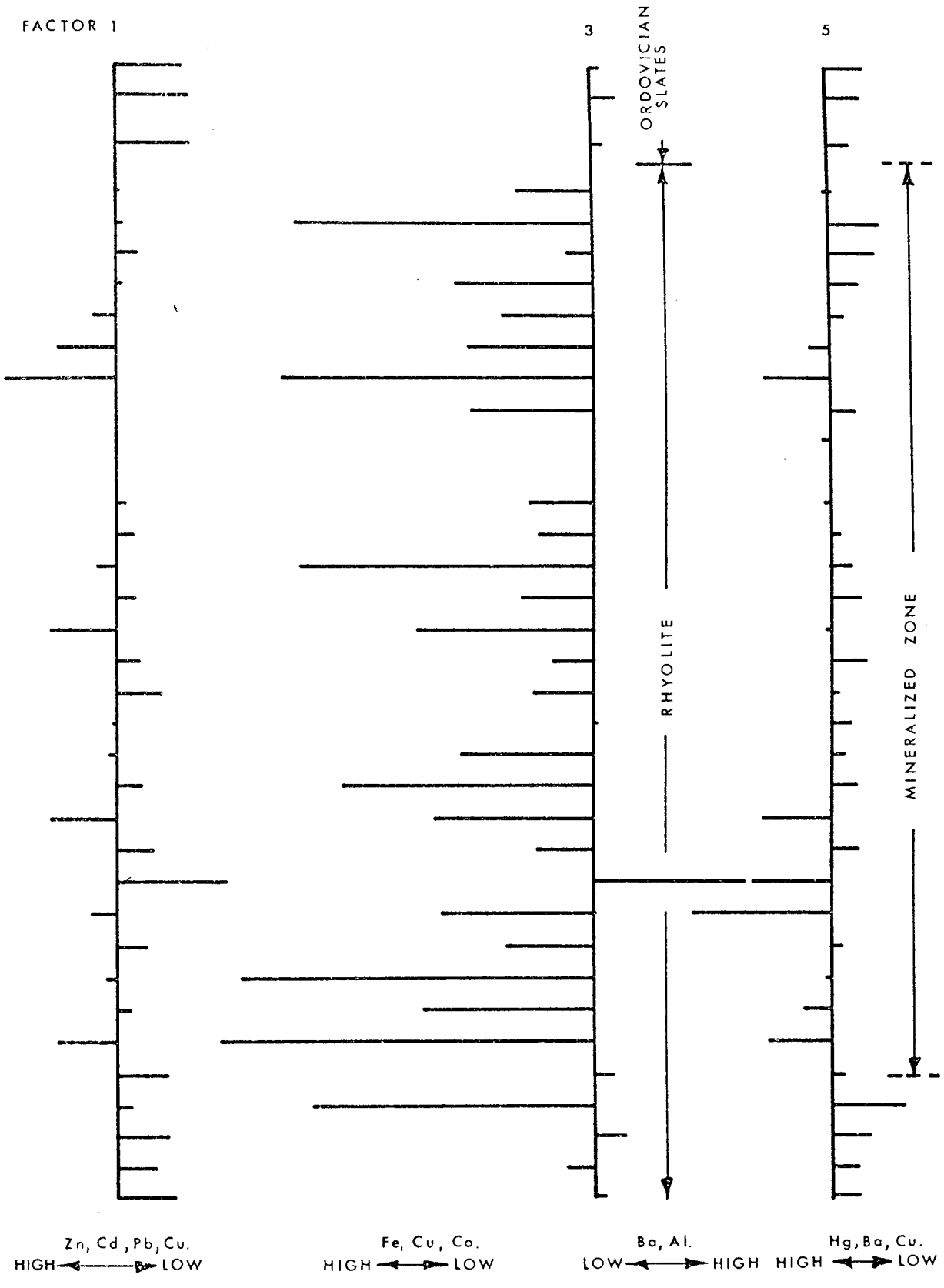

FIGURE 23 PLOTS OF FACTOR SCORES (FACTOR 1 3 and 5) ALONG BOREHOLE H17A FROM 1191 TO 1550 feet (DEPTH ALONG CORE)

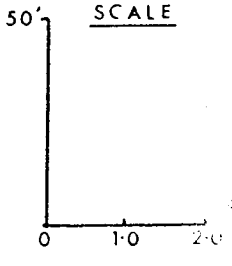

C4 (Fig.20), and in the siliceous sinter layers of borehole M10 (Fig.21). It is much higher than factor 1 in the mineralized zone of borehole H17A, but in borehole IM9 it is similar to factor 1. This is believed to be indicative of a different mineralization from that defined by factor 1. It is probably related to deposition of pyrite and chalcopyrite in the Pyritic and Copper ore types (Chapter 5), while factor 1 corresponds to the intimate association of sphalerite, galena, and chalcopyrite in the Bluestone ore type. This factor is not thought to be lithologically controlled, although higher scores are found in the rhyolitic rocks. Some high values extend outside the mineralized zone into the Ordovician slate contact with rhyolite in borehole C4 (Fig.20).

Factor 5 (Hg, Ba, Cu)

This is mainly a Hg factor, but Ba and, to a lesser extent, Cu are associated. High negative scores correspond to higher levels of Hg, Ba, and Cu. This factor does not show significantly high scores in any borehole except the top part of borehole IM9. It is believed to indicate similar effects as component 4, i.e. remobilization effects due to later tectonic deformation. However the moderately high values found in the siliceous sinter layers of boreholes C4 and M10 (Figs. 20 and 21), may be indicative of a primary association between these elements and this rock type.

The results of Principal Component Analysis and Factor Analysis of the data set of 61 samples (Tables 17, 18, and 19 - Appendix D) show variations which are related mainly to the major elements, probably because major elements have larger variance.

These are considered to be solely lithological factors. Trace element variance in this data set shows similar association as that in the other set hence is not discussed.

Discussion of the Statistical Analyses.

The factors from the multi-element data set can be divided into two groups:- a) lithologically related factors and b) mineralization related factors. The aim of the statistical analysis was to correlate trace element analyses with the mineralization factors. This has a limitation due to the magnitude of the eigenvalue (the percentage of total variance accounted for by each factor) consequently the number of factors considered to be significant is limited to a small number. These are those factors related to Zn, Pb, Cd, Cu, Hg, Ba, Ni, Co, Fe, and Al (components 1, 4, and 5 ; and factors 1, 3, and 5). Plots of these factors along the four boreholes C4, M10, IM9, and H17A (Figs. 19, 20, 21, 22, and 23) allow the interpretation that there were two major episodes of mineralization, both of which were probably associated with volcanism. This is indicated by the two mineralization factors (1 and 3) commonly associated with volcanic horizons, particularly the siliceous sinter. In some instances the two factors show higher scores in the siliceous sinter (Fig. 21) than in the mineralized zone (Fig.20).

Dispersion haloes around the mineralized zones, containing anomalous concentrations of various trace elements, are not readily definable since the main concentrations are confined to the mineralized zones, except in borehole M10 where anomalous concentrations

were found outside the mineralized zone (Fig.21).

Two general conclusions can be made:-

(1) Elements related to mineralization are closely associated with the volcanic rocks and are particularly prominent within the siliceous sinter. This suggests a common origin between the mineralization and the siliceous sinter.

(2) The effects of later tectonic deformation of the area, caused remobilization of some highly mobile elements (e.g. Hg, Ba, Ni and Co), which also have a primary relationship with the principal ore metal elements.

6.5 The Study of Wall Rock Alteration.

Wheatley (1971a) reported silicification and potassic metasomatism with the development of sericite in wall rock alteration associated with sulphide mineralization at Parys Mountain. The petrographic study indicated that alteration is present particularly silicification and carbonatization, and the development of sericite and chlorite.

In the present study 215 rock specimens were analysed, using an X-ray powder diffraction technique, in an attempt to discover if there is a zonal arrangement of the various alterations associated with mineralization in the area. This was done because alteration zones are commonly found associated with some types of sulphide mineralization (Meyer and Hemley, 1967).

This primary study indicates that alteration is present but no specific alteration zoning effects were defined. The alteration appears to reflect the mineralogy of the primary rocks, e.g. chlorite is commonly found in the more basic members or the sedimentary rocks.

CHAPTER 7

PETROGENESIS

7.1 General Statement.

Any interpretation of the genesis of the volcanic rocks of Parys Mountain must take into account their close association with the underlying Ordovician sediments, their vertical lithological variations, and variations in their lateral thickness. These are shown in the general stratigraphic sequence as illustrated by Fig.8. In the lower part of the sequence the Ordovician slates and the lowermost volcanic (dacitic) rocks are interlayered. This is followed by a thick (700m) sequence of Ordovician slates which are overlain by the main volcanic (rhyolitic) sequence.

The occurrence and interpretations of similar Lower Palaeozoic volcanic rocks in the other parts of the British Caledonides must also be taken into account in interpreting the petrogenesis of the volcanic rocks at Parys Mountain. These other occurrences form major rock units in three areas:- the Lake District, North Wales, and south-east Ireland. Those of the Lake District are the Borrowdale Volcanic Series (Green, 1919; Mitchell, 1963; Cliver, 1954; Fitton and Hughes, 1970; Soper, 1970; Wheatley, 1971b); in North Wales the Snowdonian Volcanic Series are most important (Rast, Beavon, and Fitch, 1958; Beavon, Fitch, and Rast, 1961; Bromley, 1965; Fitch, 1967; Brenchley, 1969; Rast, 1969); and in south-east Ireland the Upper Volcanic Series are the main Palaeozoic volcanic rocks (Charlesworth, 1963; Williams, 1969; Wheatley, 1971b).

7.2 The Ordovician Slates.

The Ordovician sediments at Parys Mountain have a close relationship with the volcanic rocks, and their origin and depositional environment is important to the interpretation of the volcanic rocks.

Despite the strong alteration and deformation of these rocks they still retain characteristics indicating a marine depositional environment (Brenchley, 1969; Rast, 1969; Wheatley, 1971b) i.e. very fine grain-size, and pelagic nature indicated by the occurrence of Didymograptus bifidus.

The existence of an Ordovician depositional basin in Anglesey requires the presence of an Irish Sea Landmass to explain the provenance of the Ordovician sediments.

7.2.1 The Ordovician Depositional Basin in Anglesey.

It is generally accepted that the Irish Sea Landmass (Jones, 1938) was present in Ordovician times as shown by the overstep of the Arenig and the basal Caradoc onto the Precambrian rocks in Anglesey (Brenchley, 1969). This belt of active uplift, extending from Anglesey to the extreme south-east corner of Ireland, is thought to be fault bounded (Bates, 1969; Brenchley, 1969).

The scarcity of Cambrian rocks in Anglesey has led to the idea that the Irish Sea Landmass began its emergence in this period. The presence of some early Cambrian (Arvonian) rocks indicates that, during that period, at least some parts of Anglesey were still submerged. These Arvonian rocks comprise a sequence of tuffaceous and agglomeratic sediments of the Baron Hill Group, the Bwlch

Gwyn Felsite, and a conglomeratic horizon near the village of Trefdraeth (Greenly, 1919; Wood, 1969). Wood (1969) interpreted the Bwlch Gwyn Felsite as consisting of ignimbrites, and Fitch (1967) suggested that they were deposited subaerially. The nature of the rocks of the Baron Hill Group and the conglomerate also indicates a subaerial, shallow-water, depositional environment. The above evidence, together with the absence of other rocks of Cambrian age in Anglesey, allows the conclusion that Anglesey, as part of the Irish Sea Landmass, began to emerge at this time. Following the Arvonian deposition and volcanism the area continued to emerge, the volcanic activity died out, and no further Cambrian rocks were deposited. The whole area was then probably a source of sediments for the late-Cambrain horizons in the Welsh Basin to the south.

Parts of Anglesey were submerged in the early Ordovician (Arenig) when the shallow-water Basal Grit was deposited (Bates, 1964; Williams, 1969). Volcanism reoccurred during Arenig-Llanvirn times in several parts of North Wales, e.g. the Moelwyns; Moel Llyfnant; the Arans and the Cader Idris range on the southern flank of Harlech Dome; and Mynydd Rhiw in the Lleyn Peninsula (Mitchell, 1957; Bast, 1969). Simultaneous volcanic activity occurred in Anglesey and produced differential uplift there. However as the Welsh Basin overall was subsiding, the submarine environment for the accumulation of the Ordovician sediments at Parys Mountain was produced. This volcanism continued during most of Llanvirn and Llandeilo times, and explains the occurrence of the dacitic rocks and lithic tuffs, interlayered with the sediments,

at the base of the Parys Mountain sequence.

The Anglesey area overall began to emerge again at the end of Llandeilo time and the major part probably remained as an area of uplift until the end of the Ordovician. The intense volcanic activity which produced the Caradocian rhyolitic rocks at Parys Mountain is believed to have been associated with this emergence.

Table 6 summarizes the events in the Anglesey area from Precambrian to early Silurian times, and includes an interpretation of the probable depositional environments related to the status of the Irish Sea Landmass.

It is concluded that the Irish Sea Landmass began to emerge in the early Cambrian and existed as a landmass through most of the Ordovician period, during which time several episodes of alternate differential subsidence and uplift occurred. Volcanism is believed to account for most of this instability.

7.2.2 Source of the Ordovician Sediments.

During the Ordovician the British part of the Caledonian Geosyncline received considerable supplies of sediment from areas to the north-west and south-east (Williams, 1969). Some of the mudstone and shale components in the Welsh Basin were thought to have been derived from the Borrowdale Volcanic Series of the Lake District (Brenchley, 1969). The products of the extensive Ordovician volcanism in the Welsh Basin probably contributed an enormous supply of sediment, although these rocks were localized in extent and formed relatively temporary landmasses (Brenchley, 1969; Williams, 1969). In an unstable area, like Anglesey in the

Table 6 Inferred depositional events in Anglesey from Precambrian to early Silurian, with probable depositional environments related to the status of the Irish Sea Landmass.

Age	Representative stratigraphic horizons in Anglesey	Environment	Status of the Irish Sea Landmass
Silurian	Silurian slates at Parys Mountain (Greenly, 1919; Bates, 1964)	Marine	Submerged
Ordovician*			
Bala	None	Erosional	Emerged
Ashgill	None	Erosional	Emerged
Caradoc	Rhyolites at Parys Mountain	Subaerial	Emerging
Llandeilo	Ordovician slates at Parys Mountain (Greenly, 1919; Bates, 1964)	Marine	Submerged
Llanvirn	Dacites and lithic tuffs at Parys Mountain	Marine	Submerging
Arenig	The Basal Grit (Bates, 1964; Williams, 1969)	Subaerial	Submerging
Tremadoc	None	Erosional	Emerged
Cambrian			
Upper	None	Erosional	Emerged
Lower	Conglomerate, Baron Hill Group, Bwlch Gwyn Felsite (Greenly, 1919; Wood, 1969)	Subaerial	Emerging
Precambrian	The Mona Complex (Greenly, 1919)	-	-

* The subdivision of Ordovician is after Skevington (1969).

Ordovician, extraneous sources are not thought likely to play an important role in supplying the sediments.

Jones (in Rast, 1969) estimated that the average rate of deposition in the Ordovician was 0.3m per 5000 years, although Boswell (in Rast, 1969) suggested that a rate of 0.3m per 6000 years is a more representative figure. At these rates approximately $12x10^6$ years would be necessary to accumulate the 600m of the Ordovician slates at Parys Mountain. Sedimentation rates such as these are really only applicable in a basin of continuous deposition like the Welsh Basin. In a tectonically unstable area like Anglesey deposition of materials from a source outside the area would take even longer. However the Ordovician slates at Parys Mountain were deposited mainly during Llanvirn time (approximately $9x10^6$ years) thus a more rapid rate of deposition must have operated. It is probable that a local source of sediment such as the volcanic materials erupted during the Arenig and Llanvirn, in the Anglesey area, were the main sources. This interpretation would account for the absence of volcanic horizons in the Arenig and Llanvirn of Anglesey compared with the large volumes of volcanics present in other parts of North Wales.

7.3 The Volcanic Rocks.

7.3.1 Previous Interpretations.

The pretogenesis of the volcanic rocks of Parys Mountain has been interpreted in different ways by various previous workers. The major factor that appears to have resulted in the different interpretations is the intensive rock alteration, which has removed

most of the primary volcanic characteristics from the rocks in the field.

Greenly (1919), who proposed the name felsite for these rocks, concluded that they constituted of an intrusive soda-felsite sill, but Manning (1959) suggested that they were emplaced as dyke rather than sill. The extrusive character of some of the rocks was recognized by Derry (1961), but he concluded that they were mainly intrusive. Bates (1964) was the first to interpret the felsite as being almost wholly extrusive, and based his conclusions on:- a) the absence of contact metamorphic effects in the underlying slates, and b) the agglomeratic nature of the felsite with its included slate fragments. Since then information from diamond drill holes in the area has revealed more evidence for an extrusive origin. Hawkins (1966), Wolfenden (1967), and Wheatley (1971a,b) concluded that they consist of groups of igneous rocks comprising rhyolitic lavas, tuffs, and intercalated sediments. This conclusion is borne out by the petrographic evidence gained in this study. This evidence is discussed in the next section.

7.3.2 Evidence used in the Petrogenetic Interpretation.

A description of the characteristics of the volcanic rocks of Parys Mountain, including outcrop patterns, stratigraphic relation with associated rock types, and their general appearance both in hand specimen and thin section, were previously given (Chapter 3). The features which indicate an extrusive origin, are listed below:

(1) The presence of flow textures which appear as colour bands in dacite (Plate 3A) and rhyolite (Plate 9C), stripes of

glassy and lithic characters (Plates 2F, 6D, 9B, D, and E), and lines of spherulites (Plates 2E, and 8B) in dacites and rhyolites.

(2) Spherulitic and perlitic textures resulting from devitrification of glassy rocks (Plates 6B, E, F, 7, 8, 9E, and 10F).

(3) Pyroclastic textures, with the presence of quartz and feldspar crystal fragments, and some few lithic fragments, set in a very fine grained matrix, of rhyolitic rocks (Plates 6A, C, D, 9D, and E).

(4) The mixed pyroclastic and flow-like textures in the rhyolitic tuff-lava (Plates 9C, D, E, F, 10A, B, C, and D).

(5) Lithic fragments of various sizes, shapes, and lithologies, embedded in a very fine grained matrix, of lithic tuffs (Plates 4A, B, C, D, E, and F).

(6) The presence of glassy groundmass and amygdales in the dacitic rocks (Plates 1C, 2A, B, C, E, 3D, E, and F).

The above evidence is indicative of an extrusive origin for the igneous rocks at Parys Mountain. Explosive volcanism produced the pyroclastic-type rocks and relatively quiet activity produced the flow types. Transitional, or contemporaneous, activity between the two types of volcanism probably gave rise to the tuff-lava types.

Interlayering between the volcanic rocks and the Ordovician sediments is clearly seen in the bore hole cores and indicates contemporaneous deposition of the two rock types. This contemporaneity occurred during the first episode of volcanism (dacitic rocks and lithic tuffs), and at the end of the Ordovician sedimentation

(beginning of the rhyolitic phase).

The genesis of the siliceous sinter was previously thought to be through hydrothermal agencies operating during the Caledonian (post-Silurian), or Variscan (late Devonian to Permian) orogenies (Greenly, 1919; Manning, 1959; Bates, 1964; Fitch et al., 1969). It was generally believed, by these previous workers, that this rock type formed as a series of large quartz veins. This hydrothermal activity was also thought to be responsible for the mineralization at Parys Mountain. Petrographic evidence, gained in this study, indicates that the siliceous sinter was more likely a product of fumarolic activity or volcanic emanations. Colloform layering and the occurrence of well-formed quartz crystals aligned along walls of cavities (Plates 5A, B, C, and D), indicate deposition from solutions at low temperatures (up to 100°C) in near surface, or surface, environments, rather than formation as hydrothermal quartz veins. Interpretation of this rock as the product of hydrothermal solutions at depth would require the presence of a large intrusive body in the Parys Mountain area. This would be needed to provide the hydrothermal fluids for quartz veins of this size, assuming that hydrothermal activity is the result of late stage magmatism. On the other hand, if hydrothermal fluid is considered simply as thermal water ascending from some deeper zones within the earth, regardless of its source, it is reasonable to expect that such water would penetrate weaker zones in the rocks. In the Parys Mountain area, preferred sites would be the unconformable contact between the rhyolitic rocks and the Silurian slates, and the faulted

contacts between the Precambrian Mona Complex and the Ordovician slates.

No evidence for an intrusive igneous body is present in the Parys Mountain area, and this quartz rock occurs at the most unlikely site, the gradational, interlayered contact between the Ordovician slates and the rhyolitic rocks. Furthermore, the outcrop pattern of this rock (Figs. 3 and 9) indicates that it was folded during the Caledonian orogeny (see Chapter 4) hence was formed prior to this tectonism. The main mineralization episode in the area, which is intimately associated with this rock type, was volcanogenic (see Chapter 8). Because of this the siliceous sinter is interpreted as a silica deposit formed by fumarolic processes or volcanic emanations in late Ordovician, prior to the rhyolitic phase of volcanism.

The abundance of arenaceous beds at the base and the top of the sedimentary sequence (Hawkins, 1966), indicates that although the main environment of deposition was submarine, shallow-water or subaerial environments existed during the periods of volcanism.

The Ordovician sedimentary and volcanic rocks on the southern limb of the major syncline (Fig.3) may be thinned by overthrusting of the Precambrian Mona Complex. This may, in part, account for the scarcity of dacites in the southern part of the area. Nevertheless, as was previously stated, all the volcanic rock units at Parys Mountain thin toward the south. This thinning is believed to indicate that the sources of the volcanics lie to the north of the present area.

7.3.3 Origin of Magma and Regional Tectonics.

Evidence from the bulk chemical study of the volcanic rocks of Parys Mountain indicates that they are parts of the calc-alkaline volcanic series, and vary in composition from andesite through dacite to rhyolite (Chapter 6). The intermediate and acidic types of the calc-alkaline series are the most abundant igneous rocks in the orogenic belts (Green and Ringwood, 1966), and have a close genetic relationship with island arc systems (Kuno, 1968; Miyashiro, 1974; Ringwood, 1974).

Three petrogenetic models have been commonly applied to explain the origin of this orogenic volcanic series. These are outlined below:-

1) Fractional crystallization or differentiation of basaltic magmas (Bowen, 1928; Osborn, 1959; Battey, 1965; Taylor and White, 1965; Kuno, 1968).

2) Melting of pre-existing sialic continental rocks or wet geosynclinal sediments, during orogenies (Turner and Verhoogen, 1960), or the contamination of mantle-derived basaltic magma with sialic material (dry lower crust) or recent sediments (Waters, 1955; Coats, 1962; Eichelberger, 1974).

3) Melts or their derivatives, formed from either the upper part of the oceanic lithosphere descending along subduction zones or from partial melting of mantle directly above such a subduction zone (Dickinson, 1970; Jakes and White, 1972; Miyashiro, 1974; Ringwood, 1974).

The first two models were commonly applied until plate tectonic theory was widely accepted when the third model became

increasingly popular.

The major drawbacks of the first two models are that both require many specific conditions to produce andesite magmas and the more acidic types. They also commonly fail to explain many observed features of the natural rocks (Green and Ringwood, 1966). Fractional crystallization of basaltic magmas requires the production of very large volumes of feldspathic and ferromagnesian crystal residua to account for the large volumes of andesitic magma. Green and Ringwood (1966) suggested that over 65 percent crystallization of the basaltic magma is needed to produce andesite. In the natural calc-alkaline series there is no evidence for the occurrence of such large volumes of basaltic magma associated with the volcanism. Normal fractional crystallization of basaltic magma according to Bowen's (1928) model does not always result in basalt-andesite-dacite-rhyolite series. Differentiation of basaltic magma, in the Skaergaard (Wager and Deer, 1939), produced the series olivine gabbro-gabbro-ferrogabbro-iron rich granophyre where extreme iron enrichment occurred because the magma was in a highly reduced state. Osborn's (1959) model, which involves silica enrichment and the removal of iron, requires conditions of high oxygen or water vapour pressure during fractionation, to produce early crystallization of magnetite and ferromagnesian minerals together with suppression of crystallization of plagioclase. However Green and Ringwood (1966) argued that while the available evidence is against the early formation of magnetite, in calc-alkaline rocks, early crystallization of plagioclase is commonly seen.

The second model also has some limitations because it is only applicable where sialic continental material is present to allow for a degree of contamination. This fails to explain the very common occurrence of andesites in island arcs developed on oceanic crust. The low initial strontium isotope ratios found in many andesitic rocks (Dickinson, 1970) indicates that contamination of basaltic magma by assimilation of old crust is unlikely to be an important petrogenetic process.

Basic volcanic rocks are not present in the Ordovician sequence at Parys Mountain but variation from andesite through dacite to rhyolite is present (Fig.14). In other parts of North Wales both basic and acidic magmas were available during Ordovician times at several volcanic centres, e.g. Snowdon, Arenig, and Moel Hebog. Fitch (1967) showed that a differentiation sequence from pyroxene-andesite to alkali rhyolite is present in these centres. He used the arguements of Taylor and White (1966) to suggest that basaltic magma was not involved in the genesis of the andesite, and that the calc-alkaline magmas of North Wales were produced by partial melting of a pre-existing continental crust. However the process of partial melting as suggested by Fitch (1967), and proposed by McBirney and Weill (1965) for the genesis of rhyolite magma of south-east Guatemala, cannot be applied at Parys Mountain because, although a metamorphic basement was present in the area, xenocrysts, or partially fused xenoliths, have not been found. The process of magma contamination within the volcanic pile, proposed by Eichelberger (1974) is not applicable to the rocks at Parys Mountain since the volcanic pile there was too small for such a

process to be effective.

The plate tectonic model for the formation of the andesite-dacite rhyolite magmas implies a derivation either from partial melting of the upper part of the crustal lithosphere on a Benioff zone, or by partial melting of the mantle, under high load pressures and high water pressures, above such a zone. Magmas formed in this way are believed not to be significantly contaminated during passage through the crust. However a thick continental crust may hold up the magma and allow it to differentiate to a high degree. The models proposed by Miyashiro (1972) and Ringwood (1974) (see discussion of section 6.2) for differentiation of magmas along deacending lithospheric plate, are applicable to the magma type of Parys Mountain.

The plate tectonic model, on which this interpretation is based, can be used to explain the magma variation in the British Caledonides as a whole. The scheme proposed by Fitton and Hughes (1970), for the early Palaeozoic arc-trench system in this area, has the Moffat Geosyncline as the oceanic trench, the English Lake District and the Irish Sea Landmass as the island arc system, and the English Midland Platform as part of the continental margin (Fig.24). The oceanic lithosphere descending along a Benioff zone produced tholeiitic magma in the Lake District area, calc-alkaline magma in the Irish Sea Landmass, part of which is Parys Mountain, and alkaline magma in the Welsh Basin. Parys Mountain was situated on the continental side of the arc thus magmas there would have a composition close to that of the continental margin type rather than a typical island arc andesitic magma. This is believed to

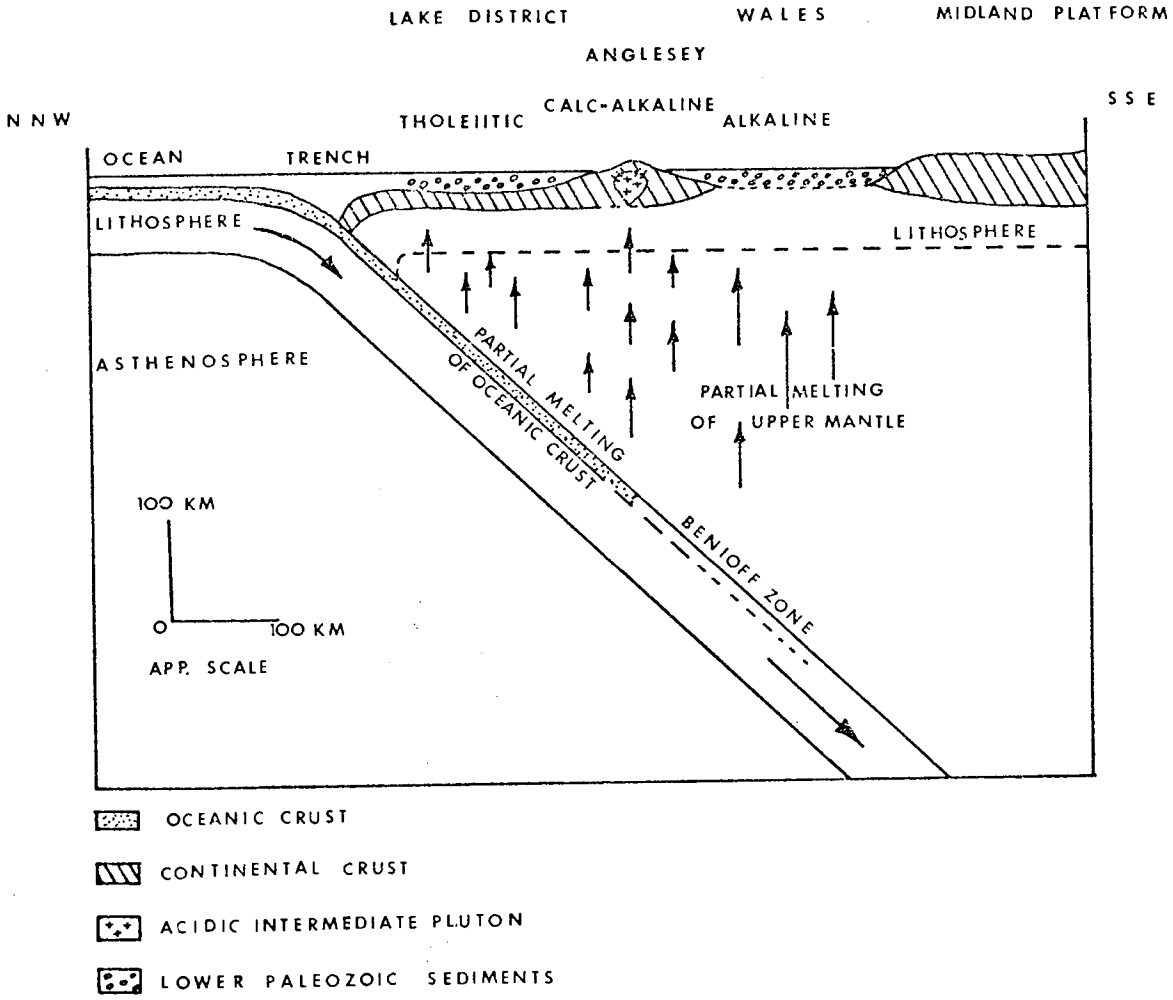

FIGURE 24 DIAGRAMATIC SECTION THROUGH ENGLAND AND WALES IN MID-ORDOVICIAN TO SHOW THE POSITION OF ANGLESEY WITH RESPECT TO THE PLATE TECTONIC INTERPRETATION OF THE REGIONAL STRUCTURE (DERIVED FROM FITTON AND HUGHES, 1970).

explain the abundance of rhyolitic rocks particularly the apparently alkali-rich rhyolites (Fig.15) of the area. Plot of MgO versus Fe_2O_3, on a Yoder's (1969) diagram, for the volcanic rocks of Parys Mountain (Fig.16) shows that their compositional trend lies in the field of continental-margin calc-alkaline series.

CHAPTER 8

ORE GENESIS

8.1 Introduction

Massive sulphide deposits, associated with both volcanic and intrusive igneous rocks, were interpreted as being formed epigenetically by hydrothermal processes. Later work has shown many of them to have a close genetic relationship with their associated volcanic rocks. Examples of such deposits are those in New Brunswick and Quebec, Canada (Suffel, 1965; Anderson, 1969; Sangster, 1971; Hutchinson, 1973), Jerome district, Arizona (Anderson and Nash, 1972), Skellefte district, Sweden (Anderson, 1969), and the Iberian Pyrite Belt, Spain and Portugal (Strauss and Nadel, 1973).

Reconsideration of the genetic aspects of these deposits, and many other massive sulphide deposits occurring in volcanic rocks, has been influenced by the volcanogenic evidence obtained from undeformed, younger deposits such as the Tertiary kuroko ores of Japan (Horikoshi, 1969), the Tertiary cupriferous pyrite deposits of Cyprus and Turkey (Suffel, 1965; Kinkel, 1966), the Pliocene massive pyrite deposits of the Izu peninsula, Japan (Sumi, 1958; Kinkel, 1966), and the pyrite deposits of Pleistocene and recent ages of Taiwan, which have a direct relationship with hotspring and fumarolic activities (Kinkel, 1966). The metal bearing brines of the Red Sea are perhaps the most recent examples of metal concentrations associated with areas of high heat flow and volcanism (Miller, et al., 1966; Degens and Ross, 1969).

Sulphide deposits with similar characteristics to those at Parys Mountain, i.e. similar oremineral assemblages (pyrite, chalcopyrite, galena, and sphalerite), and similar host rocks (submarine/subaerial silicic volcanic rocks with interbedded sedimentary rocks), are found in many parts of the world. Examples include those of:- Mt Lyell and Mt Isa, West Tasmania (Solomon and Elms, 1965; Bennett, 1965; Loftus-Hills and Solomon, 1967); Adak Area, Northern Sweden (Nairis, 1971); Caucasus and Urals, U.S.S.R. (Smirnov, 1971); Cyprus and Turkey (Hutchinson, 1965; Suffel, 1965; Kinkel, 1966); Matagami Lake, Noranda, and New Brunswick, Canada (Stanton, 1959; Suffel, 1965; Kinkel, 1966); the Iberian Pyrite Belt of South Portugal and Southwest Spain (Schermerhorn, 1970; Strauss and Madel, 1973); and the kuroko deposits of Japan (Horikoshi, 1969; Watanabe, 1970). In these places the mineralization is considered to have a close genetic relationship with volcanism (Suffel, 1965; Kinkel, 1966; Anderson, 1969; Hutchinson, 1973).

Anderson (1969) summarized the literature on massive sulphide deposits associated with volcanic rocks, and classified them into four categories, base on the major sulphide mineral assemblages. Of some 100 major sulphide deposits that he considered, two-thirds are equally divided between silicic and mafic volcanic host rocks, and the remainder occur within sedimentary rocks interbedded with volcanoclastics. He defined "massive sulphide" as being any solid, compact, mass of pyrite and/or pyrrhotite commonly containing one or more sulphides of Cu, Pb, and Zn. Later, Hutchinson (1973) discussed volcanogenic sulphide deposits and their general geological characteristics, i.e. their associated

volcanic rock types, types of volcanism and sedimentation, their associated precious metals (Au and Ag), and their related tectonism. He divided these volcanogenic sulphide deposits into three distinct varieties on the basis of their mineralogy and rock associations, e.g. pyrite-sphalerite-chalcopyrite bodies in differentiated, mafic-to-felsic volcanic rocks; pyrite-galena-sphalerite-chalcopyrite bodies in more felsic, calc-alkaline volcanic rocks; and pyrite-chalcopyrite bodies in mafic, ophiolitic volcanic rocks.

Table 7 is derived from the works of Anderson (1969) and Hutchinson (1973), and shows the classification of volcanogenic sulphide mineral assemblages, their general geological characteristics, the distribution of each type of the sulphide assemblages in conjunction with their host rocks, and their age of formation. The deposits listed are those which form tabular or lenticular bodies which are generally conformable with the bedding, or the foliation, of the host rocks. Various terms have been applied to these tabular or lenticular sulphide bodies, and these include:- "stratabound","stratiform", "bedded", "banded", and "kuroko type" (Suffel, 1965; Kajiwara, 1970; Sangster, 1971; Smirnov, 1971; and Hutchinson, 1973).

The mineral deposits of Parys Mountain commonly form tabular or lenticular bodies, generally conformable with the bedding and cleavage of the host rocks (Chapter 5), hence can be classified as stratiform, pyritic deposits with appreciable polymetallic sulphides, i.e. galena, sphalerite, and chalcopyrite, associated with felsic, calc-alkaline volcanic rocks. They correspond to type 3 of Table 7.

Table 7 Mineral Assemblages Found in Volcanogenic Sulphide Deposits, and Their General Geological Characteristics.

Mineral Assemblages	Precious Metal Association	Associated Volcanic Rock Types	General Geological Type of Volcanism	Characteristics Type of Sedimentation	Tectonism	Distribution of Major Deposits Host Rocks		Age	
1 Py and/or po, cp, and sl	Both Au (with high Cu) and Ag (with high Zn)	Fully differentiated suites of intermediate bulk composition; tholeiitic to calc-alkaline : basalt-andesite-dacite-rhyolite	Initial deep, subaqueous mafic platform, with differentiation toward felsic volcanism, building domical centres	Chemical:cherts,iron-formations Clastic:immature,first cycle,volcanogenic greywackes,volcanoclastics	Early eugeosynclinal orogenic stage; major subsidence	Silicic Mixed Mafic Sedimentary	16 4 14 9	Precambrian E Palaeozoic Devonian L Palaeozoic Triassic Cretaceous and Palaeocene	21 11 3 1 1 3
2 Py and/or po and sl	Mainly Ag	ditto	ditto	ditto	ditto	Sil-1;Mixed-2 Maf-3;Sed - 1		Precambrian L Palaeozoic	5 1
3 Py and/or po,cp,sl, and gn	Mainly Ag	Intermediate to felsic calc-alkaline volcanic suites; andesite-dacite-rhyolite-porphyry-crystal tuff, etc.	Felsic centres of explosive,pyroclastic and ignimbritic activity; subaqueous to subaerial	Epiclastic predominates; immature volcanogenic greywackes, manganiferous shales, graphitic shales and argillites, siltstones; Chemical : minor, cherts and iron formation Sulphate gangue common	Later eugeosynclinal orogenic stage, associated with crustal instability, uplift balances subsidence	Silicic Mixed Mafic Sedimentary	10 2 4 12	Precambrian E Palaeozoic Devonian Triassic	6 17 2 3
4 Py and/or po and cp	Mainly Au	Poorly differentiated mafic-ultramafic (ophiolitic) suites; tholeiitic, basaltic pillow lavas, serpentinite, etc.	Deep subaqueous, quiescent fissure eruptions	Chemical predominates; cherts, ironstones, manganostones. Clastics insignificant	Early stage of continental plate rifting; tension,separation, graben	Silicic Mixed Sedimentary Mafic	8 2 4 11	Precambrian E palaeozoic Devonian L palaeozoic Cretaceous and Palaeocene	3 3 4 5 3

After Hutchinson (1973) and Anderson (1969); Numbers in column 7 and indicate numbers of major deposits or districts.
Py - pyrite ; po - pyrrhotite ; cp - chalcopyrite ; sl - sphalerite ; gn - galena

8.2 Previous Interpretation.

The mineralization at Parys Mountain has long been considered to be of an epigenetic nature, that is, having been formed by the processes of metasomatism, or hydrothermal deposition (Greenly, 1919; Manning, 1959; Bates, 1964). This interpretation was generally accepted on the basis of 1) the occurrence of mineralization as crosscutting veins, stringers, and stockworks in the host rocks, 2) the interpretation of the 'felsite' as a post-Silurian intrusive igneous body, hence a likely source of the ore fluids, 3) the age of the mineralization interpreted as being post-Silurian.

Mining has removed the main mineralized materials, however, recorded descriptions of the ores note that the exploitable ore occurred as lenses or tabular bodies rather than veins (Greenly, 1919; Derry, 1961). Therefore the veins, stringers, stockworks of ores should not be interpreted as being truely representative of the ore bodies. Moreover the drilling programme, which started in 1961, has provided evidence (Chapter 3) that the felsite is extrusive rather than intrusive (Hawkins, 1966; Wheatley, 1971a). This led Wheatley (1971a) to suggest that the mineralization at Parys Mountain had a close genetic relationship with the extrusive, felsitic rocks, and that it is probably syngenetic in origin.

Petrographic evidence presented in this work (Chapter 3) shows that the 'felsite' consists of a succession of rhyolitic materials, and that those rocks previously called 'greenstone' are dacitic lavas. The majority of the ore bodies have lens-like or tabular forms which are generally conformable with the enclosing rocks. Textural evidence from the ore minerals allow the

interpretation that the sulphide deposit at Parys Mountain is volcanogenic. The evidence for this interpretation is discussed in a later section of this chapter.

8.3 Depositional Environment and Method of Emplacement of Stratiform Massive Sulphide Deposits.

Kinkel (1966) suggested that stratiform, massive sulphide, deposits, related with volcanism, were formed in the uppermost pyroclastic parts of submarine volcanic piles. They formed in the closing stage of submarine volcanism from volcanic emanations both by deposition in porous, in part, unconsolidated material, and by replacements within flows and pyroclastic beds. Stanton (1972) made similar interpretations and added that the deposition (or replacement) occurred on (or just beneath) the seafloor, in many cases, at volcanic centres where submarine fumaroles or hot springs debouched.

The submarine environment was emphasised by both authors though Davidson (1963-64) suggested that volcanic emanations may not be adequate in volume or in content to form large mineral deposits. In a submarine depositional environment, the ore material would be accumulated and concentrated in or near the volcanic centres. Evolution of gases and liquids in solfataric areas is commonly continuous over a long period hence a large mineral deposit can be formed (Kinkel, 1966). This does not rule out the possibility of a volcanic origin for the deposits occurring in shallow-water or subaerial volcanic rocks, such as those of Parys Mountain. The original ore metal content of the magma, which formed the volcanic rocks at Parys Mountain, may have been sufficiently concentrated to form the deposits there, with sulphur

also being provided by the magma. Alternatively, gases and liquids of hot springs or volcanic emanations are capable of leaching large quantities of material, particularly Fe and Si, along their channel ways (Burbank, 1950; Lovering, 1950; Morozumi, 1961; Naboko, 1959; Kinkel, 1966). Leaching of suitable basement rocks such as the Precambrian Mona Complex (the average ore metal content of equivalent Precambrian rocks at West Avoca, analysed by Wheatley (1971a) is as follows: Cu 249ppm, Zn 242ppm, and Pb 462ppm), to provide the base metals and leaching of the thick section of Ordovician sediments to provide iron, would provide sufficient metals for the mineral deposit at Parys Mountain. The sulphur for such a mineral deposit again would need to have been provided by an extraneous source. In addition the kuroko deposits of Japan have a very similar mineral content and occur in volcanic rocks similar to those at Parys Mountain. As pointed out by Sillitoe (1973) the typical deposits of kuroko ore are related to dacitic or rhyolitic domes and explosive vents emplaced in a shallow marine environment. They consist of zones of syngenetic massive pyritic ores enriched in Zn-Pb-Cu-Ag, and chalcopyrite at the top. These zones are underlain by silicified stockworks and disseminated chalcopyrite mineralization which represent the feeder channels for the ascending fluids. The concentration of ore metals, in this instance, was interpreted as being produced by processes operating during andesitic magma production by partial melting on subduction zone (Sillitoe, 1973). A similar process is possible for the formation of the Mineralization at Parys Mountain as the magmas which produced the volcanic rocks probably were formed on a

subduction zone as discussed in Chapter 7.

Fundamental environmental and structural conditions for sulphide deposition in felsic calc-alkaline volcanic and sedimentary basins are summarized below, from the following works on volcanogenic sulphide deposits:- Kinkel, 1966; Anderson, 1969; Schermerhorn, 1970; Holmes, 1971; Ivanov, 1971; Jenks, 1971; Ferguson and Lambert, 1972; Stanton, 1972; Hutchinson, 1973; Sillitoe, 1973; Strauss and Madel, 1973; and Ferguson et al., 1974.

1. Presence of regional weaknesses (faults or rifts) that have controlled and localized volcanism.

2. Development of active island arc/continental margin environments, or island arcs, along convergent plate margins where volcanism is active above subduction zone. Volcanism is of the explosive vent type resulting in the formation of massive piles of fragmental volcanics of the andesite-dacite-rhyolite type. The final explosive stages are accompanied and/or followed by gaseous venting (hot springs or volcanic emanations) around the central parts of the pile. The depositional environment varies from submarine to subaerial depending upon the size and stage of evolution of the island arc.

3. An active subsiding depositional basin in which the volcanic-sedimentary materials accumulate is present. Argillic-pyroclastic and/or black shales are deposited in depressions in the basin, commonly close to the peripheral areas of the pile. These subsidiary depressions are generally fault controlled, and sulphides are commonly localized within them.

4. Active faulting in the pile area controls gaseous venting

into the basin.

5. The calc-alkaline suite, of basalts, andesites, dacites, and rhyolites, is typical of these convergent plate margins, and pyroclastic units are particularly common. The depositional environment of island arc volcanism is more commonly subaqueous than that of continental margins, where submarine activity is normally restricted to the early stages of orogenic development. Sulphide deposits formed in this environment are commonly confined to the pyroclastic units which are situated at the top of the volcanic pile.

6. Deformation features are common in these deposits. These form by submarine sliding and brecciation, immediately following the ore formation when the rocks are still in a relatively unconsolidated state.

7. Redeposition of sulphide minerals as sediments result in clastic depositional ore textures. These are produced by submarine erosion and the products are deposited in depressions created, in the seafloor, by repeated volcano-tectonic movements.

8.4 Genesis of Sulphide Deposits at Parys Mountain and Their Relationship with volcanism.

The characteristics of the sulphide deposits at Parys Mountain, and their associated volcanic-sedimentary rocks, are similar to volcanogenic sulphide deposits occurring in other parts of the world (section 8.1 and Table 7). The environmental and structural conditions at Parys Mountain have great similarity to those listed in the previous section (8.3) for volcanogenic

sulphide deposits. The genesis of the mineralization, and sequence of events associated with it, at Parys Mountain is interpreted as follows:-

In the early Ordovician Parys Mountain was a part of an active Irish Sea Landmass in the Southern Caledonian Belt (Williams, 1969; Wheatley, 1971b). Although most of the Irish Sea Landmass was in a stage of uplift during this period (Brenchley, 1969), the area around Parys Mountain and the central-western part of Anglesey was submerged as indicated by the occurrence of marine Ordovician sediments in these areas. Subaqueous volcanic activity, producing dacites and lithic tuffs, began with the early stages of deposition of the Ordovician sediments. The volcanism at this time was intermittent, and of short duration. Only a limited quantity of volcanic rocks were produced, and volcanic horizons were not produced during the main stage of sedimentation of the Ordovician. Volcanism began again with the eruption of dacite (c), during the final stages of Ordovician sedimentation. This was followed by the formation of the siliceous sinter, indicating the presence of fumarolic activity probably at the end of this particular volcanic episode. The depositional environment was mainly subaqueous as some Ordovician sediments also were deposited. Mineralization began during this period with the deposition of the Copper ore and Pyritic ore in the dacite (c), siliceous sinter, and the interbedded sediments. This was immediately followed by the main stage of volcanism during which a thick pile of rhyolitic rocks were formed. The depositional environment gradually changed from subaqueous to subaerial as indicated by interlayering between Ordovician sediments in the lower parts of the rhyolitic sequence, the absence of the

sediments higher in the sequence, and the occurrence of subaerially deposited rhyolitic ignimbritic rocks. The Copper ore and the Bluestone ore were the major mineralizations formed during this stage although their accumulation and concentration was developed most strongly while the depositional environment was subaqueous. Deposition of the low grade Lead-Zinc ore followed the Bluestone ore, during the final stages of volcanism, and probably represents the final episode of mineralization.

The stringer and stockwork-type ore, which consists mainly of pyrite and chalcopyrite and is most commonly present in the Ordovician slates, may represent the feeder channels of the ore fluids for the main mineralization (Sillitoe, 1973). However the other vein-type mineralization, consists mainly of pyrite, with minor quantities of chalcopyrite, accompanying quartz veins. This mineralization penetrates all rock types, belongs to the latest of mineralization, and probably was formed by hydrothermal processes during later tectonic deformation, i.e. the Caledonian and Variscan orogenies. The extensive metamorphism and deformation formed during these orogenies commonly obliterated primary textures in both the ore mineralization and the volcanic rocks, and has made genetic interpretations of these difficult. Deformation and metamorphism may cause remobilization of previously formed sulphides (Sorensen, 1963; Vokes, 1971). Sulphide minerals, particularly pyrite and chalcopyrite, can be mobilized, and may migrate for varying distances (Vokes, 1971). This can occur within the ore body itself or in its immediate host rocks. The mobilized segregations later may recrystallize and form coarse grained pegmatitic or vein-like

bodies, and are commonly associated with vein quartz. Many metamorphic phenomena, such as pressure shadows (Plate 14C), tension fractures (Plates 24C and D), and compression vortices (Plates 29E and 30E), are common in the sulphide deposits and are interpreted as being produced by metamorphic remobilization (Natale, 1969). It is, therefore, probable that tectonic deformation, during Caledonian and Variscan orogenies, remobilized some of the sulphides. This has resulted in the production of vein-like structures with crosscutting relationships; variations in the apparent paragenetic sequence; apparent epigenetic textures.

Despite severe deformation of the ore bodies, and remobilization of some sulphides, many ore textures are preserved that indicate that the ore minerals were deposited in a sedimentary-volcanic basin. Such textures include colloform and framboidal textures in pyrite, colloform layering of pyrite, layering of Ordovician slate inclusions in massive chalcopyrite masses, interlayering of chalcopyrite, sphalerite, and pyrite, and slump textures of detrital pyrite grains (Chapter 5). Many textural features of the ore minerals indicate that the main mineralization was closely associated with the volcanism, prior to the tectonic deformation of the area. These textures include:- the cataclastic textures of pyrite (Plates 24B, C, D, E, and F), fragments of Ordovician slates containing pyrite grains being cemented by barren quartz (Fig. 11E), and folding of a layer containing both pyrite and chalcopyrite (Fig. 11F).

The mineralization of Parys Mountain is thus interpreted as being of synsedimentary-exhalative origin of late Ordovician age

which has been modified by mobilization of some sulphides producing apparent epigenetic features.

CHAPTER 9

SUMMARY OF CONCLUSIONS

9.1 Introduction

Interpretation of the relationship between mineralization and petrology at Parys Mountain requires the solution of three main problems:-

(1) Origin of the 'felsite', the Carreg-y-doll, and the White Rock Formations.

(2) Relationship between the rocks in problem (1) and the enclosing sedimentary strata (Ordovician and Silurian slates).

(3) Origin of the mineral deposits.

The answers to these problems as reached in this study are summarized below.

9.2 Origin of the 'felsite', the Carreg-y-doll, and the White Rock Formations.

The evidence available from petrographic study, bulk chemical analyses, field observations and drill core logging, allows the origin of these rocks to be interpreted as follows:-

The three rock types, together with the rocks previously identified as 'greenstone', represent a succession of volcanic rocks, comprising dacite, lithic tuff, siliceous sinter, rhyolitic tuff, rhyolitic ignimbrite, rhyolitic tuff-lava, and rhyolitic lava. The results of 61 bulk chemical analyses indicate that these volcanic products belong to an orogenic calc-alkaline magma series which formed in a continental margin/island arc environment. The magmas

probably formed either from partial melting of the crustal part of the oceanic lithosphere on a Benioff zone, or from partial melting of the mantle,above a Benioff zone, under high load pressures and high water pressures.

The plate tectonic model, on which this interpretation is based, can be used to explain the magma variation in the British Caledonides as a whole. The arc-trench system of this model, as proposed by Fitton and hughes (1970), has the Moffat Geosyncline as the oceanic trench, the English Lake District and the Irish Sea Landmass as the island arc system, and the English Midland Platform as part of the continental margin. The oceanic lithosphere descending along a Benioff zone produced tholeiitic magma in the Lake District area, calc-alkaline magma in the Irish Sea Landmass area, and alkaline magma in the Welsh Basin as a result of the processes outlined above. Parys Mountain, as part of the Irish Sea Landmass, was situated on the continental side of the arc thus magmas there would have a composition close to that of the continental margin type rather than a typical island arc magma, i.e. andesitic magma. This is believed to explain the abundance of rhyolitic rocks particularly the apparently alkali-rich rhyolites of the area. The highly siliceous Carreg-y-doll and White Rock Formations are believed to have formed as a siliceous sinter associated with this highly siliceous volcanism.

9.3 Relationship Between the Volcanic Rocks and the Enclosing Sedimentary Strata.

Contact relations, as seen both in outcrop and in drill

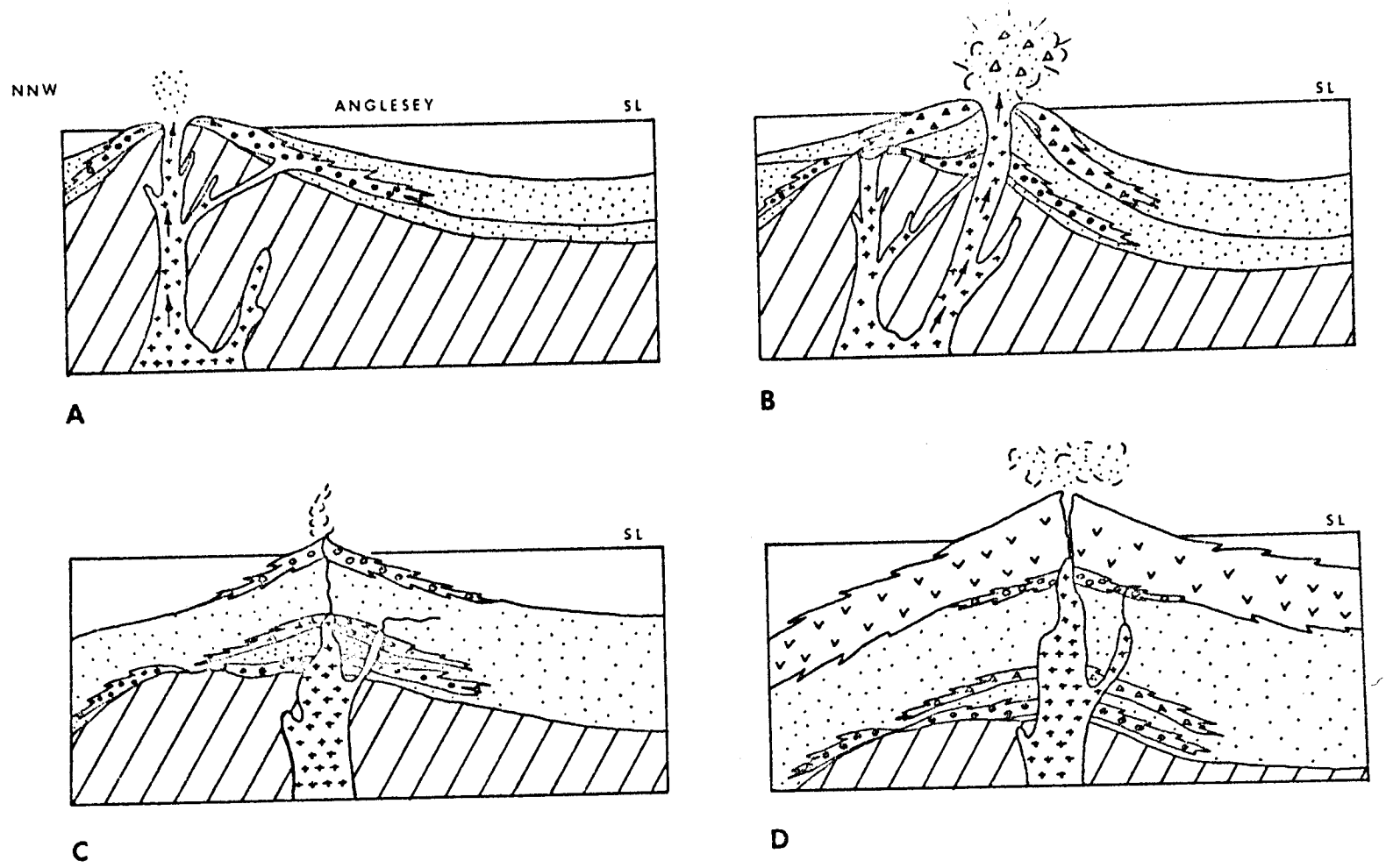

FIGURE 25 SKETCH DIAGRAMS TO SHOW THE DEVELOPMENT OF THE ORDOVICIAN VOLCANISM AND SEDIMENTATION AT PARYS MOUNTAIN (NOT TO SCALE)

: RHYOLITE

: SILICEOUS SINTER

: LITHIC TUFF

: DACITE

: MAGMA

: ORDOVICIAN SEDIMENTS

: PRECAMBRIAN BASEMENT

cores, between these rocks are interpreted to show that the volcanism was closely associated with deposition of the Ordovician slates. Two phases of volcanic activity occurred separated by a period in which some of the Ordovician sediments was deposited. The first volcanic phase was represented by dacite and lithic tuff, and the second by siliceous sinter, dacite and rhyolite. Rhyolitic rocks are the most abundant of the volcanic products though are confined to the second volcanic episode. The volcanic succession is thus interpreted to be Ordovician in age. The Silurian sediments were deposited after the end of the volcanism. The contact with the volcanics is unconformable thus the Silurian succession may be partly derived from the Ordovician volcanics.

Sketch diagrams to illustrate the proposed Ordovician volcanic and sedimentary events at Parys Mountain are shown in Fig.25.

9.4 Origin of the Mineral Deposits.

The ore textures and paragenesis, the general characters of the ore bodies, and their relationship with the host rocks, i.e. occurrence as lenses and tabular bodies conformable with the host rocks, are the main lines of evidence for the origin of the deposits. The mineralization at Parys Mountain is interpreted as being of a synsedimentary-exhalative origin of late Ordovician age. These deposits were probably later modified by remobilization of some sulphides to produce apparent epigenetic features.

The study of trace element chemistry (Cu, Zn, Pb, Ni, Co, Cd, Cr, Ba, and Hg) on 350 specimens, detected anomalous concentrations

of these elements in and around the mineralized zones, though some were found where no mineralization was apparent. Dispersion haloes are not distinct and cannot readily be defined. This is probably due to the collection of insufficient specimens from around the mineralized zones.

Principal Component Analysis and Factor Analysis operated on the analytical results produced two general conclusions:

(1) The elements related to mineralization reflect two types of mineralization: the Pyrite and Copper ores, and the Bluestone ore. The ore metal elements of both types show a close association with the volcanic succession, particularly the siliceous sinter. This is believed to indicate a genetic relationship between the mineralization and the siliceous sinter.

(2) Later tectonic deformations resulted in the remobilization of the more highly mobile elements. Hg was particularly susceptible to this though it also has a primary association with the main elements of the ore minerals.

The overall geological history of the main events in the area, including the mineralization and volcanism is interpreted as follows:-

(a) Deposition of the Ordovician sediments in a marine environment with volcanism producing dacites and lithic tuffs at the end of the main sedimentation.

(b) Continued Ordovician sedimentation after the first period of volcanism was followed by the formation of the siliceous sinter along with deposition of the pyritic and some copper ores.

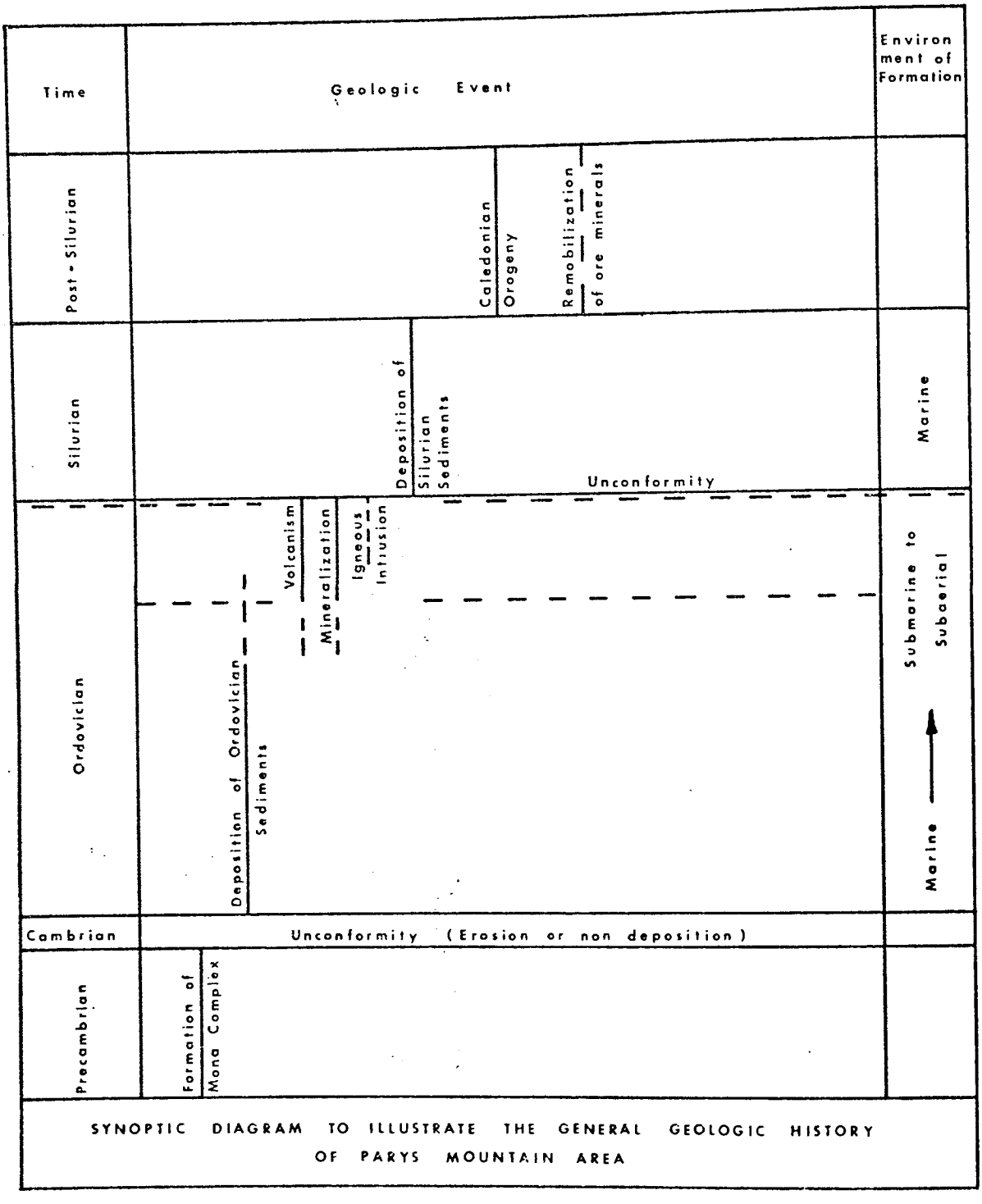

Figure 26 Time relationships for the geological events of Parys Mountain area

Facing page 204

(c) The main stage of volcanism followed, in which the rhyolitic succession formed. At this time the depositional environment changed from subaqueous to subaerial. Formation of the main units of copper ore and the Bluestone ore constituted the major mineralization during this stage.

(d) The area stood as a landmass and an erosional environment existed at the end of the Ordovician. In the Silurian the area was submerged and Silurian sediments accumulated, receiving parts of their sediment supply from the erosion of the pre-existing Ordovician volcanics and sediments.

(e) The sediments and volcanics were deformed and metamorphosed during Caledonian and Variscan orogenies. Remobilization of some of the sulphides in the mineral deposits occurred at this time.

These events at Parys Mountain are shown in a synoptic diagram (Fig.26).

REFERENCES CITED

Anderson, C.A., 1969, Massive sulphide deposits and volcanism: Econ. Geol., v. 64, p. 129-145.

_____., and Nash, J.T., 1972, Geology of the massive sulphide deposits at Jerome, Arizona - a re-interpretation: Econ. Geol., v. 67, p. 845-863.

Angino, E.E., and Billings, G.K., 1967, Atomic Absorption Spectrometry in geology: Methods in Geochemistry and Geophysics, Elsevier Publishing Company, Amsterdam, London and New York.

Bates, D.E.B., 1964, The stratigraphy, structure and palaeontology of the Lower Palaeozoic rocks of Anglesey: Ph.D. Thesis, Queen's University Belfast.

_____., 1966, The geology of Parys Mountain: Welsh geol. Quart., v. 2, no. 1, p. 27-29.

_____., 1969, Some aspects of the Arenig faunas of Wales: in "The Precambrian and Lower Palaeozoic rocks of Wales, A. Wood, ed. (University of Wales Press, Cardiff), p. 155-160.

Battey, M.H., 1965, The "Two-Magma Theory" and the origin of ignimbrites: Paper read at the IAV International Symposium on Volcanology, sci. session, p.407-423.

Beavon, R.V., Fitch, F.J., and Rast, N., 1961, Nomenclature and diagnostic characters of ignimbrites with reference to Snowdonia: Lpool. Manchr. geol. J., v. 2, p. 600-611.

Belt, C.B.Jr., 1964, Atomic Absorption Spectrophotometry and the analysis of silicate rocks for Cu and Zn: Econ. Geol., v. 59, p. 240-258.

Bennett, E.M., 1965, Lead-zinc-silver and copper deposits of Mt. Isa: in Geology of Australian ore deposits, 2nd ed., Melbourne, Australasian Inst. Min. Met., p.233-246.

Bernas, B., 1968, A new method for decomposition and comprehensive analysis of silicates by AA Spectrometry: Anal. Chem., v. 40, p. 1682-1686.

Billings, G.K., and Adams, J.A.S., 1964, The analysis of geological materials by AA Spectrometry: AA Newsletter, no. 23, p. 1-7.

Boswell, P.G.H., 1961, The case against a Lower Palaeozoic geosyncline in Wales: Lpool. Manchr. geol. J., v. 2, p. 612-624.

Bowen, N.L., 1928, The evolution of the igneous rocks: Princeton, N.J., Princeton Univ. Press, 332p.

Brenchley, P.J., 1969, The relationship between Caradocian volcanicity and sedimentation in North Wales: in The Precambrian and Lower Palaeozoic rocks of Wales, A. Wood, ed. (University of Wales Press, Cardiff), p.181-202.

Bromley, A.V., 1965, Intrusive quartz latites in the Blaenau Ffestiniog area, Merioneth.: Geol. J., v. 4, p.247-256.

Burbank, W.S., 1950, Problems of wall-rock alteration in shallow volcanic environments: Colo. School Mines Quart., v. 45, p. 287-319.

Charlesworth, J.K., 1963, Historical geology of Ireland: Oliver and Boyd Ltd.(Edinburgh, London), p.73-107.

Coats, R.R., 1962, Magma type and crustal structure in the Aleutian arc, in crust of the Pacific basin: Geophys. Monograph 6, p. 92-109.

Davidson, C.F., 1963, Discussion: Inst. Min. Met. Trans., v. 72, p. 381-383.

_____., 1964, Uniformitarianism and ore genesis: Min. Mag. (London), v. 110, p.176-185, 244-253.

Degens, E.T., and Ross, D.A., eds., 1969, Hot brines and recent heavy metal deposits in the Red Sea. A geochemical and geophysical account: Springer-Verlag, Berlin, Heidelberg and New York, 600 p.

Derry, D.R., 1961, Parys-Mona Mines, Anglesey, Wales: Unpublished report.

Dickinson, W.R., 1970, Relations of andesites, granites, and derivative sandstones to arc-trench tectonics: Rev. Geophys. Space Phys., v. 8, p.813-860.

_____., 1971, Plate tectonic models of geosynclines: Earth and Planetary Sci.Letters, v. 10, p. 165-174.

Eichelberger, J.C., 1974, Magma contamination within the volcanic pile: Origin of dacite and andesite: Geology, v. 2, p. 29-33.

Evans, T.F., 1878, The mines of the Parys Mountain, Anglesey: Trans. Manchr. geol. Soc., v. 14, p.357-372.

Ferguson, J., and Lambert, I.B., 1972, Volcanic exhalations and metal enrichments at Matupi Harbour, New Britain,T.P.N.G.: Econ. Geol., v. 67, p. 25-37.

_____., Lambert, I.B., and Jones, H.E., 1974, Iron sulphide formation in an exhalative-sedimentary environment, Talasea, New Britain, P.N.G.: Mineral. Deposita, v. 9, p. 33-47.

Fitch, F.J., 1967, Ignimbrite volcanism in North Wales: Bull. Volcan., v. 30, p. 455-475.

_____., and Miller, J.A., 1964, Age of the paroxysmal Variscan orogeny in England: Quart. J. geol. Soc. Lond., v. 1205, p. 159-173.

_____., Miller, J.A., Evans, A.L., Grasty, R.L., and Meneisy, M.Y., 1969, Isotopic age determinations on rocks from Wales and the Welsh Borders: in A. Wood, ed., The Precambrian and Lower Palaeozoic Rocks of Wales (University of Wales Press, Cardiff), p. 23-46.

Fitton, J.G., and Hughes, D.J., 1970, Volcanism and plate tectonics in the British Ordovician: Earth and Planetary Sci. Letters, v. 8, p. 223-228.

Green, J.F.N., 1919, The vulcanicity of the Lake District: Proc. geol. Assoc. Lond., v. 30, p. 153-189.

Green, T.H., and Ringwood, A.E., 1966, Origin of the calc-alkaline igneous rock suite: Earth and Planetary Sci. Letters, v. 1, p. 307-316.

Greenly, E., 1919, The geology of Anglesey: Mem. Geol. Surv. Gt. Br., 2 vols, 980 p.

Hatch, F.H., Wells, A.K., and Wells, M.K., 1972, Petrology of igneous rocks, 13th edition: Thomas Murby & Co., London, 551 p.

Hawkes, H.E., and Webb, J.S., 1962, Geochemistry in mineral exploration: Harper and Row, New York and Evanston, 415 p.

Hawkins, T.R.W., 1966, Boreholes at Parys Mountain, near Amlwch, Anglesey: Bull. Geol. Surv. Gt. Br., no. 24, p. 7-18.

Holmes, S.W., 1971, Massive sulphide environment - volcanic-sedimentary basins (Abstract): Econ. Geol., v. 66, p. 207.

Horikoshi, Ei, 1969, Volcanic activity related to the formation of the kuroko-type deposits in the Kosaka district, Japan: Mineral. Deposita, v. 4, p. 321-345.

Hutchinson, R.W., 1965, Genesis of Canadian massive sulphides reconsidered by comparison to Cyprus deposits: C.I.M. Bull., v. 58, p. 972-986.

_____., 1973, Volcanogenic sulphide deposits and their metallogenic significance: Econ. Geol., v. 68, p. 1223-1246.

Irvine, T.N., and Baragar, W.R.A., 1970-1, A guide to the chemical classification of the common volcanic rocks: Canadian J. Earth Sci., v. 8, p. 523-548.

Ivanov, M.V., 1971, Bacterial processes in the oxidation and leaching of sulphide-sulphur ores of volcanic origin: Chem. Geol., v. 7, p. 185-211.

Jakes, P., and White, A.J.R., 1972, Major and trace element abundances in volcanic rocks of orogenic areas: Geol. Soc. America Bull., v. 83, p. 29-40.

Jenks, W.F., 1971, Tectonic transport of massive sulphide deposits in submarine volcanic and sedimentary host rocks: Econ. Geol., v. 66, p. 1215-1224.

Jones, O.T., 1938, On the evolution of a geosyncline: Quart. J. geol. Soc., Lond., v. 94, lx-cx.

Kajiwara, Y., 1970, Syngenetic features of the kuroko ore from the Shakanai Mine: in Volcanism and Ore Genesis, T. Tatsumi, ed., Univ. of Tokyo Press, p. 197-206.

Kinkel, A.R. Jr., 1966, Massive pyritic deposits related to volcanism and possible methods of emplacement: Econ. Geol., v. 61, p. 673-694.

Krauskopf, K.B., 1967, Introduction to geochemistry: McGraw-Hill , 721 p.

Kraynov, S.R., Volkov, G.A., and Korol'kova, M.Kh., 1966, Distribution and the mode of migration of trace elements Zn, Cu, Hg, Li, Rb, Cs, As, and Ge: Geochem. Internat., v. 3, p. 108-123.

Kuno, H., 1966, Lateral variation of basalt magma type across continental margins and island arcs: Bull. Volcan., v. 29, p.195-222.

_____., 1968, Origin of andesite and its bearing on the island arc structure: Bull. Volcanol., v. 32, p. 141-176.

Loftus-Hills, G., and Solomon, M., 1967, Cobalt, nickel and selenium in sulphides as indicators of ore genesis: Mineral. Deposita, v. 2, p.228-242.

Lovering, T.S., 1950, The geochemistry of argillic and related types of rock alteration: Colorado School Mines Quart., v. 45, p. 231-260.

Manning, W., 1959, The Parys and Mona mines in Anglesey: in The future of non-ferrous mining in Great Britain and Ireland (London, Inst. Min. Met.), p. 313-328.

Meyer, C., and Hemley, J.J., 1967, Wall rock alteration: in Geochemistry of Hydrothermal Ore Deposits, H.L. Barnes, ed., Holt, Rinehart and Winston Inc., p. 166-232.

Miller, A.R., Densmore, C.D., Degens, E.T., Hathaway, J.C., Manheim, F.T., McFarlin, P.F., Rochlington, R., and Jokela, A., 1966, Hot brines and recent iron deposits in deeps of the Red Sea: Geochim. Cosmochim. Acta, v. 30, p. 341-359.

Miller, J.A., and Fitch, F.J., 1964, Potassium-argon methods with special reference to basic igneous rocks: Quart. J. geol. Soc. Lond., v. 1205, p. 55-69.

Mitchell, G.H., 1957, Ordovician volcanoes: Advance Sci., v. 14, p. 34-47.

_____., 1963, The Borrowdale volcanic rocks of the Seathwaite Fells, Lancashire: Lpool. Manchr. geol. J., v. 3, p. 289-300.

Mitchell, A.H., and Reading, H.G., 1969, Continental margins, geosynclines, and ocean floor spreading: J. Geol., v. 77, p. 629-646.

Miyashiro, A., 1972, Metamorphism and related magmatism in plate tectonics: Am. Jour. Sci., v. 272, p. 629-656.

_____., 1974, Volcanic rock series in island arcs and active continental margins: Am. Jour. Sci., v. 274, P. 321-355.

Moorbaths, S., 1962, Lead isotope abundance studies on mineral occurrences in the British Isles and their geological significance: Phil. Trans. Roy. Soc.(A), v. 254, p. 295-360.

Moorhouse, W.W., 1959, The study of rocks in thin section: Harper and Row, New York, 514 p.

_____., 1970, A comparative atlas of textures of Archean and younger volcanic rocks: J.J. Fawcett, ed., The Geol. Assoc. Canada, special paper no. 8, 22 p.

Morozumi, M., 1961, Exo- and endomagmatic hydrothermal differentiation observed along the chemical components exhaled by Horibetsu volcanic activity: Japan Geol. Surv. Bull., v. 12, p. 627-645.

McBirney, A.R., and Weill, D.F., 1965, Rhyolite magmas of central America: Paper read the IAV International Symposium on volcanology (New Zealand), scientific session of Nov.27, p. 435-446.

McElhinny, M.W., 1973, Palaeomagnetism and plate tectonics: Cambridge Univ. Press, 358 p.

McPherson, G., 1956, Unpublished report on mineralization of Parys Mountain.

Naboko, S.I., 1959, Volcanic exhalations and products of their reactions as exemplified by the Kamchatka-Kuriles volcanoes: Bull. Volcanol., ser II, v. 20, p. 121-136.

Nairis, B., 1971, Endogene dispersion aureoles around the Rudtjebacken sulphide ore in the Adak area, Sweden: Con. Inst. Min. Met., special volume no. 11, Primary Halos and Lithogeochemical methods, p. 357-374.

Natale, P., 1969, Recrystallization and remobilization in some stratiform pyrite deposits of the Western Alps: in Remobilization of ores and minerals, P. Zuffardi, ed., p. 129-143.

Oliver, R.L., 1954, Welded tuffs in the Borrowdale Volcanic Series, English Lake District, with a note on similar rocks in Wales: Geol. Mag. Lond., v. 91, p. 473-483.

Osborn, E.F., 1959, Role of oxygen pressure in the crystallization and differentiation of basalt magma: Am. Jour. Sci., v. 257, p. 609-647.

_____., 1962, Reaction series for subalkaline igneous rocks based on different oxygen pressure conditions: Am. Mineral., v. 47, p. 211-226.

Oxburgh, E.R., and Turcotte, D.L., 1970, Thermal structure of island arcs: Geol. Soc. America Bull., v. 81, p. 1665-1688.

Ramdohr, P., 1969, The ore minerals and their intergrowths: Pergamon Press, 1174 p.

Ramsay, A.C., 1881, The geology of North Wales: Mem. Geol. Surv. Grt. Br., v. 13.

Rankama, K., and Sahama, Th. G., 1950, Geochemistry: The Univ. Chicago Press, 912 p.

Rast, N., 1969, The relationship between Ordovician structure and volcanicity in Wales: in The Precambrian and Lower Palaeozoic rocks in Wales, A. Wood, ed. (Univ. Wales Press, Cardiff), p.305-336.

_____., Beavon, R.V., and Fitch, F.J., 1958, Subaerial volcanicity in Snowdonia: Nature, Lond., v. 81, p. 508.

Ringwood, A.E., 1974, Petrological evolution of island arc systems: Quart. J. geol. Soc., v. 130, p. 183-204.

Sangster, D.F., 1971, Geological significance of stratabound sulphide deposits: Geol. Assoc. Canada, Proc., v. 23, p. 69-72.

Schermerhorn, L.J.G., 1970, The deposition of volcanics and pyrite in the Iberian Pyrite Belt: Mineral. Deposita, v. 5, p. 273-279.

Schindler, M.R., 1966, Unpublished report on mineralization at Parys Mountain.

Shackleton, R.M., 1969, The Precambrian of North Wales: in The Precambrian and Lower Palaeozoic rocks of Wales, A. Wood, ed., (Univ. Wales Press, Cardiff), p. 1-22.

Sillitoe, R.H., 1973, Environments of formation of volcanogenic massive sulphide deposits: Econ. Geol., v. 68, p. 1321-1336.

Skevington, D., 1969, The classification of the Ordovician system in Wales: in The Precambrian and Lower Palaeozoic rocks of Wales, A. Wood, ed. (Univ. Wales Press, Cardiff), p. 161-180.

Smirnov, V.I., 1971, Temperature conditions of the origin of stratabound pyritic volcanogenic ore deposits: Soc. Mining Geol. Japan, Special Issue 3, p.221-225. (Proc. IMA-IAGOD meetings '70, IAGOD Vol).

Smith, R.L., 1960, Ash flow: Bull. Geol. Soc. America, v. 71, p. 795-842.

Solomon, M., and Elms, R.G., 1965, Copper ore deposits of Mt. Lyell: in Geology of Australian ore deposits, 2nd ed., Melbourne, Australasian Inst. Min. Met.,p. 478-484.

Soper, N.J., 1970, Three critical localities on the junction of the Borrowdale Volcanic rocks with the Skiddaw slates in the Lake District: Proc. York. geol. Soc., v. 37, p. 461-493.

Sorensen, A.H., 1963, A re-examination of some suggested mechanisms for remobilization of sulphide ore bodies: Econ. Geol., v. 58, p. 1071-1088.

Stanton, R.L., 1959, Mineralogical features and possible mode of emplacement of the Brunswick mining and smelting ore bodies, Gloucester County, New Brunswick: Trans. Can. Inst. Min. Met., v. 62, p. 339-351.

Stanton, R.L., 1972, Ore petrology: McGraw-Hill Inc., 713 p.

Steiner, A., 1963, Crystallization behaviour and origin of the acidic ignimbrites and rhyolite magma in the North Island of New Zealand: Bull. Volcano., v. 25, p. 217-241.

Strauss, G.K., and Madel, J., 1975, Geology of massive sulphide deposits in the Spanish-Portuguese pyrite belt: Geologische Rundschau, v. 63, p. 191-211.

Suffel, G.G., 1965, Remarks on some sulphide deposits in volcanic extrusives: C.I.M. Bull., v. 58, p. 1057-1063.

Sumi, K., 1958, Explanatory text of the geologic map of Japan, Mikomotojima quadrangle: Japan Geol. Surv., Tokyo, 6 p. English summary.

Taylor, S.R., and White, A.J.R., 1965, Geochemistry of andesites and the growth of continents: Nature, v. 208, p. 271.

_____., 1966, Trace elements abundance in andesites: Bull. Volcano., v. 29, p. 177-194.

Thomas, J.E., Dodson, M.H., Rex, D.C., and Ferrara, G., 1966, Caledonian magmatism in North Wales: Nature, v. 209, p. 866-868.

Thornton, C.F., and Tuttle, O.F., 1960, Chemistry of igneous rocks I. Differentiation index: Am. Jour. Sci., v. 258, p. 664-684.

Turner, F.J., and Verhoogen, J., 1960, Igneous and metamorphic petrology: 2nd ed., New York, Toronto and London, McGraw-Hill, 649 p.

Vlodavetz, V.I., 1966, The problem of tuff lavas and ignimbrites: in Tufflavas and Ignimbrites, New York, American Elsevier, p. 1-15.

Vokes, F.M., 1971, Some aspects of the regional metamorphic mobilization of pre-existing sulphide deposits: Mineral. Deposita (Berl.), v. 6, p. 122-129.

Wager, L.R., and Deer, W.A., 1939, The petrology of the Skaergaard intrusion, Kangerdlugssuaq, East Greenland, Meddel om Gronland, v. 105, 352 p.

Watanabe, T., 1970, Volcanism and ore genesis: in Volcanism and Ore Genesis, T. Tatsumi, ed., Univ. Tokyo Press, p. 423-432.

Waters, A.C., 1955, Volcanic rocks and tectonic cycle: Bull. Geol. Soc. Am. Special Paper 62, p. 703.

Wheatley, C.J.V., 1971a, Economic geology of the Avoca mineralized belt, south-east Ireland, and Parys Mountain, Anglesey: Ph.D. Thesis, University of London.

_____., 1971b, Aspects of metallogenesis within the Southern Caledonides of Great Britain and Ireland: Trans. Inst. Min. Met., v. 80, p. B211-B223.

Williams, A., 1969, Ordovician faunal provinces with reference to brachiopod distribution: in The Precambrian and Lower Palaeozoic rocks of Wales, A. Wood, ed.(Univ. Wales Press, Cardiff), p. 117-154.

Wilson, H.D.B., Andrews, P., Maxham, R.L., and Ramlal, K., 1965, Archaean volcanism in the Canadian Shield: Canadian J. Earth Sci., v.2, p. 161-175.

Wolfenden, E.B., 1967, Evaluation of pyrite deposits on Parys Mountain, Amlwch, Anglesey: report (unpublished).

Wood, D.S., 1969, The base and correlation of the Cambrian rocks of North Wales: in The Precambrian and Lower Palaeozoic rocks of Wales, A. Wood, ed. (Univ. Wales Press, Cardiff), p. 47-66.

Yoder, H.S.Jr., 1969, Calcalkalic andesites : experimental data bearing on the origin of their assumed characteristics: Proc. of the Andesite Conference, A.R. McBirney, ed., Oregon Dept. Geol. Mineral Ind. Bull. 65, p. 77 -89.

APPENDIX A

SPECIMEN COLLECTION

The use of a simple sampling plan for surface sampling was not possible because of the very irregular outcrop pattern (Fig.27), and problems of contamination from previous mining operations. However representative specimens were collected over most of the general area (Fig.28). The average size of the specimens collected was 8 x 8 x 6cm (average weight approximately 600g). Samples, of approximately 400g weight, were collected at intervals of 1.5 and 3m from a number of drill cores (Fig.29). Four different core sizes of 7, 6, 4.5, and 3.5cm diameter, were used by the various companies exploring Parys Mountain, consequently the core samples collected vary from 6 to 15cm in length. The specimens were almost exclusively taken from the volcanic sequence although some Mona Complex, doleritic rock and slate specimens were collected. Core materials containing sulphide mineralization were selectively sampled, for reflected light studies. These materials were taken from both within and outside the zones described as being mineralized in the core logs.

A total of 491 rock specimens were collected for study. General information concerning types of specimens, the number collected, and the number of specimens studied by various methods, is given in Table 8. Some 29 specimens were collected from outcrops of acidic igneous rocks in areas to the east and west of Parys Mountain. The location for each specimen is indicated by its sample number which corresponds to its grid reference (Sheet Nos. 92, 93, 94, 105, 106).

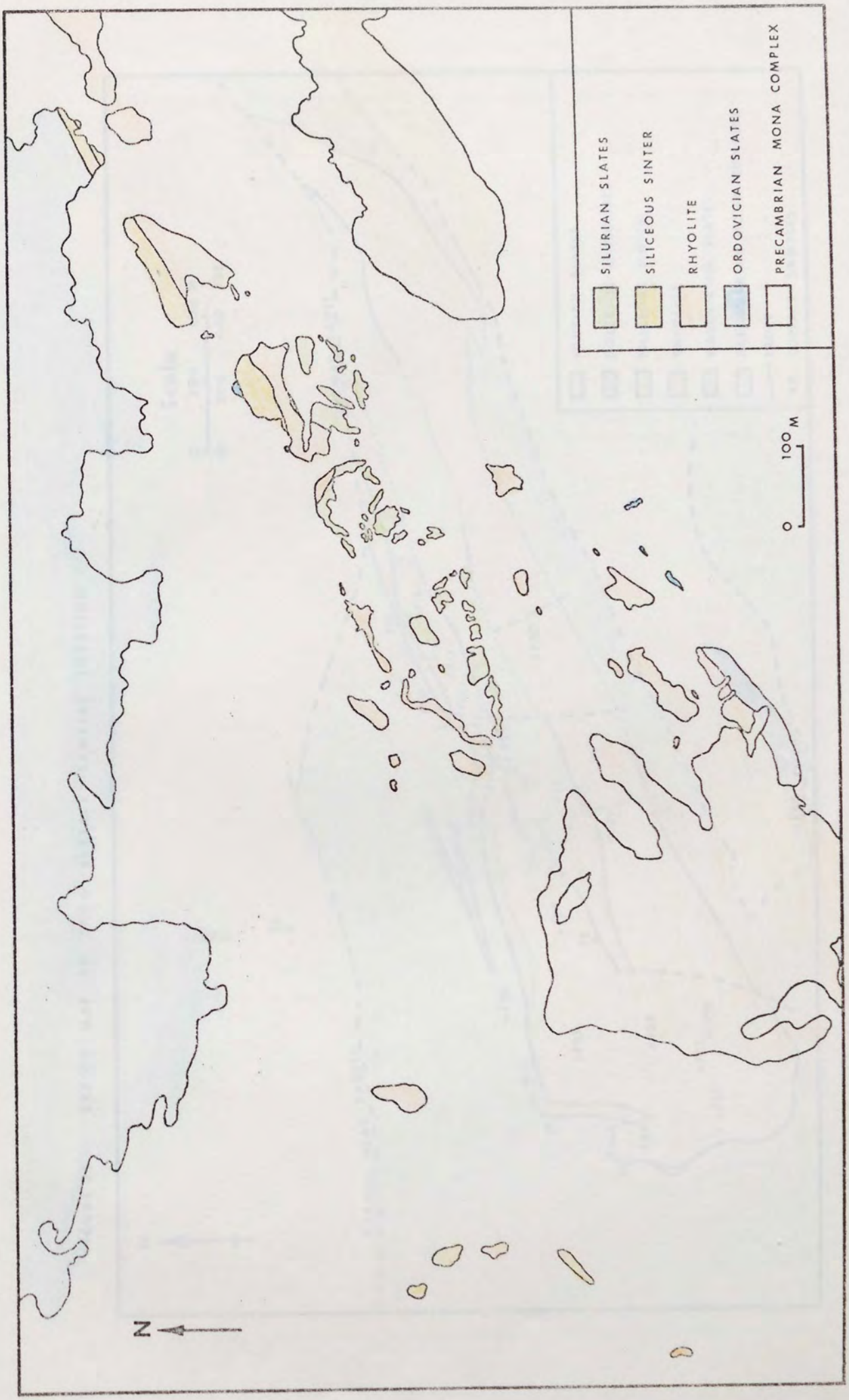

FIGURE 27 SKETCH MAP TO SHOW THE EXPOSURE AREAS OF ROCKS AT PARYS MOUNTAIN

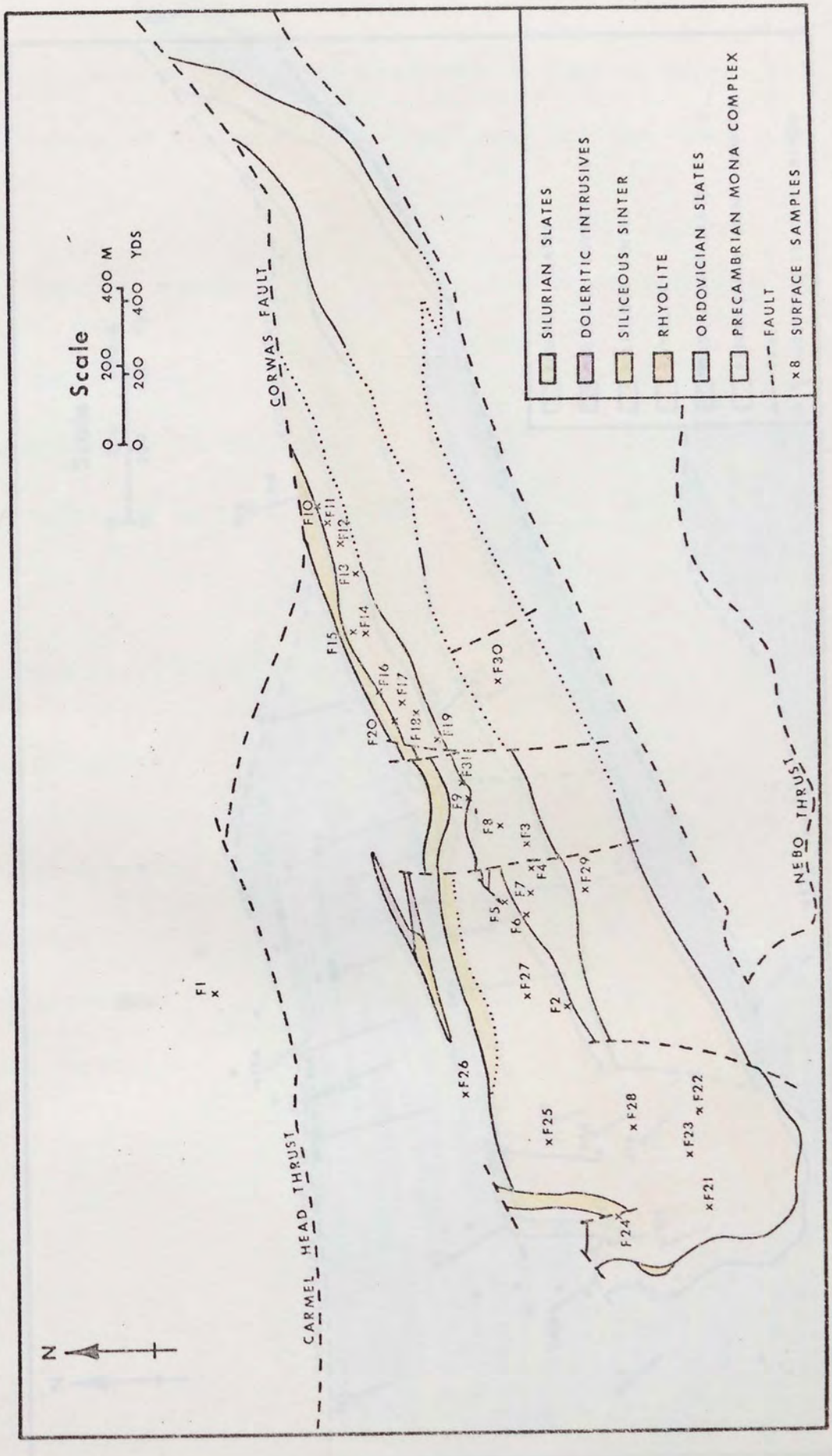

FIGURE 28 SKETCH MAP TO SHOW SURFACE - SAMPLES' LOCATION

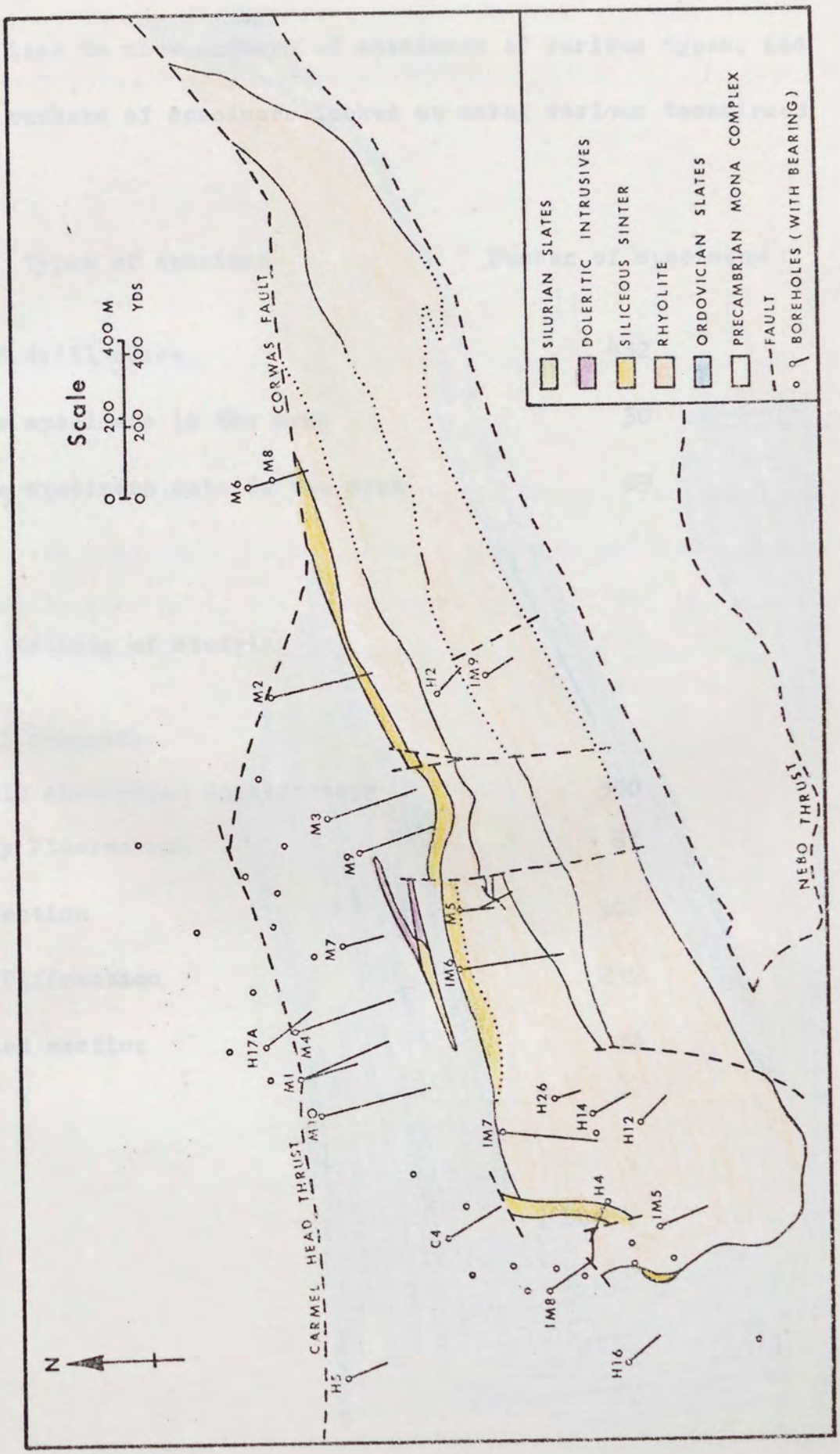

FIGURE 29 SKETCH MAP TO SHOW POSITION (WITH BEARING) OF DIAMOND DRILL HOLES

Table 8 : List to show numbers of specimens of various types, and numbers of specimens looked at using various techniques

Types of specimen	Number of specimens
Diamond drill cores	432
Surface specimens in the area	30
Surface specimens outside the area	29
Methods of studying	
Chemical analysis	
Atomic Absorption Spectroscopy	350
X-ray Fluorescent	61
Thin section	308
X-ray Diffraction	215
Polished section	73

Details of the types of study made on each specimen, together with results of geochemical analyses (A.A.S.), are given in Table 9.

APPENDIX B

Sketch Geologic Sections for the Various Diamond Drill Holes and Correlations between them.

Sections are for the 20 diamond drill holes, from which most specimens were collected. Variation of rock types and their apparent thicknesses in each hole, are illustrated by Figs. 30A, B, and C. A tentative correlation between various borehole is illustrated in Fig. 31.

EXPLANATION OF TABLE 9

ROCK NUMBER from 293919 to 483913 :- surface specimens collected from outside the Parys Mountain area. The number are their grid references.

from R1 to R3 :- are from Rhosmynach area.

from F1 to F31 :- are surface specimens from the Parys Mountain area. Location are shown in Figure

from C4-700 to IM9-431'6" :- are specimens from diamond drill holes in the Parys Mountain area. The first figure represent the number of the borehole e.g. C4 , and the last figures represent the depth in feet. The locations and bearing of each diamond drill hole are shown in Figure 29

TABLE 9

ROCK NUMBER	Powder number	Thin section	Polished section	XRD	XRF	ATOMIC ABSORPTION (ppm) - oxide in %												
						Al_2O_3	Ba	Cd	Co	Cr	Cu	Fe_2O_3	Hg	Ni	Pb	SiO_2	Sr	Zn
293919	T133	X		X	X	14.047	511.0	0.585	36.040		75.075	4.015	0.067	13.418	26.403	75.866	31.118	79.658
293923	T134	X		X		3.572	158.0	0.367	12.907		0.589	0.592	0.063	3.391	35.013	87.903	3.776	7.069
303922		X																
384895/1		X																
384895/2		X																
385895	T81	X		X		10.319	81.900	2.324	34.708		2.374	3.628	0.029	13.453	49.567	70.762	619.0	29.737
385895/1		X																
385895/S		X																
385896	T159	X		X		14.628	492.0	3.707	54.593	1.941	113.0	5.283	0.052	32.002	30.017	70.377	219.0	117.0
419913		X																
422913		X																
448922/1		X																
448922/2A		X																
448922/2B		X																

TABLE 9 CONT.

ROCK NUMBER	Powder number	Thin section	Polished section	XRD	XRF	ATOMIC ABSORPTION (ppm) - oxide in%												
						Al_2O_3	Ba	Cd	Co	Cr	Cu	Fe_2O_3	Hg	Ni	Pb	SiO_2	Sr	Zn
463922		X																
469920		X																
469920/1		X																
479917/1		X																
479917/2		X																
479917/3		X																
480917		X																
481902/G1		X																
481902/G2		X																
481902/G3		X																
482912		X																
483913	T305	X		X	X	13.687	549.969		36.428		3.183	0.774	0.004	3.001	37.215	82.088	6.838	0.490
R1		X																
R2		X																
R3		X																
F1		X																
F2	T66			X		5.443	78.326	1.616	3.327		18.323	0.269	0.176	0.305	491.0	85.060	28.258	58.977
F3		X																
F5		X																
F6		X																
F7	T96	X		X		2.288	122.0	0.499	32.875		62.381	1.158	0.167	2.297	291.0	86.023	24.222	71.113
F9	T83	X		X		3.779	71.117		72.114		4.637	1.411	0.084	2.566	50.038	85.638	23.112	1.096
F10	T156	X		X		18.672	750.0	2.058	76.652	19.966	295.0	5.309	0.058	38.826	41.652	70.634	32.328	122.0
F11	T304	X		X	X	10.710	109.664		31.685		47.988	5.282	0.026	3.963	55.354	77.868	5.607	35.046
F12	T68			X		7.352	162.0	1.207	31.509		7.011	0.404	0.053	3.384	106.0	79.730	17.513	10.852
F13	T88	X		X		7.371	233.0	1.011	59.569		26.071	2.736	0.072	6.607	183.0	79.131	26.170	25.758
F14	T144	X		X		6.085	18.353		9.471		145.0	5.812	0.046	3.229	54.721	85.552	1.075	62.494
F15	T95	X		X		2.230	322.0		37.298		84.090	3.771	0.064		251.0	83.968	22.516	58.674

TABLE 9 CONT.

ROCK NUMBER	Powder number	Thin section	Polished section	XRD	XRF	ATOMIC ABSORPTION (ppm) -oxide in %											
						Al_2O_3	Ba	Cd	Co	Cr	Cu	Fe_2O_3	Hg	Ni	Pb	SiO_2	Sr	Zn
F15		X																
F17		X																
F18	T85	X		X		5.670	221.0		36.943		7.743	1.110	0.058	4.334	91.075	84.461	26.001	7.019
F19		X																
F20		X																
F21		X																
F22	T97	X		X		7.503	332.0		44.818		19.368	1.197	0.060	6.129	105.0	82.235	35.251	22.989
F23	T98	X		X		5.972	342.0	1.010	32.532		3.135	1.998	0.051	3.307	25.621	80.993	18.332	403.0
F24		X																
F24/1		X																
F25	T157	X		X		11.661	1003.0	1.893	89.578		24.382	0.521	0.430	6.673	371.0	81.550	53.443	58.856
F26		X																
F27	T84	X		X		3.912	149.0		52.271		3.359	1.651	0.594	3.297	148.0	85.552	18.118	6.641
F28	T93	X		X		5.046	162.0		38.414		10.346	0.803	0.477	0.206	1684.0	87.543	22.625	16.912
F29	T158	X		X		4.101	149.0	1.242	71.239		27.694	0.629	0.095	0.265	369.0	86.237	13.816	23.437
F30																		
F31		X																
C4-700	T324					21.764	354.0	1.194	86.011	41.263	121.0	6.893	0.040	67.192	46.429	46.031	166.0	93.660
C4-705	T113			X		6.482	29.698	43.806	32.400	2.388	11393.0	9.428	0.253	7.522	7694.0	57.149	82.057	18411.0
C4-710	T325					22.472	397.0		97.013	28.028	123.0	10.676	0.149	76.764	71.859	41.671	135.0	99.588
C4-715	T326					22.334	638.0	1.913	97.041	44.790	238.0	9.354	0.026	87.316	32.802	42.285	129.0	89.884
C4-720	T327					22.621	649.0	0.826	114.0	44.233	16.712	7.760	0.109	85.051	31.355	48.392	124.0	40.415
C4-725	T328					23.097	622.0	0.843	104.0	51.451	18.465	8.211	0.031	79.440	38.320	45.155	88.256	63.458
C4-730		X																
C4-735	T329		X			15.887	12.613	6.856	95.197	148.0	631.0	18.162	0.110	57.665	2015.0	24.872	59.435	3690.0
C4-745	T330		X			11.668	37.902	5.537	45.065		38.085	9.832	0.305	64.216	1361.0	21.953	137.0	2723.0
C4-750	T209					21.678	582.0	0.218	84.358	131.0	54.916	10.317	0.157	78.815	77.902	59.084	145.0	200.0
C4-755	T331		X			13.018	104.0	0.336	60.740		0.739	10.273	0.178	58.249	186.0	42.611	101.0	232.0

TABLE 9 CONT.

ROCK NUMBER	Powder number	Thin section	Polished section	XRD	XRF	ATOMIC ABSORPTION (ppm)-oxide in%											
						Al_2O_3	Ba	Cd	Co	Cr	Cu	Fe_2O_3	Hg	Ni	Pb	SiO_2	Sr	Zn
C4-773	T109			X		0.471	41.750	298.0	212.0	92.292	19939.0	3.662	0.242	42.233	21218.0	47838	169.0	73540.0
C4-785	T114					15.251	140.0	4.013	111.0	314.0	438.0	13.085	0.291	100.0	516.0	40.753	99.277	1115.0
C4-803	T101			X		4.139	30.573	2.867	77.140	74.451	86.797	4.333	0.199	56.627	126.0	75.523	101.0	963.0
C4-813	T332		X			2.175	50.670	49.195	78.615		986.0	13.533	0.396	6.039	12853.0	59.105	64.296	15159.0
C4-830	T111			X		2.306	56.938	31.793	18.022		5932.0	6.629	0.219	2.657	8633.0	75.096	75.750	20193.0
C4-845	T117					8.278	208.0	10.875	21.530	6.299	1393.0	8.239	0.003	15.307	2253.0	57.080	99.793	7470.0
C4-861	T112					1.758	71.207	67.009	34.520		2616.0	7.185	0.283	2.356	13424.0	77.504	89.977	34000.0
C4-871	T107			X		1.137	40.631	61.732	173.0	51.704	1155.0	3.851	0.071	33.205	20359.0	70.805	105.0	27934.0
C4-881	T115					4.460	213.0	3.989	38.645	3.918	966.0	8.305	0.344	56.397	665.0	76.413	85.805	1171.0
C4-891	T116					7.711	305.0	2.762	20.815	6.235	31.667	4.923	0.106	7.419	369.0	80.565	72.287	201.0
C4-906	T110			X		0.297	41.226	52.840	45.735		2975.0	3.685	0.070	4.432	9744.0	85.702	78.223	28772.0
C4-920			X															
C4-930	T333		X			0.922	65.089	197.0	141.0		5429.0	5.669	0.119	0.316	26733.0	66.445	40.547	82181.0
C4-940	T108					1.947	106.0	3.823	115.0	3.116	616.0	1.839	0.288	22.778	1053.0	78.938	54.877	2619.0
C4-950	T127			X		0.544	42.223	6.397	27.948		1437.0	3.156	0.473	0.702	1972.0	94.563	48.235	3050.0
C4-960	T334		X			0.185	32.657	4.435	132.0		6783.0	3.545	1.417	0.328	2511.0	82.266	59.694	2922.0
C4-970	T104			X		0.136	26.278	12.993	127.0		2228.0	3.000	1.477	26.106	4185.0	83.455	45.731	7332.0
C4-981	T103					0.968	83.688	5.832	157.0	74.100	2499.0	4.029	0.213	54.052	991.0	80.651	108.0	2679.0
C4-991	T335		X			2.000	155.0	13.575	77.374		825.0	4.726	1.312	2.466	3181.0	77.188	57.626	6467.0
C4-1001	T130			X		0.067	8.462	4.707	48.113		2896.0	2.137	1.084	1.843	16501.0	95.634	59.204	2697.0
C4-1011	T126					0.111	24.419	5.547	144.0		5735.0	2.801	0.813	1.834	2214.0	94.025	37.089	2937.0
C4-1021	T129					0.062	21.751	7.889	44.822		507.0	1.048	0.940	6.024	3259.0	97.710	40.589	5634.0
C4-1031	T102					0.422	65.694	126.0	185.0		2155.0	2.284	0.030	40.695	17547.0	75.642	83.145	47163.0
C4-1040	T105			X		1.373	140.0	63.023	192.0	64.465	3945.0	3.131	0.035	61.629	18853.0	74.593	108.0	35779.0
C4-1043	T48			X		11.472	488.0	18.206	40.299	77.242	1656.0	19.533	0.522	28.359	3719.0	51.306	18.277	8676.0
C4-1048	T45					11.698	962.0	1.481	35.931		61.791	1.058	0.167	10.449	34.255	79.837	17.154	101.0
C4-1050	T60					7.541	615.0	3.291	131.0		132.0	0.859	0.246	40.952	64.784	77.098	59.660	567.0
C4-1053	T61					9.563	664.0		13.115		68.593	0.884	0.171	7.650	58.392	81.956	13.138	78.279

TABLE 9 CONT.

ROCK NUMBER	Powder number	Thin section	Polished section	XRD	XRF	ATOMIC ABSORPTION (ppm) - oxide in %												
						Al_2O_3	Ba	Cd	Co	Cr	Cu	Fe_2O_3	Hg	Ni	Pb	SiO_2	Sr	Zr
C4-1058	T74			X		10.073	1032.0	2.730	55.471		117.0	0.817	0.293	48.169	38.109	77.440	125.0	116.0
C4-1060	T305	X		X	X	12.379	877.084		75.669		4.053	0.922	1.005	4.410	59.539	80.075	100.403	131.809
C4-1063	T62					15.062	1247.0	0.387	30.576		499.0	1.184	0.944	18.790	90.923	74.893	91.721	313.0
C4-1068	T44					0.122	19.271	3.360	138.0		404.0	2.134	0.324	26.675	808.0	91.567	27.320	1311.0
C4-1070	T336	X				11.127	362.0		28.200			1.488	0.037	4.132	43.648	65.148	113.0	19.339
C4-1073	T45					6.785	297.0		5.238		61.375	1.896	0.054	0.573	53.656	59.221	116.0	77.349
C4-1078	T49			X		12.530	811.0	1.999	74.042		665.0	1.211	0.017	45.034	25.349	66.567	94.480	258.0
C4-1080		X																
M1B-392		X																
M1B-415.5	T143	X						1.104	68.665	0.813	80.972	6.370	0.050	24.282	33.156			85.771
M2-618	T202	X		X	X	9.604	195.459	0.882	30.300		5.148	5.751	0.011	3.596	29.741	77.796	4.396	55.539
M2-627	T210	X				7.711	146.0	0.520	33.570		3.973	5.649	0.018	6.099	32.463	84.774	38.747	60.383
M2-643	T 163 204	X		X		9.520	333.0	1.740	76.435	3.277	5.940	1.647	0.015	6.977	32.209	86.836	76.416	33.070
M2-752	T211	X		X		8.976	480.0		44.035		8.732	2.120	0.051	6.258	36.467	68.704	72.534	19.339
M2-763	T205	X		X		10.282	333.0	0.242	63.970		14.446	3.344	0.068	7.828	19.765	82.568	57.825	31.219
M2-773	T206	X		X		9.130	288.0	1.054	67.838		2.661	1.656	0.075	5.255	38.695	87.795	49.925	14.925
M2-977	T203	X		X		9.836	263.0	1.300	65.374		6.092	0.871	0.111	7.381	37.879	84.903	43.381	21.443
M2-1064	T201	X		X	X	9.988	137.152	0.838	28.777		28.055	6.194	1.018	5.826	78.935	70.025	55.009	403.549
M2-1212	T164,207	X		X		15.413	350.0	0.363	37.761		1.315	1.083	0.014	6.403	30.294	78.534	57.697	16.060
M2-1452	T146	X				13.995	1255.0	2.328	49.885		14.846	1.421	0.095	3.564	20.921	83.549	30.623	10.775
M2-1461	T208	X		X	X	7.078	1100.536		46.699		16.919	2.658	3.475	3.666	71.504	73.217	432.240	34.975
M3-763	T307	X		X	X	8.950	68.585		16.036		3.476	12.296	0.010	3.284	40.725	71.958	2.822	68.800
M3-862	T215	X		X		13.216	374.0	0.869	96.086		7.426	1.547	0.031	10.156	35.184	76.443	69.083	6.270
M3-957	T145	X		X	X	16.793	268.491	0.931	43.296		17.472	3.986	0.045	7.718	33.203	71.488	16.262	29.088
M3-1002	T310	X				5.564	165.0		76.024		914.0	1.962	0.141	1.043	50.840	85.857	50.663	0.342
M3-1063	T135	X		X		14.166	315.0	0.362	23.262		35.979	1.101	0.077	9.666	147.0	75.791	48.453	50.020
M3-1148	T148	X		X	X	9.842	128.420	0.153	33.173		74.080	2.425	0.050	3.673	18.493	82.885	6885	44.588
M4-937	T221	X						1.305	70.394	584.0	8.362	18.219	0.019	216.0	52.707			267.0

TABLE 9 CONT.

ROCK NUMBER	Powder number	Thin section	Polished section	XRD	XRF	ATOMIC ABSORPTION (ppm) - oxide in %												
						Al_2O_3	Ba	Cd	Co	Cr	Cu	Fe_2O_3	Hg	Ni	Pb	SiO_2	Sr	Zn
M4-947		X																
M4-1052	T150	X						3.347	45.389		8.462	6.228	0.057	7.912	41.348			72.415
M4-1072	T222	X							40.402		0.859	2.562	0.057	8.866	34.021			26.668
M4-1097		X																
M4-1129	T153	X						0.398	33.888		24.725	3.217	0.042	1.304	21.628			134.0
M5-27	T152	X		X	X	11.209	231.159	1.693	54.920		95.924	3.128	0.062	1.574	40.772	79.986	6.461	30.569
M5-189	T308	X		X	X	15.277	216.546		78.121		10.352	3.272	0.023	6.090	69.899	75.234	4.274	68.677
M6-426	T154	X						0.542	92.217		1331.0	21.446	0.066	18.407	82.526			201.0
M7-491	T224	X							83.008	560.0	322.0	11.276	0.025	346.0	53.782			113.0
M7-504	T219	X		X				0.975	80.340	785.0	6.245	18.248	0.002	371.0	66.602			249.0
M7-674	T220	X		X	X	9.916	538.099	0.087	32.791		3.541	9.657	0.038	4.857	29.565	70.014	4.132	91.088
M7-713	T229	X						0.228	42.793		16.473	5.481	0.043	3.648	18.459			71.343
M7-767	T291	X		X	X	11.930	181.926		22.645		0.139	6.716	0.003	3.104	19.803	74.772	4.011	38.599
M9-41	T147	X						1.180	56.795	51.301	358.0	14.519	0.056	161.0	57.396			372.0
M9-550.5	T311	X				13.513	484.0	1.091	76.710		277.0	4.729	0.042	8.772	61.523	68.814	51.590	29.291
M9-731		X	X															
M9-849.5	T312	X				8.391	133.0		96.149			2.870	0.002	3.921	26.604	77.697	94.818	46.483
M9-856	T212	X							62.166			1.485	0.051	16.618	66.722			16.626
M10-249	T72	X		X	X	20.093	647.967	5.641	46.543	21.096	79.354	7.495	0.045	61.305	22.323	63.381	74.207	69.942
M10-690	T73	X		X		12.303	454.0	5.619	38.937		44.633	6.107	0.031	45.911	32.149	57.898	55.289	94.579
M10-1089	T125			X		6.123	18.752	4.742	31.125	3.560	7044.0	19.301	0.153	33.516	179.0	64.876	55.824	468.00
M10-1095	T105			X		0.041	23.722	3.444	172.0		95.522	7.093	0.029	14.117	86.777	76.263	45.297	103.0
M10-1279	T313			X		10.293	675.0	0.482	86.350	24.638		8.470	0.012	61.213	15.991	55.622	85.740	49.856
M10-1284	T 314			X		19.453	682.0	0.726	87.041	26.545	7.677	7.857	0.028	70.760	24.373	55.501	85.095	39.980
M10-1289	T315			X		19.619	740.0	0.303	82.230	35.329	4.726	5.962	0.009	55.656	48.065	58.679	97.479	47.756
M10-1294	T316			X		24.224	1387.0	0.943	114.0	63.995	64.490	10.212	0.179	76.571	302.0	43.057	71.989	534.0
M10-1299	T63			X		0.279	302.0	5.365	134.0		5028.0	2.473	0.223	32.174	2299.0	89.640	41.565	301.0
M10-1304	T50					0.266	96.539	3.656	107.0		1220.0	0.743	0.030	30.535	95.676	89.148	45.268	117.0

TABLE 9 CONT.

ROCK NUMBER	Powder number	Thin section	Polished section	XRD	XRF	ATOMIC ABSORPTION (ppm) - oxide in %												
						Al_2O_3	Ba	Cd	Co	Cr	Cu	Fe_2O_3	Hg	Ni	Pb	SiO_2	Sr	Zn
M10-1308		X																
M10-1309	T51			X		0080	121.00	4.362	138.00		610.00	0.767	0.282	23.444	96.311	94.178	23.756	551.00
M10-1311	T137					0.218	22.141	4.099	229.00		185090	26.834	0.246	20.978	149.0	31.306	54.933	243.00
M10-1318	T317	X				20.790	2158.0	1.531	95.708	38.139	2265.0	9.686	0.104	73.974	106.0	50.031	42.415	465.0
M10-1332	T139			X		0.541	386.0	4.103	121.0		7959.0	3.590	0.366	23.860	418.0	81.571	52.739	705.0
M10-1357	T136			X		0.103	93.931	2.404	285.0		82080	2.197	0.112	42.361	184.0	85.253	69.928	116.0
M10-1388	T138			X		0.624	128.00	4.733	122.0		9075.0	3.010	0.081	18.764	141.0	79.502	22.594	104.0
M10-1408	T142			X		0.089	53.340	13.898	244.0		123400	2.485	0.251	31.364	1984.0	92.359	60.475	4275.0
M10-1410			X															
M10-1421	T123					0.332	139.0	8.769	120.0		5249.0	2.375	0.508	5.523	310.0	94.092	86.878	4410.0
M10-1431	T124			X		0.308	119.0	29.030	112.0		6949.0	3.526	0.064	6.626	448.0	89.812	72.358	12337.0
M10-1441	T121					0.247	58.585	17.408	92.892		7219.0	2.234	0.562	17.728	1700.0	95.847	62.550	5769.0
M10-1451	T141			X		0.100	20.610	15.975	147.0		2082.0	1.526	0.994	19.217	44820	92.402	42.428	6919.0
M10-1472	T318					0.929	231.0		89.888			1.198	0.042	0.414	53.917	88.306	91.618	33.191
M10-1483	T122					0.307	76.017	22.255	92.601		335840	3.723	0.321	35.322	1849.0	83.883	77.219	7320.0
M10-1491	T140					0.700	172.0	11.650	142.0		1218.0	5.000	0.093	15.767	389.0	81.015	36.467	2623.0
M10-1501	T128			X		0.322	40.776		143.0		3061.0	5.871	0.219	3.705	67.352	84.824	121.0	24.897
M10-1512			X															
M10-1521			X															
M10-1529	T131			X		6.237	672.0	4.632	29.661	4.770	2093.0	2.587	0.261	31.472	275.0	85.360	85.771	351.0
M10 1540		X	X															
M10 1548	T319		X(2)			0.252	98.059	86.984	183.0		31794.0	9.257	0.247	0.195	51292.0	60.693	51.183	50801.0
M10-1562	T320		X			0.226	28.969	8.476	215.0		1663.0	2.147	0.244	0.202	3264.0	86.520	50.427	3985.0
M10-1572			X															
M10-1584	T321	X	X			0.474	52.653	66.083	73.794		3048.0	1.505	1.554	0.596	10511.0	64.026	36.395	23145.0
M10-1589	T322		X(2)			0.333	41.037	363.0	126.0		9750.0	2.681	0.144	0.396	58048.0	58.639	26.629	13.674
M10 1599	T323	X	X			0.107	32.608	0.899	339.0		649.0	1.490	0.129	0.422	4412.0	88.130	50.541	1159.0
M10-1608		X	X															

TABLE 9 CONT.

ROCK NUMBER	Powder number	Thin section	Polished section	XRD	XRF	ATOMIC ABSORPTION (ppm) - oxide in %												
						Al_2O_3	Ba	Cd	Co	Cr	Cu	Fe_2O_3	Hg	Ni	Pb	SiO_2	Sr	Zn
M10-1620			X															
M10-1630			X															
H4-456			X															
H4-460			X															
H4-464			X															
H4-474			X															
H4-491			X															
H4-581			X															
H5-638'10"		X																
H7-553	T161	X						0.185	19.080		15.483	1.429	0.045	9.605	20.710			52.079
H11-169'8"	T91	X						2.090	48.922		139.0	1.361	0.051	9.274	52.554			214.0
H12-594'6"	T90	X		X				1.961	80.730		13.794	3.291	0.064	16.188	24.661			34.096
H12-674	T79	X		X				1.707	76.223		4.769	1.395	0.032	17.549	18.618			23.357
H12-741		X																
H14-171		X	X(2)															
H14-195		X	X(2)															
H14-267	T67	X		X	X	9.404	73.713				13.618	0.303	0.233	1.367	1921.130	68.029	5.051	224.093
H14-285	T76	X		X		11.679	346.0	4.821	34.758		175.0	1.375	1.660	33.615	51.009	73.074	49.553	86.446
H14-318	T75	X		X		8.467	261.0	4.479	36.179		18.742	1.931	2.201	4.284	44.707	71.254	44.616	112.0
H14-373	T57	X		X		10.867	293.0	0.905	15.667		241.0	3.677	0.449	6.378	69.106	79.006	23.648	940.0
H14-395	T59	X		X		11.697	219.0		30.218		39.809	2.170	0.392	22.328	61.578	75.514	21.579	45.629
H14-406	T55	X		X		14.854	296.0	0.964	36.882		30.707	1.328	0.175	13.445	33.947	71.468	26.198	29.336
H14-412	T71	X		X		17.557	399.0		48.013		35.172	0.818	0.045	56.435	40.012	69.799	27.691	26.173
H14-421	T58	X		X		14.004	290.0		32.393		51.248	0.957	0.065	50.515	37.675	74.443	29.177	29.621
H14-438	T160	X		X		11.037	260.0	4.672	26.081		10.282	2.097	0.090	25.233	27.923	69.178	42.033	67.515
H14-464	T74	X		X	X	23.108	258.149	6.516	32.857		80.860	6.655	0.096	2.113	11.549	57.343	11.201	290.622
H14-472	T65	X		X		9.582	168.0		2.784		70.675	3.563	0.017	23.280	49.675	52.226	164.0	106.0
H14-526	T70	X		X		8.807	242.0		6.979		46.774	2.075	0.031	11.851	30.457	74.914	41.412	64.986

TABLE 9 CONT.

ROCK NUMBER	Powder number	Thin section	Polished section	XRD	XRF	ATOMIC ABSORPTION (ppm) - oxides in %												
						Al_2O_3	Ba	Cd	Co	Cr	Cu	Fe_2O_3	Hg	Ni	Pb	SiO_2	Sr	Zn
H14-526	T70	X		X		8.807	242.0		6.979		46.774	2.075	0.031	11.851	30.457	74.914	41.412	64.986
H14-548	T69	X		X	X	16.336	246.297		21.176		160.679	1.389	0.026	21.176	71.178	74.998	8.642	135.678
H14-186			X (2)															
H14-265			X															
H15-108	T228	X							47.905		3.306	1.615	0.043	10.502	135.0			278.0
H15-275	T226	X						0.718	63.318		3.101	2.499	0.047	28.363	78.049			187.0
H15-361	T227	X						0.367	37.235		6.572	1.164	0.045	18.685	32.648			36.972
H16-36	T342	X				21.217	315.0	0.785	102.0	46.153	6.258	7.311	0.065	72.259	31.931	39.803	168.0	305.0
H16-47	T343	X				19.434	518.0	0.985	85.125	35.289	9.419	6.959	0.047	72.821	41.038	41.237	126.0	158.0
H16-329'1"	T69	X		X		22.395	1006.0	5.504	48.910		16.932	0.742	0.129	9.378	20.986	56.293	82.056	88.655
H16-340'7"	T87	X		X		11.339	645.0	5.165	77.241		3.633	1.806	0.071	13.950	37.845	70.997	92.449	151.0
H16-350'4"	T119	X		X		14.514	1084.0	4.309	30.320		40.932	1.727	0.186	5.227	171.0	67.509	102.0	42.981
H16-357	T149	X		X	X	17.998	673.924	4.162	50.171		92.375	2.764	0.044	33.387	33.383	68.756	30.507	83.004
H16-367'5"		X																
H16-385	T344	X		X		13.769	51.096		65.133		109.0	10.725	0.021	56.187	37.928	39.751	101.0	736.0
H16-395	T345	X				11.734	71.099	0.019	74.788		31.435	10.590	0.026	42.698	50.272	41.968	125.0	398.0
H16-402	T346	X				12.719	75.198	0.906	79.006		29.105	11.180	0.108	48.760	74.619	29.678	485.0	640.0
H16-412'2"	T80	X		X		12.345	800.0	1.228	44.410		72.690		0.075	24.038	27.529		82.334	437.0
H16-417'2"	T162	X				14.928	1058.0	1.206	48.121		43.651	4.169	0.051	23.041	23.998	75.505	33.945	202.0
H16-421	T155	X		X	X	17.330	886.758	4.658	96.888	88.870	108.915	63.43	0.068	76.523	31.931	61.570	19.991	260.197
H16-437	T99	X		X		16.536	1580.0	4.886	41.437		45.661	2.912	0.404	9.548	29.181	54.452	55.869	410.0
H16-438'2"	T132	X				15.081	1576.0	1.713	39.991		175.0	2.211	0.246	17.513	154.0	67.380	29.632	453.0
H17A-1191	T17			X		17.992	6900	1.824	74.342	45.031	11.552	8.724	0.010	51.968	38.777	58.412	180.0	251.0
H17A-1196	T26			X		18.464	721.0	2.194	96.046	49.392	7.014	7.049	0.031	79.409	35.819	61.473	42.574	55.608
H17A-1201	T337					22.221	666.0	1.172	82.921	53.098		7.461	0.009	74.165	46.391	47.427	97.542	44.960
H17A-1206	T21					8.504	219.0	1.420	39.223	5.212	175.0	7.987	0.096	15.523	44.242	77.333	135.0	102.0
H17A-1211																		
H17A-1216	T338					18.563	644.0	0.175	83.606	23.065	1.312	8.600	0.012	66.721	26.778	51.352	69.095	47.154

TABLE 9 CONT.

ROCK NUMBER	Powder number	Thin section	Polished section	XRD	XRF	ATOMIC ABSORPTION (ppm) - oxide in %											
						Al_2O_3	Ba	Cd	Co	Cr	Cu	Fe_2O_3	Hg	Ni	Pb	SiO_2	Sr	Zn
H17A - 1220'10	T339					9.776	361.0		144.0		5118.0	20.659	0.427	44.770	74.120	43.082	61.895	106.0
H17A - 1221'2	T23			X		16.007	754.0	1.700	75.497	46.176	97.989	6.778	0.093	50.497	57.253	63.570	82.053	156.0
H17A - 1225	T11			X		0.945	19.331	0.245	249.0	3.244	937.0	6.303	0.121	8.339	96.249	90.539	87.151	24.709
H17A - 1231	T1			X		1.474	10.405	0.718	8.190	3.018	5485.0	8.253	0.309	3.677	109.0	82.352	53.583	157.0
H17A - 1236	T35					0.217	26.238	4.177	297.0	82.958	2315.0	1.123	0.096	47.273	22.637	91.567	122.0	24.381
H17A - 1241	T31			X		0.409	10.171	1.767	76.000		2090.0	4.330	0.521	382.0	128.0	94.092	179.24	18.399
H17A - 1246	T36			X		0.501	10.894	2.600	86.925	11.500	24621.0	27.491	0.385	4.682	322.0	51.113	20.212	903.0
H17A - 1251	T2					0.567	56.354	0.662	0.757		1523.0	5.217	0.016	5.300	66.306	94.820	196.0	47.135
H17A - 1261	T34			X		0.388	2.171	0.001	493.0		2107.0	2.538	0.137	59.535	124.0	91.032	20.756	54.177
H17A - 1271	T3					1.096	66.681		8.102		10289.0	6.000	0.160	4.650	57.456	90.589	225.0	65.810
H17A - 1281	T4			X		0.359	12.053	0.749			18362.0	3.781	0.014	7.709	70.937	91.652	54.415	81.628
H17A - 1291	T14					0.265	83.002	0.002	318.0		23071.0	12.355	0.485	4.669	223.0	68.750	151.0	54.343
H17A - 1301	T27			X		0.283	8.166	2.121	337.0		3212.0	3.522	0.126	72.282	96.223	88.677	17.153	279.0
H17A - 1321	T5			X														
H17A - 1331	T6					0.132	31.379		14.777		3229.0	7.689	0.553	0.680	151.0	80.308	110.0	44.761
H17A - 1341	T41					0.132	16.265	4.243	245.0		360.0	1.594	0.486	26.599	28.670	91.888	44.790	24.034
H17A - 1351	T40			X		0.113	7.558		1135.0		98.197	5.204	0.082	18.233	53.717	88.934	20.451	33.754
H17A - 1361	T29					0.321	65.522	0.142	228.0		691.0	5.050	0.020	1.642	359.0	92.402	69.680	20.934
H17A - 1371	T16			X		0.227	8.823	5.925	434.0		7138.0	6.939	0.192	7.921	1542.0	86.965	19.826	3265.0
H17A - 1381	T30			X		0.103	22.243	0.143	230.0		65.295	1.092	0.099	11.868	48.225	91.945	45.515	13.058
H17A - 1391	T13			X		8.164	587.0	1.475	166.0	18.864	106.0	12.356	0.062	32.317	214.0	76.413	55.427	58.574
H17A - 1401	T24					3.175	274.0	2.704	101.0	2.641	146.0	3.484	0.183	2.755	3558.0	92.038	89.600	810.0
H17A - 1411	T38			X		0.334	6.447	1.302	397.0		4485.0	4.058	0.147	23.341	269.0	92.380	22.210	22.708
H17A - 1421	T28					0.170	30.813	0.148	604.0		660.0	1.951	1.365	458.0	262.0	94.063	70.200	16.778
H17A - 1431	T10			X		4.800	426.0	1.467	119.0	8.356	20863.0	7.741	0.253	17.002	181.0	77.954	29.717	87.997
H17A - 1441	T22					6.444	37.245	0.603	30.691	4.022	255.0	10.678	0.076	15.690	85.775	74.529	83.428	118.0
H17A 1451	T214			X		22.814	2468.0		121.0	146.0	16.433	5.442	0.652	67.322	100.0	67.652	53.840	77.994
H17A 1461	T39					0.310	24.546	3.251	582.0		4654.0	4.457	2.637	28.790	59.342	85.210	49.926	32.654

TABLE 9 CONT.

ROCK NUMBER	Powder number	Thin section	Polished section	XRD	XRF	ATOMIC ABSORPTION (ppm) - oxides in %												
						Al_2O_3	Ba	Cd	Co	Cr	Cu	Fe_2O_3	Hg	Ni	Pb	SiO_2	Sr	Zn
H17A-1471	T18			X		8.410	15.028	1.209	65.618	10.635	962.0	13.414	0.185	15.979	41.729	66.931	30.164	185.0
H17A-1481	T37					14.628	36.537	1.784	136.0	71.542	4937.0	39.735	0.061	49.647	36.640	25.214	94.071	335.0
H17A-1486	T7					13.796	6.519	3.213	141.0	5.006	2556.0	29.303	0.127	61.692	72.081	37.757	49.507	264.0
H17A-1491	T340					7.964	324.0	0.878	111.0		3137.0	21.458	0.266	36.878	213.0	48.444	37.764	149.0
H17A-1496	T15					5.859	206.0	0.963	132.0	5.065	19084.0	12.745	0.104	9.287	247.0	66.931	146.0	152.0
H17A-1501	T341					8.299	19.941	0.221	288.0		13035.0	30.657	0.291	37.237	195.0	31.173	22.969	314.0
H17A-1506	T216					7.794	17.773		36.846	55.490		10.397	0.076	12.981	70.901	82.155	50.786	140.0
H17A-1510'10"	T33			X		7.144	562.0	1.516	134.0	13.462	14.955	2.154	0.108	49.711	69.684	79.987	37.925	45.660
H17A-1511' 2"	T8			X		11.018	1051.0	1.678	25.464	8.233	40.825	2.644	0.308	13.745	70.145	78.211	226.0	59.951
H17A-1516	T19			X		0.983	8.251	1.449	407.0		8599.0	9.444	0.319	18.578	173.0	75.214	21.455	126.0
H17A-1521	T32			X		4.819	366.0	1.684	697.0	9.555	1306.0	4.155	0.139	475.0	1623.0	81.635	24.457	247.0
H17A-1526	T12					6.936	104.0	1.326	96.113	4.457	69.995	8.705	0.092	12.111	41.650	73.437	198.0	131.0
H17A-1531	T43			X		9.015	430.0	0.156	33.459	93.128	47.834	2.731	0.056	33.915	17.963	83.262	25.276	301.0
H17A-1536	T9					8.599	564.0	0.980	6.855	7.144	58.718	0.731		8.411	62.953	86.580	207.0	91.359
H17A-1541	T42					12.889	460.0	0.468	55.153	128.0	12.791	9.477	0.264	48.439	35.774	60.231	28.208	46.602
H17A-1546	T25			X		0.183	45.819	1.299	75.493	10.411	37.150	13.316	0.060	23.157	53.394	68.500	28.178	98.337
H17A-1550	T20			X		10.394	497.0	1.409	38.004	7.909	3.705	6.884	0.087	15.107	54.567	74.486	182.0	35.662
H19-538	T100	X						3.347	37.911		195.0	1.996	0.080	13.584	45.503			74.929
H25-80	T225	X						0.691	86.181	93.125	6.495	7.830	0.038	52.048	52.018			69.753
H25-867	T86	X						2.329	59.918		4.550	1.445	0.072	10.479	42.621			41.974
H26-206	T64	X						1.000	28.555		17.514	3.287	0.087	11.692	144.0			37.308
H26-237	T54	X							3.032		26.353	0.703	0.039	3.892	16.082			89.220
H26-257	T56	X				8.996	221.0		12.897		23.712	1.529	0.082	9.370	37.399	76.370	14.284	96.367
H26-292	T54	X							15.457		16.282	1.229	0.028	2.259	2.949			58.531
H28-387	T118	X						1.860	39.881		80.504	2.618	0.070	7.898	86.351			194.70
H28-391	T120	X						1.485	35.629		87.597	1.104	0.128	5.481	29.268			203.0
H28-396	T151	X						3.222	56.137		14.880	1.834	0.151	10.836	35.298			85.677
H28-410		X																

TABLE 9 CONT.

ROCK NUMBER	Powder number	Thin section	Polished section	XRD	XRF	ATOMIC ABSORPTION (ppm) - oxides in %												
						Al_2O_3	Ba	Cd	Co	Cr	Cu	Fe_2O_3	Hg	Ni	Pb	SiO_2	Sr	Zn
H28 - 440	T94	X						0.798	74.376		1.142	0.936	0.105	10.493	33.367			17.746
H28 - 461	T92	X						1.601	60.303		6.051	1.346	0.160	12.869	49.363			34.945
H29 - 175		X																
H29 - 294	T82	X						2.436	56.644	25.823	69.113	8.324	0.039	22.523	197.0			465.0
H29 - 649		X																
H29 - 657		X																
H32 - 181		X																
H32 - 424		X																
H32 - 675		X																
H32 - 917		X																
H33 - 734		X																
H34 - 35	T217	X							66.311	25.009	4.161	2.570	0.022	16.956	57.364			49.384
H34 - 720		X																
H35 - 304	T223	X							71.621	31.183	8.147	17.590	0.022	42.104	35932			60.959
H36A - 1061	T218	X							50.125			3.361	0.006	6.679	60.504			16.004
H38 - 678	T213	X							74.111	53.428		3.961	0.048	15.856	87.434			258.0
H38 - 701	T309	X		X	X	20.001	452.042	0.876	73.399	261.198	1281.418	16.493	0.006	59.271	23.977	50.122	9.258	190.650
H38 - 702		X																
H38 - 705		X																
H38 - 706' 8"		X																
H38 - 743' 3"		X																
H43 150	T53	X						0.260	23.550		89.698	2.366	0.012	6.990	31.079			64.282
H43A - 1837'8"			X															
H43A - 1845'9"			X															
H43A - 1847'7"			X															
H43A - 1850'9"			X															
H43A - 1855'1"			X															
H43A - 1855'6"			X															

TABLE 9 CONT.

ROCK NUMBER	Powder number	Thin section	Polished section	XRD	XRF	ATOMIC ABSORPTION (ppm) - oxides in %												
						Al_2O_3	Ba	Cd	Co	Cr	Cu	Fe_2O_3	Hg	Ni	Pb	SiO_2	Sr	Zn
H43A-1913'10"		X																
H43A-1915		X																
H43A-1957		X																
H43A-1986		X																
H45A-144	T77	X						1.691	84.949		25.312	9.496	0.051	63.659	34.700			77.186
H45A-149	T78	X						1.020	80.564		145.0	7.843	0.053	67.401	31.962			72.345
H45A-192		X																
IM5-59	T277	X		X	X	21.529	412.131	1.193	43.770			1.512	0.015	5.545	67.629	67.866	18.547	356.372
IM5-114	T278	X		X	X	15.689	423.576		39.089		0.997	1.272	0.021	3.369	70.362	77.065	6.994	116.322
IM5-178	T279	X		X	X	14.865	307.111		46.240	12.904	39.098	14.110	0.001	42.187	45.490	51.330	65.256	121.377
IM6-81	T235	X		X	X	15.893	347.562	1.907	71.687		57.752	0.680	0.069	1.773	214.000	78.432	7.115	22.754
IM6-129	T236			X		12.417	325.0	1.630	77.401		37.542	1.086	0.044	4.465	55.667	81.314	39.422	13.809
IM6-141'6"	T245			X		9.147	225.0	1.176	88.263		67.723	1.057	0.078	2.414	59.235	84.877	25.438	25.693
IM5-152	T246			X		12.114	236.0	1.166	47.708		70.713	2.086	0.065	3.593	24.654	82.513	24.618	53.788
IM6-153'6"	T247			X		9.979	150.0	1.392	56.029		49.227	1.022	0.044	2.353	16.171	86.173	41.926	26.919
IM6-180	T261	X		X	X	25.271	382.458	0.654	85.609		4.042	2.308	0.042	6.282	27.681	62.841	5.721	21.298
IM6-194	T262	X				24.766	467.0	1.450	65.742		71.912	2.840	0.048	8.858	58.422	60.295	49.409	25.046
IM6-208	T263	X				17.349	327.0	0.420	64.831		4.704	2.156	0.055	8.164	40.804	70.056	15.737	21.537
IM6-223	T248	X		X		6.085	115.0	1.408	71.049		4.847	2.096	0.039	3.573	32.719	91.310	31.117	10.483
IM6-236.5	T249			X		6.785	164.0	0.747	58.321		2.678	2.719	0.045	3.582	41.022	89.683	39.146	1.754
IM6-254		X																
IM6-261.5	T250			X		3.400	337.0	0.782	89.751		165.0	3.794	0.130	1.749	84.488	88.378	49.022	46.705
IM6-283	T251	X				6.426	181.0		99.714		3.494	3.701	0.113	1.194	32.603	86.986	38.485	8.702
IM6-299	T237	X		X		9.279	203.0	0.765	106.0		3.441	1.969	0.070	6.308	21.825	86.323	42.687	10.729
IM6-308	T252	X		X	X	11.249	131.843	0.777	59.102		1.563	1.472	0.060	2.490	17.021	81.897	4.623	10.204
IM6-319		X																
IM6-351	T234	X		X		8.080	330.0	0.067	62.945		167.0	3.105	0.062	0.909	28.277	88.238	88.139	37.591
IM6-372'4"	T253	X		X	X	12.663	90.751	0.334	37.176		2.192	2.094	0.034	2.180	88.892	79.627	4.334	13.792

TABLE 9 CONT.

ROCK NUMBER	Powder number	Thin section	Polished section	XRD	XRF	ATOMIC ABSORPTION (ppm) - oxides in%												
						Al_2O_3	Ba	Cd	Co	Cr	Cu	Fe_2O_3	Hg	Ni	Pb	SiO_2	Sr	Zn
IM6-385' 10"	T238	X		X		7.578	250.0	0.336	82.958		2.567	2.562	0.037	3.730	43.350	86.665	43.214	19.361
IM6-390	T254	X				7.446	166.0	0.168	28.848		0.681	1.965	0.031	2.048	42.757	90.090	34.663	13.874
IM6-408'4"	T239	X		X		7.843	224.0	0.327	73.836		4.379	2.711	0.052	3.745	39.938	88.206	31.319	66.435
IM6-416	T240	X		X		6.293	180.0	0.340	91.255		0.975	1.146	0.041	3.138	24.057	91.539	47.327	12.488
IM6-436	T255	X				6.237	176.0	1.170	69.692		22.591	2.203	0.153	3.639	75.822	90.946	40.256	15.643
IM6-447' 10"		X																
IM6-470		X																
IM6-480		X																
IM6-496	T279	X		X	X	11.472	131.461		98.005		58.533	1.090	0.007	0.496	45.129	83.474	5.911	18.063
IM6-516' 6"			X															
IM6-535			X															
IM6-574' 10"	T256	X		X	X	9.410	108.328	1.491	72.077		0.669	3.403	0.074	2.169	55.585	84.234	5.835	58.039
IM6-580			X															
IM6-599	T257					5.122	206.0	0.340	21.752		2.061	2.605	0.775	1.335	50.368	88.720	41.593	64.177
IM6-620	T241	X		X		6.633	327.0	0.738	60.089		5.334	2.939	0.427	1.811	55.639	88.420	30.592	50.297
IM6-647	T258	X				6.539	218.0	0.661	49.461		2.341	1.788	0.067	1.729	28.002	89.555	56.583	50.978
IM6-652	T264	X		X	X	9.261	155.833	1.797	48.739		3.520	8.354	0.071	4.036	64.423	74.785	4.504	143.703
IM6-660	T265					5.046	219.0	0.665	64.071		2.523	2.813	0.048	2.473	56.998	92.187	34.041	57.344
IM6-696' 3"	T259					7.257	258.0	0.748	64.730		0.158	3.214	0.046	4.352	24.635	82.855	49.707	109.0
IM6-720	T242			X		7.560	226.0	0.752	82.511		0.766	4.225	0.074	3.078	25.768	86.494	45.410	85.843
IM6-727	T266	X				5.878	151.0	1.998	29.764		5.725	5.504	0.354	0.996	65.749	82.705	31.738	128.0
IM6-745			X															
IM6-747	T260					6.331	265.0	0.684	89.610		6.557	1.160	0.062	2.833	36.210	90.860	72.357	71.383
IM6-757	T243			X		6.010	205.0	0.734	87.500		18.481	3.192	0.118	2.403	35.655	88.870	38.889	136.0
IM6-762			X															
IM6-770			X															
IM6-779			X															
IM6-805	T267	X		X	X	8.740	110.301	2.070	66.442		1.239	19.206	0.040	3.424	77.146	60.871	2.065	247.315

TABLE 9 CONT.

ROCK NUMBER	Powder number	Thin section	Polished section	XRD	XRF	ATOMIC ABSORPTION (ppm) - oxides in %												
						Al_2O_3	Ba	Cd	Co	Cr	Cu	Fe_2O_3	Hg	Ni	Pb	SiO_2	Sr	Zn
IM6 - 859.5	T244	X		X		6.293	80.439	0.327	57.506		0.062	1.681	0.065	2.345	32.286	89.297	26.158	73.456
IM6 - 886' 2"	T268	X				7.333	165.0	0.762	31.754		1.216	3.181	0.048	2.517	32.922	86.066	31.407	128.0
IM6 - 896	T269					5.707	98.698	1.163	35.436		1.060	3.72	0.069	2.468	48.462	84.889	44.00	136.0
IM6 - 902	T233	X		X		4.276	98.974		40.904			1.878	0.025	0.008	20.997	90.808	110.0	112.0
IM6 - 923		X																
IM6 - 959.5	T270	X		X	X	19.719	485663	1.186	53.583		0.136	2.824	0.042	6.717	42.819	70.196	4.697	60.738
IM6 - 1005	T271	X				6.388	75.804		47.875			6.678	0.031	3.957	12.800	83.815	8.873	213.0
IM6 - 1025	T272	X				7.484	23.540		38.136		9.837	8.329	0.041	2.727	36.167	80.433	18.580	229.0
IM6 - 1044'8"			X															
IM6 - 1085'6"	T230	X		X		5.357	182.0	0.238	22.407			1.947	0.029	5.418	30.482	91.963	69.892	55.122
IM6 - 1091	T273	X				6.520	119.0		14.958		2.961	5.173	0.043	3.494	34.466	81.764	38.505	132.0
IM6 - 1101			X															
IM6 - 1104	T274	X		X	X													
IM6 - 1108			X															
IM6 - 1120	T275	X				9.204	124.0		22.201		2.123	9.204	0.022	6.064	31.885	80.244	14.817	237.0
IM6 - 1134			X															
IM6 - 1142	T231	X		X		7.349	91.023		25.54		0.272	7.657	0.016	3.448	44.224	84.265	70.191	150.0
IM6 - 1152	T232	X		X		7.565	556.0		54.112		11.837	2.651	0.019	0.883	20.048	87.700	88.897	76.249
IM6 - 1160			X															
IM6 - 1179			X															
IM6 - 1200		X																
IM6 - 1210		X																
IM6 - 1231			X															
IM6 - 1240	T280	X		X	X	9.149	23.229		56.402		42.004	13.530	0.003	4.577	14.987	62.722	4.391	229900
IM6 - 1271		X																
IM6 - 1365			X															
IM6 - 1392			X															
IM6 - 1442'8"		X																

TABLE 9 CONT.

ROCK NUMBER	Powder number	Thin section	Polished section	XRD	XRF	ATOMIC ABSORPTION (ppm) - oxides in %												
						Al_2O_3	Ba	Cd	Co	Cr	Cu	Fe_2O_3	Hg	Ni	Pb	SiO_2	Sr	Zn
IM6 -1502'7"	T281	X		X	X	17.678	311.322	2.026	79.488	36.830	65596	16.614	0.001	48.129	31.762	48.737	56.151	105.297
IM6 -1574	T282	X		X	X	25.248	347.357		78.502	1.572	0.918	3.768	0.001	27.260	40.925	52.274	205.824	1.070
IM6 -1619	T283	X		X	X	17.974	420.012		60.564		0.178	10.373	0.015	42.991	15.265	51.356	230.636	32.673
IM7 - 93	T284	X		X	X	15.198	167.496		36.443		4.622	1.691	0.010	3.791	26.338	77.147	6.394	72.257
IM7 - 167	T285	X		X	X	17.177	306.890		25.639			2.154	0.010	5.012	13.256	72.696	14.481	22.705
IM7 - 231.5	T286	X		X	X	28.083	466.139		47.108		13.956	0.635	0.099	17.138	44.577	61.643	12.226	0.802
IM7 - 312	T287	X		X	X	17.991	332.177		40.952		5.729	2.793	0.038	5.791	45.620	68.029	22.349	23.875
IM7 - 426	T288	X		X	X	18.599	164.905		49.115		1.132	3.284	0.030	2.631	43.605	71.089	8.590	36.708
IM7- 520	T289	X		X	X	27.960	518.629		43.748		0.453	1.886	0.020	12.966	29.671	59.697	10.918	9.255
IM7 - 640	T290	X		X	X	16.371	49.476		24.261		1.436	12.636	0.004	4.989	13.621	59.324	4.400	93.354
IM7 - 871	T292	X		X	X	15.544	319.995	0.235	60.613		278.255	1.315	0.009	3.134	47.404	76.802	13.327	5.344
IM7- 1232.5	T293	X		X	X	14.379	20.275	0.233	64.159		2.868	28.062	0.011	29.981	60.794	36.175	8.473	231.814
IM7 - 1338	T294	X		X	X	21.540	1224.076		36.646		0.143	0.967	0.018	7.317	20.415	70.143	13.970	3.795
IM7 - 1607	T295	X		X	X	14.861	300.984		53.678	4.358	16.715	6.021	0.003	7.039	34.322	70.242	220.584	35.346
IM8 - 276	T296	X		X	X	23.446	339.894		35.505		8.742	4.242	0.025	7.372	46.161	62.977	14.107	258.734
IM8 - 279		X																
IM8 -282		X																
IM8 -297.5		X																
IM8 -316	T297	X		X	X	19.980	495.621		31.799		3.556	1.428	0.033	4.836	55.391	69.979	9.701	547.210
IM8 -363	T298	X		X	X	13.980	393.071		24.648		0.932	2.125	0.004	5.854	30.119	76.248	9.761	665.201
IM8-427	T299	X		X	X	13.732	432.470		39.987			1.040	0.005	4.295	19.990	77.834	52.947	36.233
IM8-435		X																
IM8-470		X																
IM8- 504	T300	X		X	X	14.117	432.470		39.987		0.939	0.863	0.073	4.208	34.290	78.494	21.457	1.022
IM8- 610	T301	X		X	X	22.504	666.325	0.448	25.948			1.737	0.002	7.480	32.265	65.564	40.599	19.811
IM8-767	T302	X		X	X	21.202	625.735	2.043	17.213			1.715	0.020	6.528	49.927	68.055	17.167	47.226
IM8-894	T303	X		X	X	15.709	794.135	0.662	31.288		4.469	2.019	0.119	5.869	76.525	74.767	11.623	430.809
IM9-47.5			X															

TABLE 9 CONT.

ROCK NUMBER	Powder number	Thin section	Polished section	XRD	XRF	ATOMIC ABSORPTION (ppm) - oxides in %											
						Al_2O_3	Ba	Cd	Co	Cr	Cu	Fe_2O_3	Hg	Ni	Pb	SiO_2	Sr	Zn
IM9 - 50		X				15.788	1290.0	1.059	35.663		1.602	0.365	0.184	6.836	40.715	80.273	45.506	9.225
IM9 - 50.5	T172	X		X	X	7.163	1153.0	2.043	19.498		1.155	0.298	0.127	6.715	58.545	90.153	4.920	11.016
IM9 - 51	T174	X		X		9.175	1967.0	1.389	41.829		5.453	0.467	0.096	5.528	32.447	87.129	86.581	9.502
IM9 - 53	T184	X		X		13.494	2020.0	1.947	97.676		3.685	0.455	0.090	29.171	13.086	72.753	50.473	14.310
IM9 - 56.5	T177	X		X		10.582	1848.0		56.738		16.026	1.755	0.442	1.736	56.508	71.002	36.310	1.661
IM9 - 59	T 347	X				7.503	1804.0	1.906	38.929		6.432	0.733	0.093	6.870	30.169	82.684	21.172	13.835
IM9 - 72' 9"	T171	X		X		8.599	1711.0	1.021	74.559		3.754	0.678	0.194	21.933	35.052	79.623	46.927	16.358
IM9 - 74	T179	X		X		11.520	3301.0	0.652	41.137		7.272	1.131	0.257	4.659	36.720	83.917	31.907	15.789
IM9 - 77	T187	X		X		10.054	3037.0	1.267	107.0		16.362	0.675	0.271	27.269	19.358	79.538	75.841	78.163
IM9 - 85	T178	X		X		8.202	2649.0	3.357	109.0		7.093	0.824	3.941	25.269	18.00	77.354	166.0	158.0
IM9 - 97.5	T168	X		X		12.380	3119.0	1.882	45.693			0.672	2.390	9.559	33.925	75.097	78.952	46.070
IM9 - 100	T197	X		X														
IM9 - 102			X			9.077	2433.0	0.475	29.931		6.386	2.364	6.681	1.915	23.456	84.961	55.014	61.345
IM9 - 107	T181	X		X														
IM9 - 115		X				19.837	3140.0	3.131	50.803		2.434	3.698	2.544	14.372	68.936	76.267	56.422	475.0
IM9 - 119.5	T198	X		X		14.023	2084.0	1.394	41.473		5.945	1.892	1.577	8.096	23.728	83.318	17.191	139.0
IM9 - 122.5	T182	X		X		5.898	378.0	0.251	72.361		6.007	0.504	0.633	1.554	32.681	84.378	43.357	210.0
IM9 - 145	T191, 348	X		X		17.521	1129.0	2.282	56.950		7.666	0.481	0.988	11.394	38.643	76.450	24.352	408.0
IM9 - 158	T192	X		X		20.199	1038.0	3.067	61.858		9.516	0.735	0.810	15.485	24.324	77.558	26.799	377.0
IM9 - 167.5	T183	X		X		11.104	540.0	1.417	52.216		9.062	0.655	0.308	6.318	29.914	85.786	29.327	182.0
IM9 - 175.5	T188	X		X		13.124	634.0	1.412	46.207		13.961	1.798	0.413	7.500	134.0	82.377	40.451	183.0
IM9 - 194.5	T193	X		X		10.482	550.0	0859	40.984		10.202	1.097	0.221	6.075	95.194	86.525	58.941	101.0
IM9 - 197	T194	X		X		23.970	625.476	2.624	63.457		33.784	1.292	1.033	14.095	162.156	67.037	13.820	766.655
IM9 - 200.5	T196	X		X	X	13.021	569.0	4.322	70.247		28.420	1.022	0.170	16.773	36.397	72.239	94.481	113.0
IM9 - 204	T165	X		X		11.515	424.0	1.278	41.389		35.104	1.278	0.328	7.285	77.797	85.884	53.296	186.0
IM9 - 208	T199	X		X		10.186	367.0	1.075	30.158		13.913	1.452	0.428	8.551	123.0	84.304	20.808	194.0
IM9 - 215.5	T186	X		X		8.644	522.0	1.656	45.368		12.631	1.821	0.352	3.470	92.198	88.115	99.920	169.0
IM9 - 225	T195	X		X														

TABLE 9 CONT.

ROCK NUMBER	Powder number	Thin section	Polished section	XRD	XRF	ATOMIC ABSORPTION (ppm) - oxides in %												
						Al_2O_3	Ba	Cd	Co	Cr	Cu	Fe_2O_3	Hg	Ni	Pb	SiO_2	Sr	Zn
IM9 - 231.5	T175	X		X		9.015	264.0	1.820	30.493		11.058	1.419	0.289	6.922	390.0	79.003	30.114	478.0
IM9 - 244	T349	X				12.389	464.0		34.980		9.997	3.081	0.277	16.985	267.0	66.118	42.722	575.0
IM9 - 251.5	T350	X				11.131	324.0	0.712	54.219		15.255	1.922	1.293	5.132	430.0	40.037	45.241	1125.0
IM9 - 265'4"	T351					7.147	265.0	0.014	25.515		216.0	1.532	0.437	5.047	583.0	76.232	29.479	933.0
IM9 - 269			X															
IM9 - 283																		
IM9 - 284.5	T190	X		X	X	9.961	159.751	0.910	142.828		7.418	0.582	0.153	1.275	168.958	86.621	7.553	198.833
IM9 - 285.2			X (3)															
IM9 - 288		X																
IM9 - 292.5		X																
IM9 - 294.5		X																
IM9 - 299	T173			X		8.013	144.0	3.448	18.944		37.911	0.520	0.117	6.996	96.203	80.158	17.150	348.0
IM9 - 300.5	T185	X		X		11.275	233.0	0.927	44.033		11.192	1.351	0.056	5.986	249.0	85.607	18.215	85.468
IM9 - 310		X																
IM9 - 320	T170	X		X		8.297	176.0	3.187	25.353		18.384	0.868	0.186	8.316	143.0	78.639	23.624	537.0
IM9 - 334	T180	X		X		8.294	296.0	1.445	94.856		5.615	0.991	0.097	1.815	24.383	88.108	93.945	17.163
IM9 - 355	T169	X		X		8.977	223.0	2.871	61.655		9.819	0.976	0.098	11.299	68.102	76.991	70.078	25.055
IM9 - 364'2"			X															
IM9 - 365'4"			X															
IM9 - 376	T176	X		X		11.131	589.0	3.047	30.316		905.0	2.289	0.067	7.603	49.085	71.126	40.544	18.238
IM9 - 380	T189	X		X		15.015	819.0	1.182	60.693		8.872	1.292	0.061	11.836	35.588	78.419	21.758	42.918
IM9 - 384	T200	X		X		13.650	753.0	0.860	69.738	4.930	3.892	0.541	0.047	6.576	39.944	83.223	31.094	7.246
IM9 - 388		X																
IM9 - 395.5	T352	X				12.479	740.0		52.962			2.314	0.080	14.050	57.702	68.496	26.465	3.285
IM9 - 403'3"	T166	X		X		10.924	720.0	3.267	75.489		119.0	1.284	0.067	14.426	35.113	72.667	39.260	30.239
IM9 - 410		X																
IM9 - 413.5	T167	X		X	X	13.720	419.050	3.008	125.670	13.377	118.408	1.061	0.119	28.218	8.033	81.072	13.324	17.688
IM9 - 415.5		X																
IM9 - 423.5	T353			X		16.518	659.0		65.195		144.0	1.866	0.953	26.275	39.293	63.343	67.735	0.549
IM9 - 431.5		X																

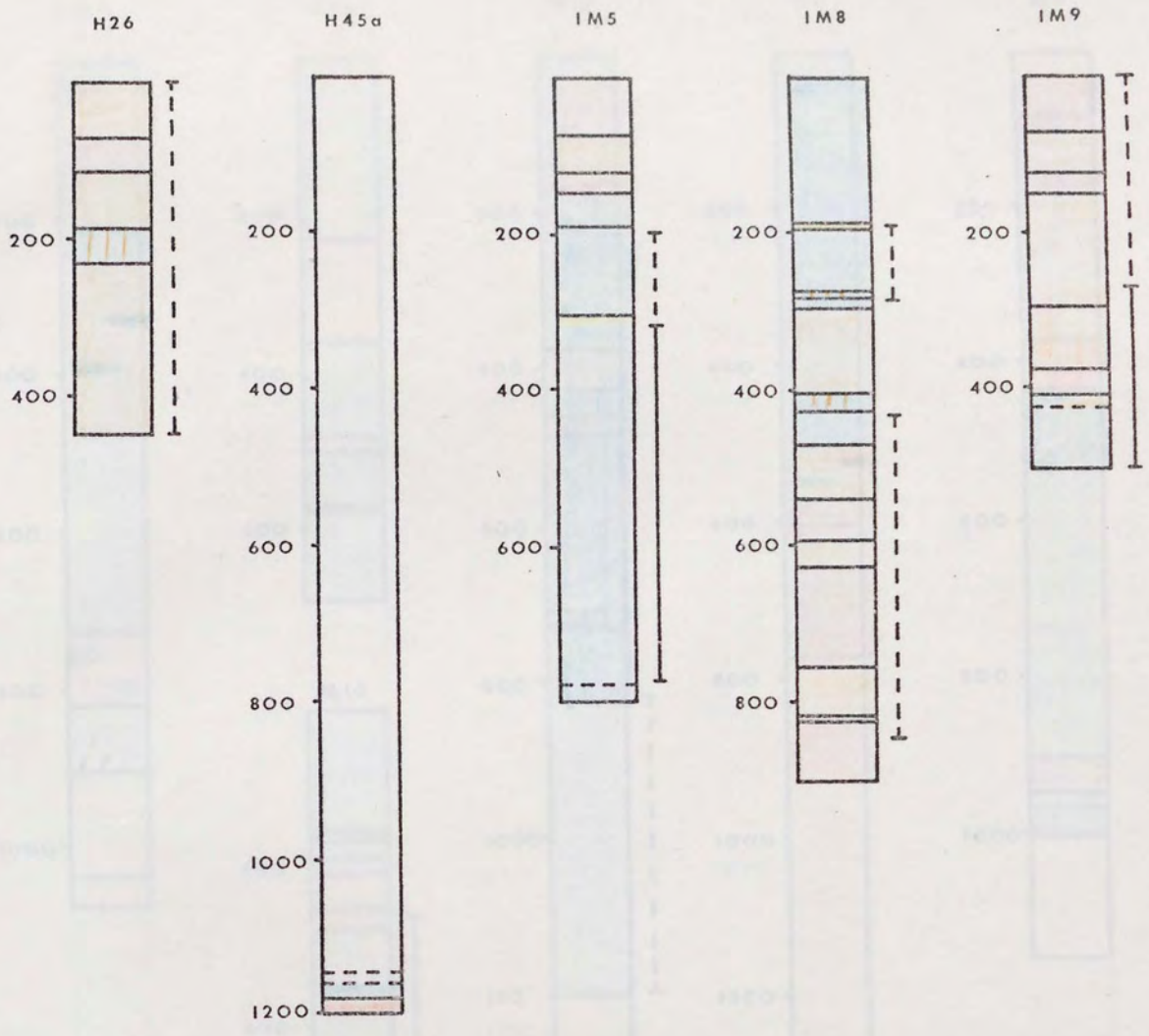
H26
H45a
IM5
IM8
IM9
200
400
600
800
1000
1200

FIGURE 30A

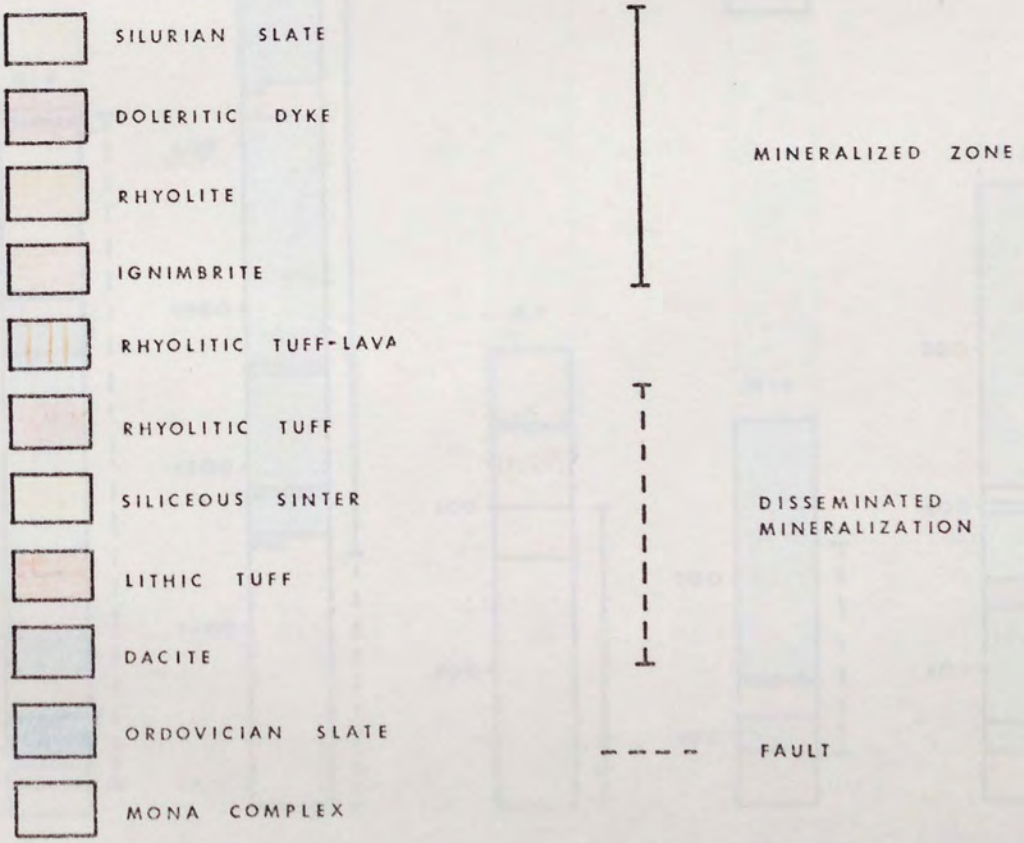
SILURIAN SLATE
DOLERITIC DYKE
RHYOLITE
IGNIMBRITE
RHYOLITIC TUFF-LAVA
RHYOLITIC TUFF
SILICEOUS SINTER
LITHIC TUFF
DACITE
ORDOVICIAN SLATE
MONA COMPLEX
MINERALIZED ZONE
DISSEMINATED MINERALIZATION
FAULT

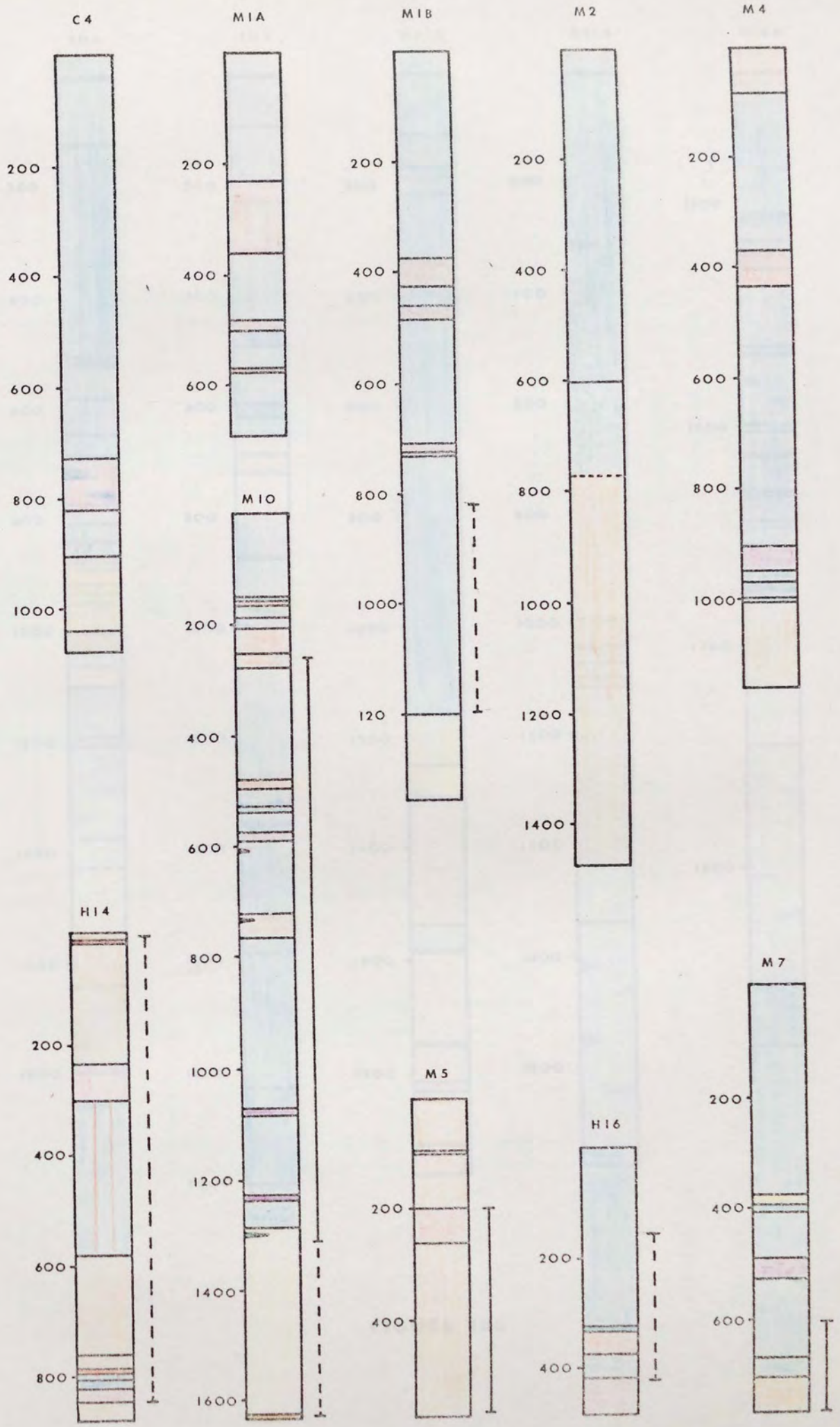
C4
200
400
600
800
1000
M1A
200
400
600
M10
200
400
600
800
1000
1200
1400
1600
M1B
200
400
600
800
1000
120
M2
200
400
600
800
1000
1200
1400
M4
200
400
600
800
1000
H14
200
400
600
800
M5
200
400
H16
200
400
M7
200
400
600

FIGURE 30 B

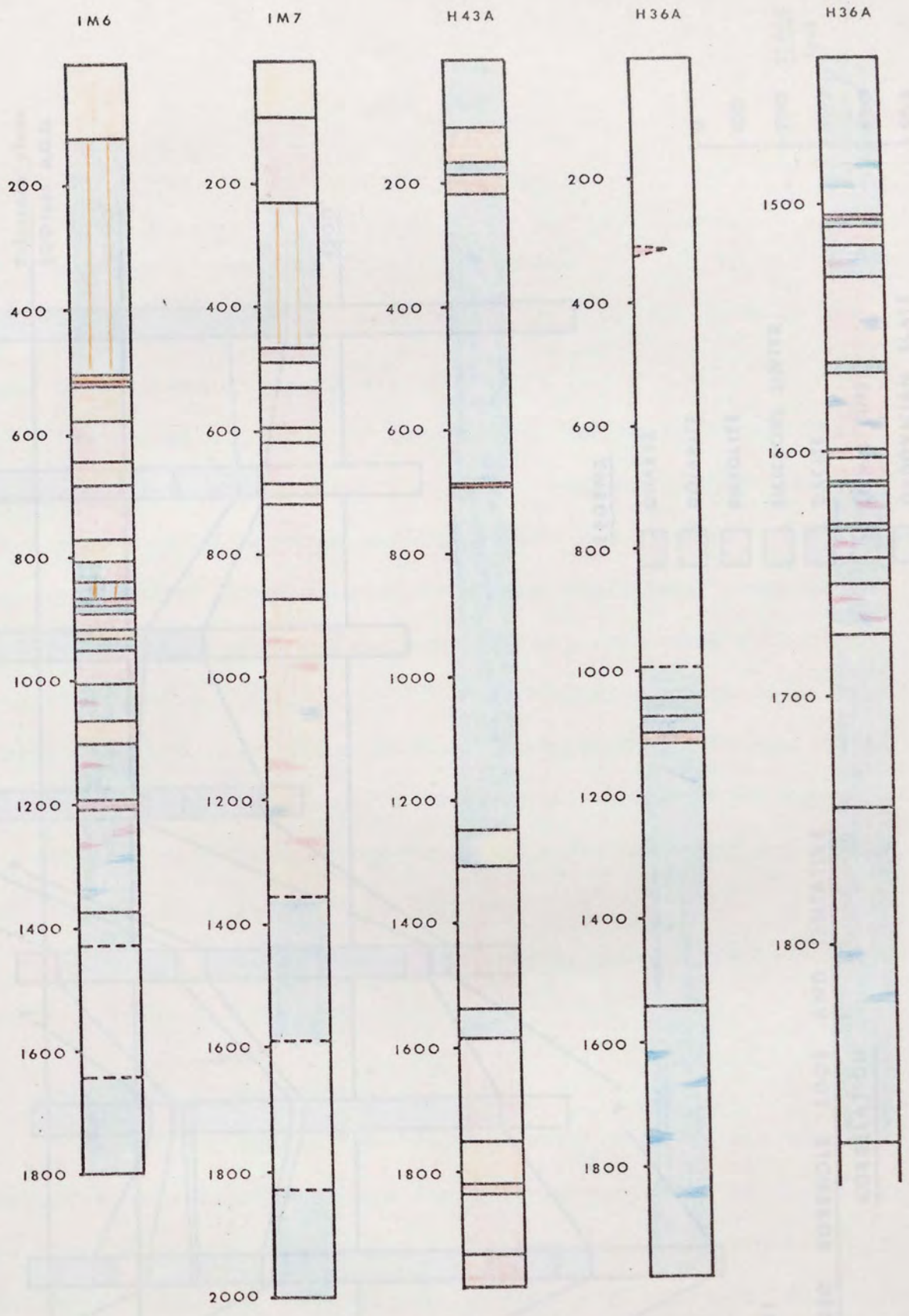
IM6
IM7
H43A
H36A
H36A
200
400
600
800
1000
1200
1400
1600
1800
2000
1500
1700

FIGURE 30C

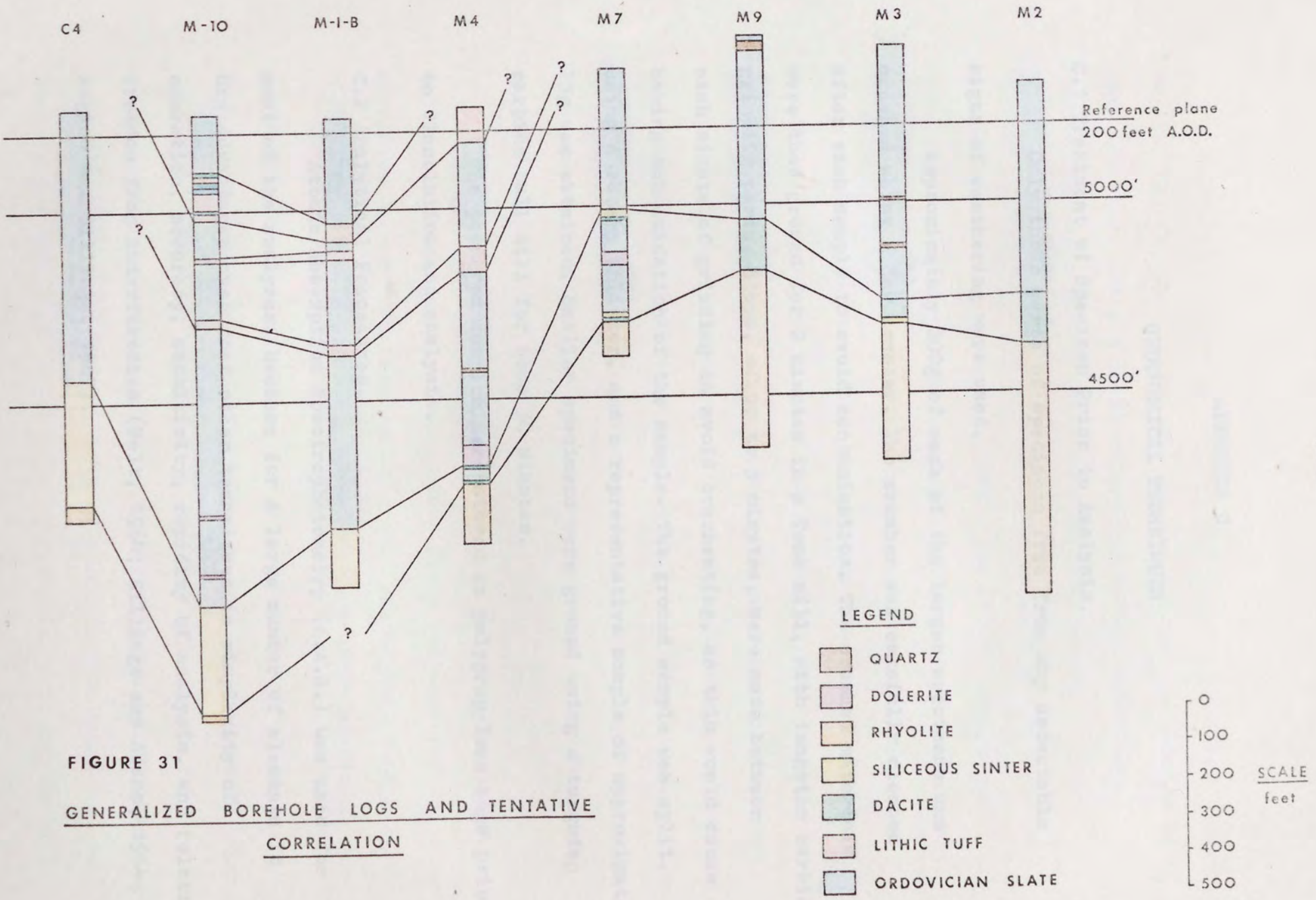

FIGURE 31

GENERALIZED BOREHOLE LOGS AND TENTATIVE CORRELATION

APPENDIX C

GEOCHEMICAL TECHNIQUES

C.1 Treatment of Specimen Prior to Analysis.

Only those parts of specimens free from any detectable signs of weathering were used.

Approximately 200g of each of the larger specimens was crushed using a jaw crusher. The crusher was carefully cleaned after each sample to avoid contamination. The crushed materials were then ground for 2 minutes in a Tema mill, with tungsten carbide grinding parts. Stops, of up to 5 minutes, were made between each minute of grinding to avoid overheating, as this would cause baking and oxidation of the sample. The ground sample was split, using a rotary splitter, and a representative sample of approximately 25g was obtained. Smaller specimens were ground using a tungsten carbide ball mill for some 30 minutes.

The powdered samples were stored in polypropylene bags prior to dissolution and analysis.

C.2 Analytical Procedures.

Atomic Absorption Spectrophotometry (A.A.S.) was used for most of the analyses, because for a large number of elements it has advantages over most other techniques in simplicity of operation, accuracy, sensitivity, rapidity of analysis, and relative freedom from interferences (Belt, 1964; Billings and Adams, 1964; Angino and Billings, 1967).

Three major elements (Si, Al, and Fe) and ten trace elements (Ba, Cd, Co, Cr, Cu, Hg, Ni, Pb, Sr, and Zn) were determined by this technique, using a Perkin-Elmer 303 Atomic Absorption Spectrophotometer with a chart recorder attachment.

The method used to decompose the samples is one modified from that described by Bernas (1968). The ground samples were decomposed by heating with aqua regia and 48 percent hydrofluoric acid, in a polypropylene bottle, and a full description of the technique is given in the next section. In the determination of Ba, Cd, Co, Cr, Cu, Ni, Sr, and Zn, a blank solution, of approximately the same composition as the sample except for these elements, was used to compensate for background absorption effects. An alkaline salt, sodium citrate, of 1000 to 2000ppm concentration, was added to both standard solutions, and unknown sample solutions to protect against ionization interference when Ba and Sr were measured.

A nitrous oxide-acetylene flame was used for the Al, Ba, Si, and Sr analyses, and an air-acetylene flame was used for the other elements. Hg was determined using a cold vapour method of A.A.S. and details of this technique are given in a later section.

C.3 Sample Dissolution.

Approximately 0.2g of powdered sample was accurately weighed into a polypropylene bottle. It was wetted by adding 0.5ml of aqua regia, and gently swirling the bottle. This was done to dissolve carbonate minerals, especially those containing Ca ions, in order to prevent the formation of CaF_2 with hydrofluoric acid in the main

part of the dissolution. Five ml of 48 percent hydrofluoric acid was then added and the bottle capped with a polypropylene stopper. The bottle was heated at 90°C in an oven for 30-40 minutes, then removed and allowed to cool to room temperature. 50ml of saturated boric acid solution was added in order to obtain a salt-free, single matrix system (Bernas, 1968). The bottle was then reheated at 90°C for a further 30-40 minutes. After cooling the solution was washed into a 100ml volumetric flask and made up to volume, using double-distilled water. The solutions were analysed within 48 hours of preparation because losses of elements, present in low concentrations, occur by absorption on the sides of the bottle, if stored for longer periods.

C.4 Preparation of Blank (Matrix) Solution

Determination of the trace element content of geological materials requires the use of a blank solution, to eliminate background absorption effects caused by 'matrix' interferences. A molecular absorption, due to high salt content in the sample solution, is also common (Angino and Billings, 1967). Both these interferences were compensated for by using a blank solution of approximately the same composition as the sample, but without the elements of interest, The blank solution was added to the standard solutions and the spectrophotometer was calibrated to ensure that the background absorptions were similar for both standard and test solutions.

Some of the volcanic rocks from Parys Mountain have approximately 72 percent of SiO_2, 15 percent of Al_2O_3, and 9 percent total alkalis (Wheatley, 1971a). The majority of the samples used in this study were volcanic rocks, similar to and from the same area as, those analysed by Wheatley, thus a similar composition was

assumed. The blank solution contained similar proportions of these constituents. The solution was made by accurately weighing approximately 1.4g of SiO_2 powder into a Teflon-lined decomposition vessel (Bernas, 1968)(Fig. 32). 20ml of 48 percent hydrofluoric acid was added to the powder and the vessel was capped and heated in an oven at 200°C, for 30-40 minutes. The decomposition vessel was used to prevent volatilization losses during dissolution. After cooling to room temperature, the solution was transferred into a 1000ml polythene beaker and 30ml of 48 percent hydrofluoric acid, 10ml of aqua regia, 100ml of double-distilled water, 500ml of saturated boric acid solution, 2.6677g of aluminium ammonium sulphate, and 12.79g of sodium citrate were added. The solution was then transferred to a 1000ml flask and made up to volume with double-distilled water. This solution had 1.4g SiO_2, 0.3g Al_2O_3, and 9000ppm sodium citrate in 1000ml.

C.5 Preparation of Standards

Standards for the analysis were prepared from a stock solution containing approximately 1000ppm of the element to be determined. The stock solutions were made from weighed quantities of either spec pure metal, or an appropiate stoichiometric salt dissolved in a suitable acid or solvent. Table 10 lists the types and quantities of the materials and solvents used in the preparation of each stock solution. Double-distilled water was used to make the volume up to 1000ml, and the solution was stored in a polythene bottle. Standard solutions, used in analysis, were prepared from these stock solutions by dilution with blank solution, using an autodiluter.

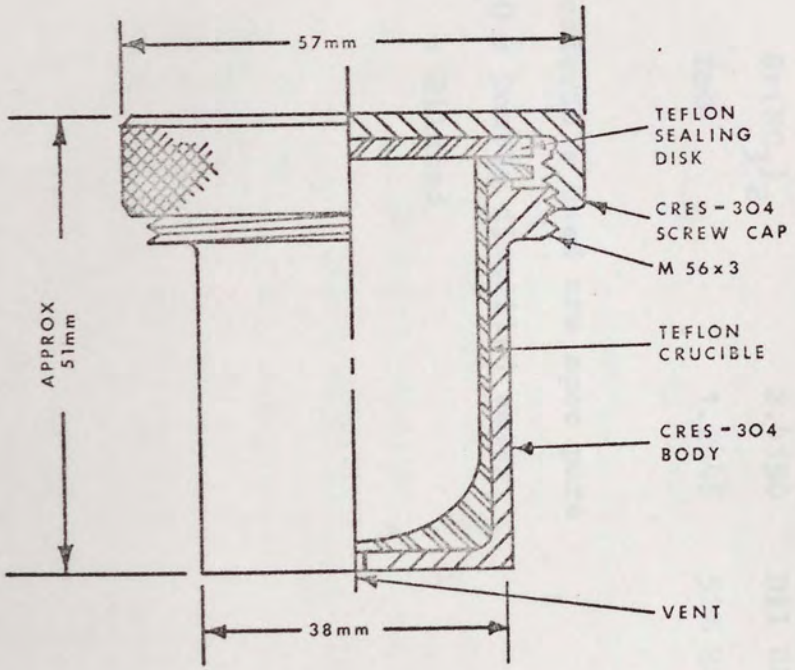

DECOMPOSITION VESSEL

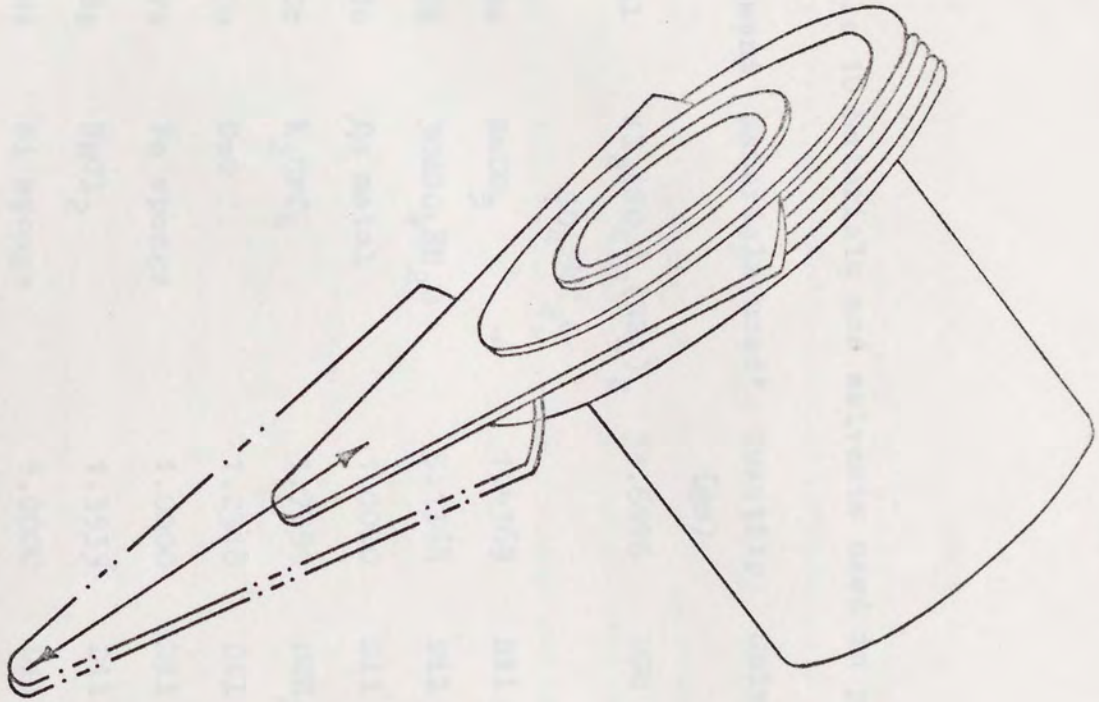

DECOMPOSITION VESSEL WITH SPOUT

FIGURE 32

DIAGRAM TO SHOW THE CONSTRUCTION OF THE DECOMPOSITION VESSEL USED FOR DISSOLUTION OF SAMPLES FOR ATOMIC ABSORPTION SPECTROPHOTOMETRY.

Table 10 Materials and solvents used in preparation of stock solutions.

Element	Materials used*	Quantity (gm)	Solvents	Concentration
Al	$Al_2(SO_4)_3(NH_4)_2SO_424H_2O$	33.6176	DDH O	1000 ppm
Ba	$BaCO_3$	1.4369	Dil HCl	1000 ppm
Cd	$3CdSO_48H_2O$	5.1368	Dil HCl	1000 ppm
Co	Co metal	1.0000	Dil HCl	1000 ppm
Cr	K_2CrO_4	3.7350	DDH_2O	1000 ppm
Cu	CuO	1.2518	Dil HNO_3	1000 ppm
Fe	Fe sponge	1.0000	Dil HCl	1000 ppm
Hg	$HgCl_2$	1.3535	Dil HCl	1000 ppm
Ni	Ni sponge	1.0000	Dil aqua regia	1000 ppm
Pb	$Pb(NO_3)_2$	1.5986	DDH_2O	1000 ppm
Si	SiO_2	8.5616	48% HF	4000 ppm
Sr	$Sr(NO_3)_2$	2.4150	Dil HNO_3	1000 ppm
Zn	ZnO	1.2448	50% HCl	1000 ppm

* All materials used are spec pure

DDH_2O : Double distilled water

Dil : Diluted

For the analyses blank solution, standard solutions, and sample solutions were run in a strict sequence each time in order to correct for background absorption, to achieve correspondance between the order of data input and to facilitate the programme used in calculating the results. The sample handling sequence for the analyses, i.e. the sequence of aspirating blank solution, standard solutions, and the unknown solutions was as follows:-

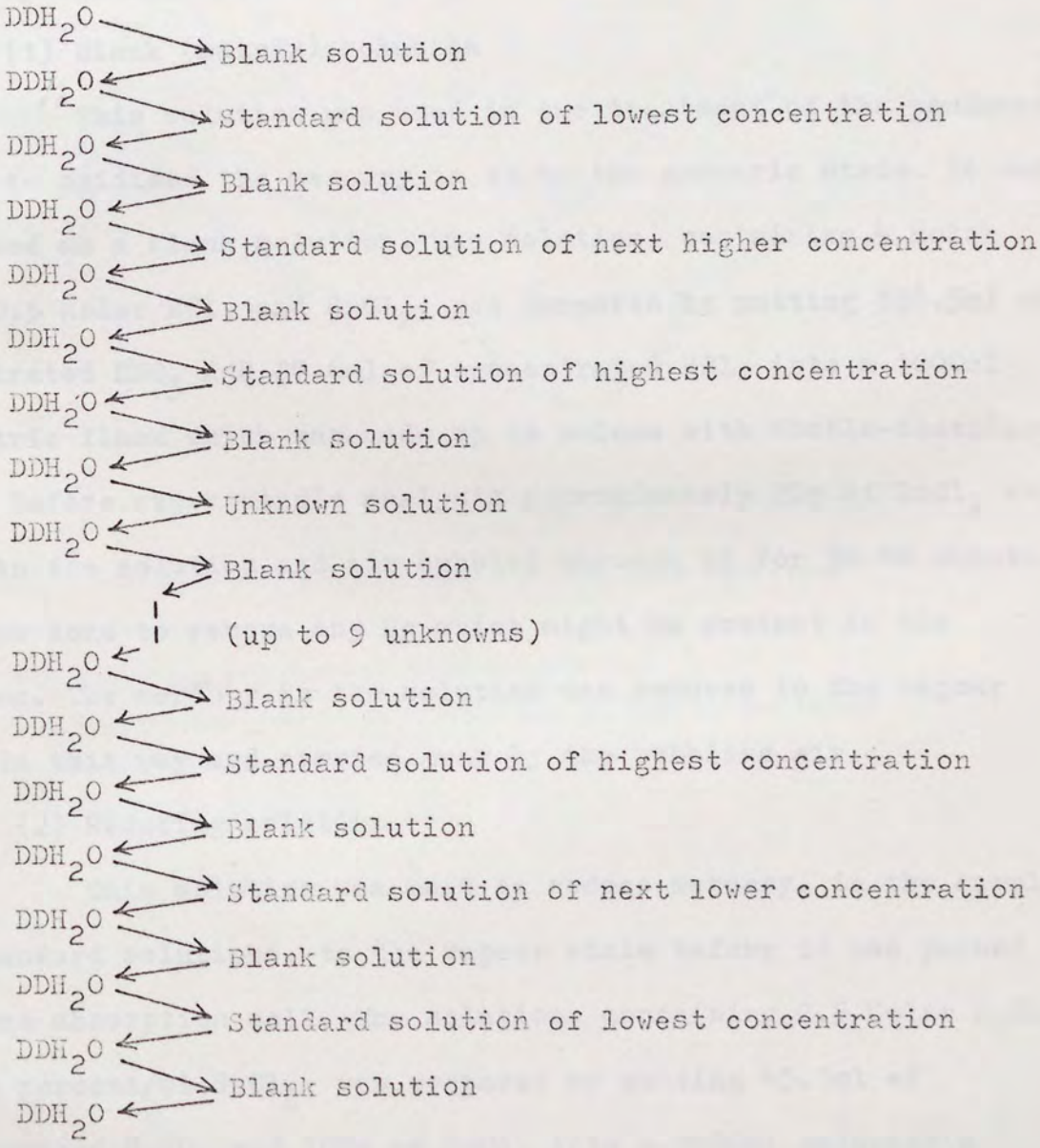

C.6 Cold Vapour Method for Determination of Mercury.

In this method sample solutions are not ionized in a flame in the path of the light beam, instead mercury (Hg) is taken from the solution into the vapour state and passed through a tube sitting in the path of a mercury light beam. The absorption produced by Hg vapour is measured (Fig.33) as in the other A.A.S. techniques and the Hg content calculated. The following solutions were prepared and used:-

(1) Blank (matrix) solution

This solution was used in the treatment of the powdered sample to oxidised the mercury in it to the mercuric state. It was also used as a blank solution. The solution, containing 4 Molar HNO_3, 0.5 Molar HCl, and $SnCl_2$, was prepared by putting 358.5ml of concentrated HNO_3 and 27.6ml of concentrated HCl, into a 1000ml volumetric flask which was made up to volume with double-distilled water. Before every single analysis approximately 20g of $SnCl_2$ was added to the solution and air bubbled through it for 30-40 minutes. This was done to remove any Hg which might be present in the solution. The mercury in the solution was reduced to the vapour state in this way and carried away by the bubbling air.

(2) Reducing solution

This solution was used to reduce mercury, in the sample and standard solutions, to the vapour state before it was passed into the absorption cell. The solution, containing 0.5 Molar H_2SO_4 and 10 percent/wt $SnCl_2$, was prepared by putting 45.1ml of concentrated H_2SO_4 and 100g of $SnCl_2$ into a 1000ml volumetric flask which was made up to volume with double-distilled water. The

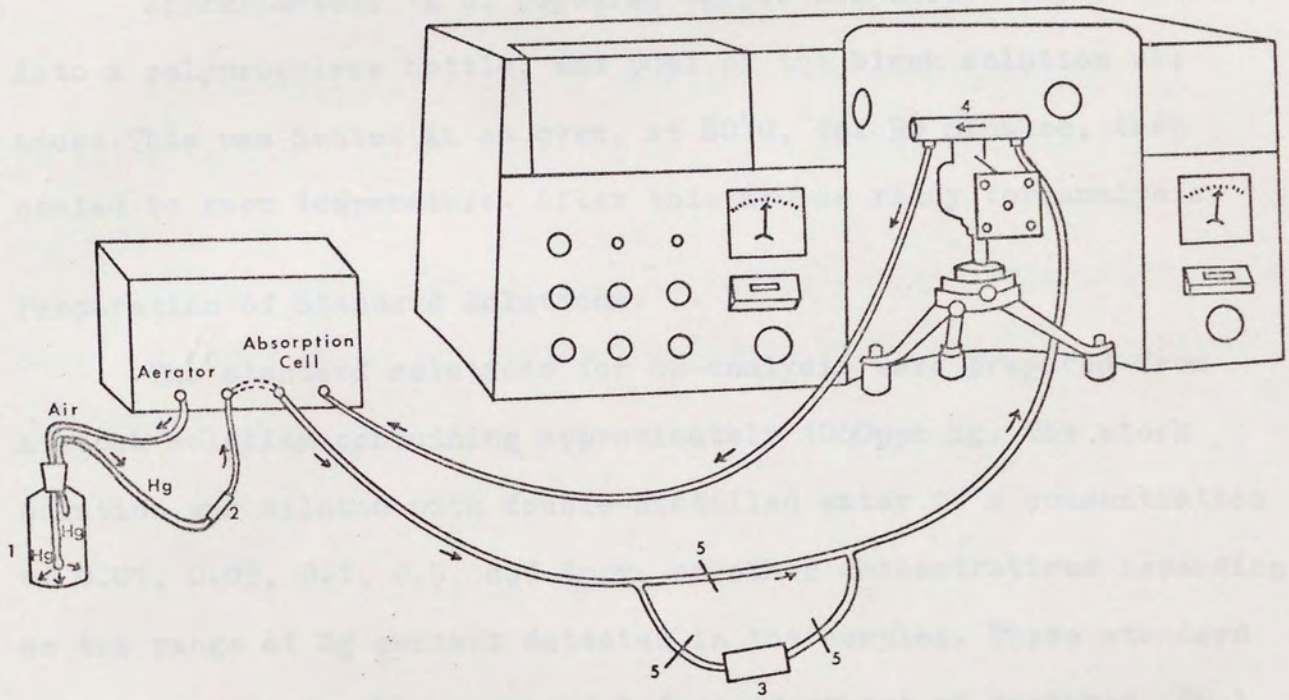

Figure 33

Sketch diagram to show instrumental set up for the determination of mercury by cold vapour method.

1. Bottle used for aerating Hg vapour.

2. Tube containing material which absorbs moisture (Magnesium perchlorate).

3. Tube containing activated carbon used to absorb Hg vapour after absorbance has been recorded.

4. Mercury tube aligned along the path of mercury light beam.

5. Clips used to control the path of Hg vapour.

solution was treated with air bubbles for 30-40 minutes in order to render it Hg-free.

Preparation of Sample Solution for Hg-analysis.

Approximately 1g of powdered sample was accurately weighed into a polypropylene bottle, and 50ml of the blank solution was added. This was heated in an oven, at 80°C, for 90 minutes, then cooled to room temperature. After this it was ready for analysis.

Preparation of Standard Solutions.

The standard solutions for Hg-analysis were prepared from a stock solution containing approximately 1000ppm Hg. The stock solution was diluted with double-distilled water to a concentration of 0.01, 0.05, 0.1, 0.5, and 1ppm, or other concentrations depending on the range of Hg content detected in the samples. These standard solutions were freshly prepared before every set of analyses. 50ml of matrix solution was added to each standard solution before use, e.g. if the concentration range of the standard solutions required was between 0.01 to 0.5ppm, four standard solutions of 0.01, 0.05, 0.1, and 0.5ppm concentration were prepared. This was done by putting 1ml of each concentration into four separate bottles and adding 50ml of matrix solution to each of them.

Analytical Procedure.

(1) 50ml of matrix solution, and 10ml of reducing solution (both now Hg-free) were put into the aerating bottle (Fig. 33) and the absorbance recorded. This was used as the base line for calculation of the results.

(2) The standard solution, which also contained 50ml of matrix solution, was transferred to the aerating bottle and 10ml of reducing solution added. The absorbance for each standard solution was recorded, from the lowest concentration to the highest, before analysis of the unknown solution.

(3) The sample (unknown) solution was transferred to the aerating bottle, 10ml of reducing solution added, and the absorbance recorded.

The Hg content of each sample was calculated from the results obtained above using the programme written by Frost (1972, personal communication).

APPENDIX D

BULK CHEMICAL ANALYSES

Whole rock chemical analyses were done on 61 specimens, by Dr G. Hendry of the University of Birmingham, using X-ray fluorescence techniques. The specimens selected for analysis were fresh, apparently unaltered rocks taken from both drill cores and surface exposures. The specimen locations are shown in Fig.28 and listed in Table 9 (Appendix A). Two surface specimens of rhyolitic rocks, from the Rhosmynach (N.G.R. 483913) and Carmel Head (N.G.R. 293919) areas were analysed. These were included because thin section studies indicated that they were similar to rhyolitic rocks of Parys Mountain and may have been formed in the same volcanic episode. Of the 61 specimens; 43 were rhyolitic rocks, 13 were dacitic rocks, 4 from the Precambrian Mona Complex, and 1 of the Ordovician slate.

The specimens were ground in a Tema mill (see Appendix C), and pelletized using MOWIOL 8-38 as binding agent. Internal standards used in the analysis were obtained from samples, which were internally analysed, using wet chemical techniques, and calibrated and checked against standard rocks, e.g. G-1, W-1, etc. The analyses were double checked using both sides of the pellets. The analytical results are given in Table 11. CIPW Norms, Niggli numbers, and Differentiation Indices were also calculated (Table 12).

ABLE 11 BULK CHEMICAL ANALYSIS RESULTS (XRF) TRACE ELEMENTS VALUES ARE ALSO GIVEN

Rock Type	Sample Number	Powder Number	Pellet Number	MAJOR ELEMENT										Original Total	TRACE ELEMENT									
				SiO_2	TiO_2	Al_2O_3	Fe_2O_3	MnO	MgO	CaO	Na_2O	K_2O	P_2O_5		S	Ba	Sr	Rb	Cu	Zn	Pb	Ni	Co	Cd	Cr	Hg
Rhy	IM5-59	T 276	9878	67.866	0.138	21.529	1.512	0.028	3.052	0.488	0.099	5.287	0.001	96.944	554.146	412.131	18.547	173.898		356.372	67.629	5.545	43.770	1.193		0.015
Rhy	IM5-114	T 277	9879	77.055	0.099	15.689	1.272	0.013	2.055	0.053	0.015	3.374	0.005	100.605	278.091	423.576	6.994	153.095	0.997	116.322	70.362	3.359	39.089			0.021
Dac	IM5-178	T 278	9880	51.300	2.249	14.865	14.110	0.162	5.991	7.139	1.759	1.825	0.559	89.419	367.113	307.111	65.256	40.604	39.098	121.377	45.490	42.187	46.240		12.904	0.001
Rhy	IM6-81	T 235	9881	78.432	0.156	15.893	0.680	0.008	0.719	0.005	0.193	3.467	0.021	103.768	4257.400	347.562	7.115	128.243	57.752	22.754	214.000	1.773	71.687	1.907		0.069
Rhy	IM6-180	T 261	9882	62.841	0.253	25.271	2.308	0.008	1.042	0.024	0.203	6.273	0.024	102.410	7530.535	382.458	5.721	201.292	4.042	21.298	27.681	5.282	85.609	0.654		0.042
Rhy	IM6-308	T 252	9883	81.897	0.097	11.249	1.472	0.013	0.765	0.329	0.097	2.482	0.015	105.528	15827.138	131.843	4.623	100.489	1.563	10.204	17.021	2.490	59.102	0.777		0.060
Rhy	IM6-372	T 253	9884	79.627	0.096	12.663	2.094	0.013	0.734	0.020	0.031	2.851	0.012	106.159	8589.331	90.751	4.334	116.475	2.192	13.792	88.982	2.180	37.176	0.334		0.034
Rhy	IM6-496	T 279	9885	83.474	0.116	11.472	1.090	0.006	0.501	0.005	0.055	2.358	0.016	105.452	8069.841	131.461	5.911	106.920	58.533	18.063	45.129	0.495	98.005			0.007
Rhy	IM6-574.5	T 255	9886	84.234	0.087	9.410	3.403	0.045	1.356	0.003	0.090	1.366	0.006	103.380	1814.692	108.328	5.835	57.076	0.669	58.039	55.585	2.169	72.077	1.491		0.074
Dac	IM6-652	T 264	9887	74.785	0.126	9.251	8.354	0.120	6.400	0.019	0.020	0.556	0.020	94.378	3890.621	155.833	4.504	16.796	3.520	143.703	64.423	4.036	48.739	1.797		0.071
Rhy	IM7-231.5	T 265	9888	61.643	0.260	28.083	0.635	0.004	1.803	0.238	0.096	6.784	0.030	99.781	4234.631	466.139	12.226	233.189	13.956	0.802	44.577	17.138	47.138			0.099
Rhy	IM7-167	T 285	9889	72.696	0.225	17.177	2.154	0.039	2.770	0.600	0.027	4.286	0.026	98.640	979.417	306.890	14.481	170.652		22.705	13.255	5.012	25.639			0.010
Rhy	IM7-93	T 284	9890	77.147	0.192	15.198	1.691	0.011	1.596	0.030	0.005	4.096	0.033	99.072	1421.838	167.496	6.394	202.886	4.622	72.257	26.338	3.791	36.443			0.010
Mona	IM5-161.5	T 283	9891	51.356	1.642	17.974	10.373	0.365	4.707	7.167	2.684	2.726	1.005	90.926	1277.393	420.012	230.636	86.000	0.178	32.573	15.265	42.991	60.564			0.015
Mona	IM5-157.4	T 282	9892	52.274	1.453	25.248	3.788	0.314	1.941	7.957	2.283	4.162	0.579	94.177	1009.131	347.357	205.824	171.560	0.918	1.070	40.926	27.260	78.502		1.572	0.001
Mona	IM6-150.2	T 281	9893	49.737	2.657	17.678	16.614	0.165	4.173	4.325	0.838	3.410	0.514	90.263	3393.721	311.322	56.151	81.407	65.596	105.297	31.762	48.129	79.488	2.026	36.830	0.001
Dac	IM6-424.0	T 280	9894	62.722	0.152	9.149	13.530	0.124	14.252	0.023	0.009	0.022	0.018	91.012	1178.452	29.229	4.391	<1	42.004	229.900	14.987	4.577	56.402			0.003
Dac	IM6-410.4	T 274	9895	74.229	0.043	7.477	11.915	0.122	6.109	0.006	0.052	0.043	0.004	95.457	643.478	27.245	4.238	<1		101.464	30.409	1.852	9.673			0.054
Rhy	IM6-393.5	T 270	9896	70.196	0.951	19.719	2.824	0.020	2.226	0.044	0.172	3.824	0.014	98.838	430.000	485.663	4.697	142.862	0.136	60.738	42.819	6.717	53.583	1.185		0.042
Dac	IM6-805	T 267	9897	60.871	0.118	8.740	19.206	0.222	9.940	0.018	0.020	0.525	0.020	109.709	3200.000	110.301	2.065	0.531	1.239	247.315	77.146	3.424	66.442	2.070		0.040
Rhy	IM7-312	T 287	9898	68.029	0.207	17.991	2.793	0.050	4.543	2.182	0.094	4.081	0.030	95.327	2160.000	332.177	22.349	149.153	5.729	23.875	45.620	5.791	40.952			0.038
Rhy	IM7-426	T 288	9899	71.089	0.086	18.599	3.284	0.023	2.775	0.023	0.031	4.087	0.003	100.722	703.934	164.905	8.590	78.654	1.132	36.708	43.605	2.631	49.115			0.030
Rhy	IM7-520	T 289	9900	59.697	0.310	27.960	1.886	0.008	3.663	0.225	0.076	5.836	0.037	97.676	3030.000	518.629	10.918	223.821	0.453	9.255	29.671	12.966	43.748			0.020
Rhy	IM7-640.5	T 290	9901	59.324	0.177	16.371	12.636	0.139	4.801	1.633	0.072	4.242	0.027	107.008	5775.689	49.476	4.400	4.618	1.436	93.354	13.621	4.989	24.261			0.004
Rhy	IM7-871	T 292	9902	76.802	0.149	15.544	1.315	0.063	1.509	0.750	0.049	3.789	0.030	101.572	830.577	319.935	13.327	145.851	278.255	5.344	47.404	3.134	60.613	0.235		0.009
Slate	IM7-1232	T 293	9903	36.175	0.242	14.379	28.062	0.392	19.202	0.651	0.292	0.015	0.030	89.579	5590.469	20.275	8.473	0.800	2.868	231.814	60.794	29.981	64.159	0.233		0.011
Rhy	IM7-1338	T 294	9904	70.143	0.135	21.540	0.967	0.022	1.152	0.311	0.135	5.120	0.003	100.615	4720.808	1224.076	13.970	207.525	0.143	3.795	20.415	7.317	36.646			0.018
Mona	IM7-1607	T 295	9905	70.242	0.601	14.861	6.021	0.138	1.788	1.224	3.446	1.587	0.092	96.990	976.699	300.984	220.584	81.565	16.715	36.346	34.322	7.039	53.678		4.358	0.003
Rhy	IM8-276	T 296	9906	62.977	0.264	23.445	4.242	0.203	3.141	1.101	0.069	4.515	0.041	99.554	1220.624	339.894	14.107	127.732	8.742	258.734	46.161	7.372	35.595			0.025
Rhy	IM8-315	T 297	9907	69.979	0.202	19.980	1.428	0.015	3.193	0.084	0.097	4.998	0.023	99.455	2264.012	495.621	9.701	135.986	3.556	547.210	55.391	4.836	31.799			0.033
Rhy	IM8-353	T 298	9908	76.248	0.176	13.980	2.125	0.032	3.860	0.054	0.036	3.463	0.025	99.509	531.173	393.071	9.761	106.121	0.932	665.201	30.119	5.854	24.648			0.004

LE 11 CONT.

ck	Sample	Powder	Pellet	MAJOR ELEMENT										Original Total	TRACE ELEMENT										
be	Number	Number	Number	SiO_2	TiO_2	Al_2O_3	Fe_2O_3	MnO	MgO	CaO	Na_2O	K_2O	P_2O_5		S	Ba	Sr	Rb	Cu	Zn	Pb	Ni	Co	Cd	Cr	Hg
y	IM8-427	T299	9909	77.834	0.158	13.732	1.040	0.036	1.546	0.701	0.006	4.932	0.015	102.368	1026.456	432.470	52.947	127.524		36.233	19.990	4.295	39.987			0.005
y	IM8-504	T300	9910	78.494	0.160	14.117	0.863	0.009	0.463	0.128	0.242	4.887	0.021	104.319	6429.543	671.111	21.457	109.730	0.939	1.022	34.290	4.208	29.692			0.073
y	IM8-616	T301	9911	65.564	0.261	22.504	1.737	0.003	3.745	0.123	1.539	4.486	0.038	95.849	113.943	666.325	40.599	105.786		19.811	32.265	7.480	25.948	0.448		0.002
y	IM8-767	T302	9912	68.065	0.212	21.202	1.715	0.008	3.977	0.111	0.341	4.340	0.026	96.951	627.542	625.735	17.167	141.208		47.226	49.927	6.528	17.213	2.043		0.020
y	IM8-894	T303	9913	74.764	0.103	15.709	2.019	0.043	3.555	0.050	0.124	3.630	0.003	98.056	946.009	794.135	11.623	147.899	4.469	430.809	76.525	5.869	31.288	0.652		0.119
y	IM9-505	T172	9914	79.393	0.064	16.496	0.381	0.010	0.294	0.004	0.026	3.326	0.006	104.489	1566.572	1290.233	12.651	77.659	1.602	9.225	40.715	6.836	35.663	1.059		0.184
y	IM9-2005	T195	9915	67.037	0.119	23.970	1.292	0.014	1.051	0.093	0.049	5.302	0.004	102.936	10689.005	625.476	13.820	195.336	33.784	766.655	162.156	14.095	63.457	2.624		1.033
y	IM9-2845	T190	9916	86.621	0.039	9.961	0.582	0.014	0.388	0.012	0.029	2.025	0.001	109.140	3281.462	159.751	7.553	86.929	7.418	198.833	168.958	1.275	142.828	0.910		0.153
y	IM9-4035	T167	9917	81.072	0.389	13.720	1.061	0.010	0.201	0.041	0.012	2.697	0.008	106.506	7892.334	419.050	13.324	89.950	118.408	17.686	8.033	28.218	125.670	3.008	13.377	0.119
y	F11	T304	9918	77.868	0.049	10.710	5.282	0.039	4.770	0.008	0.008	1.305	0.009	99.062	179.361	109.664	5.607	42.836	47.988	35.046	55.354	3.963	31.685			0.026
y	C4-1060	T305	9919	80.075	0.149	12.379	0.922	0.033	0.116	0.132	3.446	1.966	0.009	103.999	8082.203	877.084	100.403	51.995	4.063	131.809	59.539	4.410	75.669			1.005
c	M2-518	T202	9920	77.795	0.048	9.604	5.751	0.051	5.552	0.011	0.065	1.112	0.009	97.538	566.052	195.459	4.396	32.219	5.148	55.539	29.741	3.596	30.300	0.882		0.011
c	M2-1064	T201	9921	70.026	0.043	9.988	6.194	0.072	5.865	2.280	0.025	1.650	0.019	99.931	38375.713	137.152	55.009	52.461	28.055	403.649	78.935	5.826	28.777	0.838		1.018
y	M2-1461	T208	9922	73.217	0.036	7.078	2.658	0.154	3.632	5.933	0.225	5.117	0.003	98.344	19475.653	1100.536	432.240	82.215	16.919	34.975	71.504	3.666	46.699			3.475
c	M3-763	T307	9923	71.958	0.127	8.950	12.296	0.112	4.768	0.005	0.071	0.412	0.009	95.968	12825.287	68.585	2.822	10.372	3.476	88.800	40.726	3.284	16.036			0.010
y	M3-957	T145	9924	71.488	0.062	16.793	3.986	0.102	1.810	1.341	0.199	3.850	0.003	100.250	3840.259	268.491	16.262	110.191	17.472	29.088	33.203	7.718	43.296	0.931		0.045
y	M3-1148	T148	9925	82.885	0.043	9.842	2.425	0.055	1.007	0.317	0.033	2.139	0.004	106.125	12504.895	128.420	6.885	90.693	74.080	44.588	18.493	3.673	33.173	0.153		0.050
y	M5-27	T152	9926	79.986	0.132	11.209	3.128	0.009	0.887	0.043	0.024	2.315	0.016	106.640	22511.034	231.159	6.461	88.443	95.924	30.569	40.772	1.574	54.920	1.893		0.052
y	M5-189	T308	9927	75.234	0.104	15.277	3.272	0.004	0.997	0.033	0.133	3.129	0.010	97.883	18059.704	216.546	4.274	157.922	10.352	68.677	69.899	6.090	78.121			0.023
c	M7-674	T220	9928	70.014	0.140	9.916	9.657	0.019	9.679	0.017	0.062	0.388	0.017	94.148	538.099	66.110	4.132	12.846	3.541	91.088	29.565	4.857	32.791	0.087		0.038
c	M7-767	T291	9929	74.772	0.137	11.930	6.716	0.077	4.421	0.002	0.053	1.870	0.022	95.223	1620.000	181.926	4.011	60.761	0.139	38.559	19.803	3.104	22.645			0.003
y	M10-249	T72	9930	63.381	0.901	20.093	7.495	0.203	1.773	0.762	1.348	3.805	0.238	96.463	1242.762	647.967	74.207	122.736	79.354	699.42	22.323	61.305	46.543	5.641	21.096	0.045
y	H14-257	T67	9931	88.029	0.054	9.404	0.303	0.001	0.280	0.007	0.020	1.898	0.004	107.935	1479.208	73.713	5.051	77.592	13.618	224.039	1921.130	1.367				0.233
y	H14-454	T74	9932	57.343	0.145	23.108	6.655	0.030	7.883	0.109	0.128	4.596	0.003	94.380	306.065	258.149	11.201	143.014	80.850	290.622	11.549	2.113	32.857	6.516		0.096
y	H14-548	T69	9933	74.998	0.081	16.336	1.389	0.019	3.216	0.166	0.016	3.775	0.004	100.462	254.022	246.297	8.642	172.923	160.579	135.678	71.718	21.176	15.009			0.026
ac	H16-357	T149	9934	58.756	0.252	17.998	2.764	0.054	6.770	0.874	0.025	2.477	0.030	94.472	447.880	673.924	30.507	87.235	92.375	83.004	33.883	33.387	50.171	4.162		0.044
ac	H16-421	T155	9935	61.570	0.782	17.330	6.343	0.021	11.010	0.121	0.884	1.850	0.088	91.922	184.611	886.758	19.991	57.836	108.915	260.197	31.931	76.523	96.888	4.658	88.870	0.068
ac	H38-701	T309	9936	50.122	2.405	20.001	16.493	0.393	5.926	0.488	0.001	3.743	0.428	91.561	2149.485	452.042	9.258	57.395	1281.418	190.650	23.977	59.271	73.399	0.876	261.198	0.006
hy	283919	T133	9937	75.866	0.663	14.047	4.015	0.028	1.057	0.050	0.061	4.100	0.112	99.685	279.371	511.303	5.512	171.374	75.075	79.658	26.403	13.418	36.040	0.585		0.067
hy	483913	T305	9938	82.088	0.053	13.687	0.774	0.009	0.282	0.007	0.178	2.917	0.005	104.531	139.327	549.969	6.838	102.243	3.183	0.490	37.215	3.001	36.428			0.004

Table 12 Bulk Chemical Analyses - Calculated Values

Pellet No	9879	9880	9881	9882	9883	9884	9885	9886	9887	9888	9889	9890
CIPW Norm												
Qtz	59.53	12.46	63.29	36.76	71.16	68.71	73.86	76.47	63.23	32.15	50.80	59.09
Cor	11.54	-	11.91	18.48	7.97	9.70	8.93	7.79	8.67	20.31	11.46	10.78
Or	22.06	10.78	20.57	37.73	14.90	17.17	14.05	8.07	3.30	40.26	25.33	24.20
Ab	0.13	14.88	1.64	1.75	0.83	0.27	0.47	0.76	0.17	0.82	0.23	0.05
An	0.23	27.27	0.11	0.04	1.53	0.02	0.08	0.02	0.04	0.99	2.81	0.07
En-Hy	5.12	14.91	1.80	2.64	1.94	1.86	1.51	3.38	15.99	4.51	6.90	3.97
Il	0.03	0.35	0.02	0.02	0.03	0.03	0.01	0.10	0.24	0.01	0.08	0.02
Hm	1.27	14.11	0.68	2.35	1.50	2.13	1.10	3.40	8.36	0.64	2.15	1.69
Ru	0.08	0.85	0.15	0.25	0.08	0.08	0.11	0.04	-	0.26	0.18	0.18
Ap	0.01	1.42	0.05	0.06	0.04	0.03	0.04	0.01	0.05	0.07	0.06	0.08
Tn	-	2.98	-	-	-	-	-	-	-	-	-	-
Mt	-	-	-	-	-	-	-	-	0.03	-	-	-
Niggli No												
Fm	25.6	50.5	11.9	14.7	20.7	22.3	17.1	41.5	13.1	13.0	29.9	24.0
Al	58.8	22.5	70.1	66.4	60.7	62.1	67.3	49.8	25.1	67.8	52.4	58.7
C	0.4	19.6	0.0	0.1	3.2	0.2	0.1	0.0	0.1	1.0	3.3	0.2
Alk	15.2	7.4	18.0	18.7	15.4	15.4	15.5	8.6	1.7	18.1	14.3	17.2
Si	490.0	131.7	587.1	280.4	750.2	662.9	831.2	757.1	343.4	252.733	376.559	505.365
Mg	0.760	0.454	0.674	0.471	0.505	0.408	0.520	0.437	0.599	0.848	0.714	0.650
K	0.99	0.41	0.92	0.95	0.94	0.98	0.97	0.91	0.95	0.979	0.991	0.998
D.I.	81.72	38.13	85.50	76.24	86.89	86.15	88.38	85.30	66.70	73.23	76.36	83.34
Rock Type	Rhy	Dac	Rhy	Rhy	Rhy	Rhy	Rhy	Rhy	Dac	Rhy	Rhy	Rhy

Table 12 continued

Pellet No	9891	9892	9893	9894	9895	9896	9897	9898	9899	9900	9901	9902
CIPW Norm												
Qtz	5.79	4.76	21.37	41.35	64.44	51.19	44.09	40.50	51.09	31.18	32.28	58.25
Cor	-	3.91	-	9.11	7.34	15.25	8.18	9.62	14.09	21.26	8.81	10.07
Or	16.10	24.59	20.21	0.13	0.25	22.60	3.11	24.11	24.15	34.59	25.21	22.39
Ab	22.70	19.31	7.11	0.08	0.44	1.46	0.17	0.80	0.26	0.64	0.61	0.41
An	28.93	35.68	18.15	-	-	0.13	0.04	10.63	0.09	0.88	7.97	3.52
En-Hy	11.71	4.83	4.52	35.49	15.21	5.54	24.83	11.31	6.91	9.15	12.02	3.76
Il	0.78	0.67	0.35	0.27	0.08	0.04	0.22	0.11	0.05	0.02	0.30	0.13
Hm	10.37	3.79	16.21	13.53	11.73	2.82	19.00	2.79	3.28	1.89	12.71	1.31
Ru	1.22	1.10	2.48	0.01	-	0.94	-	0.15	0.06	0.30	0.02	0.08
Ap	2.38	1.37	1.22	0.04	0.01	0.03	0.05	0.07	0.01	0.09	0.06	0.07
Tn	0.03	-	-	-	-	-	-	-	-	-	-	-
Mt	-	-	-	-	0.27	-	0.38	-	-	-	-	-
Niggli No												
Fm	40.1	17.5	50.7	85.3	80.2	27.7	84.2	36.3	32.7	25.1	54.2	20.9
Al	28.1	43.4	28.5	14.6	19.4	58.9	14.7	43.2	54.1	60.1	31.2	58.3
C	20.3	24.9	12.7	0.1	0.0	0.2	0.1	9.5	0.1	0.9	5.7	5.1
Alk	11.5	14.2	8.2	0.1	0.3	13.2	1.0	11.0	13.0	13.9	9.0	15.7
Si	136.088	152.502	136.052	169.701	327.559	355.767	174.048	277.148	351.123	217.902	191.674	488.618
Mg	0.464	0.481	0.336	0.674	0.501	0.608	0.503	0.759	0.624	0.793	0.426	0.683
K	0.401	0.545	0.728	0.617	0.352	0.936	0.945	0.966	0.989	0.981	0.975	0.981
D.I.	44.61	48.67	48.69	41.56	65.35	75.25	47.37	65.43	75.50	66.41	58.10	81.05
Rock Type	Mona	Mona	Mona	Dac	Dac	Rhy	Dac	Rhy	Rhy	Rhy	Rhy	Rhy

Table 12 continued

Pellet No	9903	9904	9905	9906	9907	9908	9909	9910	9911	9912	9913	9914
CIPW Norm												
Qtz	12.21	47.61	39.10	38.37	45.42	56.99	55.16	57.89	33.71	43.38	54.76	66.08
Cor	-	15.29	5.47	16.54	14.31	10.13	7.15	8.30	14.98	15.80	11.49	12.86
Or	0.09	30.40	9.38	26.68	29.53	20.46	29.14	29.06	26.51	25.65	21.45	19.65
Ab	2.49	1.15	29.15	0.58	0.82	0.30	0.05	2.06	13.02	2.89	1.05	0.22
An	2.87	1.53	5.47	5.19	0.27	0.10	3.38	0.50	0.36	0.38	0.23	0.02
En-Hy	35.38	2.88	4.45	7.82	7.95	9.61	3.85	1.09	9.33	9.90	8.85	0.73
Il	0.46	0.05	0.30	0.43	0.03	0.07	0.08	0.02	0.01	0.02	0.09	0.02
Hm	27.83	0.97	6.02	4.24	1.43	2.12	1.04	0.87	1.74	1.72	2.02	0.38
Ru	-	0.11	0.45	0.04	0.19	0.14	0.12	0.15	0.26	0.20	0.05	0.05
Ap	0.07	0.01	0.22	0.10	0.05	0.06	0.04	0.05	0.09	0.06	0.01	0.01
Tn	-	-	-	-	-	-	-	-	-	-	-	-
Mt	0.58	-	-	-	-	-	-	-	-	-	-	-
Niggli No												
Fm	84.2	13.0	33.6	31.0	27.8	41.2	20.6	10.0	28.0	31.5	36.8	5.8
Al	14.2	67.2	40.3	53.2	56.1	46.0	53.5	63.4	53.8	54.5	49.8	77.1
C	1.1	1.8	6.0	4.5	0.4	0.3	5.0	1.0	0.5	0.5	0.3	0.0
Alk	0.5	18.0	20.0	11.3	15.6	12.5	20.9	25.6	17.7	13.5	13.1	17.0
Si	60.816	371.426	323.219	242.353	333.394	425.566	515.093	598.566	266.142	296.787	401.995	629.889
Mg	0.572	0.697	0.364	0.582	0.814	0.780	0.739	0.497	0.810	0.820	0.773	0.597
K	0.033	0.961	0.233	0.977	0.971	0.984	0.998	0.930	0.657	0.893	0.951	0.988
D.I.	14.79	79.16	77.64	65.63	75.77	77.75	84.35	89.01	73.24	71.92	77.26	85.95
Rock Type	Slate	Rhy	Mona	Rhy	Rhy	Rhy	Rhy	Rhy	Rhy	Rhy	Rhy	Rhy

Table 12 continued

Pellet No	9915	9916	9917	9918	9919	9920	9921	9922	9923	9924	9925	9926
CIPW Norm												
Qtz	45.19	78.36	70.88	65.73	52.50	64.89	51.99	40.66	63.66	50.23	73.25	71.22
Cor	18.19	7.73	10.81	9.29	4.40	8.30	4.22	-	8.50	9.91	6.99	8.82
Or	31.67	12.01	16.06	7.71	11.71	6.57	10.14	30.84	2.52	22.84	12.80	13.99
Ab	0.42	0.25	0.10	0.07	29.39	0.55	0.22	1.94	0.61	1.69	0.28	0.21
An	0.44	0.05	0.15	0.02	0.60	-	11.63	3.25	0.03	6.66	1.57	0.11
En-Hy	2.65	0.97	0.50	11.88	0.29	13.82	15.19	-	12.03	4.52	2.54	2.26
Il	0.03	0.03	0.02	0.08	0.01	0.09	0.08	0.07	0.24	0.12	0.08	0.02
Hm	1.31	0.58	1.07	5.23	0.93	5.73	6.36	2.43	12.46	3.88	2.42	3.20
Ru	0.10	0.02	0.38	0.01	0.15	-	-	-	-	-	-	0.12
Ap	0.01	-	0.02	0.02	0.02	0.02	0.05	0.01	0.02	0.01	0.01	0.04
Tn	-	-	-	-	-	-	-	-	-	-	-	-
Mt	-	-	-	-	-	0.03	0.11	0.41	-	0.15	0.06	-
Niggli No												
Fm	12.6	12.5	10.1	60.7	6.7	66.2	58.9	35.0	74.5	29.2	30.9	31.1
Al	69.9	71.3	73.7	34.6	56.5	29.7	25.7	19.4	23.9	50.1	53.2	55.8
C	0.5	0.2	0.4	0.0	1.1	0.1	10.7	29.5	0.0	7.3	3.1	0.4
Alk	17.0	16.0	15.8	4.6	35.6	4.0	4.7	16.2	1.5	13.4	12.8	12.7
Si	331.816	1052.512	739.271	426.982	620.784	407.599	306.253	339.740	326.079	361.977	759.930	675.923
Mg	0.614	0.562	0.271	0.642	0.199	0.654	0.649	0.718	0.432	0.468	0.445	0.359
K	0.986	0.979	0.993	0.991	0.273	0.918	0.977	0.937	0.796	0.927	0.977	0.984
D.I.	77.28	90.62	87.04	73.15	93.60	72.01	62.35	73.44	66.89	74.76	86.33	85.42
Rock Type	Rhy	Rhy	Rhy	Rhy	Rhy	Dac	Dac	Rhy	Dac	Rhy	Rhy	Rhy

Table 12 continued

Pellet No	9927	9928	9929	9930	9931
CIPW Norm					
Qtz	62.08	53.76	60.78	37.37	80.23
Cor	11.85	9.40	9.87	12.94	7.31
Or	18.83	2.29	11.05	22.49	11.22
Ab	1.15	0.52	0.45	11.40	0.17
An	0.10	0.03	0.13	2.22	0.01
En-Hy	2.53	24.10	11.01	4.41	0.70
Il	0.01	0.23	0.16	0.43	-
Hm	3.33	9.66	6.72	7.49	0.30
Ru	0.10	0.02	0.05	0.67	0.05
Ap	0.02	0.04	0.05	0.56	0.01
Tn	-	-	-	-	-
Mt	-	-	-	-	-
Niggli No					
Fm	26.1	77.9	58.6	34.0	
Al	59.6	20.9	35.2	47.7	
C	0.2	0.1	0.0	3.3	
Alk	14.1	1.1	6.2	15.0	
Si	497.817	250.501	374.197	255.122	
Mg	0.376	0.662	0.563	0.313	
K	0.939	0.805	0.959	0.650	
D.I.	82.06	56.57	72.28	71.27	91.62
Rock Type	Rhy	Dac	Dac	Rhy	Rhy

APPENDIX E

STATISTICAL TECHNIQUES

The geochemical analytical results for both major elements and trace elements, were subjected to statistical analysis using the I.C.L. 1900 Statistical Analysis Package Mark2 computer programme. Two types of statistical analysis were carried out, these were: (1) Principal Component Analysis, and (2) Factor Analysis.

Principal Component Analysis is used to find linear combinations of variables with large variance in a set of experimental results. Initially the number of observed variables in an experiment may be large, and these need to be reduced as the deviations found in the experiments are commonly of most interest. One way of reducing the number of variables to be considered is to discard the linear combinations (components) of variables that have small variance, and to study only those components with large variance. Principal Component Analysis defines those elements with large variations and those with strong variations (Tables 15 and 18). These elemental deviations and variations were interpreted for the Parys Mountain rocks in terms of such geological controls as lithology, mineralization, etc.

Factor Analysis is a multivariate analsis which attempts to explain the common variance of observations in a set of variables as the sum of the variances of a smaller, ordered, set of uncorrelated factors. This analysis, applied to the geochemical data from the Parys Mountain rocks, picks out elements, which show similar or opposite variation trends but have a relatively small variance. This allows the correlation of elements which would

otherwise be discarded (Tables 16 and 19). The significance of these correlations with respect to the mineralization, and other geological events, in the area can thus be studied.

Table 13A Statistical Data for 289 Samples.

Element	Mean	Min.Value	Max.Value	Standard Deviation
Al	8.27	0.06	24.78	6.20
Ba	427.79	2.17	3301.00	585.60
Cd	8.14	0.00	363.00	34.37
Co	97.51	0.00	1135.00	123.70
Cr	9.96	0.00	314.00	30.92
Cu	1875.64	0.00	33584.00	4857.42
Fe	4.67	0.08	39.75	5.42
Hg	0.30	0.00	6.68	0.62
Ni	24.82	0.00	475.00	50.93
Pb	1483.56	12.80	58048.00	5939.86
Si	75.88	21.95	97.71	15.54
Sr	66.11	1.07	619.00	61.92
Zn	2811.47	0.34	99999.00	11194.30

Table 13B Statistical Data for 61 Samples.

Element	Mean	Min.Value	Max.Value	Standard Deviation
Si	70.70	36.31	89.01	10.55
Ti	0.36	0.04	2.67	0.58
Al	15.64	7.08	28.09	5.26
Fe	4.98	0.30	28.17	5.55
Mn	0.08	0.00	0.39	0.10
Mg	3.57	0.12	19.28	3.58
Ca	0.81	0.00	8.00	1.84
Na	0.37	0.00	3.45	0.80
K	3.13	0.01	6.79	1.65
P	1.81	0.00	104.53	13.49
S	4856.24	113.91	38375.70	7208.27
Ba	383.12	20.28	1290.00	290.04
Sr	33.08	2.07	432.24	71.50
Rb	102.92	0.00	233.19	60.96
Cu	48.39	0.00	1261.42	166.44
Zn	125.59	0.49	767.00	162.52
Pb	79.09	8.00	1921.00	244.68
Ni	11.12	0.50	61.31	14.50
Co	50.45	0.00	147.90	29.91
Cd	0.86	0.00	6.52	1.43
Cr	7.34	0.00	261.20	35.67
Hg	0.15	0.00	3.48	0.49

Table 14 Total Variance for Principal Component Analysis of 289 Samples.

Component Number	Eigenvalue or Component Variance	Percent of Total Variance	Accumulated Value as Percent of Total Variance
1	3.254	25.03	25.03
2	2.410	18.54	43.57
3	1.765	13.58	57.15
4	1.418	10.90	68.05
5	1.083	8.33	76.38
6	0.916	7.05	83.43
7	0.679	5.23	88.65
8	0.536	4.12	92.77
9	0.365	2.81	95.58
10	0.268	2.07	97.65
11	0.166	1.27	98.92
12	0.111	0.85	99.77
13	0.029	0.23	100.00

Table 15 Matrix of Principal Component Analysis Accounting for 76.38 percent of Total Variance for 289 Samples.

Component No.	1	2	3	4	5
Al	.268	.405	.315	.070	.166
Ba	.199	.094	.406	.458	-.187
Cd	-.494	.033	.234	.096	.151
Co	-.132	-.018	-.539	.410	.081
Cr	-.023	.413	-.026	.089	.234
Cu	-.325	.043	-.202	-.105	-.522
Fe	-.089	.438	-.264	-.214	-.376
Hg	.031	-.075	.150	.537	-.559
Ni	-.005	.224	-.401	.471	.300
Pb	-.497	.006	.200	.077	.079
Si	.050	-.588	-.060	.073	.112
Sr	-.012	.244	.044	-.123	-.038
Zn	-.512	.023	.225	.079	.131

Component 1 : Zn, Pb, Cd, Cu

Component 2 : Fe, Cr, Al vs Si

Component 3 : Ba, Al vs Co, Ni

Component 4 : Hg, Ni, Ba, Co

Component 5 : Ni vs Hg, Cu, Fe

Table16 Matrix of Factor Loadings for 289 Samples.

Factor	1	2	3	4	5	6	7
Eigenvalue	71.480	16.309	7.125	3.085	1.671	1.056	0.519
Variance	0.116	0.063	0.019	0.028	0.011	0.013	0.001
Al	.288	.732	.474	.064	.069	.061	.023
Ba	.163	.237	.550	.189	-.474	-.041	-.019
Cd	-.920	.030	.058	.025	.018	-.015	-.100
Co	-.084	-.171	-.453	.645	-.008	.036	-.001
Cr	-.065	.457	-.078	.153	.096	.009	-.073
Cu	-.371	-.022	-.474	-.101	-.231	-.031	.094
Fe	-.026	.583	-.657	-.142	-.128	.080	-.039
Hg	.010	-.081	.123	.179	-.601	-.149	-.036
Ni	.037	.192	-.232	.728	.131	-.022	.040
Pb	-.851	-.011	-.007	-.012	-.043	.042	.193
Si	.118	-.918	.185	.028	.006	.032	-.003
Sr	-.026	.265	-.054	-.050	.136	-.654	.063
Zn	-.953	.011	.027	-.001	.002	.004	.010

Factor 1 : Zn, Cd, Pb, Cu

Factor 2 : Al, Fe, Cr vs Si

Factor 3 : Ba, Al vs Fe, Cu, Co

Factor 4 : Ni, Co

Factor 5 : Hg, Ba, Cu

Factor 6 : Sr

Factor 7 : Pb

Table 17 Total Variance for Principal Component Analysis on 61 Samples.

Component No.	Component Variance	Accumulated Value as percent of Total Variance
1	5.226	23.75
2	3.608	40.15
3	2.644	52.17
4	1.723	60.00
5	1.560	67.09
6	1.201	72.55
7	1.119	77.64
8	1.075	82.52
9	0.862	86.44
10	0.768	89.93
11	0.554	92.44
12	0.431	94.40
13	0.391	96.18
14	0.222	97.19
15	0.185	98.03
16	0.153	98.72
17	0.106	99.20
18	0.070	99.52
19	0.050	99.75
20	0.032	99.89
21	0.020	99.99
22	0.003	100.00

Table 18 Matrix of Principal Component Analysis Accounting for 82.52 percent of Total Variance for 61 Samples.

Component No.	1	2	3	4	5	6	7	8
Si	.36	.08	.07	.25	.26	.10	.08	.08
Ti	-.36	-.16	-.03	.02	.22	-.03	.00	.17
Al	-.07	-.41	-.24	-.25	-.15	-.09	-.05	-.01
Fe	-.34	.28	-.02	-.10	-.11	-.06	-.08	-.09
Mn	-.38	.07	.09	-.06	.02	-.16	-.06	-.07
Mg	-.25	.28	-.06	-.15	-.34	.05	.05	-.19
Ca	-.26	-.16	.37	-.12	.06	-.10	-.05	.11
Na	-.18	-.16	.29	-.17	.22	.22	.19	.21
K	.09	-.46	-.10	-.04	-.13	-.23	-.11	-.09
P	.05	.00	.00	-.02	.28	.13	.18	-.59
S	.06	.04	.23	.33	-.22	-.12	-.46	.07
Ba	.02	-.34	.07	.15	-.10	.26	.28	-.30
Sr	-.15	-.18	.50	.07	-.03	-.02	.08	-.07
Rb	.15	-.42	-.14	-.10	-.06	-.13	-.13	.08
Cu	-.22	-.05	-.26	.47	.18	-.18	-.07	-.10
Zn	-.02	.04	-.12	.11	-.51	-.10	.28	.16
Pb	.08	.07	.03	.11	.10	-.44	.57	.38
Ni	-.36	-.15	-.10	.06	.06	.07	.11	.07
Co	-.08	-.07	-.01	.22	.00	.51	-.26	.39
Cd	-.08	-.05	-.19	.12	-.29	.46	.29	.09
Cr	-.26	-.06	-.26	.44	.15	-.10	.01	-.10
Hg	.01	-.09	.42	.36	-.32	-.09	.08	-.20

Component 1 : Si vs Mn, Ni, Ti, Fe
Component 2 : K, Rb, Al, Ba
Component 3 : Sr, Hg, Ca, Na
Component 4 : Cu, Cr, Hg, S
Component 5 : Zn, Mg, Hg, Cd
Component 6 : Co, Cd vs Pb
Component 7 : Pb vs S
Component 8 : Co, Pb vs P, Ba

Table 19 Matrix of Factor Loadings for 61 Samples.

Factor	1	2	3	4	5	6	7
Eigenvalue	165.398	63.433	36.116	32.664	12.170	3.648	3.035
Variance	0.052	0.068	0.029	0.017	0.006	0.002	0.002
Si	.91	.01	.10	.09	.04	.01	.01
Ti	-.66	.03	.22	.38	.44	-.15	-.10
Al	-.47	-.80	.06	-.10	.00	.07	.00
Fe	-.68	.65	.01	-.19	-.02	-.06	.06
Mn	-.74	.40	-.05	.22	.07	.12	.30
Mg	-.57	.54	-.10	-.36	-.29	.12	-.14
Ca	-.50	.05	-.47	.52	.34	-.14	.08
Na	-.29	-.04	-.31	.39	.43	.44	-.13
K	-.10	-.90	-.01	.16	-.16	-.21	.12
P	.13	-.01	.04	.01	.06	.04	.02
S	.18	.11	-.16	.18	-.28	-.29	.02
Ba	-.01	-.46	-.08	.38	-.19	.12	-.36
Sr	-.20	.03	-.56	.72	-.04	.14	.05
Rb	.07	-.89	.01	.03	.00	-.12	.10
Cu	-.35	.09	.77	.40	-.19	.03	.12
Zn	-.12	.01	.03	-.14	-.29	-.10	-.23
Pb	.23	.06	.04	.05	.04	-.05	-.01
Ni	-.72	.01	.25	.31	.25	.00	-.19
Co	-.08	.01	.11	.16	.10	.01	-.19
Cd	-.17	-.08	.14	-.06	-.09	.09	-.45
Cr	-.44	.11	.74	.39	-.14	.05	-.05
Hg	.09	.06	-.44	.61	-.53	-.17	-.14

Factor 1 : Si vs Mn, Ni, Fe, Ti, Mg, Ca, Al, Cr, Cu, Na
Factor 2 : Fe, Mg, Mn vs K, Rb, Al, Ba
Factor 3 : Cu, Cr vs Sr, Ca, Hg, Na
Factor 4 : Sr, Hg, Ca, Cu, Na, Cr, Ba, Ti, Ni vs Mg
Factor 5 : Ti, Na, Ca, Ni vs Hg, Zn, Mg, S
Factor 6 : Na vs S, K
Factor 7 : Mn vs Cd, Ba

Table 20 Matrix of Principal Component Co-ordinates for Borehole C4.

Component No.	1	2	3	4	5
Depth (feet)					
700	.84	3.18	.26	-.13	.78
710	.83	3.43	.04	-.03	.37
720	.96	3.20	.18	.49	.78
735	-.30	5.43	-.70	-.43	.59
745	-.02	2.92	-.11	-.67	-.28
755	.39	2.11	-.30	-.61	-.09
773	-11.01	2.58	2.15	1.22	1.00
785	.01	6.92	-1.04	.89	2.28
803	.04	.86	-.77	-.11	.88
813	-2.60	.73	.27	-.60	-.49
830	-2.33	-.33	.44	-.83	-.41
845	-.38	.69	.23	-.97	.01
861	-3.72	-.33	1.18	-.43	.25
871	-4.02	.48	.50	.38	1.41
881	.03	.12	-.54	-.29	-.18
891	.43	-.31	.24	-.70	.16
906	-2.97	-1.06	.74	-.53	.51
930	-9.22	-.03	2.89	.67	1.49
940	-.15	-.97	-.48	-.16	.23
950	-.28	-1.72	-.10	-.53	-.20
960	-.78	-1.29	-.53	.41	-1.70
970	-.92	-1.35	-.30	.91	-.94
981	-.49	.39	-1.19	.16	.67
991	-.68	-.87	.24	.41	-.97
1001	-1.56	-1.88	.36	.22	-.63
1011	-.70	-1.82	-.74	.08	-.86
1021	-.44	-2.11	.09	.13	-.26
1031	-5.61	-.51	1.14	.71	1.60
1040	-4.43	.66	.28	.81	1.55
1050	.48	-.48	-.06	.48	.41
1063	1.17	.18	1.51	1.01	-.52
1070	.67	.30	.66	-.74	.32
1078	.76	.51	.50	.18	.48

Table 21 Matrix of Factor Scores for Borehole C4.

Factor	1	2	3	4	5	6	7
Depth (feet)							
700	1.05	4.67	.12	.58	.92	-.89	.06
710	1.11	5.11	-.31	.68	.61	-.54	.04
720	1.22	4.72	.26	1.14	.56	-.46	.00
735	-.50	7.36	-2.45	.61	.83	.35	-.34
745	-.09	4.37	-1.22	-.10	.52	-.75	.09
755	.66	3.19	-.90	-.05	.52	-.28	.03
773	-18.95	2.25	-3.11	.71	-.02	-1.22	.14
785	-.16	8.59	-2.23	2.35	1.40	-.14	-.69
803	.20	.72	-.80	.48	.84	-.36	-.15
813	-4.25	.89	-1.72	-.81	-.17	.13	.18
830	-3.79	-.66	-.98	-1.13	-.02	-.08	.26
845	-.65	1.02	-.44	-.84	.45	-.24	.05
861	-1.64	-.72	-.70	-.97	.06	-.19	.26
871	-6.85	.00	-1.17	.45	.64	-.27	.42
881	.25	.02	-.77	-.08	.17	-.22	-.01
891	.68	-.32	.36	-.73	.33	-.01	-.05
906	-5.04	-1.81	-.47	-.86	.34	-.09	.21
930	-16.24	-.55	-1.04	-.44	-.03	.39	.38
940	-.05	-1.54	-.32	-.03	.23	.06	-.02
950	-.27	-2.57	-.07	-.82	.00	.11	-.02
960	-.86	-2.10	-1.03	-.17	-1.17	-.26	.06
970	-1.32	-2.17	-.56	.31	-.97	-.11	.01
981	-.47	-.19	-1.37	.81	.64	-.45	-.09
991	-1.11	-1.28	-.20	-.31	-.89	-.17	-.05
1001	-2.41	-2.91	-.13	-.58	-.70	-.07	.47
1011	-.69	-2.91	-.86	-.18	-.55	.14	.04
1021	-.63	-3.14	.28	-.45	-.36	.07	-.01
1031	-9.75	-1.30	-.83	.45	.51	-.11	.29
1040	-7.50	.05	-1.42	1.01	.62	-.32	.43
1050	.72	-.64	.58	.54	.06	.01	-.02
1063	1.34	.76	2.22	.13	-1.04	-.49	.01
1070	.88	.71	.86	-.71	.53	-.48	.05
1078	.97	.97	1.03	.28	.24	-.35	.06

Table 22 Matrix of Factor Scores for Borehole M10

Factor	1	2	3	4	5	6	7
Depth (feet)							
1279	.77	2.44	-.39	.44	.29	-.13	-.06
1289	1.23	3.31	.73	.57	.44	-.20	-.02
1299	-.35	-2.32	-.76	.13	-.08	.20	.09
1311	-1.75	3.46	-.63	-.65	-1.11	.24	.13
1318	1.37	4.77	1.30	1.29	-1.06	.30	-.10
1332	-.34	-1.66	-1.07	-.09	-.44	.01	.08
1357	-.40	-2.25	-1.94	.88	.14	-.07	.14
1388	-.42	-1.82	-1.38	-.31	-.06	.39	.08
1408	-1.57	-2.71	-2.07	.46	-.21	-.01	.22
1421	-.56	-2.58	-.65	-.31	-.18	-.34	.04
1431	-1.96	-2.17	-1.03	-.52	.14	-.09	.03
1441	-1.23	-2.77	-.80	-.31	-.28	-.11	.08
1451	-1.35	-2.86	-.41	.24	-.47	.05	.04
1472	.51	-2.14	.08	-.52	.48	-.28	-.01
1486	-3.61	-1.84	-3.80	-.74	-1.28	-.38	.62
1491	-.26	-1.60	-.84	-.13	.24	.33	-.08
1501	.10	-1.55	-1.26	-.43	.26	-.57	.04
1529	.57	-.80	.61	-.19	-.08	-.28	.01
1548	-16.27	-.21	-4.57	-.97	-1.75	.33	.20
1562	-.81	-2.47	-.83	.08	.22	.17	.04
1584	-5.00	-2.34	.06	-.24	-1.16	-.03	.07
1589	-27.08	-.45	-.91	-.48	-.34	.59	.10
1599	-.53	-2.81	-1.13	.73	.37	.24	.09

Table 23 Matrix of Factor Scores for Borehole IM9.

Factor	1	2	3	4	5	6	7
Depth (feet)							
51	1.11	1.49	1.88	-.31	-.44	.58	-.11
59	1.33	.50	2.30	.06	-1.26	.15	-.11
72	1.23	-.65	2.28	-.05	-.91	.37	-.11
77	1.88	.41	3.98	.49	-2.25	.16	-.15
85	1.64	.52	3.24	1.03	-1.89	-.31	-.08
97	1.38	.19	3.35	1.84	-4.96	-2.14	-.21
107	1.63	-.90	4.15	1.89	-7.77	-1.57	-.49
119	2.07	1.88	4.42	1.27	-4.21	-.53	-.23
145	.78	-1.59	.85	-.28	-.25	.10	-.08
158	1.43	.48	2.46	.25	-1.10	.25	-.10
167	1.51	.77	2.48	.27	-.81	.31	-.07
175	1.07	-.95	1.40	-.29	-.03	.36	-.06
197	1.05	-.86	1.31	-.42	.10	.07	.00
204	.95	.44	1.17	-.15	.26	-.30	.02
215	.98	-.96	1.16	-.42	-.05	.43	-.07
225	.92	-.96	1.07	-.47	.04	-.39	-.09
231	.76	-.78	.88	-.55	.17	.35	-.05
244	.93	.72	.90	-.36	.07	.24	-.03
251	.77	-.03	1.03	-.16	-.18	-.03	-.09
265	.63	-.85	.73	-.59	-.01	.30	-.05
299	.71	-1.13	.84	-.67	.42	.51	-.06
320	.70	-.94	.81	-.60	.34	.43	-.06
334	.83	-1.25	.71	-.36	.46	-.26	.01
355	.76	-.56	.66	-.41	.50	-.03	.00
376	.87	.23	1.01	-.54	.11	.28	-.03
384	1.23	-.34	1.65	-.16	.09	.42	-.05
403	.94	.02	1.14	-.12	.07	.29	-.04
423	1.22	1.33	1.45	.23	-.60	-.18	.02

Table 24 Matrix of Factor Scores for Borehole H17A.

Factor	1	2	3	4	5	6	7
Depth (feet)							
1191	1.02	3.90	.17	.35	.60	-1.04	.04
1201	1.19	4.74	.41	.87	.59	-.17	-.05
1216	1.14	3.60	.15	.57	.37	.12	-.03
1231	.01	-1.10	-1.19	-1.15	-.09	.11	-.01
1241	.10	-2.16	-4.72	8.44	.79	.46	.19
1251	.36	-1.62	-.46	-1.19	.72	-1.34	.10
1261	.07	-2.97	-2.18	2.36	.40	.56	-.01
1271	-.32	-1.17	-1.44	-1.35	.20	-1.72	.29
1281	-.91	-2.30	-1.92	-1.39	-.31	.03	.30
1291	-1.73	-.09	-4.78	-.06	-1.07	-1.07	.41
1301	.00	-2.50	-1.92	1.67	.36	.55	.00
1331	.12	-1.04	-1.01	-1.10	-.13	-.55	.00
1341	.24	-2.86	-.78	.74	.14	.16	-.08
1351	-.27	-3.62	-4.52	5.06	.33	.83	-.11
1361	.27	-2.38	-1.11	.06	.45	.06	-.04
1371	-1.01	-2.41	-2.78	1.10	-.14	.59	.04
1381	.37	-2.90	-.65	.36	.50	.24	-.05
1391	.68	.90	-.97	.33	.03	.30	-.13
1401	-.02	-1.83	.02	-.40	.26	-.21	.07
1411	-.13	-2.90	-2.06	1.25	.15	.54	.00
1421	.39	-1.82	-3.95	9.01	.39	-.39	.25
1431	-1.02	-.53	-2.50	-.50	-1.06	.29	.27
1441	.56	.43	-.87	-.86	.46	-.05	-.06
1451	1.71	5.15	2.46	2.32	-1.27	.07	-.40
1461	-.31	-2.87	-2.43	2.97	-2.23	-.32	-.13
1471	.49	1.20	-1.31	-.66	.20	.54	-.13
1481	-.17	8.44	-5.53	-.37	-.05	.26	-.26
1491	.21	3.10	-2.68	-.35	-.41	.48	-.11
1501	-.90	4.67	-5.86	.02	-.92	.75	.02
1511	.78	-.61	.31	.60	.22	.30	-.07
1521	.22	-.13	-4.40	9.53	1.23	.44	.31
1531	.77	.66	.51	.28	.58	.49	-.26
1541	.69	3.74	-.45	.66	.39	.51	-.38
1550	.85	1.14	.24	-.59	.44	-1.14	.05

Table 25 Matrix of Principal Component Co-ordinates for Boreholes M10, IM9, H17A, and IM6.

Component No.	1	2	3	4	5
M10 - depth in feet					
1279	.51	1.68	-.22	.00	.25
1289	.98	2.15	.47	.21	.71
1299	-.46	-1.41	-.86	.02	-.21
1311	-1.95	2.83	-2.97	-1.55	-3.76
1318	1.22	2.99	1.07	1.52	-.17
1332	-.49	-.97	-.83	-.10	-.91
1357	-.71	-1.14	-1.95	.18	-.31
1388	-.61	-1.08	-1.09	-.55	-.67
1408	-1.43	-1.43	-1.68	.07	-.79
1421	-.56	-1.57	-.58	-.21	-.56
1431	-1.39	-1.27	-.50	-.59	-.25
1441	-.98	-1.68	-.57	-.13	-.63
1451	-.96	-1.80	-.40	.60	-.33
1472	.20	-1.40	-.28	-.62	.31
1486	-2.97	-.70	-1.79	-.85	-3.30
1491	-.35	-.98	-.77	-.36	.07
1501	-.24	-.83	-.98	-.74	-.45
1529	.38	-.57	.26	-.01	-.02
1548	-10.16	.55	.94	-.03	-2.29
1562	-.72	-1.50	-.85	-.11	.15
1584	-2.87	-1.52	1.11	.99	-.67
1589	-15.32	.19	5.44	1.63	2.50
1599	-.63	-1.65	-1.42	.24	.44
IM9 - depth in feet					
51	.87	-1.30	.94	.30	.23
59	1.17	-.06	1.56	1.01	-.46
72	1.06	-.79	1.33	.76	-.02
77	1.76	-.29	.26	2.07	-.58
85	1.51	-.04	1.95	2.20	-.40
97	1.42	-.22	2.56	4.85	-3.71
107	1.68	-1.23	3.44	6.77	-6.27
119	2.04	.59	3.29	3.96	-2.53

Table 25 continued

Component No.	1	2	3	4	5
IM9					
145	.51	-1.21	.30	.12	-.09
158	1.24	-.11	1.53	1.20	-.33
167	1.30	.08	1.49	1.05	-.05
175	.79	-.88	.64	.04	.31
197	.77	-.78	.63	-.15	.32
204	.75	.11	.66	-.08	.40
215	.70	-.88	.54	-.08	.17
225	.65	-.77	.55	-.19	.09
231	.54	-.73	.43	-.34	.26
244	.71	.24	.61	-.20	.13
251	.62	-.27	.76	.57	-.70
265	.44	-.76	.41	-.28	.01
299	.49	-.96	.34	-.56	.49
320	.49	-.83	.35	-.47	.41
334	.52	-.91	.14	-.40	.46
355	.51	-.50	.23	-.47	.48
376	.66	-.09	.66	-.36	.19
384	.94	-.50	.78	.07	.58
403	.72	-.21	.56	.02	.38
423	1.00	.60	.97	.74	-.32
H17A					
1191	.80	2.71	.35	-.15	.50
1201	.98	3.17	.37	.30	.87
1216	.85	2.33	.15	.11	.47
1231	-.27	-.67	-.58	-1.13	-.95
1241	-.82	-.18	-6.57	5.38	2.27
1251	.04	-.91	-.28	-1.40	-.12
1261	-.48	-1.53	-2.88	1.22	.63
1271	-.54	-.48	-.61	-1.54	-1.27
1281	-1.07	-1.32	-1.06	-1.46	-1.73
1291	-1.92	.58	-2.71	-.72	-3.33
1301	-.45	-1.30	-2.37	.76	.42
1331	-.15	-.60	-.42	-.99	-1.02

Table 25 continued

Component No.	1	2	3	4	5
H17A					
1341	-.12	-1.73	-1.30	.45	.21
1351	-1.08	-1.55	-5.41	2.84	.87
1361	-.15	-1.40	-1.28	-.40	.17
1371	-1.18	-1.21	-2.46	.35	-.55
1381	-.03	-1.79	-1.20	-.06	.51
1391	.28	.72	-.77	-.06	-.09
1401	-.10	-1.17	-.15	-.39	.19
1411	-.58	-1.59	-2.33	.48	.00
1421	-.48	.06	-6.07	6.33	2.12
1431	-1.15	-.10	-1.34	-.59	-2.38
1441	.20	.31	-.41	-1.14	-.21
1451	1.65	3.53	1.60	2.86	.73
1461	-.71	-1.48	-2.55	3.20	-2.20
1471	.13	.82	-.63	-.97	-.45
1481	-.59	6.19	-2.18	-1.71	-2.07
1491	-.17	2.17	-1.17	-.80	-1.50
1501	-1.31	3.54	-2.94	-1.06	-3.11
1511	.47	-.40	-.31	.40	.61
1521	-.59	1.23	-6.51	6.03	3.22
1531	.56	.61	.08	.09	1.20
1541	.52	2.80	-.13	.25	.85
1550	.58	.77	.35	-.74	.00
IM6					
129	.71	-.56	.39	-.34	.59
141	.54	-1.00	.11	-.36	.53
152	.69	-.62	.39	-.51	.51
163	.59	-.93	.24	-.58	.59
194	1.20	1.26	1.14	-.27	.60
208	.91	.19	.64	-.33	.59
223	.39	-1.34	-.13	-.58	.49
236	.45	-1.15	-.03	-.62	.41
261	.29	-1.18	-.23	-.44	.10

Table 25 continued

Component No.	1	2	3	4	5
IM6					
283	.38	-1.01	-.22	-.50	.27
299	.52	-.89	-.05	-.35	.52
351	.53	-.77	.17	-.60	.29
385	.48	-.96	-.02	-.49	.42
390	.53	-1.20	.17	-.70	.48
408	.50	-1.04	.00	-.50	.43
416	.43	-1.35	-.11	-.46	.54
436	.42	-1.28	-.05	-.47	.36
599	.47	-1.30	.28	-.12	-.34
620	.50	-1.15	.16	-.17	-.01
647	.48	-1.16	.11	-.61	.41
652	.38	-.39	-.11	-1.09	.05
660	.39	-1.36	-.11	-.57	.36
696	.46	-.76	.04	-.59	.32
720	.44	-.83	-.10	-.56	.28
727	.36	-.79	.03	-.62	-.14
747	.45	-1.21	-.01	-.44	.47
757	.38	-1.14	-.16	-.47	.29
886	.48	-.97	.11	-.73	.35
896	.42	-1.32	-.05	-.63	.49
902	.35	-1.16	-.02	-.91	.37
1005	.34	-.76	-.27	-.87	.15
1025	.33	-.40	-.25	-1.03	.02
1085	.45	-1.25	.10	-.76	.42
1091	.41	-.67	.02	-.95	.17
1120	.44	-.19	-.10	-1.00	.01
1152	.61	-.77	.36	-.48	.27

Table 26 Matrix of Factor Scores for Boreholes IM6, H14, H16.

Factor	1	2	3	4	5	6	7
IM6 - depth in feet							
129	1.01	-.53	1.05	-.35	.42	.35	-.03
141	.86	-1.26	.73	-.36	.39	.48	-.05
152	1.01	-.60	.96	-.56	.42	.52	-.05
163	.90	-1.15	.84	-.56	.54	.32	-.03
194	1.46	2.49	1.67	-.26	.42	.34	.02
208	1.20	.76	1.21	-.34	.40	.64	-.03
223	.74	-1.87	.40	-.53	.49	.43	-.06
236	.80	-1.56	.44	-.60	.45	.35	-.06
261	.63	-1.72	.09	-.46	.17	.20	-.07
283	.75	-1.41	.15	-.43	.34	.36	-.07
299	.87	-1.17	.54	-.25	.45	.32	-.04
351	.87	-1.02	.57	-.60	.40	-.17	-.01
385	.83	-1.29	.47	-.44	.41	.31	-.05
390	.87	-1.57	.71	-.75	.48	.39	-.05
408	.85	-1.38	.51	-.48	.39	.44	-.06
416	.79	-1.90	.50	-.40	.49	.25	-.04
436	.76	-1.77	.47	-.50	.35	.30	-.06
599	.76	-1.74	.64	-.61	-.31	.11	-.10
620	.83	-1.51	.63	-.45	-.03	.34	-.09
647	.80	-1.58	.62	-.64	.44	.14	-.04
652	.75	-.49	-.16	-.96	.49	.09	-.05
660	.74	-1.91	.37	-.58	.37	.39	-.07
696	.78	-.97	.39	-.55	.39	.23	-.05
720	.80	-1.10	.25	-.49	.36	.30	-.06
727	.66	-1.00	.13	-.79	.07	.37	-.11
747	.78	-1.71	.57	-.40	.46	-.03	-.02
757	.73	-1.59	.27	-.45	.32	.34	-.07
886	.80	-1.23	.50	-.76	.42	.43	-.06
896	.77	-1.80	.47	-.61	.49	.47	-.06
902	.67	-1.72	.32	-.82	.66	-.43	.02
1005	.72	-.93	-.16	-.77	.37	.72	-.11

Table 26 continued

Factor	1	2	3	4	5	6	7
IM6							
1025	.72	-.45	-.33	-.90	.40	.64	-.11
1085	.78	-1.75	.56	-.77	.53	-.01	-.02
1091	.74	-.82	.15	-.92	.43	.37	-.07
1120	.83	-.08	-.17	-.91	.34	.70	-.11
1152	.92	-.99	.83	-.57	.27	-.20	-.01
H14							
285	.88	-.10	1.20	.28	-1.08	-.19	-.10
318	.70	-.54	1.04	-.05	-1.67	-.27	-.17
373	.88	-.34	.85	-.62	-.06	.42	-.08
395	.99	-.19	.86	-.31	.15	.44	-.05
406	1.10	.37	1.20	-.39	.34	.46	-.03
412	1.29	.94	1.28	.31	.52	.46	.03
421	1.13	.22	1.03	.08	.55	.43	.01
434	.80	.26	.72	-.39	.45	.27	-.03
472	.64	1.76	.10	-.77	.80	-1.03	.11
526	.86	-.37	.71	-.72	.46	.28	-.03
H16							
36	.95	5.07	-.15	.74	.92	-.93	.04
47	1.00	4.51	.07	.68	.66	-.52	.02
329	1.37	2.59	2.26	-.15	.00	-.14	.03
340	.85	.42	.98	-.19	.25	-.26	.00
350	1.13	1.23	1.82	-.36	-.20	-.41	.01
385	.63	3.49	-1.03	-.13	.71	-.23	.04
395	.56	3.14	-1.11	-.30	.68	-.49	.04
402	.32	5.60	-1.59	-.48	1.40	-4.32	.41
412	.98	1.45	.71	-.27	.03	-.12	-.01
417	1.30	.82	1.51	-.06	-.19	.40	-.05
437	1.24	2.34	2.17	-.02	-.90	.00	-.07
438	1.35	1.26	2.24	.08	-.80	.32	-.07